

Spring 2013

# Interactions of shiga-like toxin-2 (Stx-2) from Escherichia coli O157:H7 and the Bcl-2 family of proteins during host cell programmed cell death

Lia K. Jeffrey

Follow this and additional works at: <https://scholars.unh.edu/dissertation>

---

## Recommended Citation

Jeffrey, Lia K., "Interactions of shiga-like toxin-2 (Stx-2) from Escherichia coli O157:H7 and the Bcl-2 family of proteins during host cell programmed cell death" (2013). *Doctoral Dissertations*. 728.  
<https://scholars.unh.edu/dissertation/728>

This Dissertation is brought to you for free and open access by the Student Scholarship at University of New Hampshire Scholars' Repository. It has been accepted for inclusion in Doctoral Dissertations by an authorized administrator of University of New Hampshire Scholars' Repository. For more information, please contact [nicole.hentz@unh.edu](mailto:nicole.hentz@unh.edu).

INTERACTIONS OF SHIGA-LIKE TOXIN-2 (STX-2) FROM *ESCHERICHIA COLI*  
O157:H7 AND THE BCL-2 FAMILY OF PROTEINS DURING HOST CELL  
PROGRAMMED CELL DEATH

BY

LIA K. JEFFREY

B.S. University of Massachusetts at Amherst, 1999

DISSERTATION

Submitted to the University of New Hampshire

in Partial Fulfillment

the Requirements for the Degree of

Doctor of Philosophy

in

Microbiology

May, 2013

UMI Number: 3572946

All rights reserved

INFORMATION TO ALL USERS

The quality of this reproduction is dependent upon the quality of the copy submitted.

In the unlikely event that the author did not send a complete manuscript and there are missing pages, these will be noted. Also, if material had to be removed, a note will indicate the deletion.

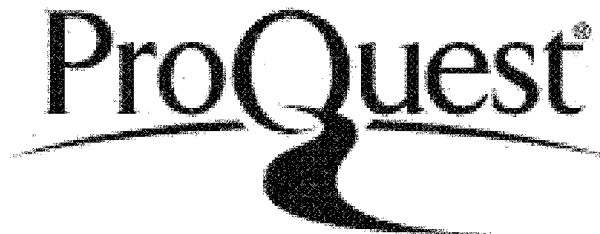


UMI 3572946

Published by ProQuest LLC 2013. Copyright in the Dissertation held by the Author.

Microform Edition © ProQuest LLC.

All rights reserved. This work is protected against unauthorized copying under Title 17, United States Code.



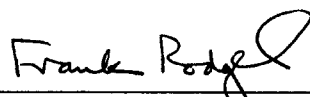
ProQuest LLC  
789 East Eisenhower Parkway  
P.O. Box 1346  
Ann Arbor, MI 48106-1346

**ALL RIGHTS RESERVED**

**© 2013**

**Lia K. Jeffrey**

This dissertation has been examined and approved.



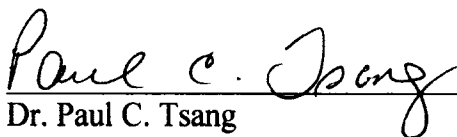
---

Dissertation Director, Dr. Frank G. Rodgers  
Professor  
Department of Molecular, Cellular, and Biomedical Sciences



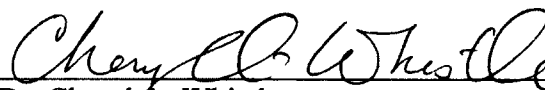
---

Dr. Aaron B. Margolin  
Professor  
Department of Molecular, Cellular, and Biomedical Sciences



---

Dr. Paul C. Tsang  
Professor  
Department of Molecular, Cellular, and Biomedical Sciences



---

Dr. Cheryl A. Whistler  
Associate Professor  
Department of Molecular, Cellular, and Biomedical Sciences



---

Dr. Andrew Laudano  
Associate Professor  
Department of Molecular, Cellular, and Biomedical Sciences

04/08/2013

---

Date

## DEDICATION

I would like to dedicate this dissertation to all of my friends and family who supported me through this process, and to my late father, Edward J. Nalewak Jr., who inspired me to be the first in my family to work towards a doctoral degree. I would especially like to thank my husband, John who was my grounding factor and kept me focused on the task at hand, my mom, Denise Tallarida who always would be there to listen when my experiments didn't go as planned, and Dr. Rodgers for giving me a truly wonderful education and mentorship I will never forget.

## ACKNOWLEDGEMENTS

I would like to acknowledge Dr. Rodgers for the opportunity to earn this degree and for all of his time and effort he spent mentoring me. I would also like to acknowledge the members of my committee for their help and guidance throughout my research project, and Adele Marone for being my designated phlebotomist. In addition, I would like to thank my colleagues at EMD Millipore, especially Kerry Roche-Lentine for supporting and allowing me the flexibility to perform my research on-site during the latter stages of these studies while maintaining my full-time position.

To all the undergraduates who worked with me on projects related to the research presented in this thesis, thank you. Your help was very much appreciated during the many hours spent performing western blots, ELISA assays, and other experimentation. I would also like to thank Kate Stefani for her friendship and support during my graduate studies; you will always be my research lab partner in crime.

I would also like to acknowledge the USDA Hatch Grant for supporting and funding this research, the University of New Hampshire's College of Life Sciences for providing fellowships and scholarships throughout my graduate degree, and the UNH Institutional Biosafety Committee and Institutional Review Board for the Protection of Human Subjects in Research for authorization to perform the recombinant DNA and human aspects of this research.

## TABLE OF CONTENTS

DEDICATION.....	iv
ACKNOWLEDGEMENTS.....	v
LIST OF CHAPTERS.....	vi
LIST OF TABLES.....	xiii
LIST OF FIGURES.....	xiv
ABSTRACT.....	xviii

<b>CHAPTER</b>	<b>PAGE</b>
1. INTRODUCTION TO <i>ESCHERICHIA COLI</i> O157:H7 INFECTION AND HOST CELL RESPONSES	
1.0 Microorganism Description.....	1
2.0 Overview of Infection.....	6
3.0 Epidemiology.....	7
4.0 Virulence Factors.....	11
4.1 Shiga-like Toxins.....	11
4.2 Adhesins.....	14
4.3 Lipopolysaccharide.....	15
4.4 Enterohemolysin.....	15
4.5 Extracellular Serine Protease.....	16



4.6	Enterotoxin.....	17
5.0	Pathogenesis of <i>E. coli</i> O157:H7 Infection .....	17
6.0	Host Response to <i>E. coli</i> O157:H7 Infection .....	23
7.0	Mechanisms of Eukaryotic Cell Death.....	27

## 2. INTERACTIONS BETWEEN THE SHIGA-LIKE TOXINS AND BCL-2 PROTEIN FAMILY

1.0	Abstract.....	36
2.0	Introduction.....	37
3.0	Hypothesis.....	39
4.0	Materials and Methods.....	39
4.1	Stx-2 Protein Sequence Analysis.....	39
4.2	Purification of Stx-2 from <i>Escherichia coli</i> O157:H7 strain 90-2380.....	40
4.3	Stx-2 Characterization.....	41
4.3.1	Native Analysis of Semi-Purified Stx-2.....	41
4.3.2	SDS-PAGE Analysis of Semi-Purified Stx-2.....	42
4.3.3	Western Blot Analysis of Semi-Purified Stx-2.....	44
4.3.4	Cleavage Analysis of Semi-Purified Stx-2 and A1 Fragment Generation.	45
4.3.5	Biological Activity Verification of Semi-Purified Stx-2.....	46
4.3.6	Quantitation of Semi-Purified Stx-2.....	47
4.4	Interactions of Stx-2 with Caco-2 Cells.....	47
4.4.1	Susceptibility of Caco-2 Cells to Stx-2.....	48
4.4.2	Protein Analysis of Caco-2 Cells.....	48
4.4.3	Interactions of Bcl-2 (from Caco-2 Cells) and Stx-2.....	51

4.4.4	Caco-2 Cell Lysate Preparation for Co-Immunoprecipitation.....	52
4.4.5	Co-Immunoprecipitation of Stx-2 and Bcl-2 Family Proteins.....	53
5.0	Results.....	56
5.1	Stx-2 Protein Sequence Analysis.....	56
5.2	Stx-2 Characterization.....	58
5.2.1	Native Analysis of Semi-Purified Stx-2.....	58
5.2.2	SDS-PAGE and Western Blot Analysis of Semi-Purified Stx-2.....	58
5.2.3	Cleavage Analysis of Semi-Purified Stx-2 and A1 Fragment Generation.	63
5.2.4	Biological Activity Verification of Semi-Purified Stx-2.....	66
5.2.5	Quantitation of Semi-Purified Stx-2.....	68
5.3	Interactions of Stx-2 with Caco-2 Cells.....	68
5.3.1	Susceptibility of Caco-2 to Stx-2.....	68
5.3.2	Protein Analysis of Caco-2 Cells.....	71
5.3.3	Interactions of Bcl-2 (from Caco-2 Cells) and Stx-2.....	76
5.3.4	Co-Immunoprecipitation of Stx-2 and Bcl-2 Family Proteins.....	78
6.0	Discussion.....	83

### 3. IMPACT OF STX-2 ON NEUTROPHIL APOPTOSIS AND NECROSIS

1.0	Abstract.....	87
2.0	Introduction.....	88
3.0	Hypothesis.....	90
4.0	Materials and Methods.....	90
4.1	Verification of Stx Genes.....	90

4.2	Isolation of Stx-2 Supernatant.....	91
4.3	Verification of Stx-2 Presence and Activity.....	93
4.4	Isolation and Cultivation of Neutrophils.....	94
4.5	Assessment of Bcl-2 Family Proteins in Neutrophils.....	96
4.6	Analysis of Neutrophil Apoptosis & Necrosis Rates when Exposed to Stx-2.....	98
5.0	Results.....	100
5.1	Verification of Stx Genes.....	100
5.2	Verification of Stx-2 Presence and Activity.....	102
5.3	Assessment of Bcl-2 Family Proteins in Neutrophils.....	105
5.4	Analysis of Neutrophil Apoptosis & Necrosis Rates when Exposed to Stx-2.....	108
6.0	Discussion.....	111

#### 4. GENERATION OF A MUTANT STX-2 PROTEIN: G225A

1.0	Abstract.....	115
2.0	Introduction.....	115
3.0	Hypothesis.....	119
4.0	Materials and Methods.....	119
4.1	Determination of <i>E. coli</i> O157:H7 strain 43888 Susceptibility Profile to Ampicillin.....	119
4.2	Creation of a Recombinant Plasmid: Mutant <i>stx2</i> with Vector pBR322...	120
4.2.1	Primer Design and PCR.....	120

4.2.2	Mutation of <i>stx2</i> using PCR SOE.....	121
4.2.3	Insertion of Mutant <i>stx2</i> into pBR322.....	122
4.3	Transformation of the Recombinant Plasmid into <i>E. coli</i> O157:H7 strain 43888.....	128
4.3.1	Preparation of Electrocompetent <i>E. coli</i> O157:H7 strain 43888.....	128
4.3.2	Electroporation of Electrocompetent <i>E. coli</i> O157:H7 strain 43888 cells with <i>stx2</i> and pBR322.....	129
4.4	Verification of Recombinant Plasmid Transformation into <i>E. coli</i> O157:H7 strain 43888.....	131
4.5	Creation of Mutant Clone Stocks.....	132
5.0	Results.....	132
5.1	Determination of <i>E. coli</i> O157:H7 strain 43888 Susceptibility Profile to Ampicillin.....	132
5.2	Creation of a Recombinant Plasmid: Mutant <i>stx2</i> with Vector pBR322....	132
5.3	Verification of Recombinant Plasmid Transformation into <i>E. coli</i> O157:H7 strain 43888.....	135
6.0	Discussion.....	143
5.	<b>THE EFFECTS OF MUTANT STX-2 AND NATIVE STX-2 WITH AN INTERLEUKIN-8 INHIBITOR ON NEUTROPHIL APOPTOSIS, NECROSIS, CASPASE-8 AND CASPASE-9 ACTIVATION</b>	
1.0	Abstract.....	145
2.0	Introduction.....	146
3.0	Hypothesis.....	148

4.0	Materials and Methods.....	148
4.1	Purification of Stx-2.....	148
4.2	Purification of Mutant Stx-2.....	149
4.3	Conjugation of STX2-11E10 Antibody.....	151
4.4	Verification of Stx-2 and Mutant Stx-2 Presence and Activity.....	152
4.5	Quantitation of Stx-2 and Mutant Stx-2 Using Enzyme Linked Immunosorbent Assay (ELISA).....	154
4.6	Isolation of Human Neutrophils.....	158
4.7	Analysis of Neutrophil Apoptosis and Necrosis Rates Following Exposure to Native and Mutant Stx-2.....	158
4.8	Analysis of Neutrophil Caspase-8 and Caspase-9 Activation Following Exposure to Native and Mutant Stx-2.....	161
5.0	Results.....	162
5.1	Verification of Stx-2 and Mutant Stx-2 Presence and Activity.....	162
5.2	Quantitation of Stx-2 and Mutant Stx-2 Using ELISA.....	167
5.3	Isolation of Human Neutrophils.....	169
5.4	Analysis of Neutrophil Apoptosis and Necrosis Rates After Exposure to Native Stx-2, Mutant Stx-2, and IL-8 Inhibitor.....	171
5.4.1	Necrosis Rates.....	171
5.4.2	Apoptosis Rates.....	175
5.5	Analysis of Neutrophil Caspase-8 and Caspase-9 Activation After Exposure to Native Stx-2, Mutant Stx-2, and IL-8 Inhibitor.....	178
5.5.1	Caspase-8.....	179

5.5.2	Caspase-9.....	182
6.0	Discussion.....	185
6.	CONCLUSIONS AND FUTURE STUDIES	
	Conclusions and Future Studies.....	193
	APPENDICES.....	199
	Appendix A Microorganisms, Media and Reagents.....	199
	Appendix B Maintenance of Eukaryotic Cell Lines.....	213
	Appendix C Institutional Review Board Project Approval.....	214
	Appendix D UNH Institutional Biosafety Committee Project Approval.....	216
	REFERENCES.....	218

## LIST OF TABLES

Table 1.1	Overview of the Pathogenic Groups of <i>Escherichia coli</i> as Outlined in Bergey’s Manual of Systematic Bacteriology.....	4
Table 1.2	The Bcl-2 Protein Family.....	30
Table 2.1	Bcl-2 Protein Family Primary Detection Antibodies.....	50
Table 2.2	Co-Immunoprecipitation Pull-Down Antibodies.....	55
Table 3.1	Primer Sequences for the Detection of <i>stx1</i> and <i>stx2</i> Courtesy of Wang <i>et al.</i> (210).....	92
Table 3.2	Neutrophil Cell Death Detection Time Point Setup.....	99
Table 4.1	Primer Sequences.....	124
Table 4.2	Samples Electroporated Into <i>E. coli</i> O157:H7 strain 43888.....	130
Table 4.3	MIC Assay for <i>E. coli</i> O157:H7 and Ampicillin.....	133
Table 5.1	Neutrophil Cell Death Detection Time Point Setup.....	160
Table 5.2	Viability of Neutrophils Collected from 3 Donors.....	170
Table 5.3	Summary of Statistical Analysis for Blood Donor B: Necrosis.....	173
Table 5.4	Summary of Statistical Analysis for Blood Donor B: Apoptosis.....	177
Table 5.5	Summary of Statistical Analysis for Blood Donor B: Relative Caspase-8 Levels.....	181
Table 5.6	Summary of Statistical Analysis for Blood Donor B: Relative Caspase-9 Levels .....	184

## LIST OF FIGURES

Figure 1.1	<i>E. coli</i> O157:H7 outbreaks by year from 1982-2002.....	9
Figure 1.2	<i>E. coli</i> O157:H7 outbreak transmission routes by year from 1982-2002.....	10
Figure 1.3	The structure of Stx.....	13
Figure 1.4	The formation of attaching and effacing (A/E) lesions, caused by <i>Escherichia coli</i> .....	19
Figure 1.5	Pathogenesis of Shiga toxin binding to cells with Gb3 receptors.....	21
Figure 1.6	Furin cleavage site of Stx-1 and Stx-2.....	22
Figure 1.7	Hypothetical sequence of events of <i>E. coli</i> O157:H7 infection from ingestion to the development of HUS.....	24
Figure 1.8	The three main pathways of apoptosis: extrinsic, intrinsic and perforin/granzyme.....	32
Figure 2.1	Western blot transfer sandwich assembly.....	43
Figure 2.2	Alignment of Stx-1 and Stx-2 protein sequences.....	57
Figure 2.3	Native Analysis of Stx-2 produced by <i>E. coli</i> O157:H7 strain 90-2380.....	59
Figure 2.4	Purification and concentration of Stx-2 produced by <i>E. coli</i> O157:H7 strain 90-2380 using Centricon devices.....	60



Figure 2.5	SDS-PAGE analysis of Stx-2 produced by <i>E. coli</i> O157:H7 strain 90-2380.....	61
Figure 2.6	Western Blot Confirmation of Stx-2 in the semi-purified toxin preparation.....	62
Figure 2.7	SDS-PAGE analysis of trypsin-treated semi-purified Stx-2.....	64
Figure 2.8	Western blot confirmation of Stx-2 cleavage and A1 fragment generation in the trypsin-treated Stx-2 preparation.....	65
Figure 2.9	Biological activity of semi-purified Stx-2.....	67
Figure 2.10	Total protein concentration of semi-purified Stx-2.....	69
Figure 2.11	Cytotoxicity of Stx-2 on Caco-2 cells.....	70
Figure 2.12	SDS-PAGE analysis of Caco-2 lysates.....	72
Figure 2.13	Western blot confirmation of Bcl-2 in Caco-2 whole cell lysate preparation with protease inhibitors.....	73
Figure 2.14	Analysis of Bcl-2 family proteins in Caco-2 whole cell lysate preparation with protease inhibitors.....	74
Figure 2.15	Far Western blot of Caco-2 whole cell lysate preparation with protease inhibitors.....	77
Figure 2.16	SDS-PAGE of Caco-2 cell lysate and Stx-2 co-immunoprecipitation interactions using Bcl-2 protein family antibodies.....	79
Figure 2.17	Western blot of Caco-2 cell lysate and Stx-2 co-immunoprecipitation interactions using Bcl-2 protein family antibodies.....	80

Figure 2.18	Western blot of Caco-2 and Stx-2 co-immunoprecipitation interactions using STX2-11E10 antibody.....	82
Figure 3.1	Sigma-Aldrich leukocyte separation method.....	99
Figure 3.2	Agarose gel analysis of PCR products.....	101
Figure 3.3	Western blot confirmation of Stx-2.....	103
Figure 3.4	Biological activity of semi-purified Stx-2.....	104
Figure 3.5	Assessment of Bcl-2 family proteins in neutrophils over 18 hours.....	106
Figure 3.6	Necrosis rates of neutrophils exposed to Stx-2 supernate for 72 h.....	109
Figure 3.7	Apoptosis rates of neutrophils exposed to Stx-2 supernate for 72 h.....	110
Figure 4.1	The Bcl-2 dimerization interface.....	118
Figure 4.2	Genome map of the <i>stx2</i> gene.....	123
Figure 4.3	Genomic sequence of <i>stx2</i> from <i>Escherichia coli</i> O157:H7 VT2-Sakai.....	125
Figure 4.4	Restriction enzyme map of the cloned <i>stx2</i> gene.....	126
Figure 4.5	Vector map of pBR322.....	127
Figure 4.6	Vector map of recombinant plasmid <i>stx2</i> -pBR322.....	134
Figure 4.7	Verification of recombinant <i>stx2</i> -pBR322 plasmids.....	136
Figure 4.8	Verification of the <i>stx2</i> insert within the recombinant <i>stx2</i> -pBR322 plasmid.....	137
Figure 4.9	Verification of recombinant plasmid size.....	138

Figure 4.10	<i>E. coli</i> clone L14 sequence alignment.....	139
Figure 4.11	<i>E. coli</i> clone L42 sequence alignment .....	140
Figure 4.12	<i>E. coli</i> clone L94 sequence alignment .....	141
Figure 4.13	<i>E. coli</i> clone L4 sequence alignment .....	142
Figure 5.1	Setup of a sandwich ELISA.....	156
Figure 5.2	Setup of the ELISA plate.....	157
Figure 5.3	SDS-PAGE analysis of semi-purified native and mutant Stx-2...	163
Figure 5.4	Western blot analysis of toxin preparations.....	165
Figure 5.5	Biological activity of semi-purified Stx-2 and mutant Stx-2 viewed at 200x magnification.....	166
Figure 5.6	Total protein concentration of toxin preparations.....	168
Figure 5.7	Necrosis rates for blood donor B.....	172
Figure 5.8	Apoptosis rates for blood donor B .....	176
Figure 5.9	Relative caspase-8 levels for blood donor B.....	180
Figure 5.10	Relative caspase-9 levels for blood donor B.....	183
Figure 5.11	The effects of mitochondrial membrane permeabilization (MMP) on programmed cell death (PCD).....	189
Figure 5.12	Apoptotic pathways leading to caspase-dependent and -independent cell death.....	190

## ABSTRACT

# INTERACTIONS OF THE SHIGA-LIKE TOXIN-2 (STX-2) FROM ESCHERICHIA COLI O157:H7 AND THE BCL-2 FAMILY OF PROTEINS DURING HOST CELL APOPTOSIS

By

Lia K. Jeffrey

University of New Hampshire, May 2013

Stx-2 is a major contributor to the pathogenesis of *Escherichia coli* O157:H7. Prior reports suggest that Stx-2 increases necrosis and apoptosis of a variety of host cells including those of endothelial origin as well as immune cells such as neutrophils (156). However, the role Stx-2 plays in delayed apoptosis of neutrophils is not fully understood given that previous studies have shown conflicting results (118, 51). The process of apoptosis is mediated by the Bcl-2 protein family (2, 46, 226). The purpose of this research was to define the molecular mechanisms of Stx-2 and Bcl-2 protein family interactions. These studies examined the binding of Stx-2 to select Bcl-2 family proteins, and outlined the effects that Stx-2 and a newly generated mutant of Stx-2 have on neutrophil apoptosis and necrosis rates as well as on caspase-8 and caspase-9 activation. Stx-2 did not bind to the select Bcl-2 family proteins examined nor did it consistently show decreased apoptosis rates in neutrophils. The mechanisms behind Stx-2-induced

neutrophil apoptosis potentially involved the endoplasmic reticulum (ER) stress response and/or interactions with other Bcl-2 family members such as Bak at the mitochondrial membrane therefore inducing mitochondrial membrane permeabilization (MMP) and its downstream effects.

## CHAPTER 1

### INTRODUCTION TO *ESCHERICHIA COLI* O157:H7 INFECTION AND HOST CELL RESPONSE

#### 1.0 Microorganism Description

*Escherichia coli* is a major human disease agent on a world-wide basis. Despite this, it was not until almost 100 years after the first description of the microbe that the most serious form of the disease it causes became apparent.

The genus name *Escherichia* was derived from its discoverer, Theodor Escherich, a German pediatrician. The genus currently consists of five species: *E. hermannii*, *E. fergusonii*, *E. vulneris*, *E. blattae*, and the type species, *E. coli*. *E. coli* was first discovered in 1885 from the feces of healthy humans and originally named *Bacterium coli commune* (21, 48). In 1895 Migula renamed the bacterium to *Bacillus coli* and in 1919 the name *Escherichia* was chosen for the genus by Castellani and Chalmers (21). The current taxonomic classification for this microorganism places it within the *Proteobacteria* phylum, *Gammaproteobacteria* class, *Enterobacteriales* order, *Enterobacteriaceae* family, *Escherichia* genus, and *coli* species (21).

*E. coli* is a Gram-negative, cylindrical, straight rod typically 1 - 1.5  $\mu\text{m}$  wide by 2 - 6 $\mu\text{m}$  in length. The cells often have a single or paired arrangement, and varying degrees of motility from non-motile to motile by way of peritrichous flagella (21). The general biochemical profile for *E. coli* is to ferment various sugars, including D-glucose (which results in the formation of gas and acid by-products), lactose, mannitol, sorbitol and mucate (which result in the formation of acid by-products only). The organism also breaks down indole and decarboxylate lysine, and can use sodium acetate as a sole carbon source (21). *E. coli* is not able to use citrate as a sole carbon source nor can it grow on potassium cyanide, use malonate, or form a yellow pigmentation like some other members of the *Escherichia* genus (21).

*E. coli* is able to survive and proliferate within a temperature range of 15-45°C (21-37°C for balanced growth) and is a neutrophilic organism that prefers to grow within a pH range of 5.0 – 9.0 (21). Due to the structure of the outer membrane, *E. coli* is intrinsically resistant to hydrophobic antibiotics such as actinomycin D, fusidic acid, macrolides, novobiocins, and rifamycins (133). Acquired resistance to other antibiotics including, but not limited to aminoglycosides, beta-lactams, chloramphenicol, tetracycline, and trimethoprim has also been previously described (158). The mechanisms for antibiotic resistance evolved through either genetic mutation or horizontal gene transfer and were developed by alteration of the target site, enzymatic detoxification of the antibiotic, decreased drug accumulation, and bypass of an antibiotic-sensitive step (158).

As a result, many diverse strains comprise the species of *E. coli* and they run the gamut from commensal to deadly pathogen. *E. coli* strains are differentiated by three distinct antigenic structures; the O antigens, the H antigens, and the K antigens. The resulting designation is referred to as the serotype of the microorganism. The O antigens are designated based upon lipopolysaccharide (LPS), H antigens on the nature of the flagella, and the K antigens on acidic capsular polysaccharide (CPS) composition (21).

In addition to these antigenic classifications, *E. coli* is also classified into groups based upon the pathogenic mechanisms and include enteropathogenic *E. coli* (EPEC), enterotoxigenic *E. coli* (ETEC), enteroinvasive *E. coli* (EIEC), enteroaggregative *E. coli* (EAaggEC), diffusely adherent *E. coli*, (DAEC), shiga toxin-producing *E. coli* (STEC), enterohemorrhagic *E. coli* (EHEC), extraintestinal pathogenic *E. coli* (ExPEC), uropathogenic *E. coli* (UPEC), and neonatal meningitis *E. coli* (NMEC) (21). These pathogenic groups are described in Table 1.1.

*E. coli* O157:H7 is the prototype organism of the STEC group, and has caused numerous outbreaks in many countries including the United States. Outbreaks had been associated with a wide variety of food types since first appearing in the early 1980's. It is hypothesized that the emergence of this microorganism as a food borne pathogen may be related to feeding practices in cattle, the nonhuman reservoir (5). *E. coli* O157:H7 is now present on most farms and appears to coincide with feeding cattle grain rather than grass (64, 65). However, the ecology of this organism is complex and not fully



**Table 1.1: Overview of the pathogenic groups of *Escherichia coli* as outlined in Bergey's Manual of Systematic Bacteriology (21)**

<b>Group Name</b>	<b>Acronym</b>	<b>Description</b>
Enteropathogenic <i>E. Coli</i>	EPEC	This was the first recognized category of diarrheagenic <i>E. coli</i> . It has most recently been described to include <i>E. coli</i> that have the ability to cause attaching and effacing (A/E) lesions without producing Shiga toxins. Many serotypes are included in this group, the most recent of which are O88:H25, O127:H40, O157:H8, O157:H16 and O157:H45.
Enterotoxigenic <i>E. Coli</i>	ETEC	This type of <i>E. coli</i> is associated with diarrhea in both humans and animals. They have the ability to produce one or more enterotoxins that can be either heat-labile or heat-stable. These toxins cause intestinal secretions and are classified based on their biological activity, receptors, and chemical and antigenic properties. Strains commonly associated with humans include O11:H27, O25:K7:H42, O48:H26, O85:H7, O119:H6, and O153:H10.
Enteroinvasive <i>E. coli</i>	EIEC	This type of <i>E. coli</i> is capable of invading and propagating within intestinal epithelial cells of the intestines. These strains obtain their virulence from multiple genes located within the bacterial chromosome and on plasmids. There are a very small number of serotypes, most of which are non-motile. These serotypes include O115:H <sup>-</sup> , O136:H <sup>-</sup> , O159:H2, O164:H <sup>-</sup> , and O173:H <sup>-</sup> .
Enterotoxigenic <i>E. coli</i>	EAggEC	This type of <i>E. coli</i> is generally associated with travelers' diarrhea and other enteric symptoms such as cramps. It is characterized by a plasmid-mediated aggregative adherence pattern to HEp-2 cells. Prominent autoagglutination of cells to each other and host cell surfaces are observed. This type of cell layering has been described as a "stacked brick" configuration. Some of the most frequently reported serotypes include O3:H2, O15:H18, O111:H12, and O125:H9.

**Table 1.1: Overview of the pathogenic groups of *Escherichia coli* as outlined in Bergey's Manual of Systematic Bacteriology (21)**

<b>Group Name</b>	<b>Acronym</b>	<b>Description</b>
Diffusely adherent <i>E. coli</i>	DAEC	This type of <i>E. coli</i> is defined by a diffuse adherence pattern to HEp-2 cells. This phenotype is a result of surface fimbriae F1845 and adhesin AIDA-I in serotype O126:H27. The role of DAEC in diarrhea is unclear.
Shiga toxin-producing <i>E. coli</i> or Vero cytotoxin-producing <i>E. coli</i>	STEC or VTEC	This type of <i>E. coli</i> is characterized by its ability to produce at least one of two distinct cytotoxins referred to as Stx-1 or VT1 and Stx-2 or VT2. The most influential serotype of this group is O157:H7.
Enterohemorrhagic <i>E. coli</i>	EHEC	This group is a subgroup of STEC/VTEC and includes all <i>E. coli</i> strains that commonly cause hemorrhagic colitis and have the same clinical and pathogenic features as <i>E. coli</i> O157:H7.
Extraintestinal pathogenic <i>E. coli</i>	ExPEC	This type of <i>E. coli</i> is commonly associated with urinary tract infections, pyelonephritis, neonatal and postneurosurgical meningitis, and septicemia. They are distinctly different from commensal and intestinal strains of <i>E. coli</i> . They typically are pathogenic clones of a limited number of O:K:H serotypes containing host defense avoidance mechanisms including capsules, serum resistance, and toxins such as $\alpha$ -hemolysin.
Uropathogenic <i>E. coli</i>	UPEC	This type of <i>E. coli</i> is commonly associated with urinary tract infections (UTIs) including pyelonephritis. They are characterized by a number of virulence factors. Predominantly this type is associated with a limited number of O groups and K antigens. The most common serotypes include O1:K1:H7, O2:K1:H4, O4:K12:H1, O4:K12:H5, O6:K2:H1, O6:K5:H1, O6:K13:H1, O16:K1:H6, and O18AC:K5:H7.
Neonatal meningitis <i>E. coli</i>	NMEC	This type of <i>E. coli</i> is frequently associated with neonatal meningitis and usually includes the O groups O7, O18ac, O1, and O6 that have the K1 antigen identical to the capsule of <i>Neisseria meningitidis</i> type B.

understood. Biochemically, *E. coli* O157:H7 differs from that of other *E. coli* strains. It is unable to ferment sorbitol, cannot produce  $\beta$ -glucuronidase which hydrolyzes a compound known as MUG (4-methylumbelliferyl- $\beta$ -D-glucuronide) which will result in cell fluorescence, and it grows poorly above 44°C (86,126). In the clinical laboratory, MacConkey agar containing sorbitol and MUG are used to detect *E. coli* O157:H7. Due to the inability to utilize sorbitol or break-down MUG, colonies will appear colorless and non-fluorescent (86). The most important differences between this strain and other non-pathogenic strains are those that aid in the pathogenicity of the microorganism and are explained below.

## **2.0 Overview of *E. coli* O157:H7 Infection**

*E. coli* O157:H7 is a major foodborne pathogen in North America and elsewhere (125, 159, 220). This serotype (STEC) produces a potent Shiga-toxin that is associated with large outbreaks (148). Although many toxic virulence factors are produced by *E. coli* O157:H7, the Shiga-like toxins are the most likely inducers of hemolytic uremic syndrome (HUS) (131). HUS, with associated hemorrhagic colitis (HC), is a rare but potentially fatal complication of infection often in children and is characterized by hemolytic anemia (a low number of red blood cells due to premature destruction), thrombocytopenia (low number of platelets), and renal injury (7).

Symptoms of disease usually present with severe abdominal cramping, nausea, and diarrhea that may be watery or bloody (87). After 5-10 days, the gastrointestinal

symptoms either resolve, or, in approximately 5% of cases, escalate to HUS (7, 87). Typical features of HUS include: swollen and detached glomerular endothelial cells, the deposition of fibrin and platelets in the renal microvasculature, and systemic thrombotic lesions in the microvasculature of the bowel, brain, and pancreas (148,161). Disease outcome depends on a number of host and organism factors including patient age, general health, and the production of the Shiga-toxins, Stx-1 and/or Stx-2 (88).

Treatment of patients with STEC infection include limiting the severity and duration of gastrointestinal symptoms, limiting life-threatening systemic complications such as HUS, and preventing spread of infection to close contacts (148). As there is no reliable treatment for patients with HUS, therapy usually involves fluid replacement, treatment of hypertension, hemodialysis and peritoneal dialysis to maintain balance (148). In general, the use of antibiotics is not recommended as they may increase toxin production and precipitate HUS (99). Clinical studies showed that children treated with antibiotics during the course of an STEC infection had a 17-fold higher chance of developing HUS than those who did not receive antibiotic therapy (219).

### **3.0 Epidemiology of *E. coli* O157:H7 Infection**

This pathogen was not recognized as a threat until the first major outbreak occurred in 1982. From 1982-2002, *E. coli* O157:H7 became broadly recognized as an important and life-threatening pathogen (162). In the US, it was the cause of 350 outbreaks in 49 states with 8,958 reported cases, 1,493 hospitalizations, 354 HUS cases,

and 40 deaths (159). The number of reported outbreaks increased after 1993 and peaked in 2000 (Figure 1.1); however, the overall size of the outbreaks decreased over time (159). It is now estimated that *E. coli* O157:H7 causes approximately 73,500 illnesses and 61 deaths per year in the US (125).

There are many routes of transmission associated with *E. coli* O157:H7 ranging from the most common foodborne-related incidences (responsible for 61% of outbreak-related cases) to the rare laboratory-related occurrences (2 cases) (159). Historically, *E. coli* O157:H7 outbreaks are most commonly associated with ground beef; however, produce, other beef and dairy products, person-to-person contact, water, animal contact, and laboratory accidents have been implicated in disease (Figure 1.2) (1, 11, 13, 30, 31, 53, 159).

A unique and troubling issue is that *E. coli* O157:H7 outbreaks remain common even with improved US food supply safety regulations (200). For example, from 2006-2011 there were 12 foodborne outbreaks in the US. These outbreaks occurred in fresh raw spinach, hazelnuts, prepackaged cookie dough, pizza, ground beef, Lebanon bologna and cheeses (29). Recently 60 cases of O157:H7 infection were associated with romaine lettuce consumed at salad bars at grocery stores in the central US region in October/November 2011 (29). Although this outbreak is considered ended the investigation is still on-going (29).

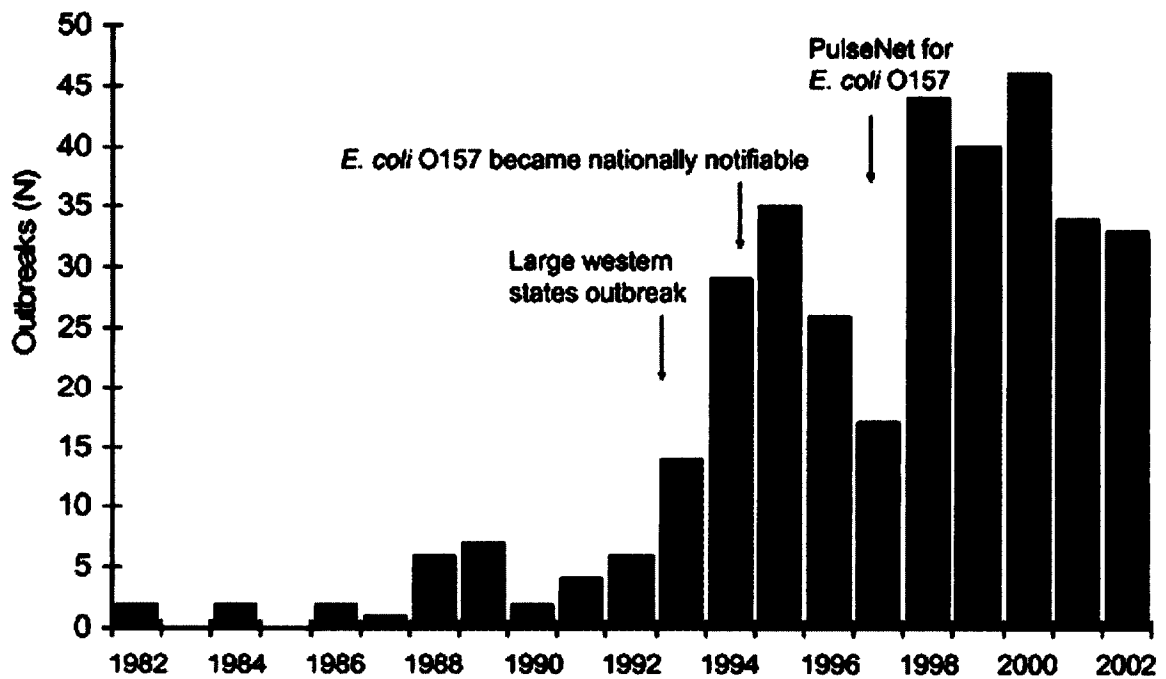


**Figure 1.1: *E. coli* O157:H7 outbreaks by year from 1982-2002.** Diagram is courtesy of Rangel *et al.* (159). A total of 350 outbreaks was recorded.

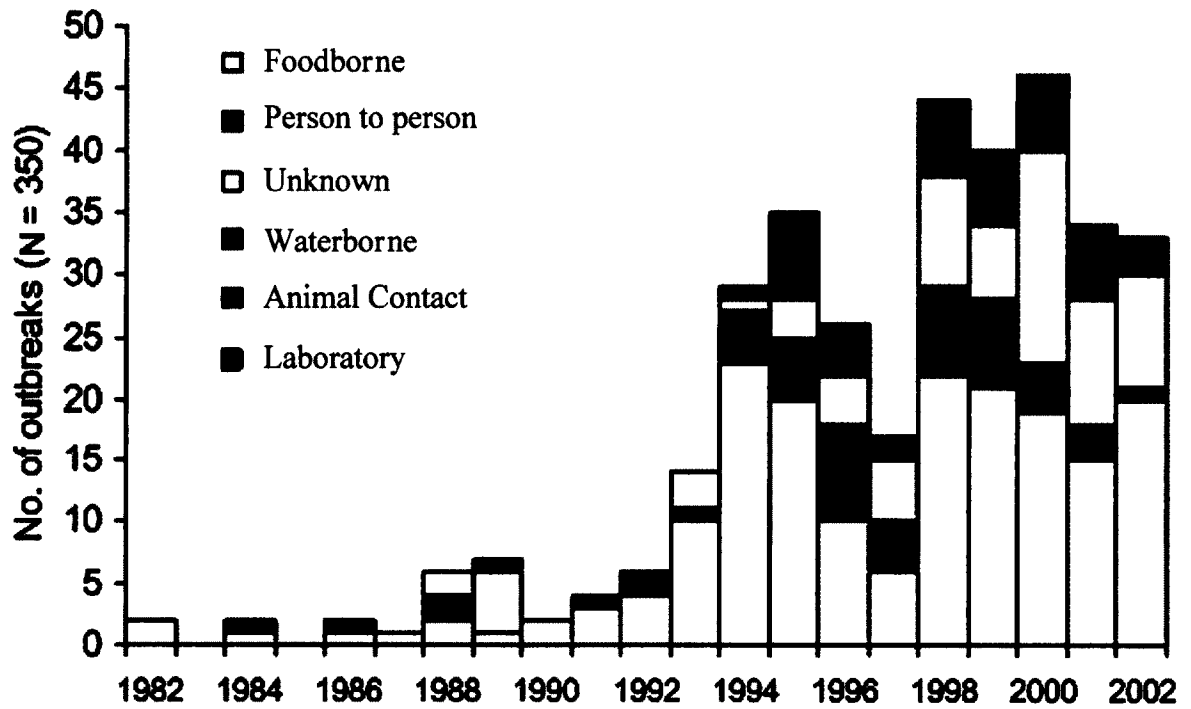


**Figure 1.2: *E. coli* O157:H7 outbreak transmission routes by year from 1982-2002.** Diagram is courtesy of Rangel *et al.* (159). The diversity of transmission routes increased over time.

About half the *E. coli* O157:H7 produce-related outbreaks are linked to cross-contamination during food preparation and the remaining half are caused by contamination during consumer preparation (159). Outbreaks related to food that is intended for raw consumption pose the most serious problem, as once the food is contaminated, prevention is difficult (14, 15). In fact, the last four *E. coli* outbreaks have been associated with foods intended for raw consumption (cheese, hazelnuts, Lebanon bologna, and romaine lettuce) (29). Key to outbreak termination is the timely recognition of *E. coli* in the food supply and this together with prevention and treatment of HUS remain top priorities.

#### **4.0 Virulence Factors of *E. coli* O157:H7**

*E. coli* O157:H7 harbors virulence factors that make it an important pathogen. Such factors include shiga-like toxins, adhesins, LPS, enterohemolysin, extracellular serine proteases, and enterotoxins. The genes for these virulence factors are located either within the chromosome itself or on a distinct virulence plasmid (pO157) within the cell.

#### **4.1 Shiga-like Toxins**

Major virulence factors that increase the pathogenicity of *E. coli* O157:H7 are the shiga-like toxins. Initially designated as verotoxins due to their remarkable cytotoxic effects on African green monkey kidney (Vero) cells, at least two of these toxins are associated with human disease: Verotoxin 1 (VT1) and Verotoxin 2 (VT2) (87). VT1 was



first identified by Konowalchuk *et al.* in 1977 (104). Both VT1 and VT2 were implicated in infantile gastrointestinal disease and children with hemolytic uremic syndrome (HUS) (89, 104, 148, 162). O'Brien *et al.* (139, 140) reported that the structure and biological activity of VT toxins were similar to those of the Shiga toxin produced by *Shigella dysenteriae* type 1, and they could be neutralized by anti-Stx antibody. This led to the current toxin nomenclature of shiga-like toxin 1 (SLT-1) or Stx-1 and shiga-like toxin 2 (SLT-2) or Stx-2 (139, 140). For simplicity and in keeping with international usage, the toxins will be referred to as Stx-1 and Stx-2 throughout this thesis and their corresponding genes designated as *stx1* and *stx2*.

Both Stx-1 and Stx-2 are compound toxins that have a total molecular weight of approximately 70,000 Daltons (70 kDa) (138). The nucleotide sequence of the genes that encode for Stx-1 and Stx-2 was discovered in the late 1980s (25, 41, 81, 82, 106, 187). The gene structure consists of an operon with a single translational unit that encodes both the individual A subunit gene and the B subunit gene (148). The AB<sub>5</sub> toxin structure (63) comprises 2 main subunits: a single 32 kDa A subunit and five 7.7 kDa B subunits (138). The B subunit gene has a stronger ribosomal binding site resulting in higher translation of the B subunit. The A-subunit has 315 amino acids for Stx-1 and 318 amino acids for Stx-2, and the B-subunit has 89 amino acids for both toxins (170).

The protein structure (Figure 1.3) follows an alpha-beta motif and each subunit has a unique function. The A-subunit has two fragments; the A1 and A2 fragments. The



**Figure 1.3: The structure of Stx.** Diagram is courtesy of the European Bioinformatics Institute PDBsum [[www.ebi.ac.uk/pdbsum](http://www.ebi.ac.uk/pdbsum)]. A) Stx holotoxin B) Stx A-subunit C) Stx B-subunit single chain. Both Stx and Stx-1 have similar structures with only minor differences in the amino acid sequence whereas Stx-2 has only 56% identity to both toxins for the A and B subunits (81).

A1 fragment is the enzymatically active portion of the toxin, and the A2 fragment is the portion that serves to bind the A1 fragment to the pentameric B-subunit structure. The B-subunit is involved in binding to specific glycolipid receptors on the surface of target cells (148). Globotriaosylceramide (Gb<sub>3</sub>) is the eukaryotic glycolipid cell surface receptor for Stx-1 and Stx-2 (115, 206).

## 4.2 Adhesins

Adhesins are important as virulence factors in that they augment the pathogenicity of *E. coli* O157:H7. These adhesins allow for pathogen binding to intestinal epithelial cells (156). *E. coli* O157:H7 attaches in a localized manner and produces attaching and effacing (A/E) lesions on host cells (156). As they bind, the bacteria trigger intercellular signals through the Type III secretion system (148). The expression of the Type III secretion system is regulated by quorum sensing (183). Proteins such as EspA, EspB, EspD, Tir (translocated intimin receptor) and intimin are involved in the intracellular signal triggering as well as the formation of the A/E lesion (148). EspA forms filamentous structures on the bacterial cell surface that bridge to the host cell surface (113). EspB is delivered into the host cell where in combination with EspD, it forms a host cell membrane pore (113). This allows other effectors (e.g. Tir) access to the host cell (113). Tir functions as the receptor for intimin which is located on the outer surface of *E. coli* O157:H7 cells. Tir-intimin binding subsequently attaches the bacterium to the host cell and triggers localized actin cytoskeleton rearrangement and pedestal formation (113).

### **4.3 Lipopolysaccharide (LPS)**

LPS serves as a third virulence factor that aids in *E. coli* O157:H7 pathogenicity. LPS is an integral part of gram-negative bacterial cell walls and it stimulates a number of immune responses including the production of tumor necrosis factor alpha (TNF- $\alpha$ ) and other inflammatory intermediates (130). It is noteworthy that high levels of circulating antibodies to LPS were observed in 20 out of 22 patients with HUS (17). In addition, increased levels of LPS binding protein were also present in patients with HC and HUS which implied that these patients had an increased acute phase response to LPS (154, 156). However, this does not suggest that Lipid A (endotoxin) is expressed (156). Finally, results from a number of studies indicated that a synergistic effect between Stx and LPS may occur both in vivo and in vitro (8, 90, 120, 156).

### **4.4 Enterohemolysin**

Bacterial enterohemolysins are well established virulence factors and this is also the case for *E. coli* O157:H7. Beutin *et al.* (16) reported that 89% of STEC strains tested showed a hemolytic phenotype different from that of the *E. coli* alpha-hemolysin (Hly). It was subsequently shown that this unique hemolysin was encoded by the 60-Mda “virulence plasmid” pO157 identified from the O157:H7 strain EDL933 (176). This 107 kDa enterohemolysin (EHEC-*hlyA*) produced by the gene *hlyA* is controlled by an operon (EHEC-*hlyCABD*) consisting of four open reading frames. This operon has 60% homology to the *E. coli* alpha-hemolysin operon (*hlyCABD*) (148). Production of this

enterohemolysin has been associated with *E. coli* O157:H7 infections that subsequently developed into HUS. Of 18 isolates from patients with HUS, 16 were enterohemolytic and positive for EHEC-*hlyA* (148). In addition, antibodies to EHEC-Hly were found in 19 of 20 patients that were recovering from O157:H7 STEC-induced HUS. It is not fully understood how EHEC-Hly contributes to the pathogenesis of STEC disease, but it is thought that the hemoglobin released by the action of the hemolysin may provide a source of iron, thereby stimulating growth of STEC in the gut (109). It was discovered that alpha-hemolysin is cytotoxic to endothelial cells and increases superoxide production by rat renal tubular cells (93, 189). The production of a combination of these enterohemolysins may lead to increased toxin production and severe damage to the tissues of the kidney and exacerbate HUS.

#### **4.5 Extracellular Serine Protease**

In addition to enterohemolysin, the pO157 plasmid encodes the putative virulence factor extracellular serine protease EspP (22). The *espP* gene encodes this 104 kDa protein which is capable of cleaving pepsin and human coagulation factor V (148). By these mechanisms it has been suggested that secretion of EspP could result in exacerbation of hemorrhagic disease in the gut (22). Antibodies to this protein were found in 5 of 6 children with STEC infection; however, it is not believed to be a universal virulence factor of STEC as not all *E. coli* O157:H7 strains produce EspP (22, 148).

#### **4.6 Enterotoxin**

To date, the most recently identified O157:H7 virulence factor that contributes to disease severity is enterotoxin EAST1 which is encoded by the *astA* gene (148). This enterotoxin was detected in 100% of 75 different O157:H7 strains tested, and may be responsible for the watery diarrhea noted in early STEC infection (172).

#### **5.0 Pathogenesis of *E. coli* O157:H7 Infection**

Induction of disease by *E. coli* O157:H7 is a complex process in which the preceding virulence factors play a major role. It should be noted that other host and microbe components also play a crucial role in disease initiation as well as in disease severity (148). Ingested organisms pass through the stomach to replicate in large numbers in the intestines. *E. coli* O157:H7 is acid-resistant, and withstands the harsh conditions in the stomach (62). As a consequence, only a relatively low number (as few as 10 organisms) is needed to cause disease (157). The incubation period of STEC infection is approximately 2-8 days with symptoms appearing, on average, after 3-4 days (157). The organisms make their way through the small intestine and typically colonize the lower portion of the small intestine and the colon (152). As indicated previously, *E. coli* O157:H7 attaches to epithelial cells of the intestine by way of adhesins that cause A/E lesions and induce structural changes in the host cell, including loss of microvilli and rearrangement of the structural cytoskeleton components resulting in formation of a pedestal (Figure 1.4) (148).

When the organism has attached and is established in the gut, toxin production increases and the toxin is translocated across the epithelial cells into the bloodstream (113). Although Stx-1 and Stx-2 favor movement from the apical to the basolateral cell surfaces (75), it appears that the mechanisms in which Stx-1 and Stx-2 cross epithelial cells differ. Stx-1 makes its way across cells in a microtubule-dependent manner, whereas Stx-2 is carried across cells independent of microtubules (75). In addition, translocation of Stx-2 is much less efficient than that of Stx-1, and Stx-2 has the ability to translocate across the cells in the opposite manner (e.g. from the basolateral to the apical cell surface) (75).

Once shiga-like toxins have reached the bloodstream, they target multiple cell types that express Gb<sub>3</sub> receptors, including endothelial cells of the colon, kidney, and central nervous system (CNS), as well as epithelial cells of the kidney (34). In addition, shiga-like toxins may also bind to red blood cells (RBCs) through the human P blood group antigens as well as the Gb<sub>3</sub>-related moiety Pk (193). The binding affinity to RBCs is dependent on the binding affinity to surrounding tissues in that when binding affinity to RBCs is high, toxin binding to tissues is diminished, thus protecting Gb<sub>3</sub> expressing tissues (193).

The concentration and nature of the lipid moiety of the Gb<sub>3</sub> receptor on the cell surface influence whether or not the cell is susceptible to the effects of shiga-like toxins (116). For instance, kidney cells express high levels of Gb<sub>3</sub>, especially in the cortical

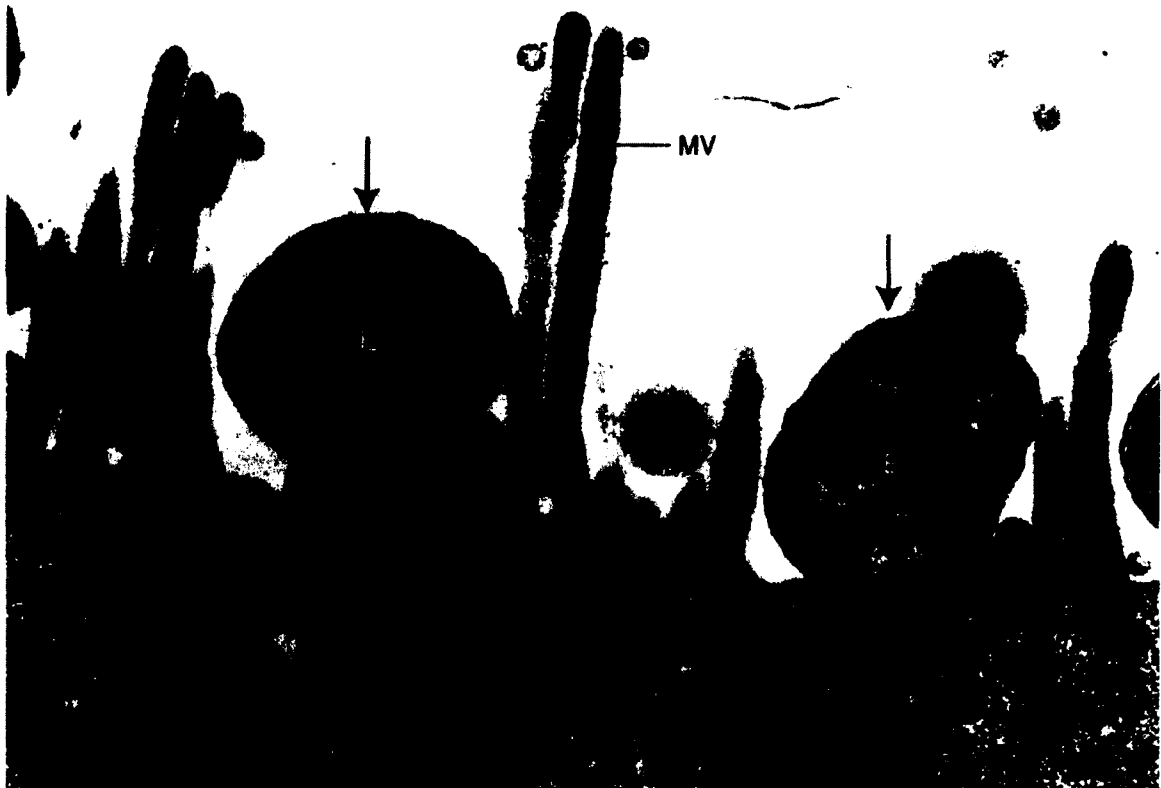


**Figure 1.4: The formation of attaching and effacing (A/E) lesions, caused by *Escherichia coli*.** This image is courtesy of Knutton *et al.* (103). The *E. coli* observed in this electron micrograph is EPEC (strain E2348); however, the mechanism of attachment for EPEC and STEC strains are similar. Bacteria are observed attached to intestinal epithelial cells on cup-like pedestals (represented by the letter E). Microvilli present on the intestinal surface have been disrupted and effaced as a result of the cytoskeletal rearrangements (represented by the letters MV) (21).



region, which is the principal region of lesions in patients with HUS (19). However, the primary cell types that exhibit histopathological lesions in HUS and hemorrhagic colitis as a consequence of exposure to the toxin are the endothelial cells (148). Endothelial cells are 10-fold to 1,000-fold more sensitive to the effects of Stx-2 than Stx-1 (75, 79, 142).

After binding to the Gb<sub>3</sub> receptor of the target cell, the shiga-like toxin triggers a specific, cellular internalization response (Figure 1.5). The entire toxin-glycolipid receptor complex is internalized from clathrin-coated pits, following the endocytotic pathway and, it is presumed, circumvents late endosomes by way of TGN38 (a Golgi-associated protein) (59, 169). The complex is subsequently transported (possibly by way of the endosomal perinuclear recycling compartment (ERC)) from sorting endosomes to the trans-Golgi network (59). Cells that are not sensitive to Stx-1 or Stx-2 internalize the toxin and confine it within lysosomes (169).

Once the toxin has entered the cell it is cleaved by furin (a membrane-bound protease) within the endosome or within the trans-Golgi network (Figure 1.6) (56). Furin recognizes the consensus sequence Arg-X-X-Arg, which is found within the loop region of the toxin between the A1 and A2 fragments of the A-subunit (56). It cleaves the A-subunit and generates a catalytically active 27 kDa N-terminal A1 fragment and a 4 kDa C-terminal A2 fragment (148). The disulfide bond between the fragments is reduced and the enzymatically active portion of the A-subunit is transported in a retrograde fashion to the endoplasmic reticulum (ER) and eventually to the cytosol (80, 191). It is possible that the A1 fragment plays a role in this transportation by directing insertion of a signal

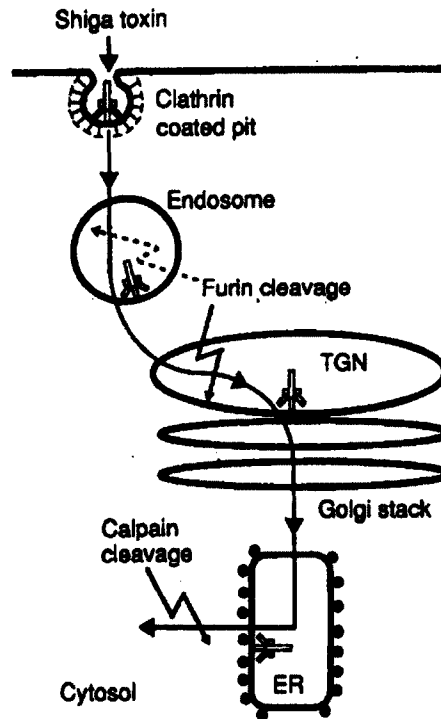


**Figure 1.5: Pathogenesis of Shiga toxin binding to cells with Gb3 receptors.** Diagram is courtesy of Sandvig *et al.* (169). The toxin is internalized by a clathrin coated pit-dependent process, cleaved by furin, and transported to the trans Golgi network, endoplasmic reticulum and eventually the cytosol.

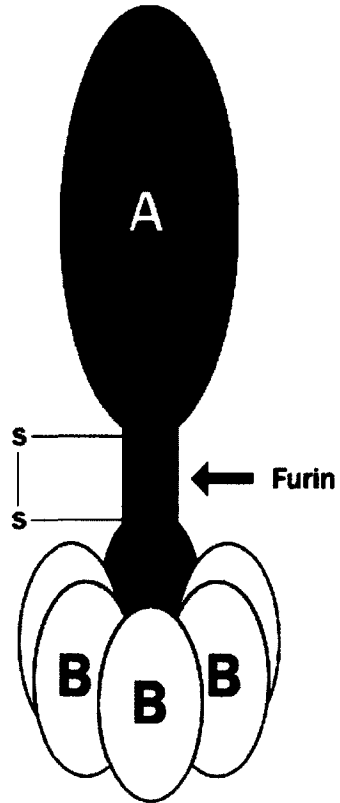


**Figure 1.6: Furin cleavage site of Stx-1 and Stx-2.** Drawing is adapted from Sandvig *et al.* (170).

sequence-like hydrophobic domain at the C-terminus into the endoplasmic reticulum membrane (167). The A1 fragment is responsible for death of the cell by way of RNA N-glycosidase activity (47,141). It inactivates the 60S ribosomal unit by cleaving the N-glycosidic bond at A-4324 in 28S ribosomal RNA (47). This inhibits elongation-factor 1 dependent binding of aminoacyl-tRNA to ribosomes and interferes with protein synthesis within the cell, impeding peptide chain elongation, and results in necrosis of the cell (47).

## **6.0 Host Response to *E. coli* O157:H7 Infection**

It is possible that not all cells exposed to toxin die from RNA N-glycosidase-related necrosis. Patients with hemorrhagic colitis and HUS have significant tissue damage which generates an inflammatory response through leukocyte activation and cytokine production and further exacerbates damage in the affected area (156). Neutrophils, macrophages, cytokines, and chemokines play an important role in the pathogenesis of disease and development of HUS (Figure 1.7) (156).

Neutrophils are the first line of cellular defense in the human's host immune system. As many as  $5 \times 10^{10}$  cells are released from the bone marrow each day (28). This number is necessary in order to maintain a sufficient level to protect against infection (28). The main reason why so many cells are required is due to their short half-life (28). In the circulation, neutrophils are constitutively undergoing apoptosis with an estimated half-life of 6 to 18 hours (3, 67, 173, 213). However, once neutrophils have crossed into the tissues they can survive for longer periods depending upon the environmental factors

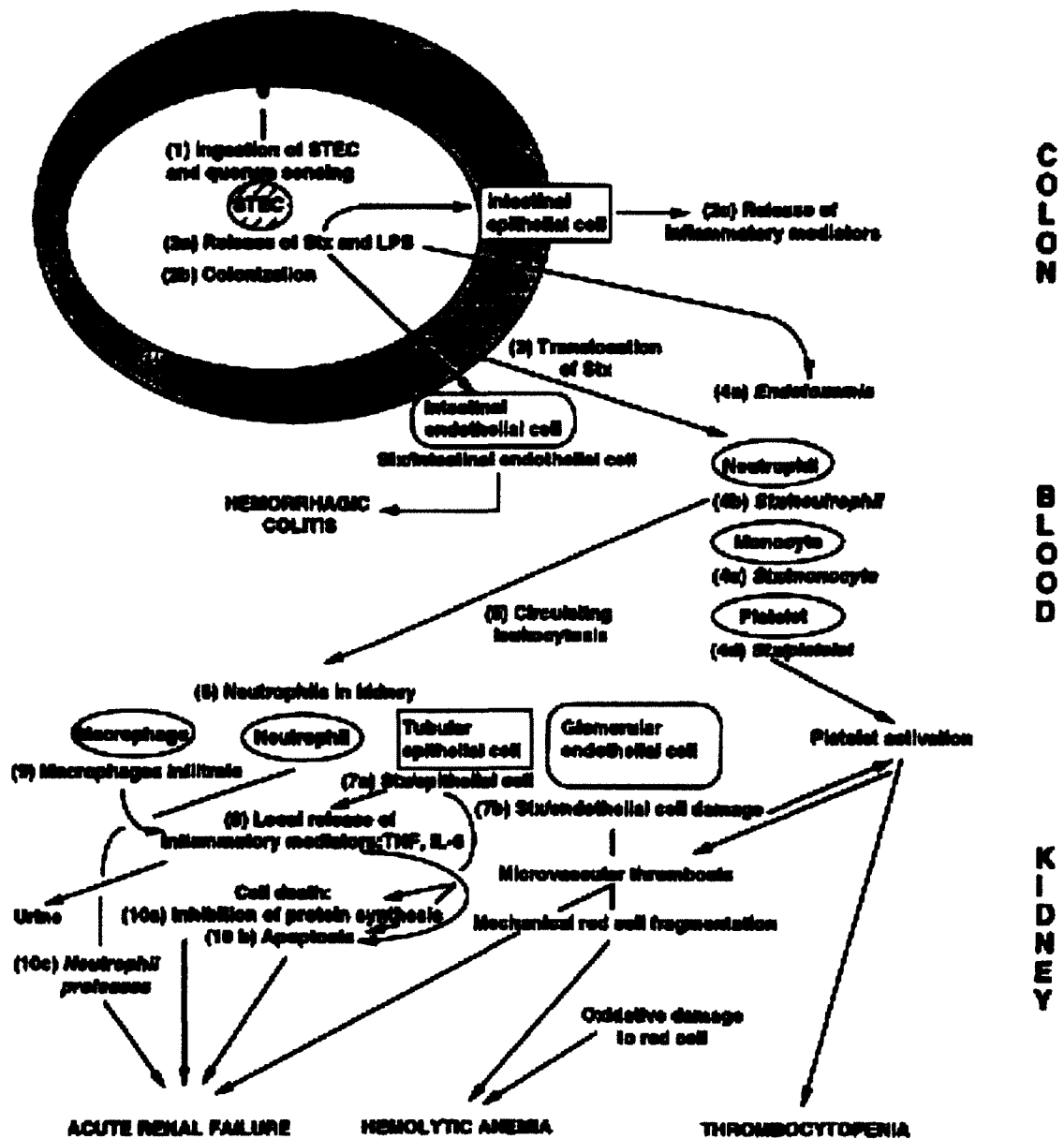


**Figure 1.7: Hypothetical sequence of events of *E. coli* O157:H7 infection from ingestion to the development of HUS.** Diagram is courtesy of Proulx *et al.* (156). The order of events is labeled numerically from 1-10. Events that may occur simultaneously are sub-bulleted by letter (e.g. 4a, 4b, etc...). Hypothesis for which data are not known or pending are shown in italics.

surrounding them (28). For instance, neutrophils can be kept alive longer by exposure to cytokines such as IL-1 $\beta$ , IL-2, IL-4, IL-15, INF- $\gamma$ , G-CSF, and GM-CSF as well as to LPS. The effect of this is to decrease their normal rate of apoptosis (20, 38, 60, 61, 102, 128, 149). Apoptotic neutrophils are incapable of normal function and will not elicit cellular responses such as chemotaxis, degranulation, adherence, phagocytosis, and the respiratory burst (28, 66, 186). In addition, cell surface receptor expression is decreased by way of either receptor shedding or internalization.

TNF- $\alpha$  can have varying effects on neutrophils depending upon where in the host the neutrophils reside. In the circulation neutrophils are more likely to undergo apoptosis when exposed to TNF-  $\alpha$  whereas apoptosis in neutrophils exposed to TNF-  $\alpha$  in tissues will be delayed. This may be due to the ability of TNF- $\alpha$  to activate a cell death caspase-activating pathway or a cell survival nuclear factor kappa B (NF- $\kappa$ B)-activating pathway (28).

The NF- $\kappa$ B pathway may be an important pathway for the control of neutrophil apoptosis (28). NF- $\kappa$ B is a transcription factor that is a central regulator of the inflammatory and immune process. It occurs as a dimer and the constituent proteins are part of the NF- $\kappa$ B /Rel family. These proteins have the ability to bind DNA through the conserved Rel homology domain, which is also required for homo- and hetero-dimerization. The role of the NF- $\kappa$ B pathway has been examined and results indicate that there is evidence to suggest that the NF- $\kappa$ B pathway does play a protective role in both spontaneous and modulated neutrophil apoptosis (45, 134, 135, 212, 214).

TNF- $\alpha$  induced NF- $\kappa$ B is more potent in the neutrophils from newborns relative to neutrophils from adults and it correlates well with the elevated IL-8 production reported in neonatal neutrophils (148). This may be important to the pathology of *E. coli* O157:H7 infection, as infants are more susceptible to the complications of HUS than are adults.

Increased circulating numbers of both neutrophils and macrophages have been associated with the severity of renal failure during HUS (156). In addition, increased numbers of neutrophils and macrophages in the glomeruli of the kidneys have been observed in children with HUS (77, 203). Leukocytosis (increased number of white blood cells) in the circulation is commonly associated with children that have HUS and is also identified as an independent risk factor for developing HUS (12, 23, 37, 49, 50, 52, 74, 122, 127, 168, 208, 218). Circulating neutrophils activated in HUS patients can be demonstrated by the increased elastase levels observed in the blood (49, 50, 52, 74). In addition, levels of granulocyte colony-stimulating factor and IL-8 have been reported in children with HUS and IL-8 levels correlated with white blood cell counts (50, 205). These neutrophils also have a higher ability to adhere to cultured human endothelium and induce injury by breaking down endothelial fibronectin (52). Stx-1 has the ability to bind to a non-Gb<sub>3</sub> receptor on human neutrophils, and in the presence of endothelial cells will relocate from the neutrophil to the endothelial cell (194). This suggests that neutrophils may also serve as an additional transport mechanism for the toxin from the intestines to the kidney (194). In addition to neutrophils, monocytes may play a role in pathogenesis by binding Stx and subsequently secreting a number of other inflammatory mediators

including TNF- $\alpha$ , IL-1 $\beta$ , IL-6, and IL-8 independent of the effects of LPS (204).

Not only do the cells of the immune system play a role in the pathogenesis of *E. coli* O157:H7, but other inflammatory mediators also have a significant effect. Interleukins, chemokines, growth factors, acute phase response proteins, and soluble adhesion molecules can all contribute to the host inflammatory response to infection (156). Patients with HUS have presented with higher levels of pro- (IL-8 and IL-6) and anti- (IL-10 and IL-1 receptor antagonist) inflammatory chemokines than those without, and these levels have been correlated to the severity of renal failure (117, 155). In addition, shiga-like toxins may induce IL-8 secretion from intestinal epithelial cells (197, 223). It appears that not all immune system cell types are involved in response to *E. coli* O157:H7 infection. Lymphokines such as IL-2, IL-4, and IL-13 were not detected in patients presenting with HC or HUS, and only low levels of interferon- $\gamma$  were detected. This infers that T-cells are not part of the host immune response (156).

## **7.0 Mechanisms of Eukaryotic Cell Death**

The two main pathways that cells follow to undergo cell death are necrosis and apoptosis. There are distinct differences between these mechanisms of cell death. A necrotic cell has undergone oncosis which is characterized by karyolysis (dissolution of the nucleus) due to DNase activity and by expansion of the cell eventually leading to leakage of the outer membrane (46). In general, necrosis is a “messy” process and will invoke an inflammatory immune response due to the contents of the cell leaking into the



extracellular matrix. In contrast, when a cell undergoes apoptosis it shrinks in size, the cytoplasm becomes denser and the organelles tightly packed, the chromatin condenses and marginalizes (pyknosis), the DNA-containing nucleus becomes fragmented (karyorrhexis), and cell fragments are separated into apoptotic bodies (“budding”) (108, 226). The apoptotic bodies are then phagocytosed by macrophages or other similarly functioning immune cells and degraded within the phagolysosome (46). Apoptosis does not elicit an immune response. This is because cellular contents are not released into the surrounding extracellular matrix, the apoptotic bodies are quickly phagocytosed after being released from the cell and the macrophages do not produce cytokines (46). This could be a beneficial way of increasing pathogenicity without the disadvantages associated with a local immune-mediated response.

Apoptosis is commonly referred to as “programmed cell death” (46). There are a number of possibilities as to why a cell may undergo apoptosis: it occurs normally during development and aging; as a homeostatic mechanism to maintain cell populations; and as a defense mechanism when cells are damaged by disease or noxious agents (136). As a result there are many stimuli and conditions that may trigger apoptosis, but the cellular response to these triggers will vary depending on the cell type (46). Apoptosis is a complicated process, and the activity of many genes influence the likelihood of a cell activating its self-destruction program (68).

The process of apoptosis is mediated by a family of proteins known as the Bcl-2 protein family. Approximately 15 proteins and 25 genes have been identified as members of the Bcl-2 family in mammalian cells (32, 39, 40, 185, 224). These proteins are

classified into two functional roles: pro-survival and pro-apoptosis; and are divided into three subfamilies: the Bcl-2 subfamily, the Bax subfamily, and the BH3 subfamily (2). The Bcl-2 subfamily promotes cell survival while the Bax and BH3 subfamilies promote apoptosis (2). Examples of proteins that belong to each subfamily are listed in Table 1.2.

All of these proteins share at least one of four possible conserved motifs (BH1, BH2, BH3 and BH4) known as Bcl-2 homology domains which are critical to the function of the proteins, and most pro-survival proteins (those that inhibit apoptosis) contain at least the BH1 and BH2 domains (2). The proteins closest in resemblance to Bcl-2 contain all four homology domains (2). Alternatively, the Bax and BH3 subfamilies (pro-apoptotic) differ in their homology domain content despite their shared cellular role (95). The Bax subfamily contains BH1, BH2 and BH3 domains and more closely resemble Bcl-2, whereas the BH3 subfamily contain only the BH3 domain (2). Both pro-survival and pro-apoptosis proteins have the ability to form homodimers and heterodimers with each other, thereby keeping themselves in balance or check. This suggests that the concentration of the proteins may be important in the outcome of the cell's fate (144). It is known that the BH1, BH2, and BH3 domains strongly influence the formation of homodimers and heterodimers, and that these regions create an elongated hydrophobic cleft to which a BH3 amphipathic alpha helix can bind (129, 171).

Heterodimerization is not required for pro-survival function, but is required for the pro-apoptosis functions of the BH3 subfamily, and it may also play a role in apoptosis in the

**Table 1.2: The Bcl-2 Protein Family**

<b>Subfamily Name</b>	<b>Function</b>	<b>Protein Members</b>
Bcl-2	Pro-survival	Bcl-2, Bcl-X <sub>L</sub> , Bcl-w, Mcl-1, A1
Bax	Pro-death	Bax, Bak, Bok
BH3	Death domain	Bik, Blk, Hrk, BNIP3, Bim, Bad, Bid

Bax subfamily (36, 95). It is noted that there may be a preference in which proteins bind, as not all pro-apoptosis and pro-survival proteins interact (2).

Apoptosis is regulated through three main pathways: the extrinsic or death receptor pathway; the intrinsic or mitochondrial pathway; and the perforin/granzyme pathway (either through granzyme A or granzyme B) (Figure 1.8) (46). The extrinsic, intrinsic, and granzyme B pathways converge into a common downstream execution pathway, which results in cellular changes commonly associated with apoptosis. Research suggests that the apoptotic pathways are linked and molecules from one pathway can interact and influence the other (76). In contrast, the Granzyme A pathway results in direct DNA cleavage (46).

The extrinsic pathway is triggered by transmembrane receptor-mediated interactions (46). When a trimeric ligand comes in contact with the surface of the cell, death receptors trimerize and bind to the ligand (119). This activates adapter proteins which in turn are recruited to the cellular membrane and bind to the death receptors (72, 207). The adapter proteins subsequently associate with procaspase-8 (the inactive form of caspase-8), form a death-inducing signaling complex (DISC), and activate procaspase-8 to form caspase-8 (101). Once caspase-8 is activated, the execution pathway is set in motion. The extrinsic pathway can be inhibited by alternative proteins which bind to adapter proteins and caspase-8, rendering them ineffective and therefore stopping the execution pathway from being set in motion (92, 174).

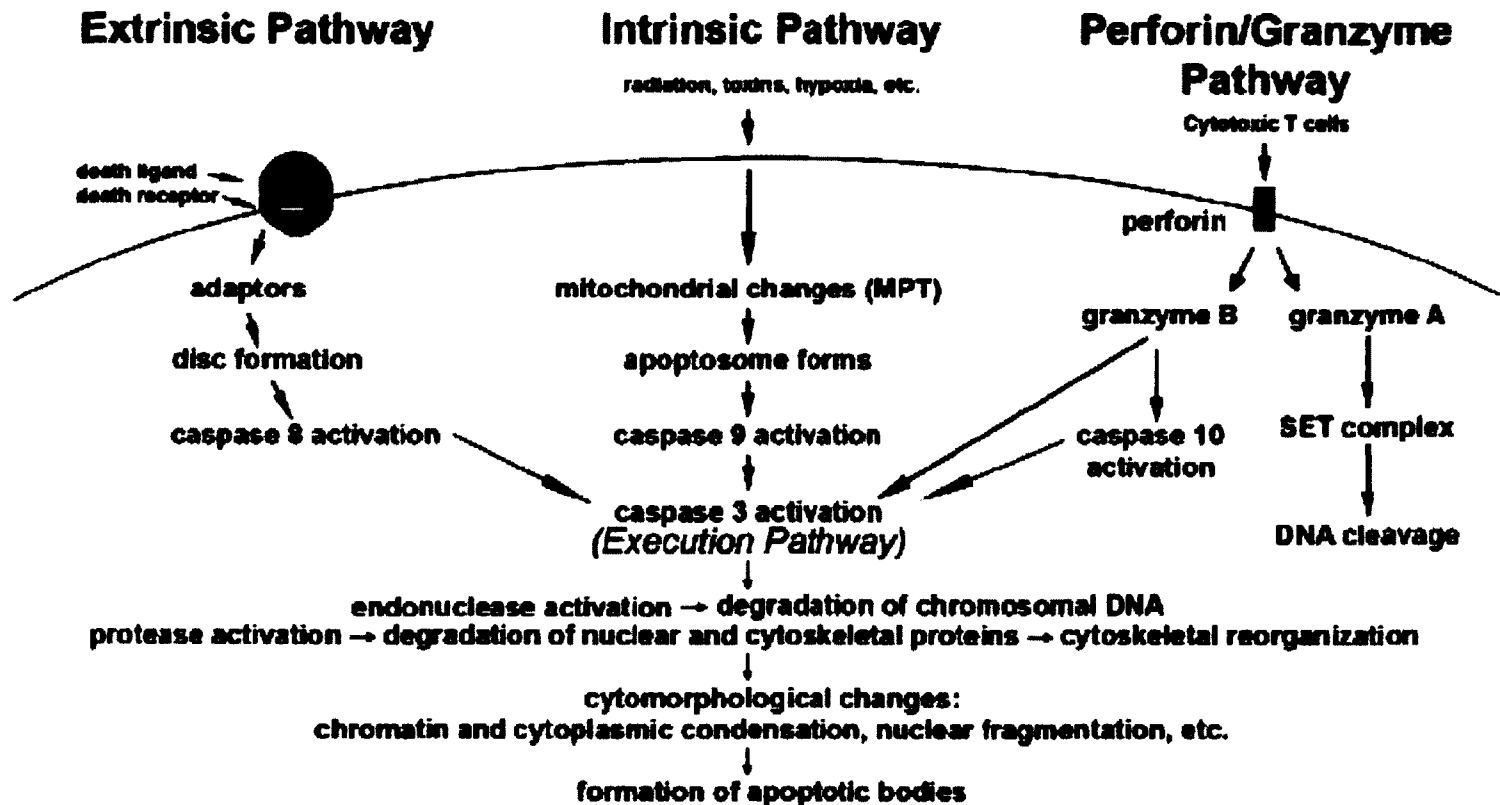


**Figure 1.8: The three main pathways of apoptosis: extrinsic, intrinsic and perforin/granzyme.** Diagram is courtesy of Elmore *et al.* (46). Each pathway activates an initiator caspase (8, 9, and 10 respectively) which in turn activates a common downstream executioner caspase-3. Note that Granzyme A has a unique pathway that is caspase-independent.

The perforin/granzyme pathway is triggered by T-cell mediated cytotoxicity. Perforin (a transmembrane pore-forming molecule) is secreted and forms pores within the target cell (198). Cytoplasmic granules are subsequently released from the T-cell into the target cell through this newly formed pore (198). These granules contain either granzyme A or granzyme B which are both known serine proteases (146).

Granzyme A activates a caspase-independent pathway (46). Once it is released into the cell, the SET complex (responsible for suppressing DNase expression and protecting DNA and chromatin structure) is cleaved (114). This results in active expression of DNase which leads to DNA nicking and apoptotic DNA degradation and thus blocks maintenance of DNA and chromatin structure integrity (46).

Granzyme B cleaves proteins at aspartate residues, and it is through this function that procaspase-10 is activated to form caspase-10 (46). Once activated, caspase-10 sets the execution pathway in motion. Granzyme B also has several other functions including the cleavage of apoptotic inhibiting factors such as inhibitor of caspase activated DNase (ICAD) (166). In addition, research has shown that Granzyme B can also use the intrinsic pathway in two other ways; by cleaving Bid which causes cytochrome C release from the mitochondria; and by directly activating caspase-3, thereby eliminating the upstream signaling pathways and setting the execution pathway into motion (9, 164).

The intrinsic pathway is triggered by a number of stimuli. These stimuli act directly on targets within the cell and are always mitochondrial-initiated events (46).

Intracellular signals are activated within the cell and cause changes within the inner mitochondrial membrane (46). Mitochondrial permeability transition (MPT) pores are opened and allow the release of two main groups of pro-apoptotic proteins into the cytosol that function in both the intrinsic and the execution pathways (165). The first group consists of cytochrome c, Smac/DIABLO, and a serine protease Htr2A/Omi, all of which are responsible for activating a caspase-dependent mitochondrial pathway where Cytochrome c binds with Apaf-1 and Procaspase-9 to form active Caspase-9 (24, 44, 57, 202). Caspase-9 or the other “initiator” caspases (caspase-8 or caspase-10) will activate caspase-3 and set the execution pathway into motion.

The execution pathway is the final pathway for apoptosis regardless of the initiation pathway type (intrinsic, extrinsic or perforin/granzyme) (46). The “executioner” caspases (caspase-3, caspase-6 and caspase-7) activate cytoplasmic endonuclease and proteases which degrade nuclear and cytoskeletal materials and proteins such as PARP, cytokeratins, alpha fodrin (a plasma membrane cytoskeletal protein), and NuMA (nuclear protein). This results in the classic morphological changes observed in apoptosis (182). In particular, Smac/DIABLO and Htr2A/Omi are responsible for preventing the activity of inhibitors of apoptosis proteins (IAP) thereby increasing the effectiveness of the pro-apoptotic response (175, 202). A second group of proteins consisting of apoptosis inducing factor (AIF), endonuclease G, and caspase-activated DNase (CAD) is also released from the mitochondria, but only in the late stages of apoptosis after cells are committed to die, and act in a caspase-independent manner (with the exception of CAD) (46). AIF translocates to the nucleus where it fragments DNA and condenses peripheral

nuclear chromatin (85). Endonuclease G is also translocated to the nucleus, and it cleaves nuclear chromatin to produce oligonucleosomal DNA fragments (112). CAD functions similarly to AIF and endonuclease G after it is translocated to the nucleus; however, it does not function until it is cleaved by caspase-3 (166). Once cleavage has occurred, CAD causes DNA fragmentation, resulting in a more pronounced (Stage II) chromatin condensation (188). In addition, Gelsolin (an actin binding protein) is cleaved by activated caspase-3 and will subsequently cleave actin filaments in a calcium-independent manner leading to cytoskeletal, intracellular transport, cell division and signal transport disruption (105).

The mechanisms of how Stx affects these cell death pathways are unclear. Toxins typically trigger apoptosis through the intrinsic pathway (46), and previous studies have shown that an interaction occurs between Stx-2 and Bcl-2 (190). The goal of this research is to confirm Stx-2 and Bcl-2 protein interactions and further examine the interactions of Stx-2 with other members of the Bcl-2 protein family in order to propose a mechanism of action. The protein interactions will be observed in cell types that are associated with the pathogenesis of HUS; human intestinal epithelial cells and neutrophils. Elucidating the mechanisms of Stx-2 action in programmed cell death can lead to a better understanding of *E. coli* O157:H7 pathogenesis and open new avenues for treatment and potential vaccines in humans.



## CHAPTER 2

### PROTEIN-PROTEIN INTERACTIONS BETWEEN SHIGA-LIKE TOXINS AND THE BCL-2 PROTEIN FAMILY

#### 1.0 **Abstract**

Data from previous studies by Suzuki *et al.* (190) indicated that Stx-2 but not Stx-1 interacts with the pentameric sequence, NWGRI within the BH1 domain (a highly conserved region) on the anti-apoptotic protein, Bcl-2 (residues 143 to 147). This interaction induces target cell death as a consequence of caspase-3 activation (190). Stx-2 contains this same sequence (residues 223-227) (190) as do other members of the Bcl-2 protein family. This may indicate that Stx-2 binds to other Bcl-2 family proteins. It is hypothesized that Stx-2 interacts with the Bcl-2 family of proteins via this NWGRI amino acid motif. If true, Stx-2 should interact with Bcl-2, Bcl-X<sub>L</sub>, Mcl-1, A1, Bax, and Bak. In order to test this hypothesis, Stx-2 was purified from *E. coli* O157:H7 strain 90-2380 and the interaction of the toxin with the various members of the Bcl-2 family of proteins isolated from Caco-2 cells was determined. The cytotoxicity of Stx-2 towards Caco-2 cells was investigated. Next, proteins produced by Caco-2 cells were examined by western blot analysis to identify the Bcl-2 family of proteins and interactions with Stx-2 were assessed by far western blot analysis and co-immunoprecipitation. Data indicated that the methods utilized did not show clear evidence that protein interactions occurred

using caco-2 cells as a model system.

## **2.0 Introduction**

Suzuki *et al.* showed that Stx-2 but not Stx-1 interacts with Bcl-2, an anti-apoptotic protein, via a pentameric amino acid sequence NWGRI located at residues 143 to 147, and this resulted in caspase-3 activated cell death (190). More precisely, this interaction occurs within the BH1 domain (residues 136 to 155) of Bcl-2 (190) which is highly conserved and critical for pro-survival protein function (180, 225). This same sequence, NWGRI, is also found on Stx-2 at residues 223-227 (190). On Stx-1 the sequence differs by one amino acid (NWGRL) and is found at residues 234-238 (190).

Evidence suggests that the ratio of anti- to pro-apoptotic proteins determines the sensitivity of a target cell to an apoptotic stimulus by mediating mitochondrial cytochrome c release (84). Therefore, it is postulated that Stx-1 and Stx-2 directly interact with these proteins and act to disrupt the equilibrium between the anti-apoptotic and pro-apoptotic members of the Bcl-2 family, thereby enhancing caspase activation and apoptosis within the cell. It is also hypothesized that since the NWGRI sequence is present on more than one type of anti-apoptotic protein, it may offer explanation as to why Stx-2 displays higher virulence during the course of disease than does Stx-1. It is also possible that Stx-2 may mimic the acceptor surface of Bcl-2 and bind either Bcl-2 or Bax depending upon its affinity for either protein. The interaction of these proteins was

investigated at the molecular level in order to determine their role in Stx-triggered apoptosis of host cells.

A study performed by Zhang *et al.* (227) reported that two distinct binding surfaces play a role in homodimerization and heterodimerization of the Bcl-2 family of host-cell proteins (227). The two surfaces, known as the “acceptor surface” and the “donor surface”, are oriented at approximately 90° to each other on the Bcl-2 protein (227). The acceptor surface has the ability to bind Bcl-2 molecules as well as Bax, while the donor surface binds only Bcl-2 (227). In healthy cells, Bax primarily resides in the cytosol of the cell and does not form dimers (227). When apoptotic stimuli occur, Bax is switched to an active conformation and is translocated to the mitochondria and endoplasmic reticulum (227). At these locations, Bax forms homo-oligomers or heterodimers with other Bcl-2 family members at the acceptor surface (227). It should be noted that the glycine at position 145 in the middle of the acceptor surface is located within the middle of the NWGRI pentameric sequence, which is the same sequence also observed in Stx-2. When this glycine in Bcl-2 was mutated to alanine, heterodimerization but not homodimerization was abolished at the acceptor surface (227). This may indicate that the NWGRI sequence was important in establishing the ratio of dimerization between anti- and pro-apoptotic proteins, and thus determines the sensitivity of a target cell to apoptotic stimuli (84). It is possible that Stx-2 may mimic this acceptor surface and bind to either Bcl-2 or Bax depending upon its affinity for either protein.

### **3.0 Hypothesis**

Extrapolating from the studies by Suzuki *et al.* (190) and Zhang *et al.* (227), it is hypothesized that Stx-1 and Stx-2 interact with the Bcl-2 family of proteins via the NWGRL or NWGRI amino acid motifs. If true, then Stx-2 should interact with Bcl-2, Bcl-X<sub>L</sub>, Mcl-1, A1, Bax, and Bak based upon its pentameric sequence (NWGRI).

### **4.0 Materials and Methods**

The bacterial strains, toxins they produce and their origins together with all media and reagent composition and preparation instructions are located in Appendix A. Authorization to complete these experiments was obtained from the Institutional Review Board for the Protection of Human Subjects In Research (IRB) under approval number 3679 (Appendix C).

#### **4.1 Stx Protein Sequence Analysis**

An analysis of Stx-1 and Stx-2 protein structures was made using ClustalX to compare these with the members of the Bcl-2 family of proteins. The purpose of this analysis was to determine if any sequence similarity was observed in other Bcl-2 family members with the NWGRI sequence, located in a highly conserved region of Bcl-2.

## 4.2 **Purification of Stx-2 from *Escherichia coli* O157:H7 strain 90-2380**

*E. coli* O157:H7 strain 90-2380 was inoculated into Luria Burtani (LB) Broth and allowed to grow overnight at 37°C with shaking. The following day, the culture was aliquoted into sterile 100x15mm Petri dishes (10mL per dish). The lids were removed, and the culture was exposed to ultraviolet (UV) light in a biosafety cabinet for 30 minutes. Subsequent to UV exposure, the dishes were transferred to a 37°C incubator and allowed to incubate for an additional 48 hours. Following incubation, the culture was pooled, centrifuged at 16,000 x g for 15 minutes at 4°C, and supernatant collected and sterile filtered using Acrodisc 0.45µm low protein-binding membranes (Pall Corp, Port Washington, NY). Ammonium sulfate precipitation was used to precipitate the toxin. Initially, ammonium sulfate was slowly added to the supernatant until the concentration reached 40% (w/v). The suspension was centrifuged and the supernatant was transferred to a new beaker. The ammonium sulfate concentration was increased to 70%, and centrifuged again. The pellet was resuspended in 15mL distilled water and dialyzed in 10mM Tris pH 7.4 for 48 hours with a 30 kDa molecular weight cut-off dialysis membrane (pre-soaked in 2% sodium bicarbonate, 1mM EDTA dialysis membrane preparation buffer at 60°C for 15 minutes).

Once dialysis was complete, the sample was concentrated using a Centricon 50 (Millipore Corp, Bedford, MA) with a 50 kDa molecular weight cut-off membrane. Then, to obtain higher purification and eliminate large proteins, the toxin was processed through a Centricon 100 (Millipore Corp) with a 100 kDa molecular weight cut-off

membrane, the filtrate was collected, and a final concentration was performed using a Centricon 50 filter unit.

### **4.3 Stx-2 Characterization**

#### **4.3.1 Native Analysis of Semi-Purified Stx-2**

Sterile-filtered supernatants from *E. coli* O157:H7 strain 90-2380 were analyzed to assess overall protein content by native gel electrophoresis. Semi-purified Stx-2 was analyzed to determine overall purity and the effectiveness of the purification method outlined in section 4.2 (page 39-40). All samples were combined with 5x sample loading buffer (5:1 ratio), loaded onto two identical 6% stacking / 12% resolving gels, and placed in a buffer tank containing native running buffer. A total of 4 gels was run at 120V for approximately 1 h, 2 of these were used to assess the purity of the sterile-filtered supernatants, and 2 to determine the purity of the semi-purified Stx-2.

Three gels were placed in Coomassie blue for at least 2 h to stain the proteins in the gel. The gels were then placed in the destaining buffer described in Appendix A, section 4.18 until the background was no longer blue, and visible protein bands were observed.

One gel was aligned onto a polyvinylidene fluoride (PVDF) membrane (Millipore Corp), and placed into a transfer sandwich consisting of fiber pads and filter paper

(Figure 2.1). The transfer sandwich was placed into a buffer tank containing Tris-Glycine buffer (Appendix A, 4.19) and proteins were transferred at 60V for 4-5 h. After transfer, the membrane was “blocked” overnight in Tris Buffered Saline containing 5% dehydrated skim milk (Appendix A, 4.20) at 4°C. On the following day, the membrane was incubated for 2 h at room temperature with 10µg/mL of primary antibody, STX2-11E10 (Toxin Technology, Sarasota, FL) raised in mice against Stx-2. Membranes were then rinsed 3x in Tris Buffered Saline containing 0.05% Tween (TTBS) (Appendix A, 4.22) for 10 min at room temperature, and subsequently treated with anti-mouse alkaline phosphatase-conjugated secondary antibody (Sigma-Aldrich, St. Louis, MO) for 2 h at room temperature. After the secondary antibody incubation, the membrane was rinsed twice in TTBS followed by one rinse in TBS for 10 min at room temperature. The blot was developed with Nitro-Blue Tetrazolium Chloride / 5-Bromo-4-Chloro-3'-Indolyphosphate p-Toluidine Salt (NBT/BCIP) tablets (Roche Diagnostics, Indianapolis, IN).

#### **4.3.2 SDS-PAGE Analysis of Semi-Purified Stx-2**

Semi-purified Stx-2 was analyzed to detect the toxin in the sample by sodium dodecyl sulfate polyacrylamide gel electrophoresis (SDS-PAGE). Samples were diluted 1:2 in sample preparation buffer (Appendix A, 4.13), boiled at 95°C for 5 min, loaded onto a 6% stacking / 12% resolving gel (Appendix A, 4.16), placed in a buffer tank containing SDS-PAGE running buffer (Appendix A, 4.14), and run at 180V for 30-40 min. The gel was removed and stained in Coomassie blue (Appendix A, 4.17) for at

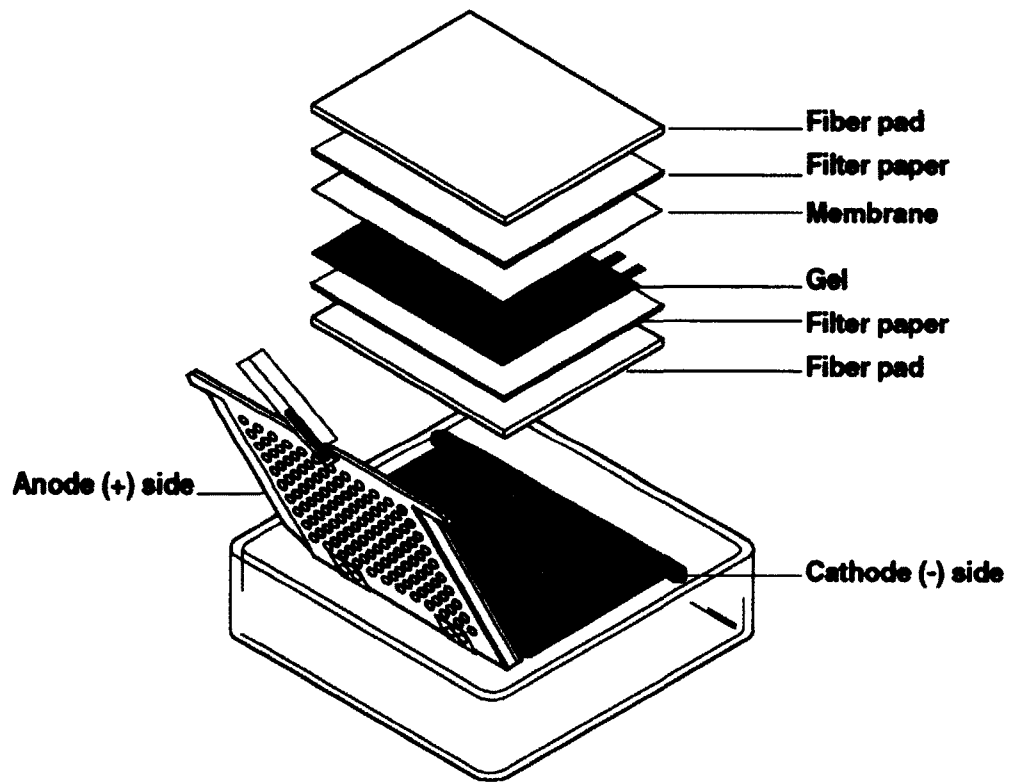


**Figure 2.1:** Western Blot Transfer Sandwich Assembly. Diagram is courtesy of Bio-Rad Trans-Blot Electrophoretic Transfer Cell Instruction Manual.



least 2 h. After staining, the gel was added to a destain buffer (Appendix A, 4.18) until the background was no longer blue, and protein bands were visible.

### **4.3.3 Western Blot Analysis of Semi-Purified Stx-2**

Triplicate samples were diluted 1:2 in sample preparation buffer, boiled at 95°C for 5 min, loaded onto a 6% stacking / 12% resolving gel, placed in a buffer tank containing SDS-PAGE running buffer, and run at 180V for 30-40 min. One set of samples was added to Coomassie blue for at least 2 h and then destained with destain buffer. The remaining samples were each divided into two separate gels and aligned on polyvinylidene fluoride (PVDF) membranes (Millipore Corp), and placed in a transfer sandwich (Figure 2.1) consisting of fiber pads and filter paper. The transfer sandwich was placed in a buffer tank containing Tris-glycine buffer (TGB) and the proteins transferred at 60V for 4-5 h. After transfer, the membranes were blocked overnight in TBS containing 5% dehydrated skim milk at 4°C. On the following day, one membrane was incubated for 2 h at room temperature with 10µg/mL STX2-11E10 (Toxin Technology) while the other remained in blocking buffer as a negative control. Both membranes were rinsed 3x in TTBS for 10 min at room temperature, and subsequently treated with anti-mouse alkaline phosphatase-conjugated antibody (Sigma-Aldrich) for 2 h at room temperature. The membranes were rinsed twice in TTBS followed by one rinse in TBS for 10 min at room temperature. The blots were developed with nitro-blue tetrazolium chloride / 5-bromo-4-chloro-3'-indolyphosphate p-toluidine Salt (NBT/BCIP) tablets (Roche Diagnostics).

#### **4.3.4 Cleavage Analysis of Semi-Purified Stx-2 and A1 Fragment Generation**

Semi-purified Stx-2 was analyzed to ensure that cleavage at the Arg-X-X-Arg consensus sequence would occur during subsequent experimentation in mammalian cells, and to obtain a semi-pure suspension of toxin containing the A1 fragment that is generated after cleavage. This was performed by mimicking the natural cleavage of furin with trypsin. Five  $\mu\text{L}$  of trypsin was added to 0.5mL of semi-pure Stx-2, vortexed briefly and incubated at room temperature for 2 min. PMSF (2.5 $\mu\text{L}$ ) and 1 $\mu\text{L}$  of beta mercaptoethanol was subsequently added to the solution to deactivate the enzyme and ensure the disulfide bond was broken.

The preparation was analyzed by SDS-PAGE to determine if cleavage had been successful. Samples were analyzed on a 6% stacking / 12% resolving gel. Ten  $\mu\text{L}$  of each sample were diluted 1:2 in sample preparation buffer. The samples were boiled at 95°C for 5 min, loaded onto the gel, placed in a buffer tank containing SDS-PAGE running buffer, and run at 180V for approximately 45 min. The gel was removed and placed in Coomassie blue for at least 2 h. After staining was complete, the gel was placed in destain buffer until the background was no longer blue, and protein bands were observed.

In addition a Western blot was performed to confirm that the A1 fragment was generated in the trypsin-treated toxin sample. A gel was prepared and run as described above and the trypsin-treated toxin and untreated toxin samples were loaded onto the gel in triplicate. Once the gel was electrophoresed, it was cut into thirds. One third was

placed in Coomassie blue to stain while the remaining two samples of the gel were prepared for a Western blot. The gels were aligned onto PVDF membranes (Millipore Corp), and placed into a transfer sandwich consisting of fiber pads and filter paper. The transfer sandwich was placed in a buffer tank containing TGB and proteins were transferred at 60V for 4-5 h. After transfer, the membranes were blocked overnight at 4°C in TBS containing 5% dehydrated skim milk. On the following day, one membrane was incubated for 2 h at room temperature with 10µg/mL STX2-11E10 (Toxin Technology) and the other remained in blocking buffer as a negative control. The membranes were rinsed 3x in TTBS for 10 min at room temperature, and subsequently treated with anti-mouse alkaline phosphatase-conjugated antibody (Sigma-Aldrich) for 2 h at room temperature. The membranes were rinsed twice in TTBS followed by one rinse in TBS for 10 min at room temperature. The blots were developed with NBT/BCIP tablets (Roche Diagnostics).

#### **4.3.5 Biological Activity Verification of Semi-Purified Stx-2**

In order to verify that the toxin preparation was biologically active after the purification procedure, African green monkey kidney (Vero) cells were exposed to the semi-purified preparation. Vero cells were grown to confluency in two 25cm<sup>2</sup> tissue culture flasks (one to serve as a toxin assay and the second as a control). Semi-purified Stx-2 (50µL) was added to the test flask. The test and control flasks were incubated at 37°C in 5% CO<sub>2</sub> for 96 h. Each flask was observed at 100x total magnification by inverted phase-contrast microscopy to look for the presence of rounded, refractile or

floating cells (indicating toxin activity). Following microscopic examination of the flasks, the media was removed and 1mL of crystal violet was added for 5 min. Monolayers in the flasks were then gently rinsed with distilled water and allowed to air dry.

#### **4.3.6 Quantitation of Semi-Purified Stx-2**

The total protein concentration of the semi-purified Stx-2 preparation was measured using the Bradford assay. A standard curve was set up in duplicate with bovine serum albumin (BSA) (1mg/mL) and the following amounts were added per well: 0, 2, 4, 8, 10, 15, and 20 $\mu$ L. The test samples were prepared by adding 1 $\mu$ L of semi-purified toxin sample to each of 6 wells. For all standards and test samples, 40 $\mu$ L of Bradford reagent was added to each well and the final volume was brought to 200 $\mu$ L using distilled water. Sample preparation was performed at the same time as the standard curve was prepared. All standards and samples were placed in the plate reader immediately, shaken for 10 sec and read at 595nm. The final protein concentration was calculated by interpolation from the average standard curve regression equation.

#### **4.4 Interactions of Stx-2 with Caco-2 Cells**

Caco-2 cells are a transformed cell line derived from a colon carcinoma, and in culture resemble enterocytes that line the small intestine and colon (69, 153). They contain microvilli on their cell surfaces and connect by way of tight junctions. These cells were examined to determine both the Bcl-2 family protein content within them, and to

assess the effects of Stx-2. They were cultured and maintained as described in Appendix B.

#### **4.4.1 Susceptibility of Caco-2 Cells to Stx-2**

Two T25 flasks were seeded with 0.1mL of a suspension of Caco-2 cells and allowed to grow for 7 days by which time the monolayers were 60-70% confluent. The media were exchanged for fresh Caco-2 media and 200 $\mu$ L of Stx-2 supernatant (sterile-filtered) was added to one flask while 200 $\mu$ L of PBS was added to the second flask. After 1 and 5 days of incubation, the cell monolayers in each flask were examined at 100x total magnification using an inverted phase-contrast microscope for rounded, refractile, and floating cells (indicating toxin induced damage). At this point, the media were removed from each flask and 1mL of crystal violet added. After 5 min, the monolayers in the flasks were gently rinsed with distilled water and allowed to air dry.

#### **4.4.2 Protein Analysis of Caco-2 Cells**

Caco-2 cells were allowed to grow to 100% confluency and harvested. Instead of resuspending the cell pellet in cell culture media, it was resuspended in 1mL of autoclaved, distilled water. The suspension was vortexed briefly and divided into 2 x 500 $\mu$ L fractions (Sample A and Sample B). Fifty  $\mu$ L of protease inhibitor cocktail was added to Sample B, and both samples were vortexed. Each sample was further divided in two to give 4 tubes (Fractions 1 and 2 from Sample A, and fractions 3 and 4 from

Sample B) each containing 250 $\mu$ L. Fractions 3 and 4 were centrifuged at 1,000 x g for 10 min. The supernatants from these tubes were transferred to fresh tubes, and the pellets were discarded.

All 4 fractions were analyzed on a 6% stacking / 12% resolving gel using SDS-PAGE. Ten  $\mu$ L of each supernatant sample of Fraction 3 and 4 was diluted 1:2 in sample preparation buffer and 5 $\mu$ L of each whole cell sample of Fraction 1 and 2 was diluted 1:4 in sample preparation buffer. All samples were boiled at 95°C for 5 min, loaded onto the gel, placed in a buffer tank containing SDS-PAGE running buffer, and run at 180V for approximately 45 min. The gel was removed and placed in Coomassie blue for at least 2 h. After staining, the gel was destained in buffer until the background was no longer blue, and protein bands were visible.

The caco-2 whole cell suspension with added protease inhibitor (Sample B) was chosen for more detailed analysis to determine if Bcl-2 family proteins were present in the cells. Gels were prepared and run as described previously and the samples were loaded onto the gel in triplicate. Once the gel was run, each triplicate sample was cut into thirds. One third was placed in Coomassie blue to stain while the remaining two thirds of the gel were prepared for Western blot. The gels were cut into 6 pieces and aligned onto PVDF membranes (Millipore Corp), and placed in a transfer sandwich consisting of fiber pads and filter paper. The transfer sandwich was placed into a buffer tank containing

**Table 2.1: Bcl-2 Protein Family Primary Detection Antibodies**

Antibody Name	Concentration
Anti-Bcl-2 (Biolegend Clone Poly 6119)	2 $\mu$ L/mL
Anti-Bcl-w (Biovision Cat #3034-100)	2.5 $\mu$ g/mL
Anti-Bcl-X <sub>L</sub> (Biovision Cat #3312-100)	2.5 $\mu$ g/mL
Anti-Mcl-1 (R&D Systems Cat#AF828)	1.5 $\mu$ g/mL
Anti-Bax (Biolegend Clone Poly 6251)	2 $\mu$ L/mL

TGB and proteins were transferred at 60V for 4-5 h. After transfer, the membranes were blocked overnight in TBS containing 5% dehydrated skim milk at 4°C. On the following day, a total of five membranes was incubated for 2 h at room temperature with one of the primary antibodies outlined in Table 2.1 and the other remained in blocking buffer as a negative control. A commercial antibody for A1 was unavailable and as a result, Bcl-w which contained the NWGRL pentameric sequence was chosen to be investigated in its place. The membranes were rinsed 3 times in TTBS for 10 min at room temperature, and subsequently treated with anti-rabbit alkaline phosphatase-conjugated secondary antibody (1:10,000 dilution) for 2 h at room temperature. The membranes were rinsed twice in TTBS followed by a rinse in TBS for 10 min at room temperature. The blots were developed with NBT/BCIP tablets (Roche Diagnostics).

#### **4.4.3 Interactions of Bcl-2 (from Caco-2 Cells) and Stx-2**

To assess the interactions of Bcl-2 and Stx-2, a far western blot was performed. For this, the Caco-2 whole cell lysate with added protease inhibitors was run in quadruplicate on two 6% stacking / 12% resolving SDS-PAGE gels. Seven  $\mu$ L of sample was added to 13 $\mu$ L of sample preparation buffer for each replicate. The samples were boiled at 95°C for 5 min, loaded onto the gels, placed in a buffer tank containing SDS-PAGE running buffer, and run at 180V for approximately 45 min. Once the gels were run, they were cut into four pieces. One fourth was placed in Coomassie blue to stain while the other three quarters of the gels were prepared for far Western blot. The samples were transferred to PVDF membranes and blocked overnight in TBS containing 5%



dehydrated skim milk at 4°C as described above. The membranes were rinsed 3 times in TTBS for 10 min each at room temperature, and then renatured with 3% Nonidet P-40 (NP-40) for 30 min. After renaturing, they were rinsed in TTBS 3x for 10 min each at room temperature. One membrane (Far WB Test) was treated with the semi-purified, trypsin-treated Stx-2 suspension containing the A1 fragment, while the control membranes (labeled as NC1 and NC2) remained in blocking solution for 2 h at room temperature. After treatment, all three membranes were rinsed as before with TTBS and two membranes (NC2 and Far WB Test) were subsequently probed with STX2-11E10, and the third (NC1) was put in blocking buffer at room temperature for an additional 2 h. After incubation in the primary antibody was complete, the membranes were rinsed in TTBS and all three membranes were treated with anti-mouse alkaline phosphatase-conjugated antibody (diluted 1:10,000) (Sigma-Aldrich) for 2 h at room temperature. Finally, the blots were rinsed twice in TTBS followed by a rinse in TBS for 10 min each at room temperature and developed with NBT/BCIP tablets (Roche Diagnostics).

#### **4.4.4 Caco-2 Cell Lysate Preparation for Co-Immunoprecipitation**

Caco-2 cells were grown in 5 x T25 flasks to give 95-100% confluency. One mL of sterile-filtered *E. coli* O157:H7 supernatant was added to each flask and incubated for an additional 24 h to collect the floating cells. The media was harvested from each flask and these were pooled, centrifuged at 1000 x g for 10 min at 4°C, and the supernatant fluid removed. The pellet was washed three times by centrifugation in 5mL PBS at 1000 x g for 10 minutes at 4°C.

To collect the attached cells from each flask, 1mL of NP-40 lysis buffer was added and the cells were removed from the flask surface using a rubber scraper. The resultant cell suspension was added to the tube containing the washed floating cells prior to the last centrifugation step and this was centrifuged at 1000 x g for 10 min at 4°C. The pellet was resuspended in 10mL of NP-40 lysis buffer and 100µL of each of the following protease inhibitors was added to the lysate: aprotinin, leupeptin, and PMSF (frozen in absolute ethanol). The cell lysate was sub-divided into 10 cryovials (1mL per vial), flash-frozen in liquid nitrogen, and stored at -80°C.

#### **4.4.5 Co-Immunoprecipitation of Stx-2 and Bcl-2 Family Proteins**

Protein A/G resin (1.5mL) was prepared by adding 10mL NP-40 lysis buffer and gently mixing. This slurry was then centrifuged at 3000 x g for 1 min. The supernatant fluid was decanted and the pellet resuspended in 10mL NP-40 lysis buffer. This washing step was repeated twice to give a total of 3 washes after which the resin was resuspended in 1.5mL lysis buffer.

The Caco-2 cell lysate was prepared for co-immunoprecipitation by centrifuging 400µL of the washed resin slurry in a separate tube at 15,000 x g for 30 sec to remove the liquid phase from the resin. One mL Caco-2 cell lysate was added to the tube and gently rocked at 4°C for 20 min to bind any molecules having high affinity for the resin. After incubation, the sample was centrifuged at 15,000 x g for 5 min at 4°C.

The antibodies were prepared for the co-immunoprecipitation by transferring 1 aliquot of each test antibody (Table 2.2) in a 1.5mL screw cap centrifuge tube. The tubes originally containing the antibody were rinsed with 100 $\mu$ L NP-40 lysis buffer and this rinse containing any residual antibodies was added to the 1.5mL screw cap centrifuge tube. One hundred  $\mu$ L of resin-treated Caco-2 lysate was added to each antibody tube and these were shaken gently, incubated on ice for 1 hour, and 75 $\mu$ L Protein A/G resin was added. The samples were then incubated on ice for an additional 30 min and centrifuged at 15,000 x g for 10 sec. Fifty  $\mu$ L of supernatant fluid was collected from each tube and set aside. One mL of NP-40 lysis buffer was added to each tube to wash and resuspend the gel, and the samples were centrifuged at 15,000 x g for 10 sec. This step was repeated four times to give a total of 5 washes. The remaining supernate was removed to just above the surface of the gel and frozen at -20°C until analyzed.

The samples were loaded onto four 6% stacking / 12% resolving SDS-PAGE gels. Ten  $\mu$ L of sample was added to 10 $\mu$ L of sample preparation buffer for each replicate. The samples were boiled at 95°C for 5 min, loaded onto the gels, placed in a buffer tank containing SDS-PAGE running buffer, and run at 150V for 45-60 min. After electrophoresis, gels were cut into pieces and stained with Coomassie blue or transferred to PVDF membranes for Western blotting as described previously. Once transfer was complete, the membranes were blocked overnight in TBS containing 5% dehydrated skim milk at 4°C. After blocking, the membranes were either left in blocking buffer (negative

**Table 2.2: Co-Immunoprecipitation Pull-Down Antibodies**

Antibody Name	Amount
Anti-Bcl-2 (Biolegend Clone Poly 6119)	10 $\mu$ L
Anti-Bcl-w (Biovision Cat #3034-100)	5 $\mu$ L
Anti-Bcl-X <sub>L</sub> (Biovision Cat #3312-100)	5 $\mu$ L
Anti-Mcl-1 (R&D Systems Cat#AF828)	5 $\mu$ L
Anti-Bax (Biolegend Clone Poly 6251)	10 $\mu$ L
STX2-11E10 (Toxin Technology)	5 $\mu$ L
NP-40 Lysis Buffer (Negative Control)	100 $\mu$ L

controls) or were probed with the following primary antibodies for 2 h: STX2-11E10 (10 $\mu$ g/mL), Anti-Bcl-2 (2 $\mu$ L/mL), Anti-Bax (2 $\mu$ L/mL), Anti-Mcl-1 (1.5 $\mu$ g/mL), Anti-Bcl-X<sub>L</sub> (2.5 $\mu$ g/mL), and Anti-Bcl-w (2.5 $\mu$ g/mL). Following incubation, the membranes were rinsed 3 times in TTBS for 10 min each at room temperature. The co-immunoprecipitation samples pulled-down with Bcl-2 family antibodies and probed with STX2-11E10 were incubated with anti-mouse alkaline phosphatase-conjugated antibody, diluted 1:10,000, (Sigma-Aldrich) for 2 h at room temperature. The samples pulled-down with STX2-11E10 and probed with the Bcl-2 family antibodies were incubated with anti-rabbit phosphatase-conjugated antibody, diluted 1:10,000, (Sigma-Aldrich) for 2 h at room temperature. Lastly, the blots were rinsed twice in TTBS followed by one rinse in TBS for 10 min each at room temperature and developed with NBT/BCIP tablets (Roche Diagnostics).

## **5.0 Results**

### **5.1 Stx-2 Protein Sequence Analysis**

Alignment of Stx-1 and Stx-2 with Bcl-2 family protein sequences were performed to examine which proteins contained the pentameric sequences NWGRI, NWGRL or NWGRV (Fig. 2.2). The NWGRI sequence was observed in Stx-2 as well as in the BH1 domain of Bcl-X<sub>L</sub>, Mcl-1, and A1. The NWGRL sequence was observed in Stx-1 as well as in the BH1 domain of Bcl-w. The proteins Bcl-X<sub>L</sub>, Bcl-w, Mcl-1, and A1 are anti-apoptotic proteins of the Bcl-2 family. The NWGRV sequence, identical except

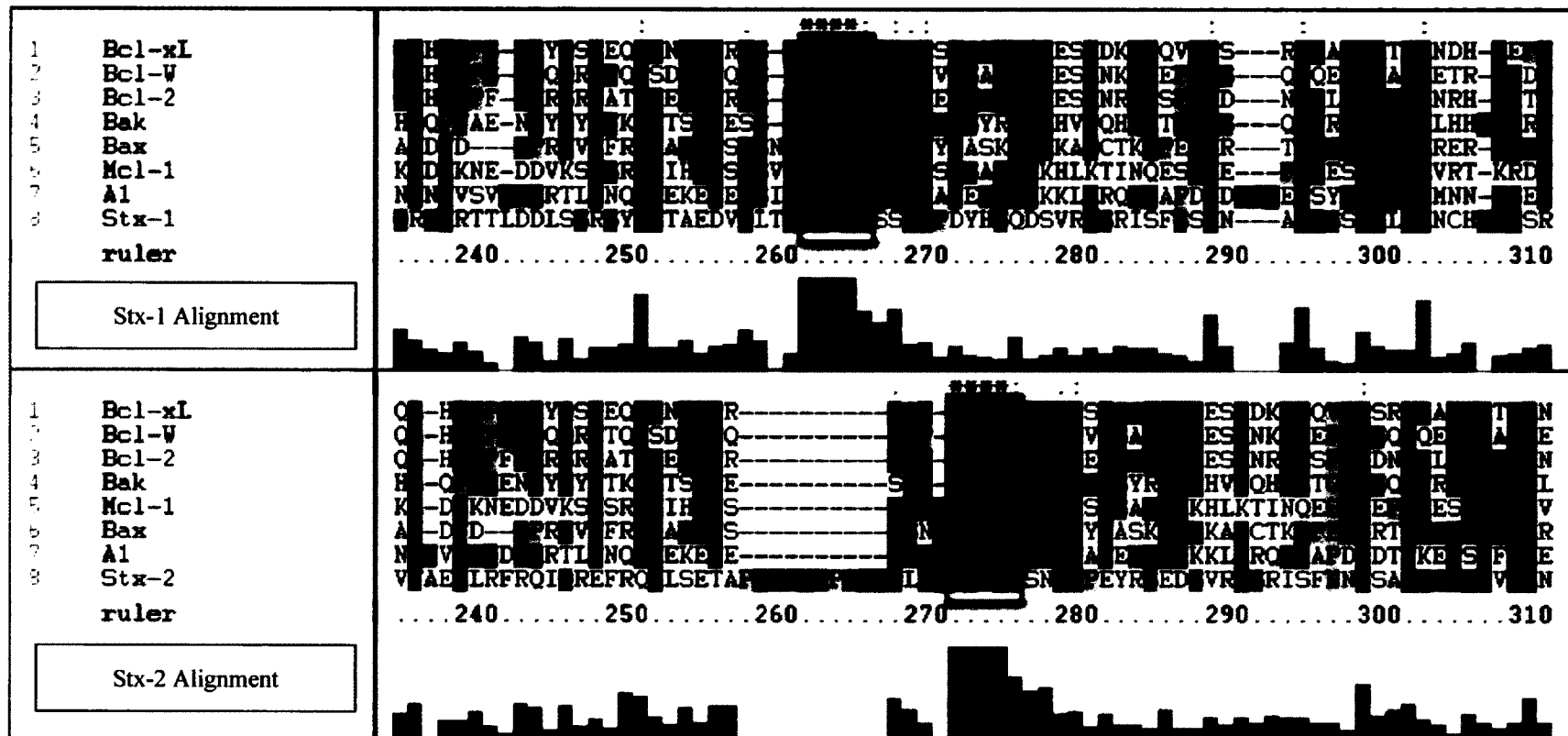


**Figure 2.2: Alignment of Stx-1 and Stx-2 protein sequences.** Exact matches between all sequences are depicted by the (\*) at the top of the outlined box. The bar graph below the aligned amino acid sequences shows relative sequence homology.

for the smaller valine [V] molecule as the final amino acid, was observed only in the BH1 domain of the Bax and Bak pro-apoptotic members of the Bcl-2 family.

## **5.2 Stx-2 Characterization**

### **5.2.1 Native Analysis of Semi-Purified Stx-2**

A native gel and western blot of UV-induced (to enhance toxin production) and non UV-induced *E. coli* O157:H7 strain 90-2380 sterile-filtered supernatant fluids (Figure 2.3) was performed to determine protein content. Lane 2 and 4 show protein band patterns of samples that had not been induced with UV light while lane 3 shows the protein band pattern of the sample that was exposed to UV light. Differences in protein content were observed between these sample types, the most important of which has been highlighted by the box in Figure 2.3. This band corresponds with the band (also boxed) observed in the Western blot that had been probed with anti-Stx-2 antibody, confirming the protein as Stx-2. Native gels illustrating the effectiveness of Centricon 100 and 50 concentration units to purify and concentrate proteins between 50-100 kDa are shown in Figure 2.4.

### **5.2.2 SDS-PAGE and Western Blot Analysis of Semi-Purified Stx-2**

The SDS-PAGE gel of semi-purified Stx-2 from *E. coli* O157:H7 strain 90-2380 is illustrated in Figure 2.5 and Figure 2.6 shows the Western blot of the semi-purified

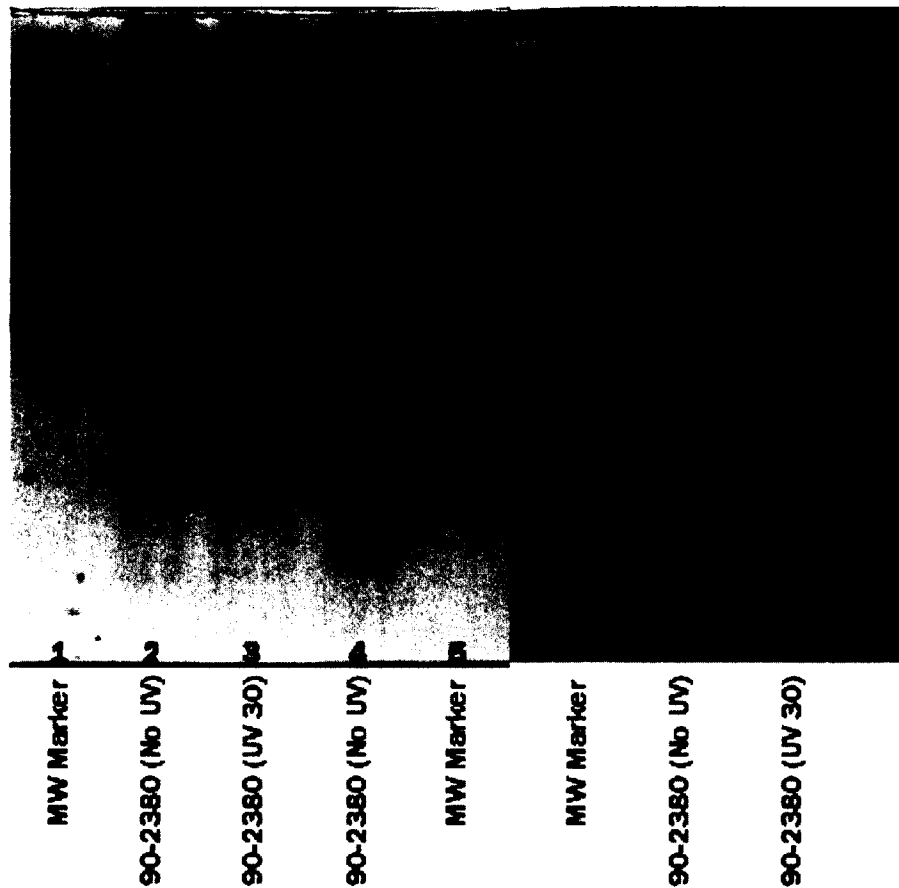


**Figure 2.3: Native analysis of Stx-2 produced by *E. coli* O157:H7 strain 90-2380. A)** Native gel of the molecular weight markers, bovine serum albumin and lysozyme (Lane 1 & 5), and non UV-induced (Lane 2 & 4) and UV-induced (Lane 3) sterile-filtered supernate from *E. coli* O157:H7 strain 90-2380. The box represents the area in which the toxin is located. B) Western Blot of non UV-induced (Lane 2) and UV-induced (Lane 3) sterile-filtered supernate from *E. coli* O157:H7 strain 90-2380. The box represents the area in which the toxin was detected.



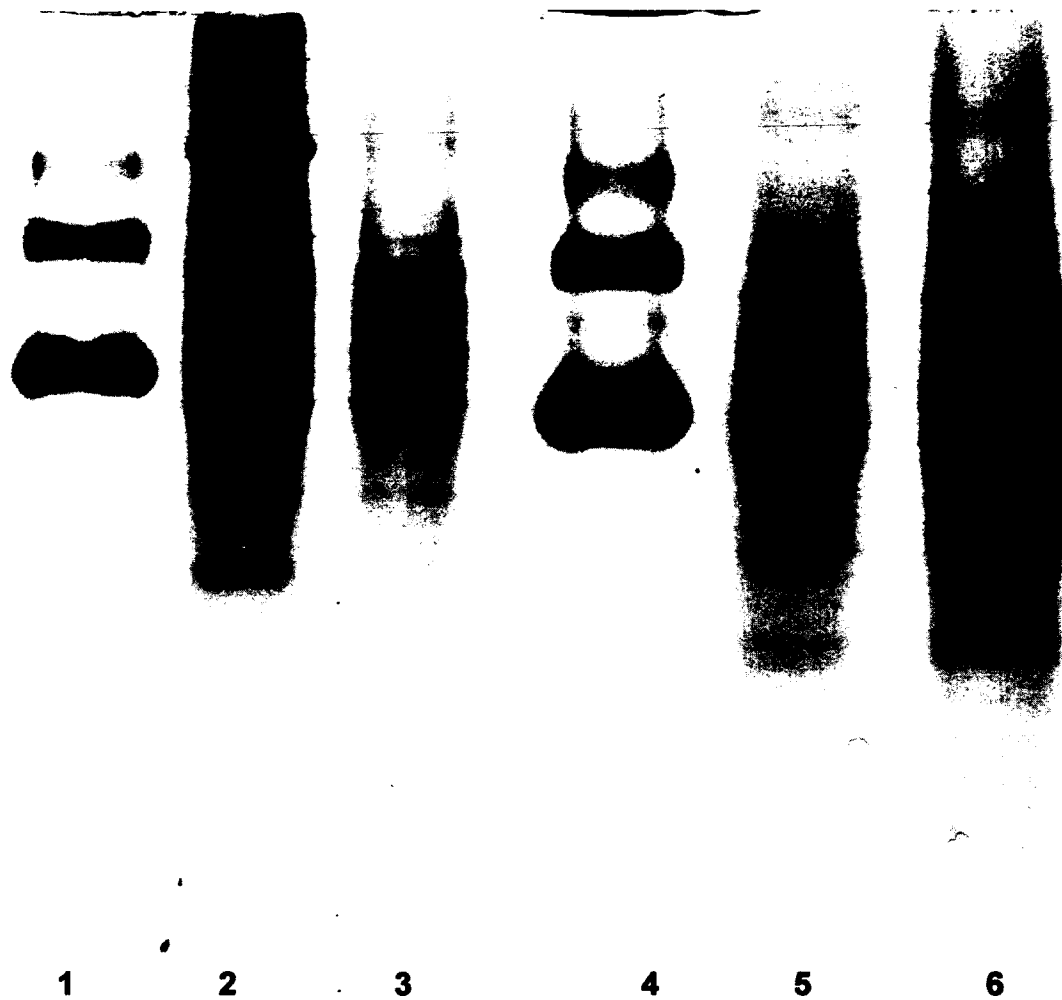


**Figure 2.4: Purification and concentration of Stx-2 produced by *E. coli* O157:H7 strain 90-2380 using Centricron devices.** Native gel of the molecular weight markers, bovine serum albumin and lysozyme (Lane 1 & 4), the semi-purified Stx-2 sample prior to Centricron 100 processing (Lane 2), the semi-purified Stx-2 sample after Centricron 100 processing (filtrate) (Lane 3 & 5), and the semi-purified Stx-2 sample after Centricron 50 processing (Lane 6).



**Figure 2.5: SDS-PAGE analysis of Stx-2 produced by *E. coli* O157:H7 strain 90-2380. Pre-stained molecular weight markers are in Lane 1 and the semi-purified Stx-2 sample is in Lane 2. The box represents the area in which the toxin is located.**

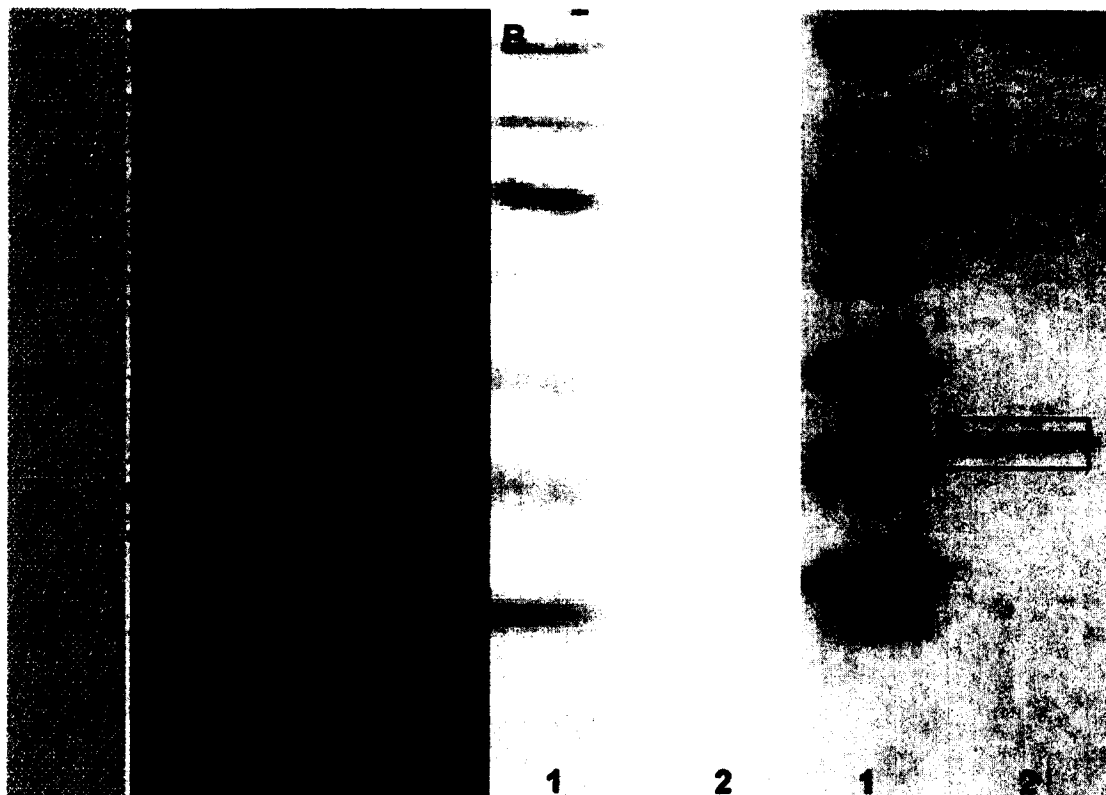


**Figure 2.6: Western blot confirmation of Stx-2 in the semi-purified toxin preparation.** Pre-stained molecular weight markers are in Lane 1 and the semi-purified Stx-2 sample is in Lane 2. A) SDS-PAGE. B) Negative control Western blot probed with anti-mouse IgG only, in the absence of Stx-2 specific antibody. No bands were detected. C) Western Blot probed with STX2-11E10 mouse antibody and anti-mouse IgG. Stx-2 was seen in the boxed areas.

Stx-2. Of interest are the bands between the 25 and 32.5 kDa markers indicating the presence of the Stx-2 A-subunit (Fig. 2.5). Pre-stained molecular weight markers were used for these procedures, and molecular weight estimates are not as accurate as unstained markers. Panel A shows the SDS-PAGE gel in which multiple bands were observed. However, the most important has been highlighted by the box and corresponds to the molecular mass of Stx-2. Panel B shows a Western blot of the negative control membrane that was treated only with secondary antibody and as expected, no bands were detected. Panel C illustrates the Western blot treated with the anti-stx-2 antibody and the secondary antibody. One band was clearly detected between the 25 and 32.5 kDa markers and confirmed the presence of the A-subunit of Stx-2 in the purified sample.

### **5.2.3 Cleavage Analysis of Semi-Purified Stx-2 and A1 Fragment Generation**

Semi-purified Stx-2 was analyzed to ensure that cleavage at the Arg-X-X-Arg consensus sequence would occur during subsequent experimentation in mammalian cells, and results indicated that trypsin treatment effectively cleaved the toxin. The Stx-2 A-subunit comprises an A1 and A2 fragment. The A1 fragment has an approximate size of 28 kDa while the A2 fragment is 4 kDa. For these experiments the generation of the larger A1 fragment was determined. Figure 2.7 shows a gel containing molecular weight markers, the trypsin treated Stx-2, and Stx-2 without trypsin treatment. Treatment of Stx-2 resulted in the disappearance of a band located at approximately 32 kDa in lane 3 of Figure 2.7. In addition, a new band was observed in the trypsin-treated sample in lane 2 of Figure 2.7 just under the 27 kDa marker. In order to ensure that this new band was not from the added trypsin (molecular weight of approximately 24 kDa) a Western blot was

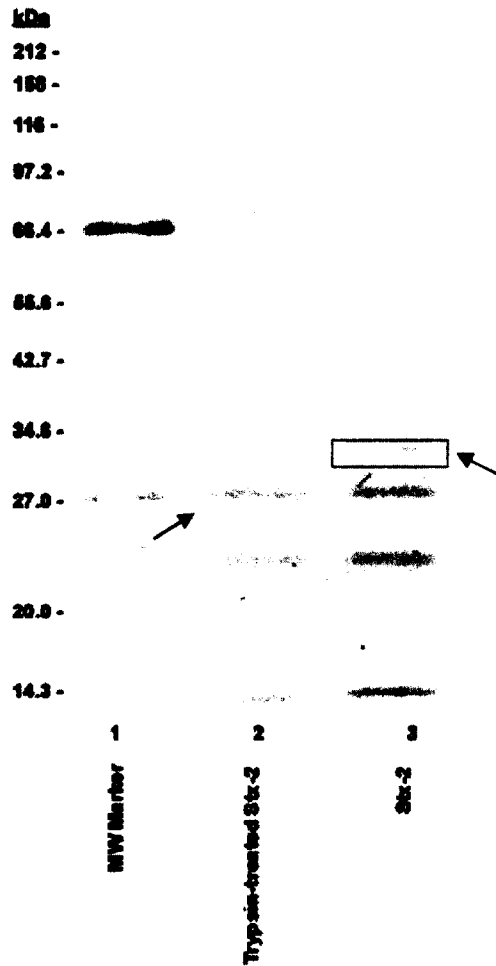


**Figure 2.7: SDS-PAGE analysis of trypsin-treated semi-purified Stx-2.** Broad range molecular weight markers are in Lane 1, trypsin-treated Stx-2 sample is in Lane 2, and the Stx-2 sample without treatment is in Lane 3. The box represents the area in which the 32 kDa A subunit of Stx-2 is located. The arrows indicate the cleavage of the A-subunit by trypsin in Lane 3, resulting in a new band (the A1 fragment) in Lane 2 that is approximately 4 kDa smaller.

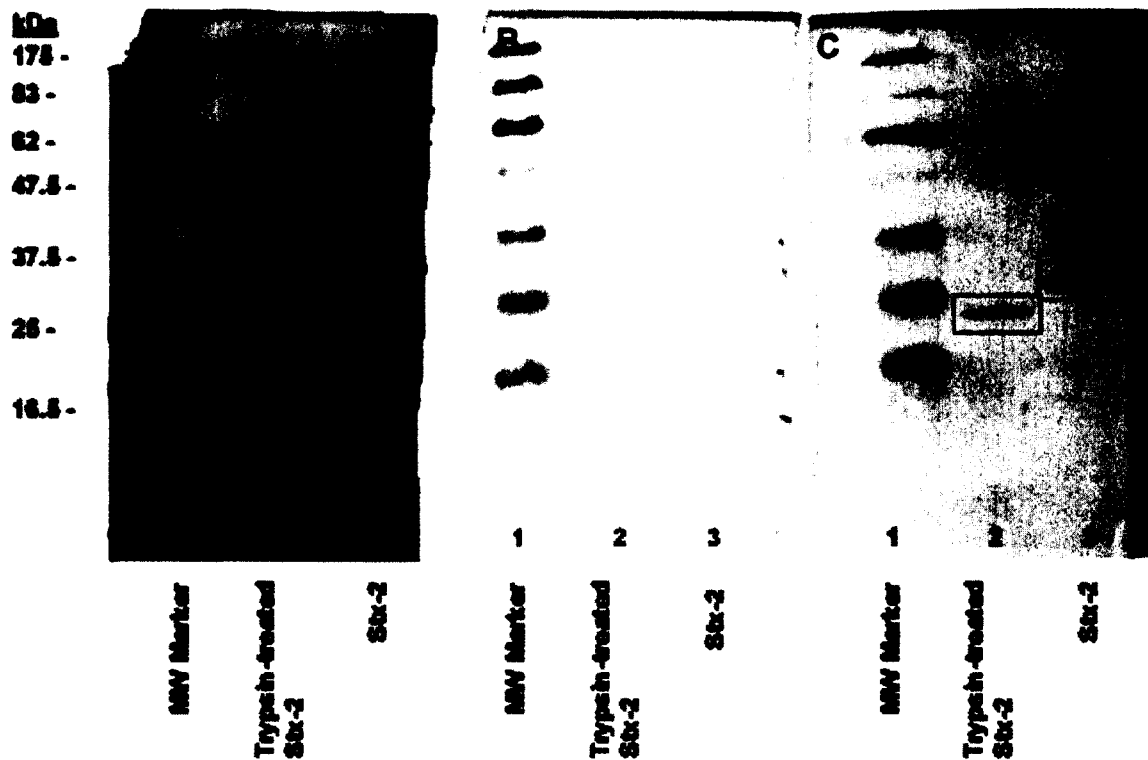


**Figure 2.8: Western blot confirmation of Stx-2 cleavage and A1 fragment generation in the trypsin-treated Stx-2 preparation.** A) SDS-PAGE of Stx-2. Pre-stained molecular weight markers are in Lane 1, trypsin-treated Stx-2 is in Lane 2, and Stx-2 without treatment is in Lane 3. B) Negative control Western blot probed with anti-mouse IgG in the absence of specific anti-Stx-2 antibody. Lanes are as outlined for A. C) Western Blot probed with STX2-11E10 anti-Stx-2 antibody and anti-mouse IgG. Lanes are as outlined for A. The band noted in the box in Lane 2, panel C, shows the A1 fragment in the sample while the box in Lane 3 shows the full (untreated) A-subunit of Stx-2. The slightly smaller size of the band in Lane 2 (A1 fragment) as compared to that in Lane 3 (whole A-subunit) corresponds to the loss of the 4 kDa A2 fragment.

performed. Results of the western blot are shown in Figure 2.8. These results confirmed that the bands observed were the toxin, and not trypsin. Pre-stained molecular weight markers were used for this procedure, and hence the molecular weight estimates were slightly smaller than those shown in the SDS-PAGE gel. However, the molecular weight of Stx-2 did correspond with the initial Western blot confirmation in Figure 2.6. Two distinct bands were observed in the samples tested, with the trypsin-treated Stx-2 band (Figure 2.8, panel C, lane 2) being approximately 4 kDa smaller than the untreated sample in lane 3. This indicated that the A-subunit of Stx-2 was cleaved by trypsin treatment (analogous to that of furin cleavage within host cells) and that the two fragments (A1 and A2) were separated and successfully detected in Western blots using the specific antibody.

#### **5.2.4 Biological Activity Verification of Semi-Purified Stx-2**

After 96 h incubation, the T25 flasks containing monolayers of Vero cells that had previously been inoculated with “semi-purified” Stx-2 preparation (as outlined in the Materials and Methods section 4.3.5) were removed from the incubator and examined for cytotoxic effects. The cells in the control flask were confluent and showed typical Vero cell morphology (Figure 2.9 A & B). There were minimal cells floating in the medium. However, the cells in the flask inoculated with 50 $\mu$ L of Stx-2 were approximately 50% confluent and were lifting off the flask surface (Figure 2.9 C & D). There were many rounded and refractile cells floating in the medium, indicating a large number of dead cells typical of Stx-2 toxicity. Once the flasks were stained with crystal violet and dried,

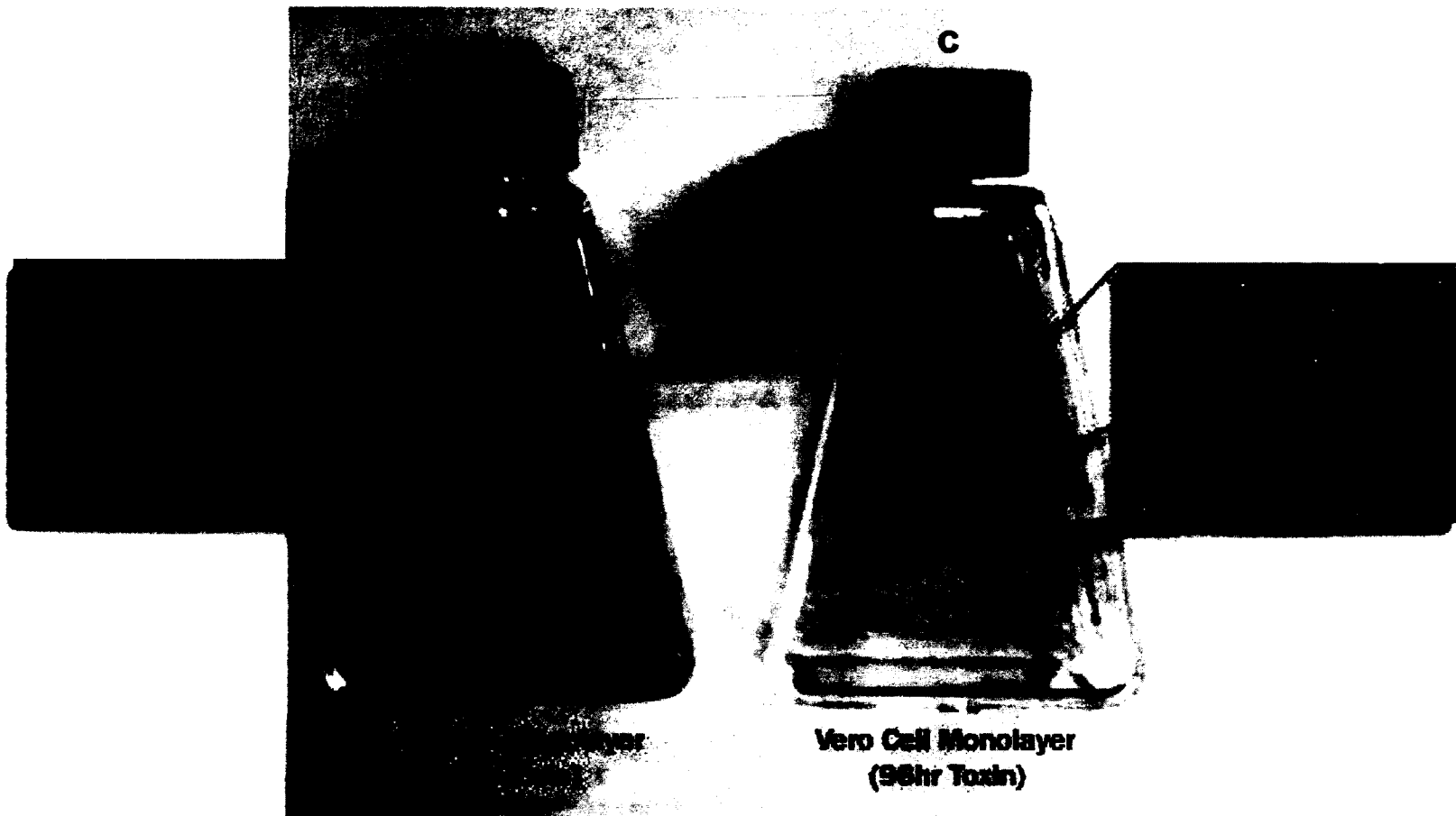


**Figure 2.9: Biological activity of semi-purified Stx-2.** A) Control flask containing no toxin and shown stained with crystal violet. The density of the cell monolayer is evident in the intensity of the crystal violet staining. B) Image of Vero cells viewed at 100x magnification. Morphology typical of healthy Vero cells is seen. C) Test flask inoculated with Stx-2 and stained with crystal violet. Note the reduced staining indicating major loss of cells from the monolayer. D) Image of Vero cells viewed at 100x magnification. Note rounded, refractile cells and loss of monolayer integrity typical of Stx-2 action.



the difference in the density of the cell monolayers between the flasks was evident (Figure 2.9).

### **5.2.5 Quantitation of Semi-Purified Stx-2**

Duplicate bovine serum albumin (BSA) standards ranging from 0 to 8 mg/mL were used to construct a standard curve to quantify the total protein concentration of the Stx-2 preparation (Figure 2.10). The average background absorbance was calculated between duplicate blanks and this value was subtracted from the total absorbance reading in each well. The duplicate standard values were averaged and plotted to produce a standard curve with a correlation coefficient ( $r^2$ ) of 0.9861. The total protein concentration for the semi-pure Stx-2 was calculated by averaging the absorbance of the six replicates assayed. This value was then entered into the standard curve regression equation, and a final protein concentration of 3.07 mg/mL was obtained.

## **5.3 Interactions of Stx-2 with Caco-2 Cells**

### **5.3.1 Susceptibility of Caco-2 Cells to Stx-2**

Caco-2 cells required 9 days of culture to achieve 100% confluency (Figure 2.11, A). These cells when subsequently exposed to Stx-2 for an additional 5 days and then stained with crystal violet (Figure 2.11, B) showed monolayer destruction as compared to the control. However, as expected this was much less pronounced than with the Vero cell

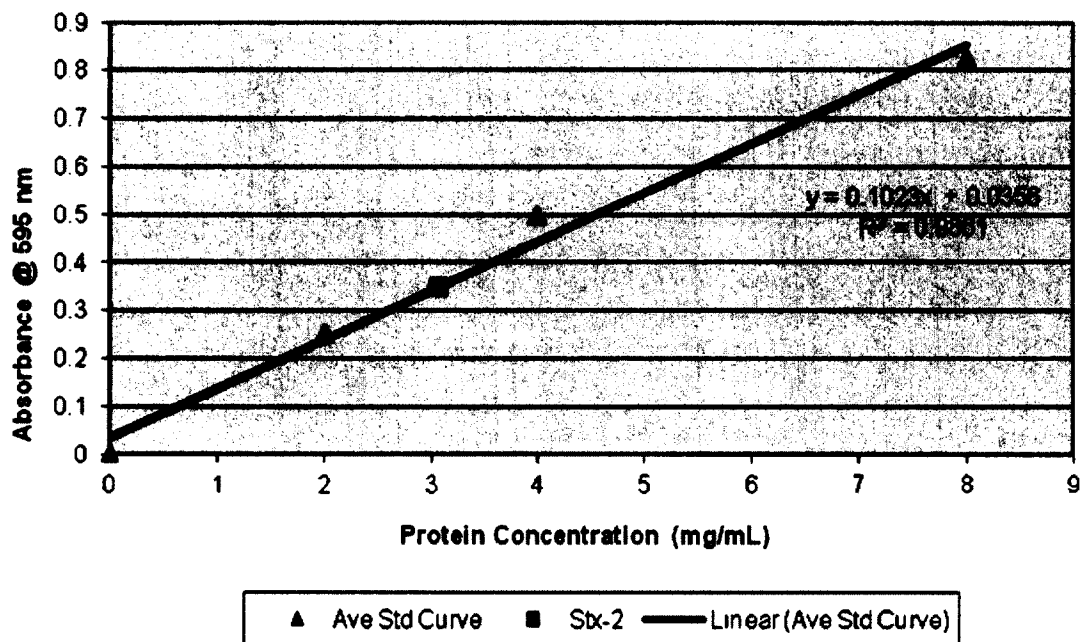


**Figure 2.10: Total protein concentration of semi-purified Stx-2.** The standard curve shown by the  $\blacktriangle$  symbol with correlation coefficient of  $r^2 = 0.9861$  and regression equation of  $y = 0.1023x + 0.0356$ . The total calculated protein concentration was 3.07mg/mL and is shown by the  $\blacksquare$  symbol.

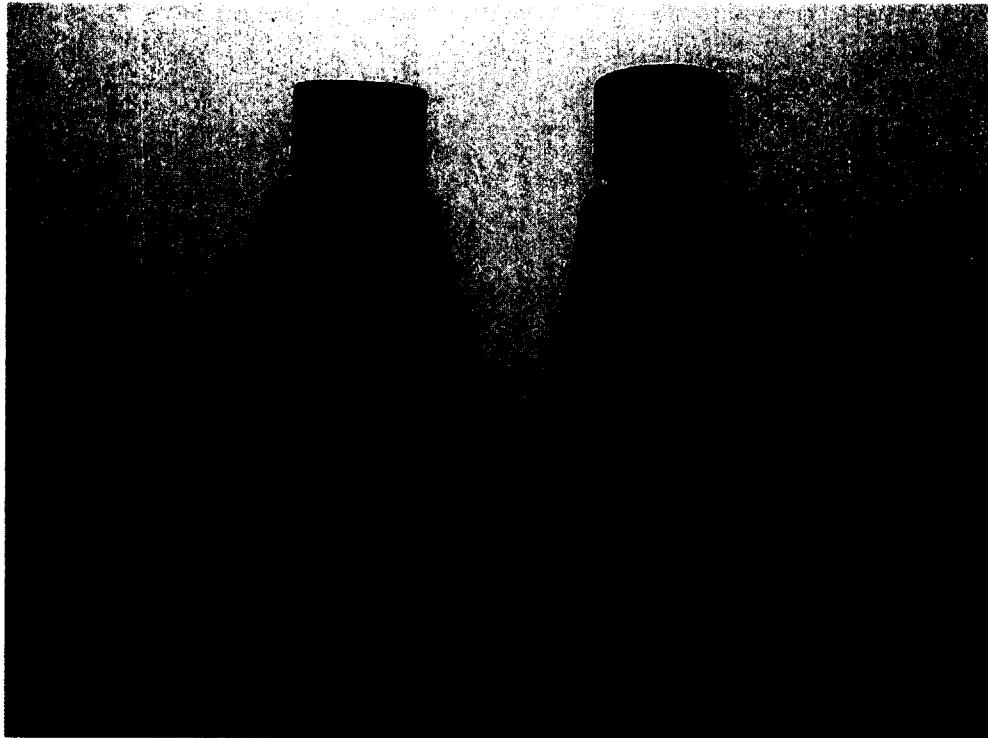


**Figure 2.11: Cytotoxicity of Stx-2 on Caco-2 cells.** Flasks were incubated for 9 days to ensure confluency of monolayers at which point the test flask was inoculated with Stx-2. Inoculated and control cells were examined daily for 5 days. After a total of 14 days of incubation, flasks were stained with crystal violet. A) Control flask with no toxin present. Note relative confluency of cell monolayer. B) Test flask inoculated with 200 $\mu$ L of sterile-filtered Stx-2 supernatant fluid. Note destruction of monolayer integrity.

monolayers which are highly susceptible to Stx, and this enhanced toxicity gave the toxin its initial name of verotoxin.

### **5.3.2 Protein Analysis of Caco-2 Cells**

SDS-PAGE of prepared Caco-2 cell lysates determined which preparation would be best suited to detect Bcl-2 family proteins. Figure 2.12 shows the results of the SDS-PAGE analysis. As can be seen, all samples resulted in preparations with multiple bands. However, the Caco-2 whole cell lysate preparations resulted in more protein bands than the supernatant fluid lysate preparations. The Caco-2 whole cell lysate preparation with added protease cocktail inhibitors was selected for Western blot to determine the presence of Bcl-2. These inhibitors would prevent proteases from degrading proteins in the lysate. Figure 2.13 panel A illustrates the SDS-PAGE of Caco-2 cell lysate following protease inhibitor treatment while panel B shows the Western blot of the negative control membrane treated with anti-rabbit IgG and without prior treatment with rabbit anti-Bcl-2 antibody. No bands were detected on the control membrane. Panel C shows the Western blot treated with rabbit anti-Bcl-2 antibody and then probed with alkaline phosphatase conjugated anti-rabbit IgG. A band was detected at approximately 26 kDa which was previously shown to correspond to the molecular weight of Bcl-2 (58). The second band was detected just above the 175 kDa marker. It is thought that this band indicates Bcl-2 oligomers.

Using a range of specific antibodies (outlined in Table 2.1 in Materials and

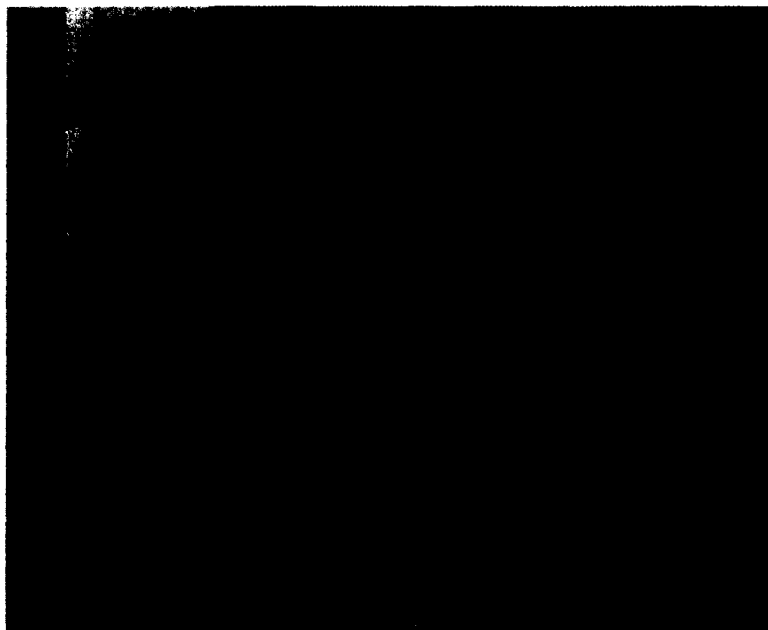


**Figure 2.12: SDS-PAGE analysis of Caco-2 lysates.** Broad range molecular weight markers are in Lane 1, Caco-2 whole cell lysate preparation is in Lane 2, Caco-2 supernatant lysate preparation is in Lane 3, Caco-2 whole cell lysate preparation with protease inhibitor cocktail is in Lane 4, and Caco-2 supernatant lysate preparation with protease inhibitor cocktail is in Lane 5. Note the increased number of bands in the whole cell lysate preparations.

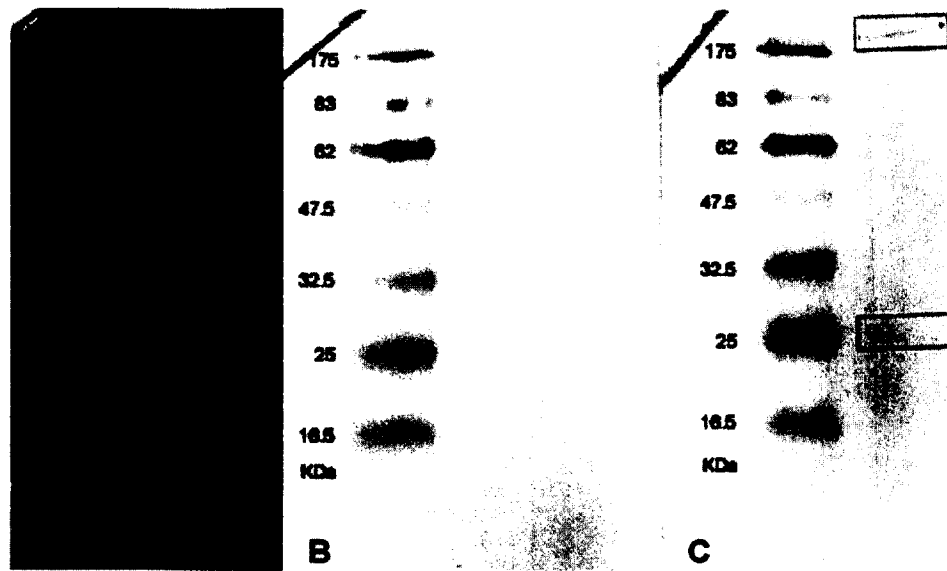


**Figure 2.13: Western Blot confirmation of Bcl-2 in Caco-2 whole cell lysate preparation with protease inhibitors.** A) SDS-PAGE. Pre-stained molecular weight markers are in Lane 1 and the Caco-2 whole cell lysate preparation with protease inhibitor cocktail is in Lane 2. The bands noted in the boxes represent Bcl-2 in the sample. B) Negative control Western blot probed with anti-rabbit IgG in the absence of specific rabbit anti-Bcl-2 antibody showing no bands. Lanes are as outlined for A. C) Western Blot probed with rabbit anti-Bcl-2 antibody and anti-rabbit IgG. Lanes are as outlined for A. The bands noted in the boxes represent Bcl-2 in the sample. The larger band is believed to be Bcl-2 oligomers.

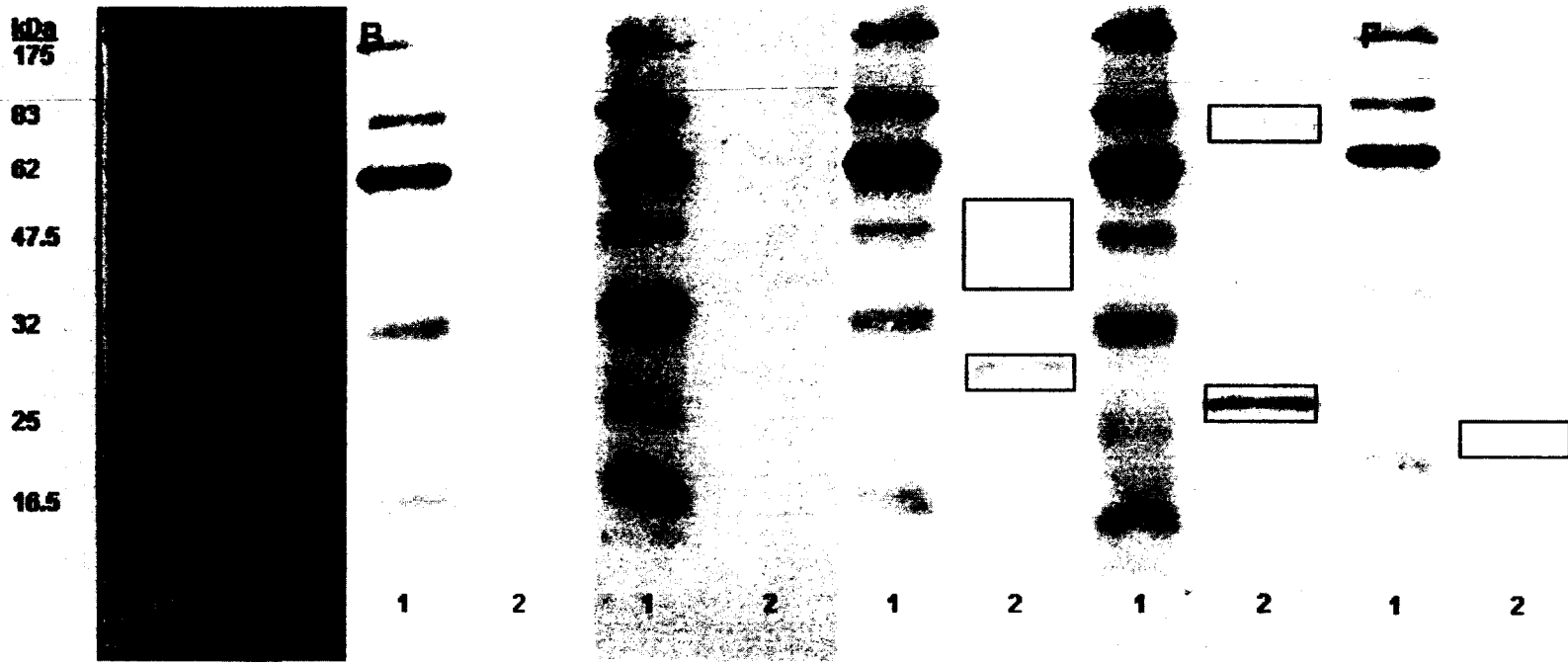


**Figure 2.14: Analysis of Bcl-2 family proteins in Caco-2 whole cell lysate preparation with protease inhibitors.** A) SDS-PAGE. Pre-stained molecular weight markers are in Lane 1 and the Caco-2 whole cell lysate preparation with protease inhibitor cocktail is in Lane 2. B) Negative control Western blot probed with anti-rabbit IgG in the absence of specific rabbit antibodies showing no bands. Lanes are as outlined for A. C) Western Blot probed with rabbit anti-Bcl-w antibody and anti-rabbit IgG. Lanes are as outlined for A. No bands were detected. D) Western Blot probed with rabbit anti-Bcl-X<sub>L</sub> antibody and anti-rabbit IgG. Lanes are as outlined for A. The bands noted in the boxes represent detected proteins. The bands detected at 28 kDa and 53 kDa are believed to be Bcl-X<sub>L</sub> and Bcl-X<sub>L</sub> dimers. The larger bands are believed to be cross-reactions of the antibody to other unknown proteins present in the caco-2 lysate. E) Western Blot probed with rabbit anti Mcl-1 antibody and anti-rabbit IgG. Lanes are as outlined for A. The bands noted in the boxes represent detected proteins. The smaller band is believed to be a cross-reaction of the antibody to another unknown protein present in the caco-2 lysate while the larger is believed to be Mcl-1 dimers. F) Western Blot probed with rabbit anti-Bax antibody and anti-rabbit IgG. Lanes are as outlined for A. The band noted in the box represents Bax in the sample.

Methods) the nature of the Bcl-2 family proteins was further investigated (Figure 2.14). There were no bands detected with the Bcl-w antibody. Bcl-w has an expected molecular weight of 22 kDa as previously reported by Wilson *et al.* (217). Since no bands were detected, this indicates that the Caco-2 cell line does not produce Bcl-w.

There were five bands detected on the membrane probed with anti-Bcl-X<sub>L</sub>. These bands were at approximately 53 kDa, 47 kDa, 45 kDa, 40 kDa, and 28 kDa. Since so many bands were detected, the specificity of this antibody to Bcl-X<sub>L</sub> appears to be poor. The expected molecular weight of Bcl-X<sub>L</sub> is 28-30 kDa (58). It is possible that the band detected at 28 kDa corresponds with the presence of Bcl-X<sub>L</sub> and that the band detected at 53 kDa corresponds with the detection of Bcl-X<sub>L</sub> dimers since pre-stained markers were used and molecular weight estimations are smaller than actual values. This would indicate that the Caco-2 cell line does in fact produce Bcl-X<sub>L</sub>; however it appears the polyclonal nature of the antibody also results in cross-reactions with other unknown proteins in the Caco-2 lysate.

There were two bands detected on the membrane probed with anti-Mcl-1. These bands were at approximately 26 kDa and 78 kDa. The expected molecular weight of Mcl-1 is 37 kDa for the short form and 42 kDa for the long form (58, 111). Neither of the detected bands matched the expected size for Mcl-1, however the 78 kDa band may be indicative of Mcl-1 dimers. The strong band detected at 26 kDa may be indicative of an antibody cross-reaction with other pro-apoptotic proteins such as Bak, which has an expected molecular weight of 25-28 kDa (58). Since the bands detected were not at the



expected molecular weight for Mcl-1 it cannot be confirmed that Caco-2 cells produce Mcl-1. Cross-reactions with other proteins in the Caco-2 lysate were due to the polyclonal nature of the antibody.

There was one band detected on the membrane probed with anti-Bax. This band was detected at approximately 20 kDa, which matches the expected molecular weight of Bax. Therefore this indicates that the Caco-2 cell line produces Bax.

### **5.3.3 Interactions of Bcl-2 (from Caco-2 Cells) and Stx-2**

Interaction of Stx-2 with the Bcl-2 family proteins was interrogated by far Western blot (Fig. 2.15). Panel A illustrates the SDS-PAGE of Caco-2 cell lysate following protease inhibitor treatment while panel B shows the far Western blot negative control membrane treated with anti-mouse IgG in the absence of Stx-2 and specific mouse anti-Stx-2 antibody. No bands were detected on this control membrane. Panel C shows the far Western blot control membrane treated with mouse STX2-11E10 antibody and then probed with alkaline phosphatase conjugated anti-mouse IgG. A band was detected at approximately 55 kDa and it is believed that this is due to non-specific binding of the primary antibody (STX2-11E10) to a highly concentrated protein band in the caco-2 lysate. Panel D shows the far Western blot incubated with Stx-2 followed by subsequent treatment with STX2-11E10 antibody and alkaline phosphatase conjugated anti-mouse IgG. A band at 55 kDa was detected, identical to the one in panel C. However, it is interesting to note that the exposure time of all membranes were the same,

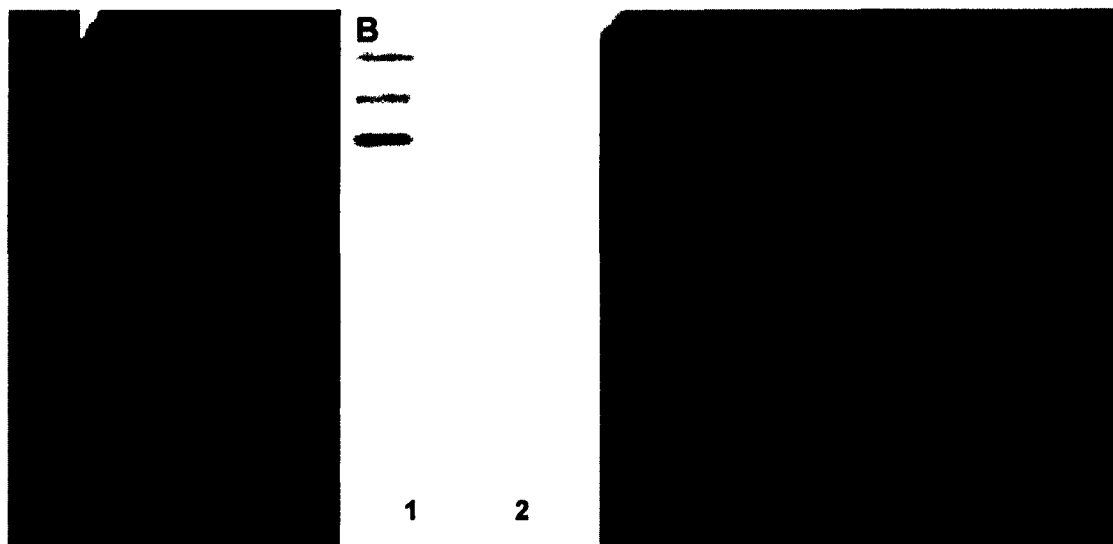


**Figure 2.15: Far Western blot of Caco-2 whole cell lysate preparation with protease inhibitors.** A) SDS-PAGE. Pre-stained molecular weight markers are in Lane 1 and the Caco-2 whole cell lysate preparation with protease inhibitor cocktail is in Lane 2. B) Negative control far Western blot probed with anti-mouse IgG in the absence of Stx-2 and specific mouse anti-Stx-2 antibody showing no bands. Lanes are as outlined for A. C) Negative control far Western blot probed with mouse STX2-11E10 antibody and anti-mouse IgG. Lanes are as outlined for A. The band noted in the box represents non-specific binding of the primary antibody (STX2-11E10) to a highly concentrated protein band in the Caco-2 lysate. D) Far Western blot probed with Stx-2 followed by mouse STX2-11E10 antibody and anti-mouse IgG. Lanes are as outlined for A. The band noted in the box corresponds with the band observed in panel C, but is of increased intensity which is believed to be a possible interaction of Stx-2 and this unidentified protein that has a molecular mass of 55 kDa.

but the intensity of the band in panel D is greater than that of the control in frame C, indicating a possible interaction of Stx-2 with this unidentified protein.

#### **5.3.4 Co-Immunoprecipitation of Stx-2 and Bcl-2 Family Proteins**

A co-immunoprecipitation was performed using two different methods. In the first method, potential immunocomplexes were isolated by binding them to the Bcl-2 family antibodies; anti-Bcl-2, anti-Bax, anti-Mcl-1, anti-Bcl-X<sub>L</sub>, and anti-Bcl-w. These samples were then probed with the Stx-2 antibody, STX2-11E10 raised in mice followed by alkaline phosphatase conjugated anti-mouse IgG antibody (Fig. 2.16 and 2.17). In all samples except the negative control, the SDS-PAGE showed protein bands at approximately 48 kDa, in particular with the Caco-2 pull-down processed with anti-Mcl-1 and anti-Bcl-X<sub>L</sub>. This most likely corresponds to the molecular weight of the heavy chain of the IgG antibodies. In addition, a second band was observed at 27 kDa in the Caco-2 pull-down processed with anti-Mcl-1. This band most likely corresponds to the light chain of the IgG antibodies. No other bands were detected. On the negative control blot, there was one very faint band detected in the Caco-2 pull down processed with anti-Mcl-1 suggesting there may be a cross reaction between anti-Mcl-1 and anti-mouse IgG antibodies. On the blot probed with STX2-11E10, there were bands detected in all lanes at approximately 48 kDa and bands detected in lane 4, 5, and 8 at approximately 27 kDa. Again it is thought that these bands correspond to the heavy and light chains of the Bcl-2 family antibodies used for the co-immunoprecipitation pull-down.

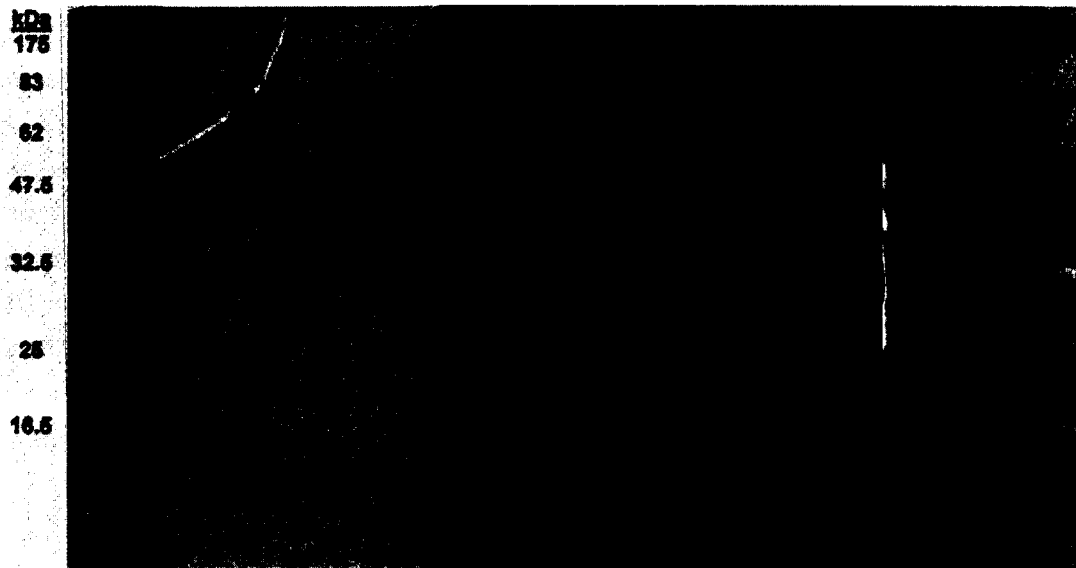


**Figure 2.16: SDS-PAGE of Caco-2 cell lysate and Stx-2 co-immunoprecipitation interactions using Bcl-2 protein family antibodies.** Pre-stained molecular weight markers are in Lane 1, 4, and 8, Caco-2 pull down with anti-Bcl-2 antibody is in Lane 2, Caco-2 pull down with anti-Bax antibody is in Lane 3, Caco-2 pull down with anti-Mcl-1 antibody is in Lane 5, Caco-2 pull down with anti-Bcl-X<sub>L</sub> antibody is in Lane 6, Caco-2 pull down with NP-40 lysis buffer (negative control) is in Lane 7, and Caco-2 pull down with anti-Bcl-w antibody is in Lane 9.

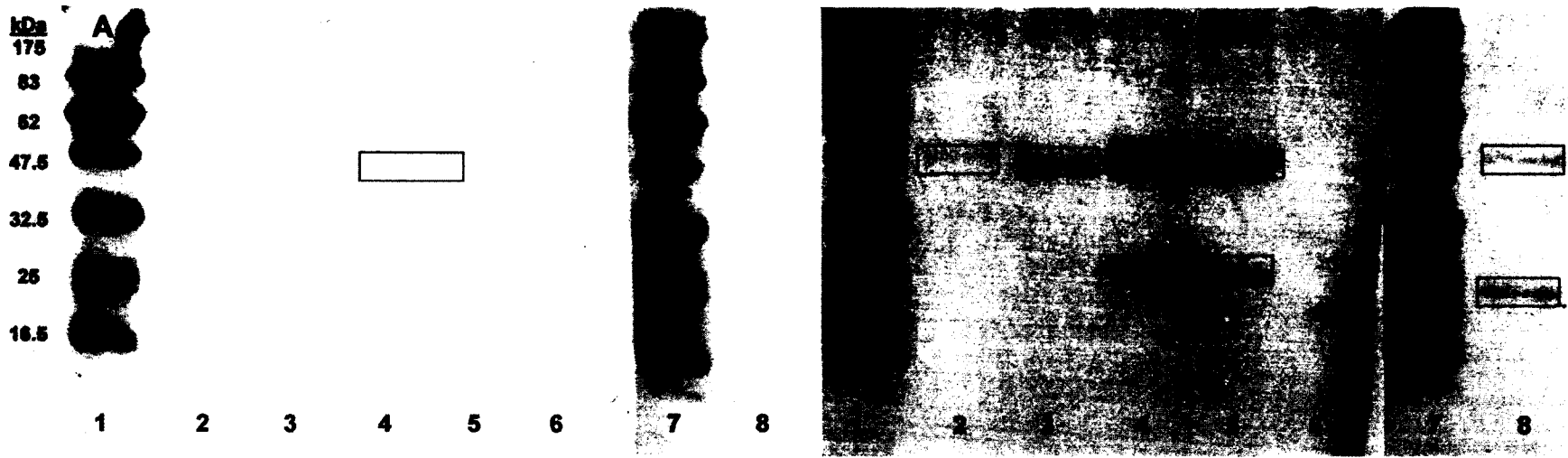


**Figure 2.17: Western blot of Caco-2 cell lysate and Stx-2 co-immunoprecipitation interactions using Bcl-2 protein family antibodies.** A) Negative control Western blot probed with anti-mouse IgG in the absence of specific mouse antibodies. Pre-stained molecular weight markers are in Lane 1 and 7, Caco-2 pull down with anti-Bcl-2 antibody is in Lane 2, Caco-2 pull down with anti-Bax antibody is in Lane 3, Caco-2 pull down with anti-Mcl-1 antibody is in Lane 4, Caco-2 pull down with anti-Bcl-X<sub>L</sub> antibody is in Lane 5, Caco-2 pull down with NP-40 lysis buffer negative control is in Lane 6, and Caco-2 pull down with anti-Bcl-w antibody is in Lane 8. The band noted in the box represents a cross reaction between anti-Mcl-1 and anti-mouse IgG antibodies. B) Western blot probed with mouse STX2-11E10 antibody and anti-mouse IgG. Lanes are as outlined in A. The bands noted in the boxes represent detected proteins. The bands detected at 48 kDa and 27 kDa are believed to be the heavy and light chains of the Bcl-2 family antibodies used for the pull-down procedure. No other bands were detected.

In the second method, potential immunocomplexes were isolated by binding them to the STX2-11E10 antibody. These samples were then probed with anti-Bcl-2, anti-Bax, anti-Mcl-1, anti-Bcl-X<sub>L</sub>, and anti-Bcl-w, and detected with the anti-rabbit IgG. The results are summarized in Figure 2.18. Neither the SDS-PAGE nor the negative control membrane showed any bands. In addition, the membrane probed with anti-Bcl-2 also did not detect any bands. However, membranes probed with anti-Bax, anti-Mcl-1, anti-Bcl-X<sub>L</sub>, and anti-Bcl-w showed the same band pattern of 6 distinct bands with molecular weights between approximately 50 kDa and 27 kDa. Since the band pattern was the same for almost all the probing antibodies, it is hypothesized that these results are most likely not true protein-protein interactions. The top and bottom bands (50 kDa and 27 kDa, respectively) appear to correspond to the heavy and light chains of the pull-down antibody (STX2-11E10) which was also observed in the previous pull-down method. The remaining 4 bands present at approximately 48 kDa, 40 kDa, 32 kDa, and 28 kDa are hypothesized to be complexes of Stx-2 and/or cross-reactions of the antibody with unknown caco-2 proteins (48 kDa and 40 kDa), whole Stx-2 A-subunit remaining in the caco-2 lysate (32 kDa), and Stx-2 that was processed by the caco-2 cells and reduced to the A1 fragment (28 kDa). Further evidence to support this hypothesis was observed as these protein-protein interactions were only detected when using the STX2-11E10 pull-down method. If a true protein-protein interaction was detected, then the interactions would have been detected using both pull-down methods. Since there was no evidence that these interactions were true, it was decided that an examination of the cross-reaction of the Bcl-2 family antibodies with Stx-2 was not necessary.

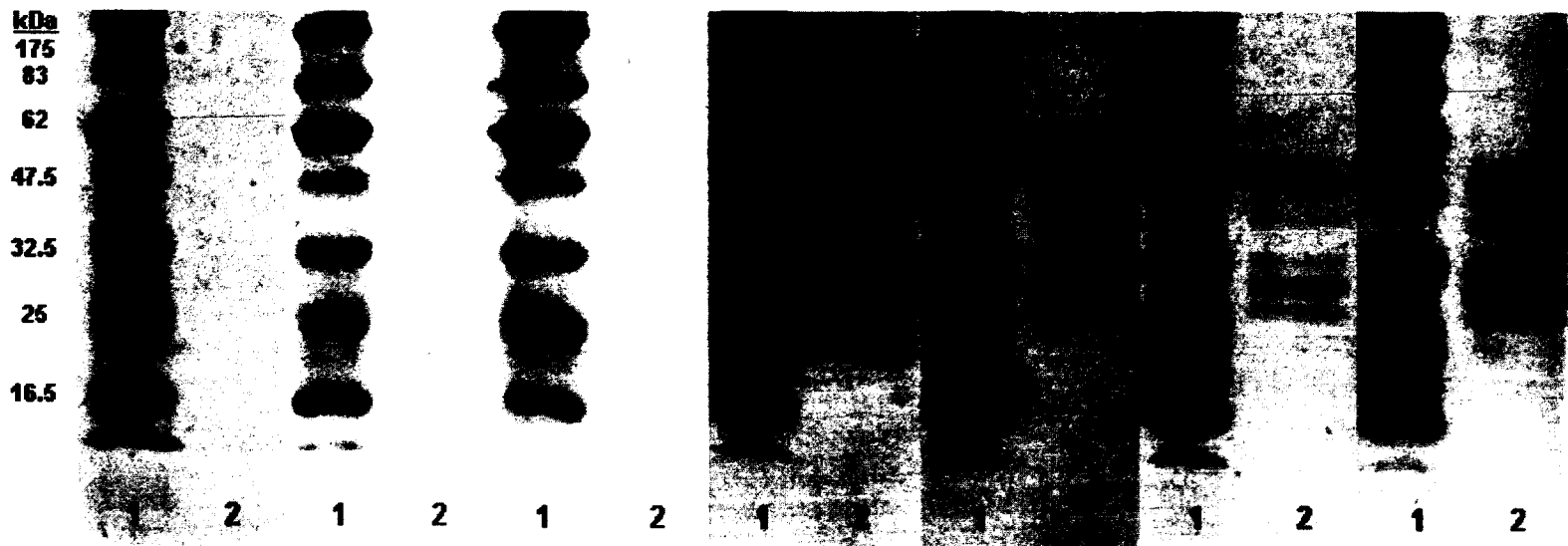


**Figure 2.18: Western blot of Caco-2 and Stx-2 co-immunoprecipitation interactions using STX2-11E10 antibody.** A) SDS-PAGE. Pre-stained molecular weight markers are in Lane 1 and the caco-2 pull down with STX2-11E10 antibody is in Lane 2. B) Negative control Western blot probed with anti-rabbit IgG in the absence of specific rabbit antibodies showing no bands. Lanes are as outlined for A. C) Western blot probed with rabbit anti-Bcl-2 antibody and anti-rabbit IgG. Lanes are as outlined for A. No bands were detected. D) Western blot probed with rabbit anti-Bax antibody and anti-rabbit IgG. Lanes are as outlined for A. E) Western blot probed with rabbit anti-Mcl-1 antibody and anti-rabbit IgG. Lanes are as outlined for A. F) Western blot probed with rabbit anti-Bcl-X<sub>L</sub> antibody and anti-rabbit IgG. Lanes are as outlined for A. G) Western blot probed with rabbit anti-Bcl-w antibody and anti-rabbit IgG. Lanes are as outlined for A. All membranes probed with anti-Bax, anti-Mcl-1, anti-Bcl-X<sub>L</sub>, and anti-Bcl-w showed 6 distinct bands with molecular weights between 50kDa and 27kDa indicating that these results are most likely not true protein-protein interactions. Instead, the top and bottom bands (50kDa and 27kDa respectively) correspond to the heavy and light chains of the pull-down antibody (STX2-11E10). The remaining 4 bands present at approximately 48kDa, 40kDa, 32kDa, and 28kDa are hypothesized to be complexes of Stx-2 and/or cross-reactions of the antibody with unknown caco-2 proteins (48kDa and 40kDa), whole Stx-2 A-subunit remaining in the caco-2 lysate (32kDa), and Stx-2 that was processed by the caco-2 cells and reduced to the A1 fragment (28kDa).

## 6.0 Discussion

Understanding what happens to Stx-2 once it has been endocytosed into the cell is critical to finding treatments for patients infected with *E. coli* O157:H7. A study published by Watanabe-Takahashi *et al.* (215) confirmed the importance of intracellular Stx-2 transport to the endoplasmic reticulum in intestinal epithelial Caco-2 cells in order for cytotoxicity to occur. Therefore, it is likely that the cytotoxic mechanisms of action occur in the endoplasmic reticulum or cytosol, where Bcl-2 family proteins are known to reside (4). The goal of these experiments was to assess the interactions of the Bcl-2 family of proteins with Stx-2 in vitro. Previous studies show there is an association between Stx-2, Bcl-2, and the NWGRI peptide that suggested binding of these proteins within a host cell by way of the BH1 domain (190). As a result, it was hypothesized that Stx-1 and Stx-2 interact with the Bcl-2 family of proteins by way of the NWGRL or NWGRI amino acid motifs, respectively. In particular, Stx-2 should interact with Bcl-2, Bcl-X<sub>L</sub>, Mcl-1, A1, Bax, and Bak based upon the pentameric sequence of its NWGRI. Bcl-2, Bcl-X<sub>L</sub>, Bax, and Bak are known to be located in the endoplasmic reticulum and cytosol of cells (73, 107, 137, 178).

The data from the Stx protein sequence analysis suggested that Stx-1 shared the NWGRL sequence only with Bcl-w, a pro-survival protein not originally within the scope of these experiments. As such, it was decided that only the Stx-2 interactions would be investigated since it is associated with the more serious form of HUS (18, 145, 179, 196). These data also indicated that Stx-2 shared the NWGRI sequence with Bcl-2, Bcl-X<sub>L</sub>,



Mcl-1, and A1, all of which are pro-survival proteins containing BH1 and BH2 domains (2). Finally, the sequence analysis suggested that the pro-apoptotic proteins Bax and Bak did not share either of these sequences, but rather they shared with each other a sequence of NWGRV. The last amino acid of each of these three pentameric sequences (NWGRI, NWGRL, and NWGRV) is isoleucine, leucine, and valine. These amino acids are nonpolar, aliphatic (do not contain nitrogen, oxygen, or sulfur in the side chain) and are hydrophobic molecules (132). The structures between valine and leucine have a higher similarity than isoleucine, and in terms of size, valine is the smallest of the three molecules. This may provide a binding advantage to proteins containing valine such as Bax and Bak by creating a binding site with the least amount of steric hindrance; thus giving these pro-apoptotic proteins the ability to interact with more molecules than their pro-survival counterparts and so encourage apoptosis. This is true especially if Stx-2 is binding these pro-survival counterparts. Although not examined as part of this work, Stx-1 may preferentially bind with Bax and Bak due to the amino acid structure similarity between valine and leucine, leading to an increase in free intracellular pro-survival proteins thus encouraging cell survival. It is possible that these interactions may explain why Stx-2 induces higher virulence compared to Stx-1 in patients with EC or HUS (18, 145, 179, 196).

Previous studies by Suzuki *et al.* (190) used human hepatoma HepG2 cells that overexpressed human Bcl-2 to study the interaction between Bcl-2 and Stx-2. Hepatocytes are not typically associated with Stx-2 pathogenesis, therefore the investigation of protein-protein interactions between Stx-2 and the Bcl-2 protein family

in the studies described herein used Caco-2 cells as the model cell line. These cells are epithelial cells of the human colon where colonization of *E. coli* O157:H7 typically occurs (152). The susceptibility of Vero and Caco-2 cells to a semi-pure preparation of Stx-2 with a total protein concentration of 3.07 mg/mL was confirmed in these studies and even though the cytotoxic effects were not as dramatic as that of Vero cells, distinct effects were observed. Previous studies by Garred *et al.* (55) have noted that the disulfide bond responsible for stabilizing the Stx-2 A-subunit also prevents dissociation of the A1 fragment from the toxin-receptor complex during transport, therefore it is critical this dissociation occurs properly to ensure toxin activity. The A-subunit of the semi-purified toxin was cleaved when subjected to trypsin treatment to produce an A1 and A2 fragment that matched the expected molecular weights of 28 kDa and 4 kDa, respectively. This cleavage mimicked the actual cleavage by Furin that occurs within cells and confirmed that the toxin would indeed function as expected once taken into the cells.

Data indicated that Caco-2 cells expressed Bcl-2, Bcl-X<sub>L</sub>, Bax, and an unknown protein corresponding to the molecular weight of Bak, however an antibody specific for Bak was not available to confirm its identity. Mcl-1 and Bcl-w were confirmed to be absent. It is important to bear in mind that detection of these pro-survival and pro-apoptotic proteins was taken at a specific point in time while the expression of the Bcl-2 family proteins is known to vary during the lifespan of the cell (163). No true protein interactions were observed between Stx-2 and Bcl-2, Bcl-X<sub>L</sub>, or Bax, however one band in the far western blot was detected in both the control and test membranes at approximately 55 kDa and this indicated that there was a cross reaction between the

mouse anti-Stx2 antibody (STX2-11E10) and an unknown protein in the Caco-2 lysate. There was an increase in the intensity of this band on the test membrane which could indicate possible binding of Stx-2 to this unknown protein, but confirmation of this interaction was not obtained using co-immunoprecipitation. There may be alterations to the Bcl-2 family proteins, such as phosphorylation, that occur within the cell during a potential interaction that can impact the binding of these proteins as has been observed in other studies (42, 83). Clearly, these alterations do not occur when the proteins have been immobilized on a PVDF membrane prior to their interaction.

The data gathered by Suzuki *et al.* (190) showed a direct correlation of Bcl-2 and Stx-2 in HepG2 cells using far Western blot and co-immunoprecipitation, however the molecular weight of these complexes and the methods used for co-immunoprecipitation were not given, making it difficult to verify the validity of this data. In addition, the effects of Bcl-2 overexpression on protein binding within the host cell are unknown. It is possible that excess concentrations of Bcl-2 lead to an interaction with Stx-2 that would not normally occur during *E. coli* O157:H7 infection.

The data gathered in this study did not show clear evidence that protein interactions occurred between Stx-2 and Bcl-2, Bcl-X<sub>L</sub>, or Bax, using either the far Western blot or co-immunoprecipitation methods, despite the previous data obtained by Suzuki *et al.* (190). This suggests that Stx-2 does not directly interact with Bcl-2, Bcl-X<sub>L</sub>, or Bax in colonic epithelial cells.

## CHAPTER 3

### IMPACT OF STX-2 ON NEUTROPHIL APOPTOSIS AND NECROSIS

#### 1.0 Abstract

Hemolytic Uremic Syndrome (HUS) is a severe complication in children and the elderly that frequently follows infection with *Escherichia coli* O157:H7. Stx-2 is a potent toxin produced by this pathogen, and it has been identified as a key player in kidney failure associated with HUS (131). Stx-2 may inhibit neutrophil apoptosis (118); however, this has yet to be confirmed (51). If true, this would have the effect of Stx-2-carrying neutrophils remaining in the bloodstream and tissues longer than normal, thus exacerbating the potential for tissue damage. Apoptosis is under the control of the Bcl-2 family of proteins (2, 46, 226). These consist of both pro-death (Bax) and pro-survival (Mcl-1) proteins. In the present study, it is hypothesized that Stx-2 decreases the normally rapid rate of neutrophil apoptosis by binding to the pro-apoptotic protein Bax resulting in a higher concentration of unbound pro-survival proteins such as Mcl-1, thus leading to an extended neutrophil lifespan. Stx-2 interactions with the Bcl-2 family proteins may occur through the amino acid motif, NWGRI, found in Stx-2 as well as in a highly conserved region of the Bcl-2 family proteins. In order to test this hypothesis, Stx-2 was harvested from *E. coli* O157:H7 and applied to human neutrophils. At intervals of 0, 6, 12, 18, 24, 48, and 72 h, samples were assayed using a cell death detection kit to

determine the impact Stx-2 had on neutrophil apoptosis rates. Data indicated that there was a significant difference in neutrophil apoptosis rates ( $p < 0.05$ ,  $n=9$ ) up to and including 12 h after the neutrophils were exposed to Stx-2. These data suggest that Stx-2 delays neutrophil apoptosis by a mechanism other than binding to Bcl-2, Bcl-X<sub>L</sub>, Bax, Bcl-w or Mcl-1.

## **2.0 Introduction**

According to the Centers for Disease Control (CDC), *Escherichia coli* O157:H7 causes 73,000 illnesses per year (159). Primary symptoms include hemorrhagic colitis (HC) but Hemolytic Uremic Syndrome (HUS), a potentially severe, often life-threatening, complication of *E. coli* O157:H7 infection, may also occur in the elderly and children under 5 years of age. Typically, HUS presents as non-idiopathic, non-immune hemolytic anemia, thrombocytopenia, acute renal failure, and occasionally central nervous system (CNS) manifestations and may lead to death (148, 156). Stx-1 and Stx-2 are major toxins produced by *E. coli* O157:H7 and they serve to increase the virulence of this organism. Stx-2 is a 74 kDa, AB<sub>5</sub> structured toxin consisting of alpha-beta motifs. The A subunit has a molecular mass of 32 kDa and each B subunit chain is 7.7 kDa (138). The role of the B subunit pentamer is to attach to the globotriaosylceramide (Gb<sub>3</sub>) receptor on host cells. After the toxin is endocytosed into the cell, it is transported to the Golgi apparatus, endoplasmic reticulum, and cytosol (59, 80, 169, 191). The A subunit is cleaved into 2 fragments within clathrin-coated pits by furin (a membrane bound protease) (56). The A2 fragment remains attached to the B subunit and is degraded by the

cell (170). The A1 fragment is the enzymatically active portion of the toxin and has been shown to elicit a necrotic response by preventing host-cell protein synthesis (47). In addition, it is thought that this fragment may also play a role in the apoptotic pathway once it is retrograde-transported into the cytoplasm of the host cell.

Apoptosis (programmed cell death) is a normal function of cells. The process is mediated by the Bcl-2 protein family (2, 46). These proteins consist of anti-apoptotic (pro-survival) and apoptotic (pro-death) proteins that possess conserved homology domains. It is through these conserved homology domains that these proteins interact with each other, and the ratio of protein type (pro-survival vs. pro-death) determines the fate of the cell (46).

Human neutrophils routinely undergo relatively rapid apoptosis and have a typical circulating lifespan of 6-18 hours (3, 67, 173, 213). Approximately  $10^{10}$  neutrophils are produced daily, and these account for 45-75% of the total white blood cell count (28). During infection, neutrophils are the first responders capable of phagocytosing invading pathogens, foreign cells, toxins, and viruses and, in an attempt to clear the infection, release reactive oxidative intermediates (28).

Previous studies have shown conflicting results on whether neutrophil apoptosis is delayed following exposure to Stx-2. Liu *et al.* (118) concluded that Stx-2 derived from *E. coli* O157:H7 exhibited both a dose- and time- dependent inhibition of spontaneous neutrophil apoptosis, possibly involving the protein kinase C pathway. Flagler *et al.* (51)

was unable to demonstrate a Stx-2 and neutrophil interaction nor did they observe an altered apoptosis rate when these cells were exposed to 1 µg/mL of Stx-1 or Stx-2. Suzuki *et al.* (190) reported that Bcl-2 bound Stx-2. Further analysis of the Bcl-2 protein family (Chapter 2, pg. 56-57) has also indicated that Stx-2 may bind with multiple Bcl-2 family members through a conserved NWGRI amino acid motif, however no binding was detected between Stx-2 and Bcl-2, Bcl-X<sub>L</sub>, or Bax using Caco-2 cells. The timing (delay or otherwise) of human neutrophil apoptosis was examined in this study over the course of 72 h following exposure to supernatant fluid from *E. coli* O157:H7, strain 90-2380; a strain that produces Stx-2.

### **3.0 Hypothesis**

Stx-2 influences neutrophil apoptosis by a mechanism unrelated to Bcl-2, Bcl-X<sub>L</sub>, Bax, Bcl-w or Mcl-1 binding, leading to a decrease in the baseline apoptosis rate and thereby extending neutrophil lifespan.

### **4.0 Materials and Methods**

#### **4.1 Verification of Stx Genes**

Four strains of *E. coli* O157:H7 (Appendix A, 1.0) were analyzed for the presence of either the *stx1* or *stx2* gene by polymerase chain reaction (PCR) using primer sequences published by Wang *et al.* (210) and shown in Table 3.1. Strains 90-2380

(*stx2+*), 95-2157 (*stx1+*), 43895 (*stx1+*, *stx2+*), and 43888 (*stx1-*, *stx2-*) were evaluated. DNA from each strain was extracted from a loopful of bacterial cells which were resuspended in 20 $\mu$ L of lysis buffer. The samples were heated in boiling water for 15 min and 180 $\mu$ L of sterile, nuclease-free water was added to each sample and then centrifuged at 13,000 rpm for 5 min. The supernatant fluid was used as the template DNA for the PCR assay. For each sample, a 25 $\mu$ L PCR reaction was prepared using 2 $\mu$ L of template DNA, 1 $\mu$ L of each primer (forward and reverse), 10 $\mu$ L PCR master mix (Promega, Madison, WI) and 11 $\mu$ L nuclease-free water. The samples were held at 94°C for 5 min and run for 30 cycles consisting of denaturation at 94°C for 30 sec, annealing at 54°C for 1 min, and extension at 72°C for 1 min. Upon conclusion of the cycling, the samples were held at 72°C for 10 min for a final extension. Five  $\mu$ L of each PCR product was loaded onto a 2.5% agarose gel along with 3.3 $\mu$ L of nuclease-free water and 1.7 $\mu$ L of 6x gel loading dye (Promega). In addition, 1.6 $\mu$ L of a 100 base pair (bp) marker was loaded into the first and last lane with 10.9 $\mu$ L nuclease-free water and 2.5 $\mu$ L 6x gel loading dye. The gel was run at 100 volts for 30-45 min.

#### **4.2 Isolation of Stx-2 Supernatant**

*E. coli* O157:H7 strain 90-2380 was grown overnight in 300mL Luria Burtani (LB) broth (Appendix A, 2.2) at 37°C, and 10mL samples were placed in Petri dishes in a BSL-2 biosafety cabinet. The lids were removed and the cultures were exposed to ultraviolet (UV) light for 30 min. After UV exposure, the cultures were incubated for an



**Table 3.1: Primer Sequences for the Detection of *stx1* and *stx2* Courtesy of Wang *et al.* (210)**

Primers	Sequence (5' to 3')	Gene Location	Amplicon Size (bp)	Genbank #
Stx1-a	TCTCAGTGGGCGTTCTTATG	777-796	338	M17358
Stx1-b	TACCCCTCAACTGCTAATA	1114-1095		
Stx2-a	GCGGTTTTATTTGCATTAGC	1228-1247	115	X07865
Stx2-b	TCCCGTCAACCTTCACTGTA	1342-1323		

additional 48 h and centrifuged at 16,000 x g for 15 min at 4°C. Each supernatant fluid was collected and filtered through Pall Acrodisc® 0.2µm Supor® membranes.

### **4.3 Verification of Stx-2 Presence and Activity**

Ten µL of sterile-filtered *E. coli* O157:H7 strain 90-2380 supernatant was analyzed to ensure that Stx-2 was present. This was achieved by sodium dodecyl sulfate polyacrylamide gel electrophoresis (SDS-PAGE) and western blot using STX2-11E10 antibody raised in mice against Stx-2. Triplicate samples were diluted 1:2 in sample preparation buffer (Appendix A, 4.13), boiled at 95°C for 5 min, loaded onto a 6% stacking / 12% resolving gel (Appendix A, 4.16), placed in a buffer tank containing SDS-PAGE running buffer (Appendix A, 4.14), and run at 180V for 30-40 min. One set of samples was placed in Coomassie Blue (Appendix A, 4.17) to stain for at least 2 h and then destained with destain buffer (Appendix A, 4.18). The remaining samples were cut to give two gels. These were aligned onto polyvinylidene fluoride (PVDF) membranes (Millipore Corp, Bedford, MA), and placed into a transfer sandwich consisting of fiber pads and filter paper. The transfer sandwich was placed into a buffer tank containing Tris-glycine buffer (TGB) (Appendix A, 4.19) and proteins were transferred at 60V for 4-5 h. After transfer, the membranes were blocked overnight in Tris buffered saline (TBS) containing 5% dehydrated skim milk (Appendix A, 4.20) at 4°C. On the following day, one membrane was incubated for 2 h at room temperature with 10µg/mL of the STX2-11E10 antibody (Toxin Technology, Sarasota, FL) and the other remained in blocking buffer as a negative control. The membranes were rinsed 3 times in Tris buffered saline

containing 0.05% Tween (TTBS) (Appendix A, 4.22) for 10 min each at room temperature, and subsequently treated with anti-mouse alkaline phosphatase-conjugated antibody (Sigma-Aldrich, St. Louis, MO) for 2 h at room temperature. The membranes were rinsed twice in TTBS followed by a rinse in TBS for 10 minutes each at room temperature. The blots were developed with nitro-blue tetrazolium chloride / 5-bromo-4-chloro-3'-indolyphosphate p-toluidine salt (NBT/BCIP) tablets (Roche Diagnostics, Indianapolis, IN).

The activity of the Stx-2 toxin was investigated using 50 $\mu$ L of sterile-filtered *E. coli* O157:H7 strain 90-2380 supernatant fluid. This was added to a 25cm<sup>2</sup> tissue culture flask with a confluent monolayer of African green monkey kidney (Vero) cells grown in DMEM modified with 5% fetal bovine serum (FBS) (Appendix A, 5.5) and allowed to incubate for 4 days. After incubation was complete, the flasks were observed at 100x magnification using an inverted phase-contrast microscope for rounded, refractile, or floating cells (indicating dead cells).

#### **4.4 Isolation and Cultivation of Neutrophils**

Neutrophils were collected from human blood using a leukocyte separation method (Sigma Aldrich) (Fig. 3.1). In a 15mL conical tube, 3mL of Histopaque™ 1119 was added followed by 3mL of Histopaque™ 1077, and 6mL of human blood. The tubes were centrifuged at 700 x g for 30 min at room temperature. After centrifugation, layer “B-Granulocytes” was aseptically transferred using a pipette to a 50mL conical tube and

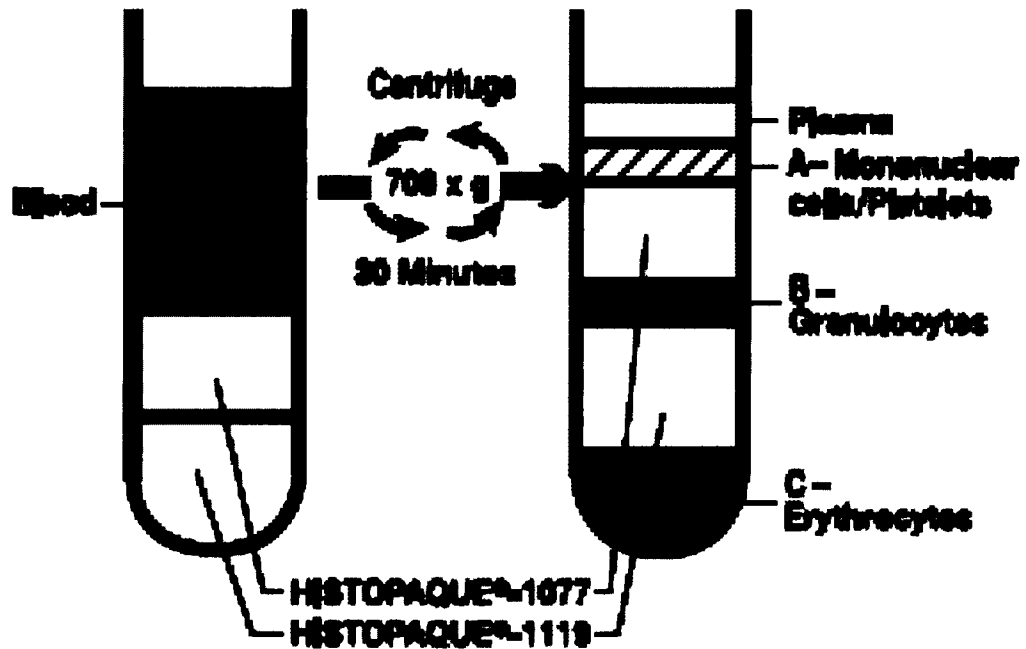


**Figure 3.1: Sigma-Aldrich leukocyte separation method.** This diagram is courtesy of Sigma-Aldrich. Whole blood is separated into its cellular components by differential centrifugation. Neutrophils are present in layer B – Granulocytes.

an equal volume of Hank's Balanced Salt Solution (HBSS) without magnesium or calcium ions was added. The cells were washed by centrifugation at 250 x g for 10 min at room temperature. Once centrifugation was complete, the supernatant fluid was removed and the pellet resuspended in 12mL of 0.2% NaCl for 30 sec to lyse any remaining blood cells. The fluid phase of the suspension was then returned to an isotonic state with the addition of 12mL of 1.6% NaCl and centrifuged at 250 x g for 10 min. This was repeated until all red blood cells were lysed. Neutrophils were subsequently stained with trypan blue (Appendix A, 5.2) to assess viability and counted using a hemocytometer. Neutrophils were seeded into a 96-well plate at a concentration of 10,000 cells in 200  $\mu$ L RPMI-1640 (Appendix A, 5.4) per well, and incubated at 37°C in a 5% CO<sub>2</sub> atmosphere.

#### **4.5 Assessment of Bcl-2 Family Proteins in Neutrophils**

Isolated neutrophils were examined for Bcl-2 family protein content at three different time points after isolation: 0 h chosen to represent healthy neutrophils, 6 h to represent early apoptotic neutrophils, and 18 h corresponding to late apoptotic neutrophils. At each time point the neutrophils were lysed with 1mL Nonidet P-40 (NP-40) lysis buffer, treated with leupeptin (10 $\mu$ M), and examined using SDS-PAGE and western blot analysis for Mcl-1, Bax, Bcl-2, Bcl-w, and Bcl-X<sub>L</sub>. Negative controls using secondary antibody only were also performed to ensure there was no cross-reaction of the antibody to the lysate.

Triplicate or quadruplicate samples (as determined by the number of test

antibodies) were diluted 1:2 in sample preparation buffer, boiled at 95°C for 5 min, loaded onto a 6% stacking / 12% resolving gel, placed in a buffer tank containing SDS-PAGE running buffer, and run at 180V for 30-40 min. One set of samples was placed into Coomassie Blue to stain for at least 2 h and then destained with destain buffer. The remaining samples were cut, aligned onto PVDF membranes (Millipore Corp), and placed into a transfer sandwich consisting of fiber pads and filter paper. The transfer sandwich was placed into a buffer tank containing TGB and proteins were transferred at 60V for 4-5 h. After transfer, the membranes were blocked overnight in TBS containing 5% dehydrated skim milk at 4°C. On the following day, each test membrane was incubated with the appropriate antibody (1.5µg/mL of Anti-Mcl-1 [R&D Systems Cat#AF828]; 2µL/mL of Anti-Bax [Biologend Clone Poly 6251]; 2µL/mL of Anti-Bcl-2 [Biologend Clone Poly 6119]; 2.5µg/mL of Anti-Bcl-w [Biovision Cat #3034-100]; or 2.5µg/mL of Anti-Bcl-X<sub>L</sub> [Biovision Cat #3312-100]) while the negative control membrane remained in blocking buffer. The membranes were rinsed 3 times in TTBS for 10 min each at room temperature, and subsequently treated with anti-mouse alkaline phosphatase-conjugated antibody (Sigma-Aldrich) for 2 h at room temperature. The membranes were washed twice in TTBS followed by one rinse in TBS for 10 min each at room temperature. The blots were developed with nitro-blue tetrazolium chloride / 5-bromo-4-chloro-3'-indolyphosphate p-toluidine salt (NBT/BCIP) tablets (Roche Diagnostics).

#### **4.6 Analysis of Neutrophil Apoptosis & Necrosis Rates when Exposed to Stx-2**

Neutrophil apoptosis and necrosis rates were measured over time at 0, 6, 12, 18, 24, 48, and 72 hours using a cell death detection ELISA kit (Roche Diagnostics). This ELISA system detects fragmented DNA and histone complexes, markers of cell death. Neutrophils were isolated as described previously, a suspension was made containing 50,000 cells/mL and 200 $\mu$ L was dispensed into each well of a 96-well plate (Table 3.2). All samples were tested at each of the time points indicated above. Three sample types were tested in triplicate in 3 individual trials. The negative control consisted of neutrophils only, the media control consisted of neutrophil suspension plus 10  $\mu$ L of LB broth, and the test sample consisted of the neutrophil suspension plus 10 $\mu$ L of Stx-2 supernatant from *E. coli* O157:H7 strain 90-2380.

At each time point, the 96-well plate was centrifuged at 200 x g for 10 min and the supernatant fluids were collected and held at 2-8°C to assay for necrosis. The cell pellet was lysed for 30 min at room temperature with the lysis buffer provided in the kit and the plate was centrifuged again at 200 x g for 10 min. The supernatant fluid was then analyzed for apoptosis. Twenty  $\mu$ L of each supernatant (pre-lysis and post-lysis), positive control (DNA-histone-complex), and background control (incubation buffer) was transferred to a strepavidin coated plate and 80 $\mu$ L of immunoreagent (consisting of incubation buffer, anti-histone biotin, and anti-DNA-POD) was added. The samples were shaken at approximately 300rpm for 2 h at room temperature, rinsed three times with 300 $\mu$ L incubation buffer, and developed with 100 $\mu$ L 2,2'-Azinobis [3-

**Table 3.2: Neutrophil Cell Death Detection Time Point Setup<sup>1</sup>**

96-well Plate Row/Column	1	2	3	4	5	6	7	8	9	10	11	12
A	C	C	C	-	-	-	-	-	-	-	-	-
B	M	M	M	-	-	-	-	-	-	-	-	-
C	T	T	T	-	-	-	-	-	-	-	-	-
D	-	-	-	-	-	-	-	-	-	-	-	-
E	-	-	-	-	-	-	-	-	-	-	-	-
F	-	-	-	-	-	-	-	-	-	-	-	-
G	-	-	-	-	-	-	-	-	-	-	-	-
H	-	-	-	-	-	-	-	-	-	-	-	-

<sup>1</sup> 10,000 cells were added to each well suspended in 200 $\mu$ L RPMI-1640. A separate plate was used for each time point.

**Sample Key:**

- 'C' = Negative Control (nothing added)
- 'M' = Media Control (10  $\mu$ L LB broth added)
- 'T' = Test Sample (10 $\mu$ L Stx-2 supernatant added)
- '-' = Blank well



ethylbenzothiazoline-6-sulfonic acid]-diammonium salt (ABTS). Absorbance was measured at 405nm using a Biorad 3550 microplate reader (Bio-Rad, Hercules, CA).

## **5.0 Results**

### **5.1 Verification of Stx Genes**

An agarose gel containing the PCR products from *E. coli* O157:H7 strains was prepared and it can be seen in Figure 3.2. Amplicons were not obtained for *stx1* or *stx2* in the negative control reactions (Lanes 2 & 3), indicating that the primers were specific to the target genes. Amplicons were also not obtained for *stx1* or *stx2* in *E. coli* O157:H7 strain 43888 reactions (Lanes 4 & 5), indicating that neither toxin is produced in this strain. An amplicon was not obtained for *stx1* (Lane 6) but an amplicon of approximately 115 bp in size was obtained for *stx2* (Lane 7) in the *E. coli* O157:H7 strain 90-2380 reactions, indicating that only Stx-2 is produced in this strain. An amplicon of approximately 340 bp in size was obtained for *stx1* (Lane 8), but no amplicon was obtained for *stx2* (Lane 9) in *E. coli* O157:H7 strain 95-2157 reactions, indicating that only Stx-1 is produced in this strain. Finally, amplicons of approximately 340 bp for *stx1* and 115 bp for *stx2* (Lanes 10 & 11) were obtained for *E. coli* O157:H7 strain 43895 reactions, indicating that both Stx-1 and Stx-2 are produced in this strain. These data confirmed that the strains in question did indeed carry the genes for the toxins as outlined in Appendix A.

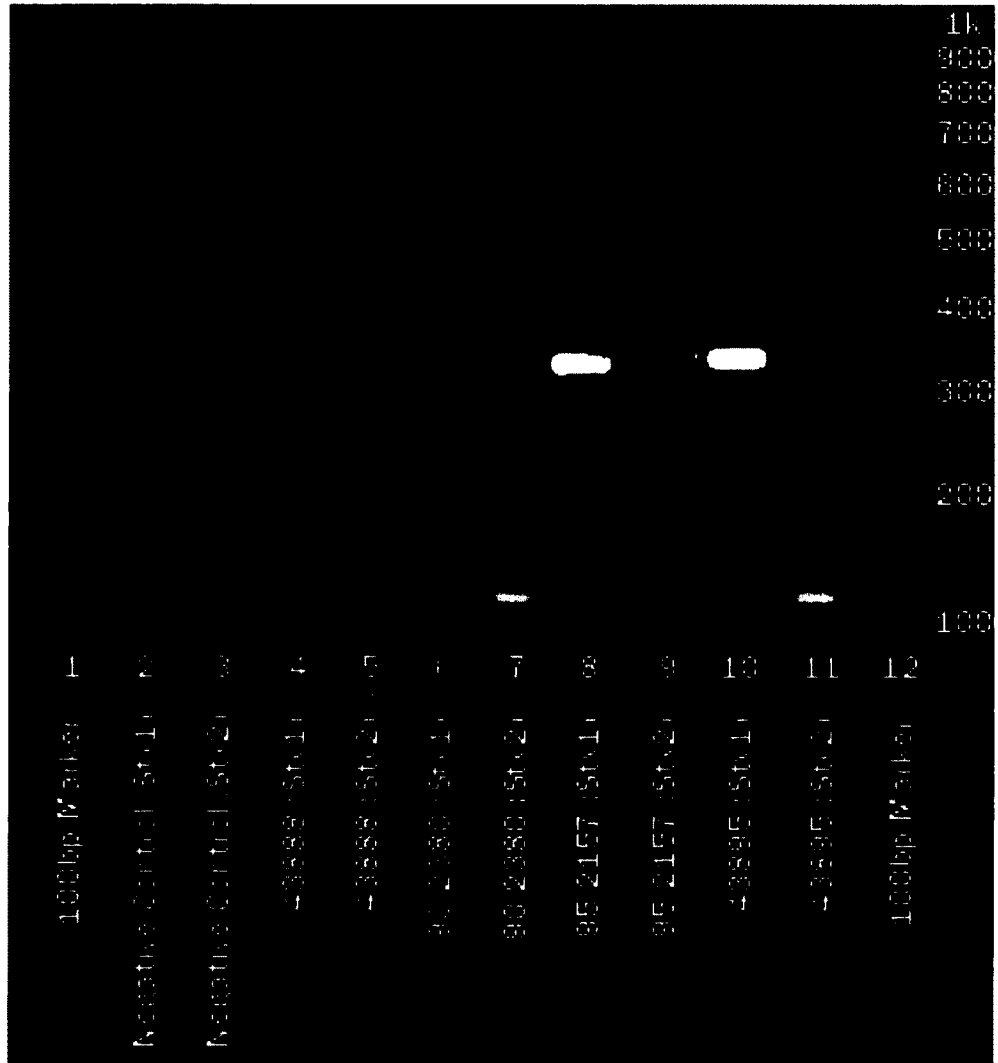


**Figure 3.2: Agarose gel analysis of PCR products.** DNA from four strains of *Escherichia coli* O157:H7 was amplified with primers specific to *stx1* and *stx2*. The 100 base pair ladder is in Lanes 1 and 12, negative controls for *stx1* and *stx2* are in Lanes 2 and 3, strain 43888 for *stx1* and *stx2* is in Lanes 4 and 5, strain 90-2380 for *stx1* and *stx2* is in Lanes 6 and 7, strain 95-2157 for *stx1* and *stx2* is in Lanes 8 and 9, and strain 43895 for *stx1* and *stx2* is in Lanes 10 and 11. Amplicons were detected for *stx1* in strains 95-2157 and 43895 and *stx2* in strains 90-2380 and 43895.

## 5.2 Verification of Stx-2 Presence and Activity

SDS-PAGE and Western blot of Stx-2 containing supernatant fluid from *E. coli* O157:H7 strain 90-2380 were prepared in Figure 3.3. Panel A shows the SDS-PAGE gel in which multiple bands were observed. However, the most important one has been highlighted by the box and corresponds to the molecular mass of Stx-2. Panel B shows a Western blot of the negative control membrane that was treated only with secondary antibody and as expected, no bands were detected. Panel C illustrates the Western blot probed with the anti-stx-2 antibody, STX2-11E10, raised in mice and the anti-mouse alkaline phosphatase conjugated secondary antibody. There was one band visible at approximately 25 kDa confirming the presence of the A-subunit of Stx-2. A second band was visible around the 47.5KD marker and this may be Stx-2 that was not completely denatured during sample processing.

Stx-2 was confirmed in the sterile-filtered supernatant and was active and able to elicit a cytotoxic response in Vero cells exposed to 50 $\mu$ L of supernatant fluid. Examination of treated and untreated monolayers at 100x final magnification showed active Stx-2 (Figure 3.4). In the control without supernatant added, a confluent cell monolayer with intact cells was observed (Fig. 3.4, A), while in the sample with 50 $\mu$ L of Stx-2 supernatant fluid, many rounded, refractile (bright), and floating cells were seen as well as a decrease in confluency of the monolayer (Fig. 3.4, B). These studies confirmed the presence of the Stx-2 gene and the production of Stx-2 by *E. coli* O157:H7 strain 90-2380.

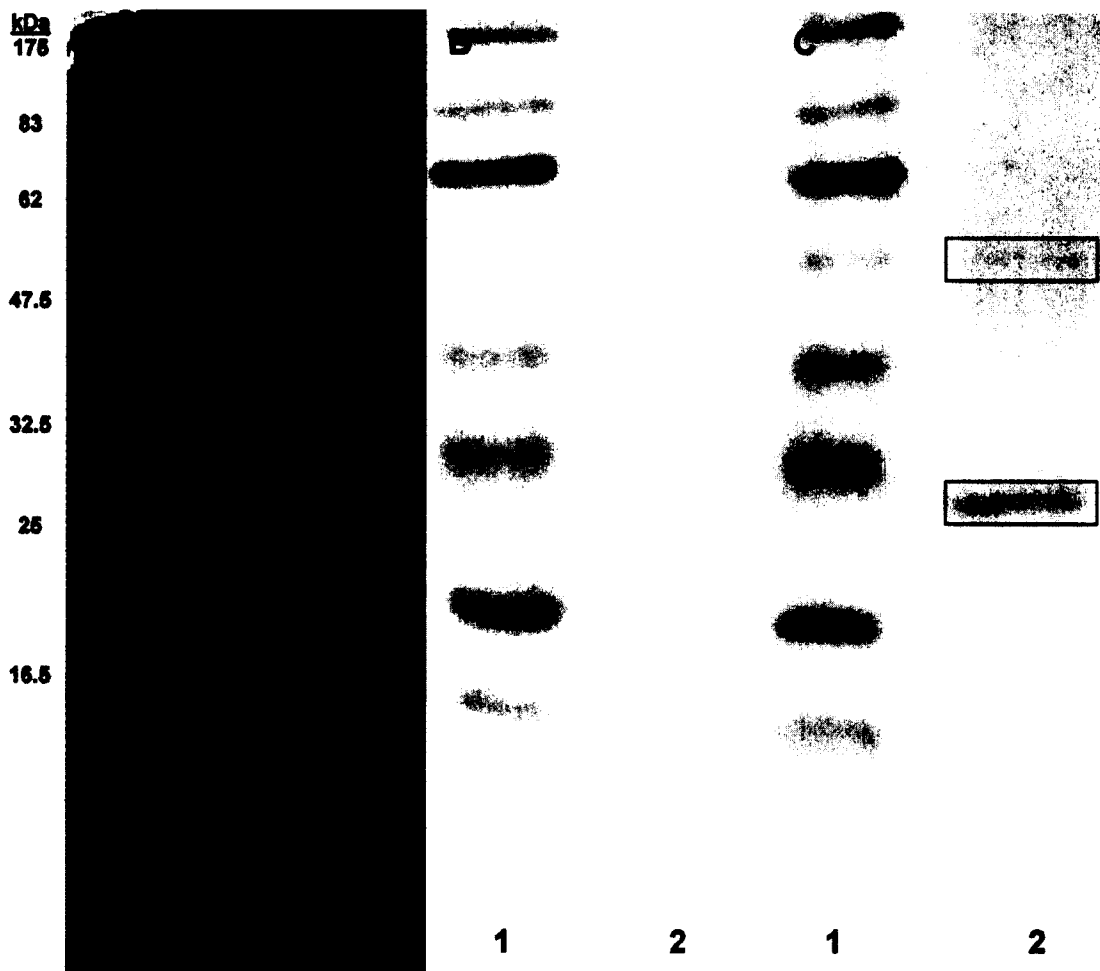


**Figure 3.3: Western blot confirmation of Stx-2.** Pre-stained molecular weight markers are in Lane 1 and the supernatant fluid containing Stx-2 is in Lane 2. A) SDS-PAGE. The band noted in the box represents Stx-2. B) Negative control Western blot probed with anti-mouse IgG only, in the absence of Stx-2 specific antibody. No bands were detected. C) Western Blot probed with STX2-11E10 mouse antibody and anti-mouse IgG. Stx-2 was seen in the boxed area just below the 25 kDa marker. The additional band is believed to be Stx-2 that was not completely denatured during sample processing.

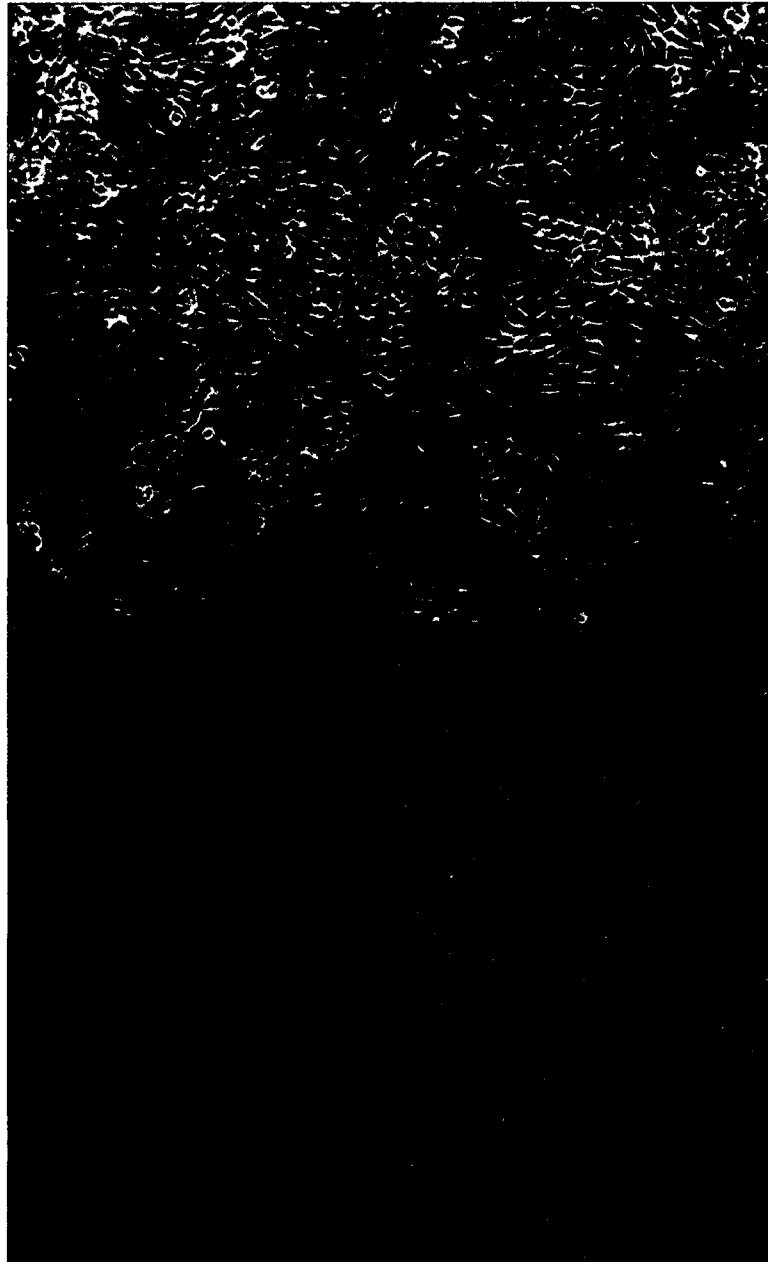


**Figure 3.4: Biological activity of semi-purified Stx-2.** A) Vero cells without *E. coli* O157:H7 strain 90-2380 supernatant fluid viewed at 100x magnification. B) Vero cells after 4 days incubation with 50 $\mu$ L *E. coli* O157:H7 strain 90-2380 supernatant fluid viewed at 100x magnification. Cytotoxic effects typical of Stx-2 are shown by the large number of rounded and refractile cells and loss of the cell monolayer confluency.

### **5.3 Assessment of Bcl-2 Family Proteins in Neutrophils**

SDS-PAGE and Western blot of the neutrophil lysates were prepared at times 0, 6, and 18 h to determine the presence of Bcl-2 family proteins. Figure 3.5 shows the results of these SDS-PAGE and Western blot analyses. In the figure, horizontal panel A illustrates the SDS-PAGE and Western blot for the assessment of Mcl-1 while horizontal panel B shows the assessment of Bax and Bcl-2, and finally, horizontal panel C presents the results for Bcl-w and Bcl-X<sub>L</sub>. In panel A, four bands were observed, one in the control blot and one at each time point on the blot probed with anti-Mcl-1. The first band on both blots observed at time 0 h corresponding to freshly isolated neutrophils was approximately 60 kDa in size; however, this was very faint and may have resulted from non-specific antibody binding due to high protein concentration of this band. Two identical bands at 26 kDa were seen in the 6 and 18 h preparations. Neither of these bands corresponded to the expected size of Mcl-1 (37 kDa for the short form and 42 kDa for the long form) (111, 128); however, these bands did correspond with previously observed similar bands from Caco-2 cells perhaps indicating an antibody cross-reaction with other pro-apoptotic proteins such as Bak, which has an expected molecular weight of 25-28 kDa (58, 111). Thus, it cannot be definitively stated that the neutrophils expressed Mcl-1 at any of the three time points.

In panel B, a band was detected at approximately 62 kDa for both Bax (column 3) and Bcl-2 (column 4) in freshly isolated neutrophils, however this band was also

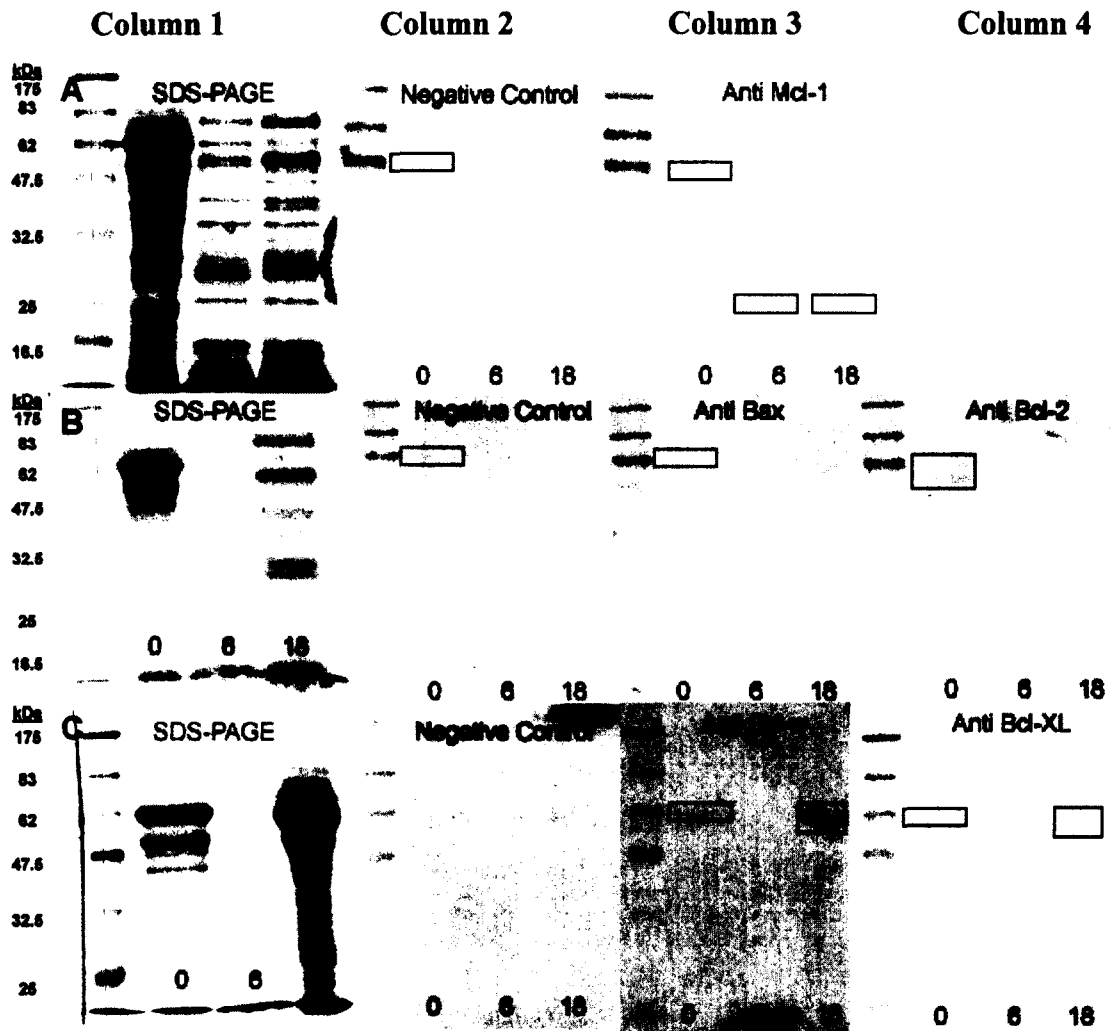


**Figure 3.5: Assessment of Bcl-2 family proteins in neutrophils over 18 hours.** A) SDS-PAGE (column 1) and western blots probed with anti-rabbit IgG (negative control, column 2) and anti Mcl-1 followed by anti-rabbit IgG (anti-Mcl-1, column 3). One non-specific interaction was noted on both blots at 60 kDa, and two bands were noted on the anti-Mcl-1 blot which are indicative of a reaction with an unknown 26 kDa protein, potentially Bak. B) SDS-PAGE (column 1) and western blots probed with anti-rabbit IgG (negative control, column 2), anti-Bax followed by anti-rabbit IgG (anti-Bax, column 3), and anti-Bcl-2 followed by anti-rabbit IgG (anti Bcl-2, column 4). One non-specific interaction was noted on all blots at 60 kDa, and one band representative of Bcl-2 dimers was observed on the blot probed with anti-Bcl-2. C) SDS-PAGE (column 1) and western blots probed with anti-rabbit IgG (negative control, column 2), anti-Bcl-w followed by anti-rabbit IgG (anti-Bcl-w, column 3), and anti-Bcl-X<sub>L</sub> followed by anti-rabbit IgG (anti-Bcl-X<sub>L</sub>, column 4). Two similar bands were observed on the blots probed with anti-Bcl-w and anti-Bcl-X<sub>L</sub> at 60 kDa but this was thought to be a non-specific interaction related to high sample protein load.

observed very faintly in the negative control (column 2). It is believed that neither result was specific for the antibody tested, and probably was the consequence of non-specific secondary antibody binding due to the high protein concentration of this band. In addition, there was a second pronounced band detected on the membrane probed with anti Bcl-2 at approximately 52 kDa. This band does not correspond to the expected size of 26 kDa for Bcl-2, although it is possible that it may represent a dimer of Bcl-2.

In panel C, a faint band was detected for both Bcl-w (column 3) and Bcl-X<sub>L</sub> (column 4) in freshly isolated neutrophils at approximately 60 kDa, however much like that of Mcl-1, it is believed that this may be a result of non-specific antibody binding due to high protein concentrations of this band as seen in the SDS-PAGE (column 1). A similar phenomenon was found in the 18 h sample and the same band was again observed for both samples due to the higher protein load as seen in the SDS-PAGE. Neither result was specific for the antibody tested, nor were Bcl-w and Bcl-X<sub>L</sub> detected in any neutrophil samples.

In summary Bcl-2 was the only protein detected in this study. These studies were not repeated since the only bands observed were associated with non-specific binding due to high protein load. Loading less protein would not increase the chances of protein detection. A study by Moulding *et al.* indicated that freshly isolated neutrophils produced Bax, Mcl-1, and very low levels of Bcl-2 (128). Even though the results in the present study do not match, it is believed that these proteins may be present at some point during the cell's lifespan and potential interactions could still occur.



#### **5.4 Analysis of Neutrophil Apoptosis & Necrosis Rates when Exposed to Stx-2**

The cell death detection ELISA was used to determine, over time, the apoptosis and necrosis rates induced by Stx-2 in neutrophils. For this assay, absorbance readings were adjusted for background interference by subtracting the average background control value from the results on each respective plate and these results were then standardized by expressing the final result as a percent of the positive control provided in the kit for each assay. This was done in order to assess the rates of apoptosis/necrosis over time since the assay development time was not standardized between plates. Necrosis rates have been summarized in Figure 3.6 and apoptosis rates in Figure 3.7. Once the data had been standardized across all tests, a t-test was performed to assess the effects of the culture medium (LB broth) and the Stx-2-containing supernatant fluid on neutrophil apoptosis and necrosis rates. The negative control (without medium or toxin) was compared to the LB medium control (medium only), and the medium control was compared to the Stx-2 containing supernatant fluid to determine if significant differences between neutrophil apoptosis and necrosis rates were observed.

There was a significant decrease ( $p < 0.05$ ) between the negative control and medium control necrosis rates up to and including 18 h suggesting that the medium may have provided some protective effect to the neutrophils against necrosis. There was also a significant decrease ( $p < 0.05$ ) in neutrophil necrosis rates between the medium control and the neutrophils exposed to Stx-2 up to and including 18 h. At 24 h, the necrosis rates

### Neutrophil Necrosis Rates Over Time

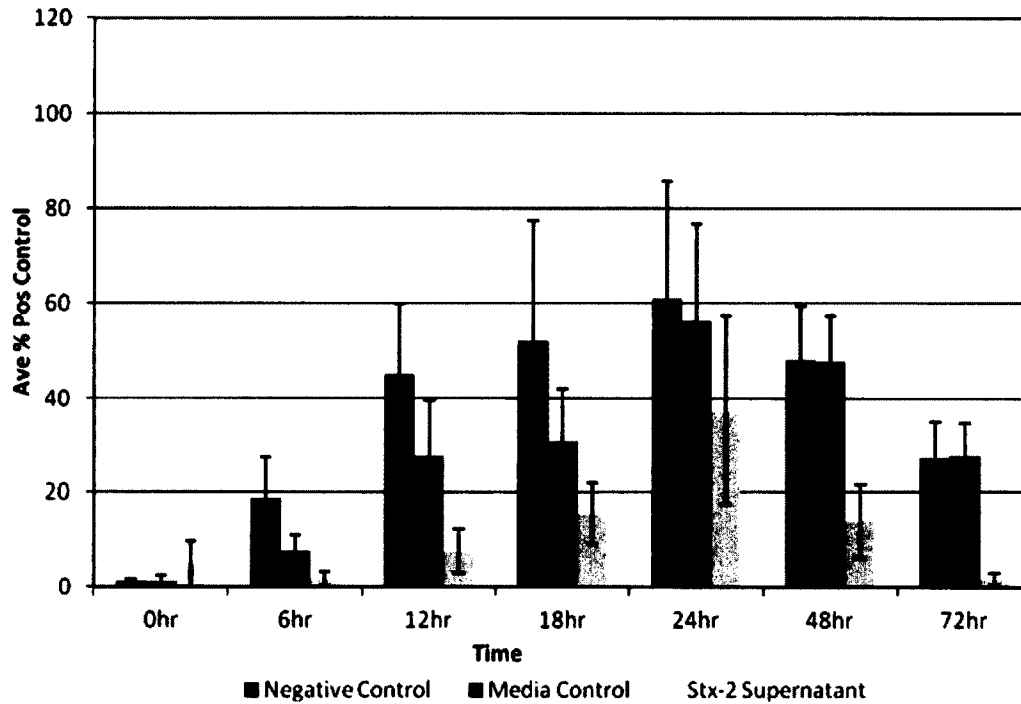


**Figure 3.6: Necrosis rates of neutrophils exposed to Stx-2 supernate for 72 h.** Data are presented as the average percent necrosis when compared to the positive assay control. Error bars represent the standard deviation calculated between the averaged triplicates. Necrosis rates of neutrophils exposed to Stx-2 were significantly reduced ( $p < 0.05$ ) at all time points except 24 h.

### Neutrophil Apoptosis Rates Over Time

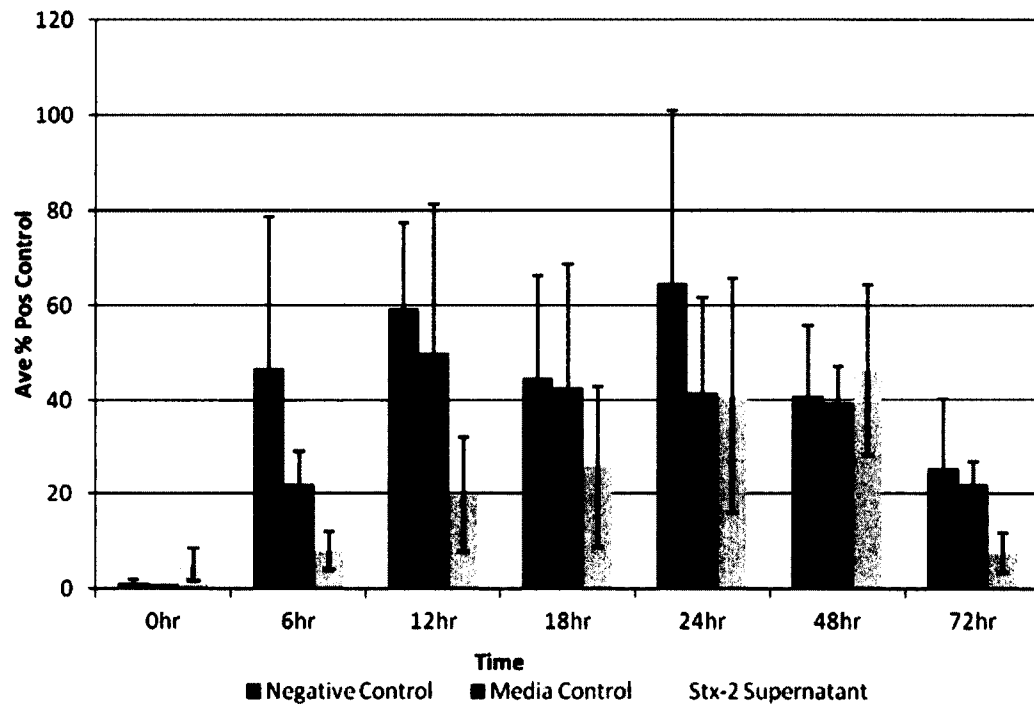


**Figure 3.7: Apoptosis rates of neutrophils exposed to Stx-2 supernate for 72 h.** Data are presented as the average percent apoptosis when compared to the positive assay control. Error bars represent the standard deviation calculated between triplicates. Apoptosis rates of neutrophils exposed to Stx-2 were significantly reduced ( $p < 0.05$ ) at the 6 h and 12 h time points.

were similar, but decreased at 48 and 72 h, most likely due to the simultaneous increase in apoptosis.

There were no significant differences observed between the negative control and medium control apoptosis rates; however, there was a significant decrease ( $p < 0.05$ ) in neutrophil apoptosis rates between the medium control and the neutrophils exposed to Stx-2 up to and including 12 h. After that point, the apoptosis rates were similar to the controls.

In summary, the data obtained during this study show that neutrophils exposed to Stx-2 have less necrosis than the untreated controls at all time points except 24 h, where the rates are similar. In addition, the data show that these neutrophils exhibit a delay in apoptosis for the first 12 h of exposure, followed by an increase in apoptosis that matched the controls for the remaining time points tested. This shows that Stx-2 did play a role in increasing neutrophil lifespan. The exact mechanism of how this occurs is still to be elucidated but it may potentially be due to the interaction of Stx-2 and pro-apoptotic proteins other than those tested in this study.

## **6.0 Discussion**

It is thought that neutrophils may provide a way for Stx-2 to be distributed throughout the body during infection (195). Therefore, during pathogenesis, it is critical that neutrophils remain within the circulation and tissues to provide maximum

distribution of the toxin, and indeed this is observed (37, 208). Previous studies on the impact of Stx-2-induced neutrophil apoptosis have shown conflicting results. Liu *et al.* (118) observed a time- and dose-dependent delay in spontaneous neutrophil apoptosis when exposed to Stx-2 whereas Flagler *et al.* (51) did not. The goal of the present experiments was to assess the effects that Stx-2-containing *E. coli* O157:H7 supernatant fluid had on neutrophil apoptosis and necrosis rates. A cell death detection ELISA was used to obtain simultaneous neutrophil apoptosis and necrosis rates following exposure to Stx-2. It was hypothesized that Stx-2 influences neutrophil apoptosis by a mechanism not related to Bcl-2, Bcl-X<sub>L</sub>, Bax, Bcl-w or Mcl-1 binding (as determined in Chapter 2) and this leads to a decrease in the baseline apoptosis rate, thereby extending neutrophil lifespan. A study by Moulding *et al.* (128) indicated that freshly isolated neutrophils produced Bax, Mcl-1, and very low levels of Bcl-2. The data obtained in this study showed that neutrophils did not contain Bcl-X<sub>L</sub>, Bax, Mcl-1 or Bcl-w at 0, 6, and 18h after isolation, but did contain Bcl-2 dimers in freshly isolated neutrophils. In addition, an unknown protein was detected in an antibody cross-reaction that corresponded to the molecular weight of Bak as seen previously with Caco-2 cells (Chapter 2), however an antibody specific for Bak was not available to confirm this. This data and data generated previously by Moulding *et al.* (128) and Ruemmele *et al.* (163) support the notion that Bcl-2 family protein expression does vary during the lifespan of the cell. This may influence the interactions of Stx-2 within the cell depending upon at what point the toxin is endocytosed.

Data produced in this study also showed that medium used to grow *E. coli* O157:H7 was protective against Stx-2 induced necrosis but had no effect on Stx-2 induced neutrophil apoptosis. The reasons for this are unknown, but it is suspected that the extra nutrients in the medium allowed the cells to live longer or prevented oxidative burst from occurring. Bax was not detected in neutrophils in this study, yet a delay in Stx-2 induced apoptosis up to and including 12 h was observed ( $p < 0.05$ ). It is possible that Stx-2 bound with the unknown protein suspected to be Bak, in turn reducing neutrophil apoptosis. A similar study performed with *Helicobacter pylori* water extracts showed that the expression of Bax and Bak was upregulated in HL-60 cells, human promyelocytic leukemia cells which can differentiate into neutrophil-like cells, during neutrophilic differentiation (98). If Bak was upregulated in the experiments performed here, it may provide high concentrations of protein for Stx-2 to bind to in the endoplasmic reticulum or cytosol, thus leaving the anti-apoptotic proteins free to promote cell survival. Stx-2 induced neutrophil necrosis was significantly decreased ( $p < 0.05$ ) at all time points except 24 h, showing an overall trend of reduced cellular necrosis. No difference in the oxidative burst of neutrophils was found between patients with and without HUS (74), therefore it seems that inhibition of oxidative burst could not be the cause of reduced necrosis. It is possible, that if Stx-2 bound Bax within the endoplasmic reticulum, there would be less Stx-2 available to elicit N-glycosidase activity on the ribosomes of the cell, which is the primary cause of Stx-2 induced cellular necrosis (47).

Overall, the data from these assays confirm that a delay in neutrophil apoptosis occurs up to and including 12 h after exposure to Stx-2 and a significant decrease in

necrosis at all time points except 24 h after exposure. It is theorized that this may be a result of Stx-2 triggering apoptosis within the endoplasmic reticulum of the cell.

## CHAPTER 4

### GENERATION OF MUTANT STX-2 G225A

#### 1.0 **Abstract**

A mutation was generated in the gene encoding Stx-2 in *E. coli* O157:H7 at amino acid position 225 using splicing by overlap extension PCR (PCR SOE). The objective of this mutation was to change this sequence from NWGRI to NWARI, thereby abolishing the ability of the mutated Stx-2 to trigger apoptosis and so demonstrating a decreased pathogenicity for the toxin. The mutated gene was ligated to pBR322 and transformed into *E. coli* O157:H7 strain 43888 (a strain that produced neither Stx-1 nor Stx-2) in order to express and purify the toxin and determine its pathogenicity compared to native Stx-2.

#### 2.0 **Introduction**

Apoptosis (programmed cell death) is a normal function of cells. It is mediated by the Bcl-2 protein family (46). These proteins are classified into two groups based on functional activity; they are either pro-survival or pro-apoptosis proteins, and they are divided into three subfamilies: the Bcl-2 subfamily, the Bax subfamily, and the BH3 subfamily (2). The Bcl-2 subfamily promotes cell survival while the Bax and BH3 subfamilies promote apoptosis (2). All of these proteins share at least one of four possible



conserved motifs (BH1, BH2, BH3 or BH4) known as Bcl-2 homology domains which play a role in the function of the proteins (2). The proteins with the closest resemblance to Bcl-2 contain all four homology domains (2). On the other hand, the Bax and BH3 subfamilies differ in their homology domain content despite their shared pro-apoptosis cellular role and contain only the BH3 domain (95).

The process by which Bcl-2 family proteins regulate apoptosis has been documented (4, 151, 177, 181). In essence, BH3-only proteins are activated by signaling pathways, and then these activate either proapoptotic proteins or inhibit antiapoptotic proteins (or both). Activated proteins form oligomers in the mitochondrial outer membrane leading to the release of cytochrome c and other proapoptotic proteins, unless they are inhibited by Bcl-2 proteins. These proteins then activate caspases which eventually cause the cell to undergo apoptosis (4, 151, 177, 181).

Both pro-survival and pro-apoptosis proteins have the ability to form homo- and heterodimers with each other, suggesting that the relative concentration of the proteins may play a role in the outcome of the cell's fate (144). It is known that the BH1, BH2, and BH3 domains strongly influence the formation of homodimers and heterodimers, and that these regions create an elongated hydrophobic cleft into which a BH3 amphipathic alpha helix can bind (129, 171). Heterodimerization is not required for pro-survival function, but it is required for the pro-apoptosis function of proteins in the BH3 subfamily and possibly also those of the Bax subfamily (2, 36, 95). It is noted that these

proteins may bind in a preferential fashion, as it has been shown that not all pro-apoptosis and pro-survival proteins interact (2).

Zhang *et al.* (227) investigated the mechanisms of Bcl-2 protein family interactions under normal and apoptotic conditions in an effort to understand homo- and heterodimerization regulation. Their work was accomplished by performing mutations to different areas of the Bcl-2 protein and measuring the resultant ability to form homo- and heterodimers. Results of the study determined that Bcl-2 dimerization involved the use of an acceptor and donor surface shown in Figure 4.1. The acceptor surface was able to bind both Bcl-2 and Bax; however, the donor surface was only able to bind Bcl-2 (227).

Suzuki *et al.* (190) investigated the binding capabilities of Bcl-2 and Stx-2 and determined that these proteins were able to bind. It is suspected that this interaction occurs by mimicking the Bcl-2 protein family. The pentameric amino acid sequence, NWGRI that is common to both Bcl-2 and Stx-2 occurs within the center of the acceptor surface described by Zhang *et al.* (227). In order to determine if Stx-2 has the ability to heterodimerize with the Bcl-2 family of proteins within neutrophils in the manner described by Zhang *et al.* (227), the present study was designed to examine the rate at which neutrophil apoptosis occurs when a point mutation at the center of the aligning NWGRI sequence (G225A) is introduced by PCR SOE, a method first described by Higuchi *et al.* (70).

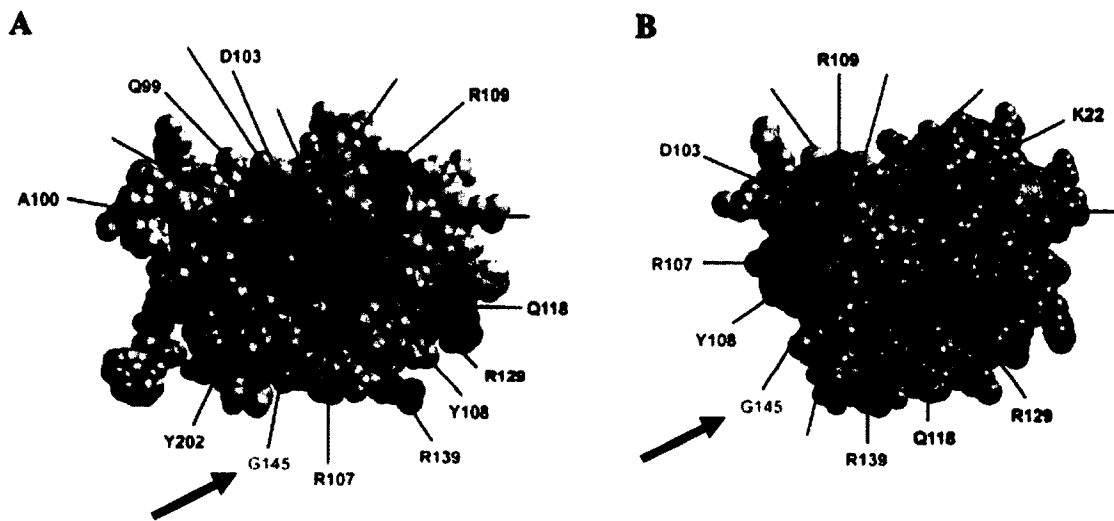


**Figure 4.1: The Bcl-2 dimerization interface.** This diagram, adapted from Zhang *et al.* (227), was modeled based upon previously determined Bcl-2 core structure (150). Two distinct surfaces were discovered: A) the acceptor surface and B) the donor surface. The middle of the binding surface is located at the G145 position (see arrows). This portion of the molecule is the same portion that contains the pentameric sequence found in Stx-2 (NWGR).

### **3.0 Hypothesis**

An introduced mutation of glycine to alanine at amino acid position 225 in Stx-2 will result in reduced virulence of Stx-2 due to the inability of the toxin to trigger the apoptotic pathways, thereby interrupting the normal apoptotic process in these cells.

### **4.0 Materials and Methods**

Authorization to complete this recombinant DNA project was obtained from the UNH Institutional Biosafety Committee (IBC) under approval number R:2-2007 (Appendix D).

#### **4.1 Determination of *E. coli* O157:H7 strain 43888 Susceptibility Profile to Ampicillin**

A minimum inhibitory concentration (MIC) assay was performed to determine the antibiotic susceptibility pattern of *E. coli* to ampicillin. A solution of ampicillin (Sigma Aldrich, St. Louis, MO) was prepared at a concentration of 25mg/mL in sterile PBS and filter sterilized. Thirty two  $\mu$ L of this solution was added to 1968 $\mu$ L of LB broth to give a final concentration of 400 $\mu$ g/mL ampicillin. A 1:2 dilution series was prepared in duplicate by transferring 1mL of this broth to a new tube containing 1mL fresh LB broth. Six tubes were prepared with ampicillin concentrations ranging from 400 $\mu$ g/mL to 25 $\mu$ g/mL. A positive control was also prepared without ampicillin. Each tube was

inoculated with 50 $\mu$ L of an overnight culture of *E. coli* O157:H7 strain 43888 and incubated at 37°C for 24 h. Two hundred  $\mu$ L of each suspension from the 6 tubes containing ampicillin and bacteria were added in duplicate to the wells of a 96 well plate, and the opacity was read at 600nm on a Biorad 3550 microplate reader (Biorad, Hercules, CA).

## **4.2 Creation of a Recombinant Plasmid: Mutant *stx2* with Vector pBR322**

### **4.2.1 Primer Design and PCR**

The sequence of Stx-2 producing *E. coli* O157:H7 VT2-Sakai (NCBI Reference Sequence NC\_002695.1) was used for primer design. The *stx2* gene comprises two parts; the Stx-2 subunit A gene and the Stx-2 subunit B gene with a promoter region. The genome encompassing these genes is depicted in Figure 4.2. Primers were created that cloned the sequence from base pair 1266525 to 1268219, and these are shown in Table 4.1. Primers were designed using the GeneFisher2 Interactive PCR Primer Design program on the Bielefeld University Bioinformatics Server (BiBiServ) and checked with NetPrimer software (Premier Biosoft, Palo Alto, CA). Primers were synthesized (Integrated DNA Technologies, Coralville, IA) and purified using standard desalting processes. The complete sequence that was cloned is listed in Figure 4.3. NEBcutter (New England Biolabs, Ipswich, MA) was used to determine the appropriate enzyme restriction sites to add to the end of the primer sequences to allow for insertion into

pBR322 (Figure 4.4), thereby eliminating the risk of cutting the cloned sequence during insertion.

#### **4.2.2 Mutation of *stx2* using PCR SOE**

*E. coli* O157:H7 strain 90-2380 was grown overnight at 37°C, and genomic DNA was isolated using the UltraClean™ Microbial DNA Isolation Kit (MoBio Laboratories Inc., Carlsbad, CA) following the manufacturer's instructions. An alternative lysis method was used in order to reduce the amount of DNA shearing and lessen the chance of unwanted damage to large DNA. PCR was performed using genomic DNA and the primers listed in Table 4.1. The mutagenesis primers were designed using Stratagene's Quick Change Primer Design Program (<http://www.stratagene.com/qcprimerdesign.com>) and the suggested guidelines for mutagenesis primer design in the QuickChange® Site-Directed Mutagenesis kit instruction manual. Primers were synthesized by Integrated DNA Technologies and purified using polyacrylamide gel electrophoresis (PAGE).

An *stx2* mutant construct was generated by PCR SOE following published protocols by Horton *et al.* (71) using the Expand Long Template PCR system and supplied Buffer 3 (Roche Applied Science, Indianapolis, IN). The outer forward and reverse primers contained engineered restriction enzyme sites (SphI and EcoRI respectively) to aid in directional cloning of the cloned *stx2* gene. Internal, complementary forward and reverse SOE primers containing a single base pair mutation (G to C, resulting in a change in protein coding from glycine to alanine) were also

designed (Table 4.1). The first two PCR amplicons were generated with 1) Stx2-SphI-F with G225A\_reverse mutagenic primer and 2) G225A forward mutagenic primer with Stx2-EcoRI-R, using the *stx2* gene (amplified with Expand HiFi plus enzyme) as a template. Following amplification, the PCR products were gel purified (Epock Biolabs, Missouri City, TX), combined at equal molarity, and a second round of SOE was performed using the purified PCR products as a template and outer primers only (Stx2-SphI-F and Stx2-EcoRI-R). A second PCR amplification was conducted with the purified SOE product to increase the yield, and the amplicon was gel purified prior to cloning. The expected size of the mutant *stx2* gene was 1743bp.

#### **4.2.3 Insertion of Mutant *stx2* into pBR322**

In order to insert the mutant *stx2* gene into pBR322 (see Fig. 4.5), both the SOE product and pBR322 were double digested with SphI and EcoRI (New England Biolabs) at 37°C for 2 h in the manufacturer's suggested buffer and this was then heat inactivated at 65°C for 20 min. This was performed to remove the tetR gene, allowing screening for inserts by sensitivity to tetracycline. Once digestion was complete, the mutant *stx2* gene was ligated into pBR322 using a 3:1 insert:vector ratio with T4 ligase (New England Biolabs). The ligation was performed overnight with thermal cycling alternating between 10°C for 30 sec and 30°C for 30 sec. This temperature-cycle ligation method was demonstrated to have higher cloning efficiency than the typical method (121).

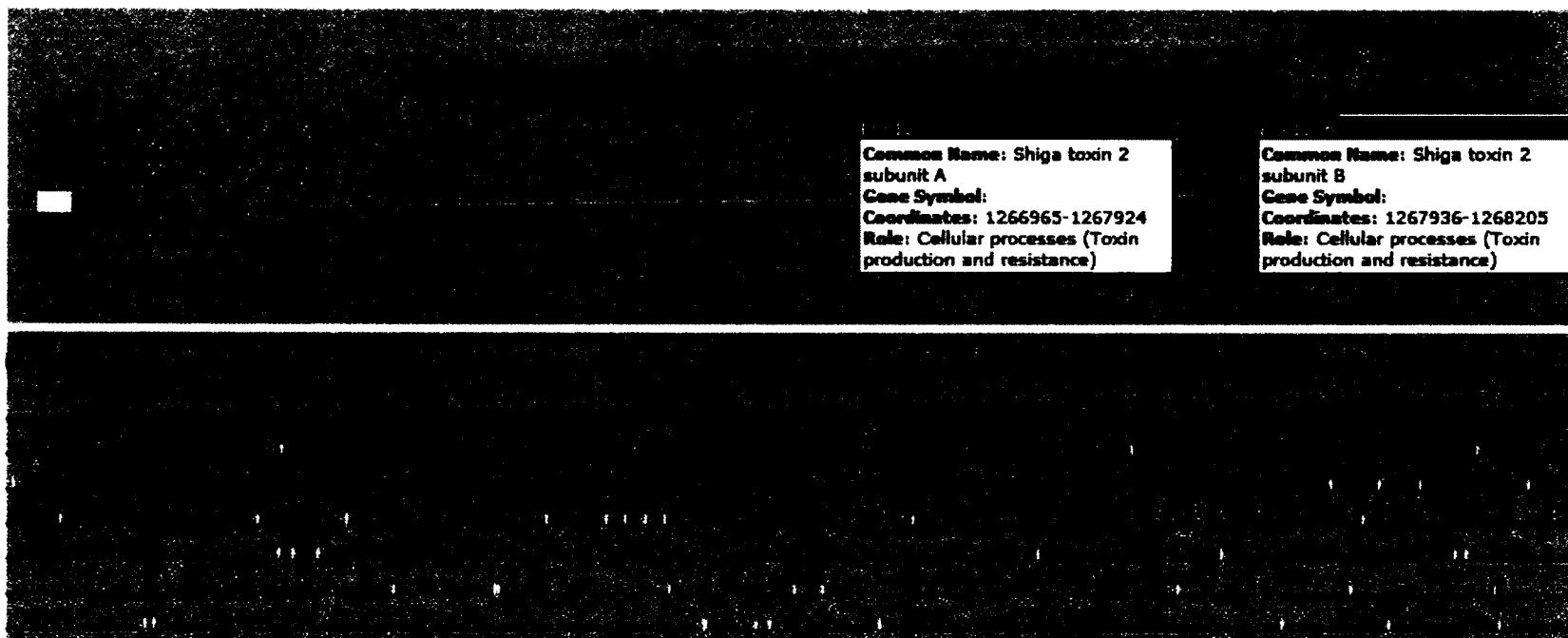


**Figure 4.2: Genome map of the *stx2* gene.** This genome map (base pair 1266525 - 1268219) is courtesy of the Comprehensive Microbial Resource (<http://cmr.jcvi.org/tigr-scripts/CMR/ComrHomePage.cgi>). This map is derived from the *Escherichia coli* O157:H7 VT2-Sakai strain (NCBI Accession # NC\_002695) and includes the *stx2* subunit A (base pair 1266965 - 1267924) and *stx2* subunit B (base pair 1267936 - 1268205) genes as well as the upstream sequence containing the gene promoters (base pair 1266525 - 1266924).



**Table 4.1: Primer Sequences**

<b>Name</b>	<b>Sequence</b>	<b>Description</b>
Stx2-SphI-F	5'- TAT TAA GCA TGC CGG GCG TTT TGA GCA -3'	Forward <i>stx2</i> primer with SphI cutting site
Stx2-EcoRI-R	5'- TAA TGA ATT CGT TAC CCA CAT ACC ACG A -3'	Reverse <i>stx2</i> primer with EcoRI cutting site
G225A <sup>1</sup>	5'- CTC ACT CTG AAC TGG GCG CGA ATC AGC AAT GTG -3'	Forward <i>stx2</i> mutagenesis primer
G225A_antisense <sup>1</sup>	5'- CAC ATT GCT GAT TCG CGC CCA GTT CAG AGT GAG -3'	Reverse <i>stx2</i> mutagenesis primer
pBR322-653-R	5'- TCT CAA GGG CAT CGG TC -3'	Reverse pBR322- <i>stx2</i> vector-insert junction primer
pBR322-4327-R	5'- GCC TCG TGA TAC GCC TA -3'	Reverse pBR322- <i>stx2</i> vector-insert junction primer
Stx2-A <sup>2</sup>	5'- GCG GTT TTA TTT GCA TTA GC -3'	Forward <i>stx2</i> primer
Stx2-B <sup>2</sup>	5'- TCC CGT CAA CCT TCA CTG TA -3'	Reverse <i>stx2</i> primer

<sup>1</sup> These mutagenesis primers were designed using Stratagene's quick change primer design program.

<sup>2</sup> These primers were previously designed by Wang *et al.* (210).

GTGCAATTGGCGTTGAGCTGGAGAG**EGGGCGTTTTGAGCAG**GACGGTCAGGGAAGT  
 TCAGAATGTAGTCAGTCAGAACGGATGATATTGCAGGATTAGTTACGTACCGTTATT  
 ATCCTGCGCCCGGCCCTTTAGCTCAGTGGTGAGAGCGAGCGACTCATAATCGCCAGG  
 TCGCTGGTTCAAATCCAGCAAGGGCCACCATATCACATACCGCCATTAGCTCATCGG  
 GACAGAGCGCCAGCCTTCGAAGCTGGCTGCGCGGGGTTGAGTCCTCGATGGCGGTC  
 CATTATCTGCATTATGCGTTGTTAGCTCAGCCGGACAGAGCAATTGCCTTCTGAGCAA  
 TCGGTCACTGGTTCGAATCCAGTACAACGCGCCATATTTATTTACCAGGCTCGCTTTT  
 GCGGGCCTTTTTTATATCTGCGCCGGGTCTGGTGCTGATTACTTCAGCCAAAAGGAAC  
 ACCTGTATATGAAGTGTATATTATTTAAATGGGTACTGTGCCTGTTACTGGGTTTTTC  
 TTCGGTATCCTATTCCCAGGAGTTTACGATAGACTTTTCGACCCAACAAAGTTATGTC  
 TCTTCGTTAAATAGTATACGGACAGAGATATCGACCCCTCTTGAACATATATCTCAG  
 GGGACCACATCGGTGTCTGTTATTAACCACACCCACCGGGCAGTTATTTTGCTGTGG  
 ATATACGAGGGCTTGATGTCTATCAGGCGGTTTTGACCATCTTCGTCTGATTATTGA  
 GCAAATAATTTATATGTGGCCGGGTTTCGTTAATACGGCAACAAATACTTTCTACCG  
 TTTTTCAGATTTTACACATATATCAGTGCCCGGTGTGACAACGGTTTTCCATGACAACG  
 GACAGCAGTTATACCACTCTGCAACGTGTGCGACGCGCTGGAACGTTCCGGAATGCAA  
 ATCAGTCGTCACCTACTGGTTTCATCATATCTGGCGTTAATGGAGTTCAGTGGTAATA  
 CAATGACCAGAGATGCATCCAGAGCAGTTCTGCGTTTTGTCAGTGTACAGCAGAAG  
 CTTACGCTTCAGGCAGATACAGAGAGAATTCGTCAGGCACTGTCTGAAACTGCTC  
 CTGTGTATACGATGACGCCGGGAGACGTGGAC**CTCACTCTGAACTGGGGCCGAAT**  
**CAGCAATGTG**CTTCCGGAGTATCGGGGAGAGGATGGTGTGAGAGTGGGGAGAATAT  
 CCTTTAATAATATATCAGCGATACTGGGGACTGTGGCCGTTATACTGAATTGCCATCA  
 TCAGGGGGCGCGTTCTGTTTCGCGCCGTGAATGAAGAGAGTCAACCAGAATGTCAGAT  
 AACTGGCGACAGGCCTGTTATAAAAATAAACAATACATTATGGGAAAGTAATACAG  
 CTGCAGCGTTTCTGAACAGAAAGTCACAGTTTTTATATACAACGGGTAAATAAAGGA  
 GTTAAGCATGAAGAAGATGTTTATGGCGGTTTTATTTGCATTAGCTTCTGTTAATGCA  
 ATGGCGGCGGATTGTGCTAAAGGTAATAATTGAGTTTTTCCAAGTATAATGAGGATGAC  
 ACATTTACAGTGAAGGTTGACGGGAAAGAATACTGGACCAGTCGCTGGAATCTGCA  
 ACCGTTACTGCAAAGTGCTCAGTTGACAGGAATGACTGTCAATCAAATCCAGTAC  
 CTGTGAATCAGGCTCCGGATTTGCTGAAGTGCAGTTTAATAATGACTGAGGCATAAC  
 CTGAT**TCGTGGTATGTGGGTAACA**AGTGTAATCTGTGTCACAATTCAGTCAGTTGA  
 CAGTTGCCTGTCAGACTGAGCATTGTGTTAAA

**Figure 4.3: Genomic sequence of *stx2* from *Escherichia coli* O157:H7 VT2-Sakai.** Nucleotides 1266500- 1268300 (forward strand). The forward and reverse primers used to clone the gene are bolded and boxed respectively near the beginning and end of the sequence. The genomic sequence representing the NWGRI protein region has been bolded and shaded.

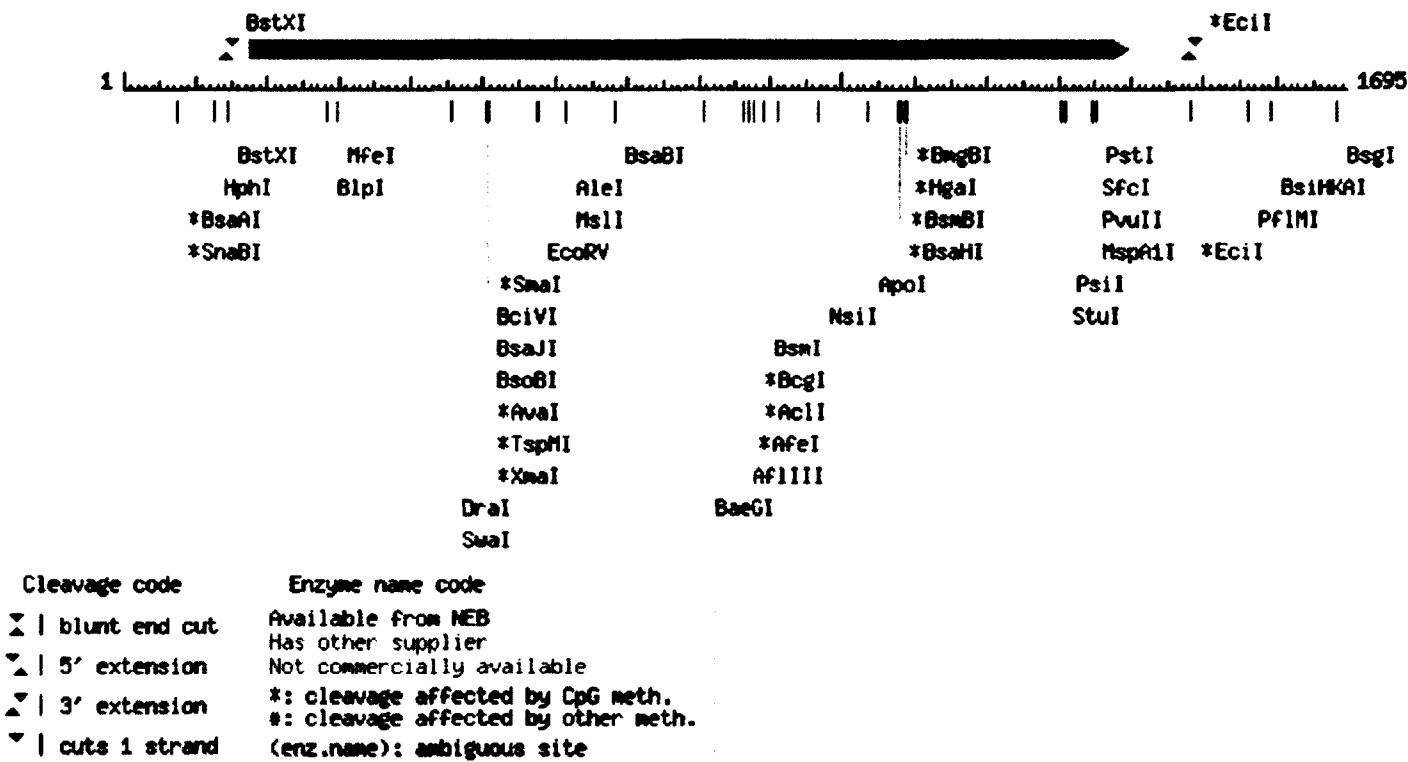


**Figure 4.4: Restriction enzyme map of the cloned *stx2* gene.** This restriction enzyme map (base pair 1266525 - 1268219) is courtesy of NEBcutter (<http://tools.neb.com/NEBcutter2/index.php>) and derived from *Escherichia coli* O157:H7 VT2-Sakai (NCBI Accession # NC\_002695). Available enzyme cutting sites are indicated by cleavage type.

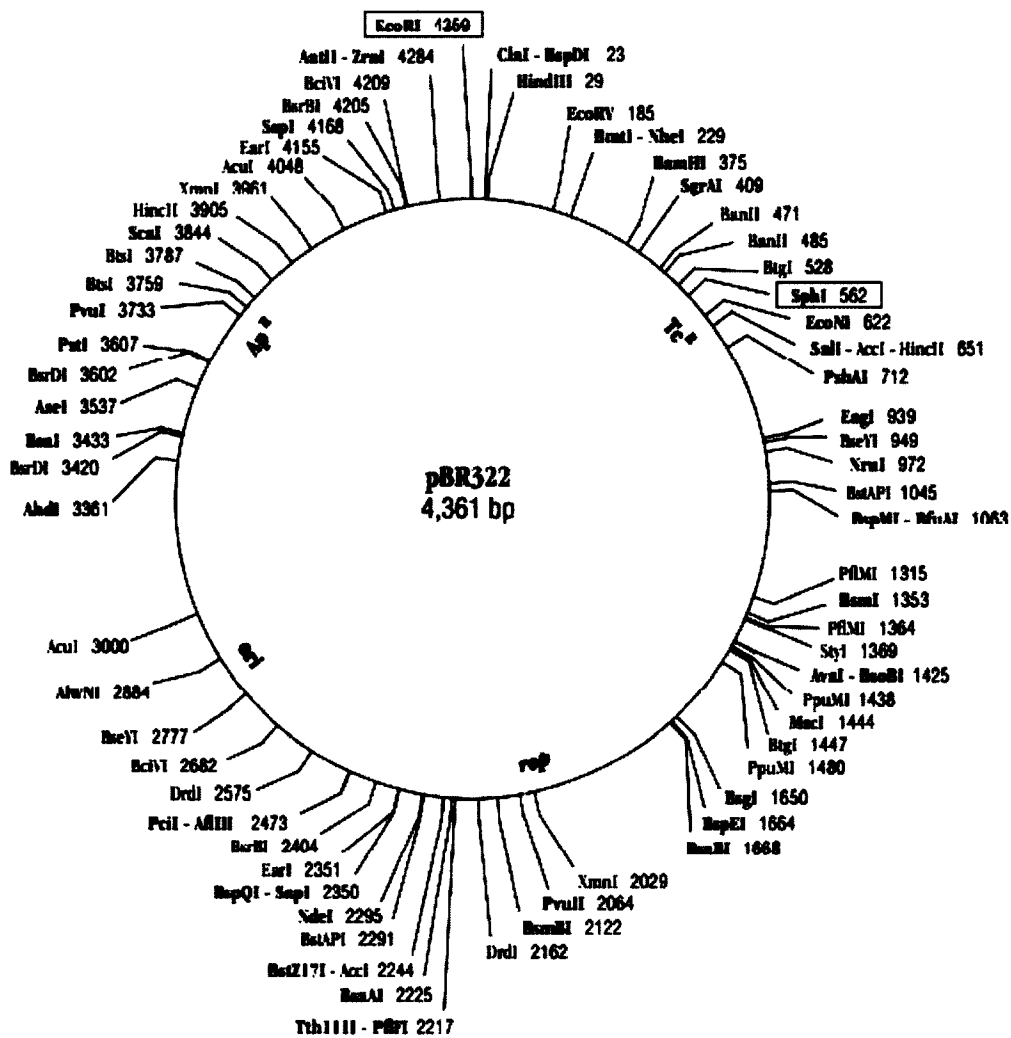


**Figure 4.5: Vector map of pBR322.** This map is courtesy of New England Biolabs. The vector will confer ampicillin and tetracycline resistance to the transformed bacteria without inserts. The mutated *stx2* segment was inserted at the EcoRI and SphI restriction sites, highlighted by the boxes above.

### **4.3 Transformation of the Recombinant Plasmid into *E. coli* O157:H7 Strain 43888**

#### **4.3.1 Preparation of Electrocompetent *E. coli* O157:H7 Strain 43888**

*E. coli* O157:H7 strain 43888 cells were made competent and prepared for electroporation through a series of ice-cold centrifugation and washing steps. Fifty mL of LB broth was inoculated with *E. coli* and allowed to incubate overnight at 37°C with vigorous shaking. On the following day, 1mL of overnight culture was transferred to 200mL of fresh LB broth and the optical density was measured at 600nm. The new culture was placed into the 37°C incubator and monitored hourly until the optical density reached approximately 0.400. At that point, the culture was placed on ice and swirled gently until well chilled. The culture was split in half, placed into 2 x 250mL pre-chilled sterilized centrifuge bottles, and centrifuged at 4,000 x g for 10 min at 4°C. The supernatant was discarded, each cell pellet was washed by resuspending in 200mL sterilized ice-cold water, and the samples were centrifuged again under the same parameters. The cells were washed once more with 100mL sterilized ice-cold water, and centrifugation was repeated a third time. The supernatant was discarded and the pellets were resuspended in 100mL sterilized ice-cold 10% glycerol and combined into one centrifuge tube. A final centrifugation at 4,000 x g for 10 min at 4°C was done and the electrocompetent cells were resuspended in 2mL sterilized ice-cold 10% glycerol. The culture was dispensed into individual microcentrifuge tubes (40µL/tube) and frozen immediately at -80°C.

#### **4.3.2 Electroporation of Electrocompetent *E. coli* O157:H7 Strain 43888 cells with *stx2* and pBR322**

Clean, sterile electroporation cuvettes with a 1mm gap between side walls were placed into an ice bucket and allowed to chill. Each sample was processed separately to ensure DNA degradation did not occur prior to exposure to electrical current. Just before electroporation, four tubes of electrocompetent *E. coli* were removed from the -80°C freezer and allowed to thaw on ice. Two µL of DNA was added to one tube containing thawed electrocompetent *E. coli* cells for each of the sample types listed in Table 4.2. The contents of each tube were subsequently transferred to pre-chilled electroporation cuvettes and immediately placed into the electroporator where 1800 volts were applied for 4 milliseconds. At this time 400µL of SOC medium (Appendix A, 2.7) was added. The suspension was immediately transferred to a sterilized 1.5mL microcentrifuge tube and the cells were allowed to recover at 37°C for 1 h with gentle shaking. Upon completion of the recovery step, each sample was spun at 10,000 x g for 30 sec, resuspended in 100mL fresh SOC medium, and plated as follows: 10µL was spread onto a LB plate as a control to ensure viability of the cells, 90µL was spread onto LB plates containing 100µg/mL ampicillin in triplicate, and 90µL was spread onto a LB plate containing 20µg/mL tetracycline.

**Table 4.2: Samples Electroporated Into *E. coli* O157:H7 strain 43888**

Number	Sample Name
1	Nuclease-free water (negative control)
2	Supercoiled pBR322 plasmid (positive control)
3	stx2 vector only ligation
4	stx2 vector and pBR322 insert ligation

#### 4.4 Verification of Recombinant Plasmid Transformation into *E. coli* O157:H7 Strain 43888

A selection of ampicillin-resistant colonies was patched onto LB agar plates with tetracycline (20µg/mL). The colonies that showed sensitivity to tetracycline were screened with PCR using Stx2-SphI-F and Stx2-EcoRI-R to determine if the mutant *stx2* insert was detected. A plasmid prep and additional PCR reaction using the same primers were also performed to confirm that the cells had the mutant *stx2*-containing plasmid. An additional PCR reaction used cross-junction primers (pBR322-653-R and pBR322-4327-R) to ensure that the mutant *stx2* gene was inserted into the plasmid at the correct location.

Plasmids were purified using the PureYield Plasmid Miniprep System (Promega, Madison, WI) according to the manufacturer's instructions. Plasmid DNA was probed with two sets of primers. Set 1 consisted of Stx2-A and Stx2-B primers, which amplify a 115bp product located within *stx2*. Set 2 consisted of Stx2-B and pBR322-653R primers, which amplify a 1649bp segment that spans the *stx2* insert and pBR322 vector junction.

Sequencing was performed on four clones (L4, L14, L42, and L94) using pBR322-653R and pBR322-4327-R primers. The sequences were blasted using NCBI Blast: Nucleotide Sequence and aligned to *E. coli* O157:H7 strain Sakai, complete genome (Accession # NC\_002695.1) to determine homology to *stx2*.



#### **4.5 Creation of Mutant Clone Stocks**

Overnight cultures of *E. coli* O157:H7 mutant clones were frozen at -80°C in LB broth containing 15% glycerol and 100µg/mL ampicillin.

#### **5.0 Results**

##### **5.1 Determination of *E. coli* O157:H7 strain 43888 Susceptibility Profile to Ampicillin**

The assay was performed with duplicate samples and results are summarized in Table 4.3. No growth was detected in any of the wells containing antibiotic indicating that *E. coli* O157:H7 strain 43888 was inhibited by ampicillin at concentrations greater than or equal to 25µg/mL.

##### **5.2 Creation of a Recombinant Plasmid: Mutant *stx2* with Vector pBR322**

Primer design, PCR SOE, enzyme digestion, and insert-vector ligation were performed and a recombinant plasmid was created as outlined in Figure 4.6. Gel electrophoresis indicated a successful PCR SOE product was obtained with a length of approximately 1734bp, and analysis of the *stx2*-pBR322 recombinant plasmid indicated successful ligation with the expected overall size of approximately 5,500bp.

**Table 4.3: MIC Assay for *E. coli* O157:H7 Strain 43888 and Ampicillin**

Sample Name	Rep #	Results (OD600)					
		0 µg/ml.	25 µg/ml.	50 µg/ml.	100 µg/ml.	200 µg/ml.	400 µg/ml.
Ampicillin (Sigma)	1	0.485	0.017	0.000	0.005	0.007	-0.001
	2	0.493	0.027	0.008	0.013	0.010	0.004
	3	0.521	0.023	0.029	0.013	0.004	0.001
	4	0.530	0.019	0.026	0.011	0.001	0.002

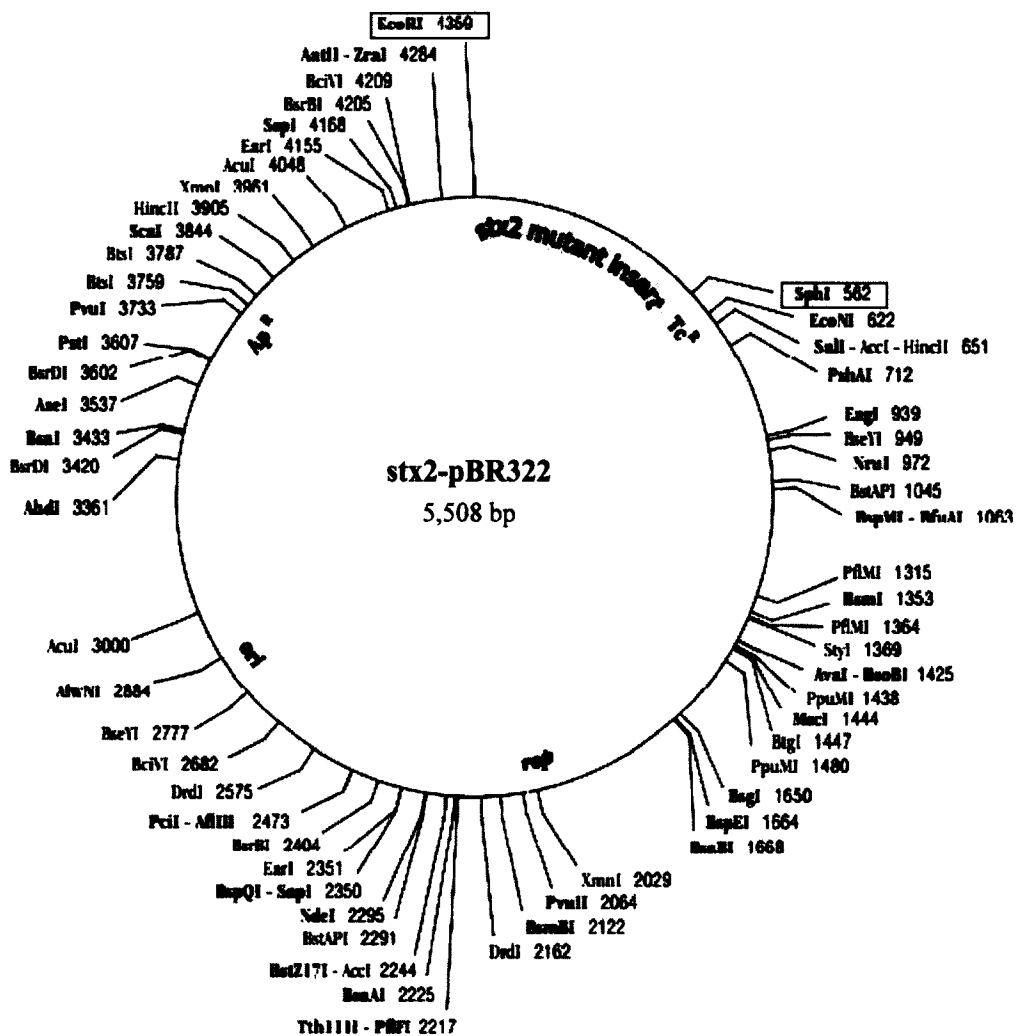


**Figure 4.6: Vector map of recombinant plasmid stx2-pBR322.** This map is adapted from New England Biolabs. The mutated *stx2* gene is shown inserted at the EcoRI and SphI restriction sites. This vector conferred only ampicillin resistance to the transformed bacteria.

### **5.3 Verification of Recombinant Plasmid Transformation into *E. coli* O157:H7 Strain 43888**

The *stx2*-pBR322 recombinant plasmid was successfully transformed into *E. coli* O157:H7 strain 43888. Nine colonies were identified to be ampicillin resistant and tetracycline sensitive. PCR results indicated that the following clones contained the mutant *stx2* inserted at the correct location within the plasmid: L4, L14, L25, L31, L42, L43, L87, L93, and L94 and these are shown in Figure 4.7. The secondary PCR showed positive results for the *stx2* specific gene primers that produced a 118bp amplicon for all samples (Figure 4.8). Results of the plasmid preparation show plasmid bands aligned approximately with the 6,000bp marker; however, the resolution of this marker was not very high so it was difficult to detect the precise molecular weight (Figure 4.9). It is suggested that this is the *stx2*-pBR322 plasmid. The remaining bands in the preparation were thought to be supercoiled and nicked plasmid DNA.

Results of the sequencing indicated that three (L14, L42, and L94) of the four clones contained the point mutation at G225 (Figure 4.10, 4.11, 4.12, and 4.13). The identity match of these clones to *E. coli* O157:H7 strain Sakai, complete genome (Accession # NC\_002695) was 94% (L14), 99% (L42), and 92% (L94). The clone that did not contain the mutation (L4) had poor sequence quality with an identity match of 78%.

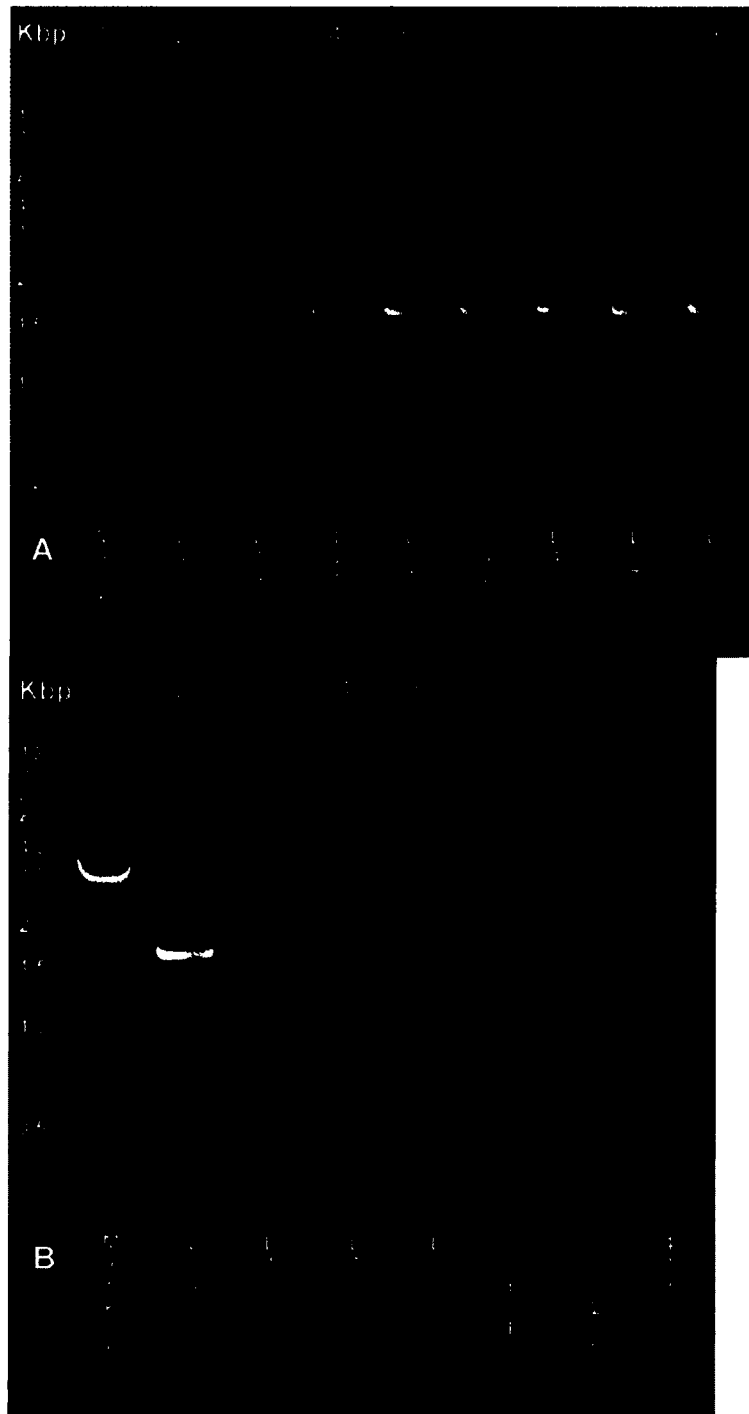
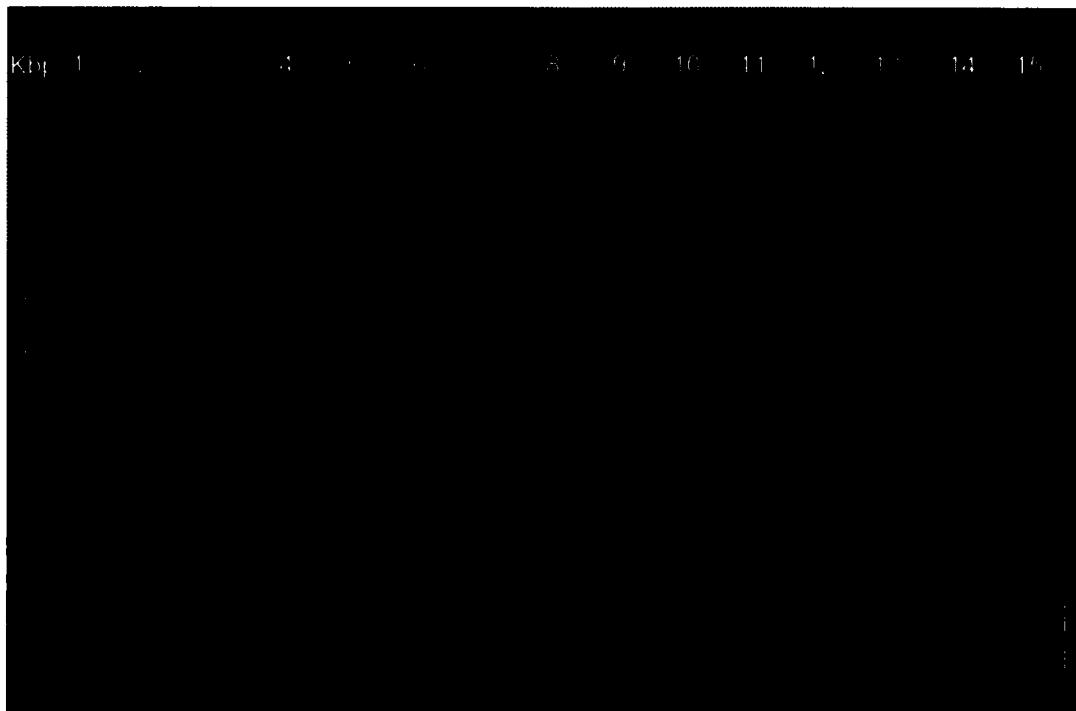
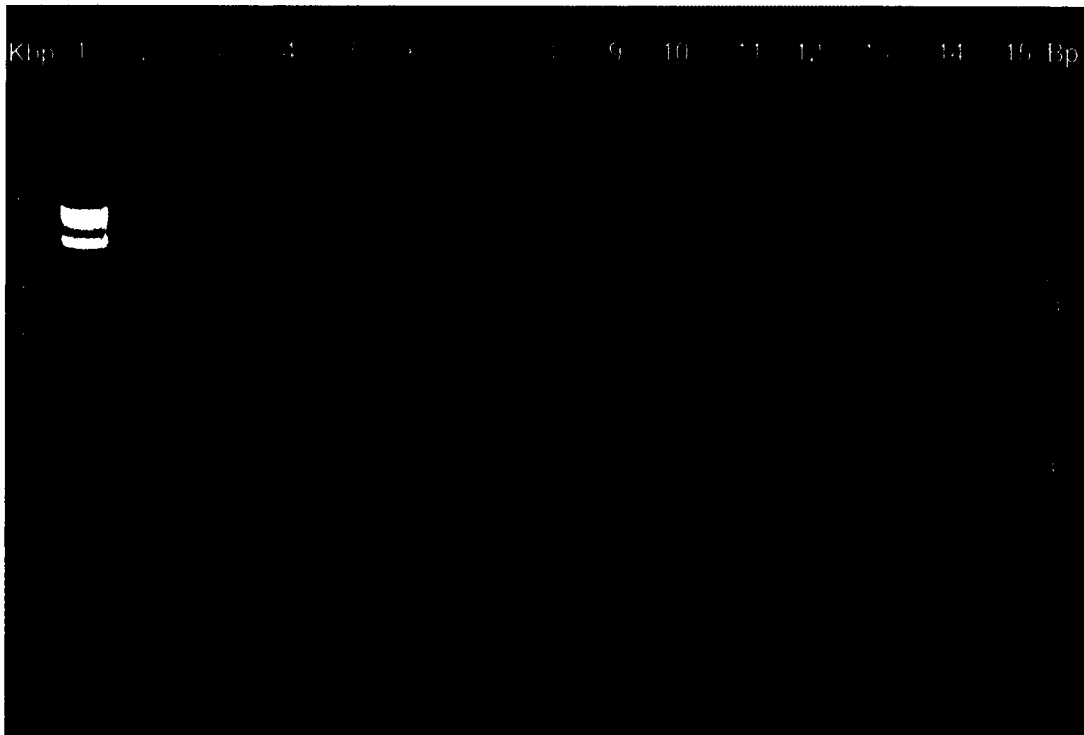


**Figure 4.7: Verification of recombinant *stx2*-pBR322 plasmids.** A) Lane 2-9 contains ampicillin resistant and tetracycline sensitive clones showing the correct insert size of 1743bp. B) Lane 2 shows ampicillin resistant and tetracycline sensitive clone L94 showing the correct insert size of 1743bp, Lane 3-5 shows clones having incorrect insert sizes, Lane 6 shows PCR SOE control (product prior to ligation with pBR3222), and Lane 7-8 show genomic DNA controls for *E. coli* O157:H7 strain 90-2380 and 43888 respectively.



Lane	Description	Lane	Description
1	500 bp – 10 kbp Ladder	9	L87
2	L4	10	L87
3	L14	11	L93
4	L25	12	L94
5	L31	13	L1 (control)
6	L31	14	L7
7	L42	15	L13
8	L43		

**Figure 4.8: Verification of the *stx2* insert within the recombinant *stx2*-pBR322 plasmid.** The boxed area shows all clones contained the *stx2* insert as illustrated by a band at approximately 120bp.



Lane	Description	Lane	Description
1	500 bp – 10 kbp Ladder	9	Plasmid prep L31
2	<i>stx2</i> SOE Product	10	Plasmid prep L43
3	90-2380 (positive control)	11	Plasmid prep L87
4	43888 (negative control)	12	Plasmid prep L42
5	water only control	13	Plasmid prep L93
6	Plasmid prep L4	14	Plasmid prep L94
7	Plasmid prep L14	15	50 bp-2 kbp Ladder
8	Plasmid prep L25		

**Figure 4.9: Verification of recombinant plasmid size.** Lane 6-14 shows ampicillin resistant and tetracycline sensitive *E. coli* O157:H7 strain 43888 clones indicating the presence of the recombinant *stx2*-pBR322 plasmid (expected size ~5.5Kbp).

```

ALIGNMENTS
>ref|NC_002695.1| Escherichia coli O157:H7 str. Sakai, complete genome
Length=5498450

Score = 1352 bits (1498), Expect = 0.0
Identities = 857/910 (94%), Gaps = 18/910 (1%)
Strand=Plus/Minus

Query 12      CTTGGAA--CTCAATTTTACCTTTTAGCACAATCCGCCGCCATTGCATTAACAGAAGCTAA 69
           |||
Sbjct 1268028 CTTGGAAAACCTCAATTTTACCTTTTAGCACAATCCGCCGCCATTGCATTAACAGAAGCTAA 1267969

Query 70      TGCAAAATAAAACCGCCATAAACATCCTTCTCCATGCTTAACTACCTTCCCTCCACCCGTCA 129
           |||
Sbjct 1267968 TGCAAAATAAAACCGCCATAAACATC--TTCTTCATGCTTAACT--CCTTTATTTACCCGTT- 1267912

Query 130     GTCTCTAAAAACAGTGACTCCATCGTCCACAGAAACGCTCGCAGCTCGTACTACTCCCCC 189
           |||
Sbjct 1267911 GTATATAAAAACGTGACTTTCTGTCCA--GAAACGCT--GCAGCT--GTATTACTTTCCC- 1267857

Query 190     ATAATCGTACCGCCTACCCCC--TAGCAGGCCCTCGTCCAGTTACCCGACACCCCTGGTCG 248
           |||
Sbjct 1267856 ATAAT--GTATTGTTTATTTTATAACAGGCCCT--GTCGCCAGTTATCTGACATTCTGGTTG 1267799

Query 249     ACTCTCTTCATTACGGCGCGAACAGAACGCCGCCCTGATGATGGCAACTCAGTATAAC 308
           |||
Sbjct 1267798 ACTCTCTTCATTACGGCGCGAACAGAACGCCGCCCTGATGATGGCAATTCAGTATAAC 1267739

Query 309     GGCCACAGTCCCCAGTATCGCTGATATATTATTAAGGATATTCTCCCCACTCTGACACC 368
           |||
Sbjct 1267738 GGCCACAGTCCCCAGTATCGCTGATATATTATTAAGGATATTCTCCCCACTCTGACACC 1267679

Query 369     ATCCTCTCCCCGATACTCCGGAAGCACATTGCTGATTCGCGCCAGTTCCAGAGTGAGGTC 428
           |||
Sbjct 1267678 ATCCTCTCCCCGATACTCCGGAAGCACATTGCTGATTCGCCCCAGTTCCAGAGTGAGGTC 1267619

Query 429     CACGCTCCCCGGCGTCATCGTATACACAGGAGCAGTTTCAGACAGTGCCTGACGAAATTC 488
           |||
Sbjct 1267618 CACGCTCCCCGGCGTCATCGTATACACAGGAGCAGTTTCAGACAGTGCCTGACGAAATTC 1267559

Query 489     TCTCTGTATCTGCCGTAAGCGTAAGGCTTCTGCTGTGACAGTGACAAAACGCAGAAGTGC 548
           |||
Sbjct 1267558 TCTCTGTATCTGCCGTAAGCGTAAGGCTTCTGCTGTGACAGTGACAAAACGCAGAAGTGC 1267499

Query 549     TCTGGATGCATCTCTGGTCATTGTATTACCACTGAACTCCATTAACGCCAGATATGATGA 608
           |||
Sbjct 1267498 TCTGGATGCATCTCTGGTCATTGTATTACCACTGAACTCCATTAACGCCAGATATGATGA 1267439

Query 609     AACCAGTGAGTGACGACTGATTTGCATTCCGGAACGTTCCAGCGCTGCGACACGTTGCAG 668
           |||
Sbjct 1267438 AACCAGTGAGTGACGACTGATTTGCATTCCGGAACGTTCCAGCGCTGCGACACGTTGCAG 1267379

Query 669     AGTGGTATAACTGCTGTCCGTTGTCATGGAACCGTTGTCACACCCGGGCCTGATATAT 728
           |||
Sbjct 1267378 AGTGGTATAACTGCTGTCCGTTGTCATGGAACCGTTGTCACACA--CCGGGCCTGATATAT 1267320

Query 729     GTGTAATAATCTGAAAAACGGTAGAAAGTATTTGTTGCCGATTAACGAACCCCGGGCCA 788
           |||
Sbjct 1267319 GTGTAATAATCTG--AAAAACGGTAGAAAGTATTTGTTGCCGATTAACGAACCC--GGCCA 1267263

Query 789     CATATAAATTAATTTTGTCAATAATCAGACGAAGATGGTCAAACGCGCTGATGGACA 848
           |||
Sbjct 1267262 CATATAAATTA--TTTTGTCAATAATCAGACGAAGATGGTCAAACGCGCTGATAGACA 1267204

Query 849     TCAAGCCCTCGTATATCCACAGCAAATAACTGCCCGGTGGGGTGTGGTTAATAACAGAC 908
           |||
Sbjct 1267203 TCAAGCCCTCGTATATCCACAGCAAATAACTGCCCGGTGGGGTGTGGTTAATAACAGAC 1267144

Query 909     ACCGATGTGG 918
           |||
Sbjct 1267143 ACCGATGTGG 1267134

```

**Figure 4.10: *E. coli* clone L14 sequence alignment.** Alignment of *E. coli* clone L14 to Accession NC\_002695.1 (*E. coli* O157:H7 strain Sakai, complete genome). Identity match was 94% and the mutation was observed (C→G) at nucleotide 409 of the query strand (see boxed area).



```

ALIGNMENTS
>ref|NC_002695.1| Escherichia coli O157:H7 str. sakai, complete genome
Length=5498450

Score = 1586 bits (1758), Expect = 0.0
Identities = 897/905 (99%), Gaps = 3/905 (0%)
Strand=Plus/Minus

Query 3      TCCTTAAACTTTGGAAACTCA-TTTTACCTTTAGCACAATCCGCCGCCATTGCATTAACA 61
            ||| ||| ||| ||| ||| ||| ||| ||| ||| ||| ||| ||| ||| ||| ||| |||
Sbjct 1268036 TCATTATACTTGAAAACTCAATTTTACCTTTAGCACAATCCGCCGCCATTGCATTAACA 1267977

Query 62     GAAGCTAATGCAAAATAAAACC GCCATAAACATCTTCTTCATGCTTAACTCCTTTATTTAC 121
            ||| ||| ||| ||| ||| ||| ||| ||| ||| ||| ||| ||| ||| ||| ||| |||
Sbjct 1267976 GAAGCTAATGCAAAATAAAACC GCCATAAACATCTTCTTCATGCTTAACTCCTTTATTTAC 1267917

Query 122    CCGTTGTATATAAAAACTGTGACTTTCTGTTTCAGAAACGCTGCAGCTGTATTACTTTCCC 181
            ||| ||| ||| ||| ||| ||| ||| ||| ||| ||| ||| ||| ||| ||| ||| |||
Sbjct 1267916 CCGTTGTATATAAAAACTGTGACTTTCTGTTTCAGAAACGCTGCAGCTGTATTACTTTCCC 1267857

Query 182    ATAATGTATTGTTTATTTTTATAACAGGCCCTGTCGCCAGTTATCTGACATTCTGGTTGAC 241
            ||| ||| ||| ||| ||| ||| ||| ||| ||| ||| ||| ||| ||| ||| ||| |||
Sbjct 1267856 ATAATGTATTGTTTATTTTTATAACAGGCCCTGTCGCCAGTTATCTGACATTCTGGTTGAC 1267797

Query 242    TCTCTTCAATTCACGGCGC GAACAGAAGCGCCCTTGATGATGGCAATTCAGTATAACGG 301
            ||| ||| ||| ||| ||| ||| ||| ||| ||| ||| ||| ||| ||| ||| ||| |||
Sbjct 1267796 TCTCTTCAATTCACGGCGC GAACAGAAGCGCCCTTGATGATGGCAATTCAGTATAACGG 1267737

Query 302    CCACAGTCCCCAGTATCGCTGATATATTATTAAGGATATTCTCCCCACTCTGACACCAT 361
            ||| ||| ||| ||| ||| ||| ||| ||| ||| ||| ||| ||| ||| ||| ||| |||
Sbjct 1267736 CCACAGTCCCCAGTATCGCTGATATATTATTAAGGATATTCTCCCCACTCTGACACCAT 1267677

Query 362    CCTCTCCCCGATACTCCGGAAGCACATTGCTGATTCGCCGCCAGTTTCAGAGTGAGGTCCA 421
            ||| ||| ||| ||| ||| ||| ||| ||| ||| ||| ||| ||| ||| ||| ||| |||
Sbjct 1267676 CCTCTCCCCGATACTCCGGAAGCACATTGCTGATTCGCCGCCAGTTTCAGAGTGAGGTCCA 1267617

Query 422    CGTCTCCCGGCGTCATCGTATACACAGGAGCAGTTTCAGACAGTGCCTGACGAAATTC 481
            ||| ||| ||| ||| ||| ||| ||| ||| ||| ||| ||| ||| ||| ||| ||| |||
Sbjct 1267616 CGTCTCCCGGCGTCATCGTATACACAGGAGCAGTTTCAGACAGTGCCTGACGAAATTC 1267557

Query 482    TCTGTATCTGCCCTGAAGCGTAAGGCTTCTGCTGTGACAGTGACAAAACGCAGAAGTCT 541
            ||| ||| ||| ||| ||| ||| ||| ||| ||| ||| ||| ||| ||| ||| ||| |||
Sbjct 1267556 TCTGTATCTGCCCTGAAGCGTAAGGCTTCTGCTGTGACAGTGACAAAACGCAGAAGTCT 1267497

Query 542    TGGATGCATCTCTGGTCATTGTATTACCACTGAACTCCATTAACGCCAGATATGATGAAA 601
            ||| ||| ||| ||| ||| ||| ||| ||| ||| ||| ||| ||| ||| ||| ||| |||
Sbjct 1267496 TGGATGCATCTCTGGTCATTGTATTACCACTGAACTCCATTAACGCCAGATATGATGAAA 1267437

Query 602    CCAGTGAGTGACGACTGATTTGCAATCCGGAACGTTCCAGCGCTGC GACACGTTGCAGAG 661
            ||| ||| ||| ||| ||| ||| ||| ||| ||| ||| ||| ||| ||| ||| ||| |||
Sbjct 1267436 CCAGTGAGTGACGACTGATTTGCAATCCGGAACGTTCCAGCGCTGC GACACGTTGCAGAG 1267377

Query 662    TGGTATAACTGCTGTCCGTTGTCATGGAAACC GTTGTACACCCGGGCACTGATATATGTG 721
            ||| ||| ||| ||| ||| ||| ||| ||| ||| ||| ||| ||| ||| ||| ||| |||
Sbjct 1267376 TGGTATAACTGCTGTCCGTTGTCATGGAAACC GTTGTACACCCGGGCACTGATATATGTG 1267317

Query 722    TAAAATCTGAAAAACGGTAGAAAGTATTTGTTGCCGTATTAACGAACCCGGCCACATATA 781
            ||| ||| ||| ||| ||| ||| ||| ||| ||| ||| ||| ||| ||| ||| ||| |||
Sbjct 1267316 TAAAATCTGAAAAACGGTAGAAAGTATTTGTTGCCGTATTAACGAACCCGGCCACATATA 1267257

Query 782    AATTATTTTGTCTAATAATCAGACGAAGATGGTCAAAACGC GCCTGATAGACATCAAGCC 841
            ||| ||| ||| ||| ||| ||| ||| ||| ||| ||| ||| ||| ||| ||| ||| |||
Sbjct 1267256 AATTATTTTGTCTAATAATCAGACGAAGATGGTCAAAACGC GCCTGATAGACATCAAGCC 1267197

Query 842    CTCGTATATCCACAGCAAAATAACTGCCCGGTGGGGGTGTGGTTAAATAACAGACACCGA 901
            ||| ||| ||| ||| ||| ||| ||| ||| ||| ||| ||| ||| ||| ||| ||| |||
Sbjct 1267196 CTCGTATATCCACAGCAAAATAACTGCCCGGT-GGGGTGTGGTT-AAATAACAGACACCGA 1267139

Query 902    TGTGG 906
            ||| |
Sbjct 1267138 TGTGG 1267134

```

**Figure 4.11: *E. coli* clone L42 sequence alignment.** Alignment of *E. coli* clone L42 to Accession NC\_002695.1 (*E. coli* O157:H7 strain Sakai, complete genome). Identity match was 99% and the mutation was observed (C→G) at nucleotide 400 of the query strand (see boxed area).

```

ALIGNMENTS
>ref|NC_002695.1| Escherichia coli O157:H7 str. Sakai, complete genome
Length=5498450

Score = 1292 bits (1432), Expect = 0.0
Identities = 851/919 (92%), Gaps = 19/919 (2%)
Strand=Plus/Minus

Query 10      CTTGGAA--CTCAATTTTACCTTTAGCACAATCCGCCGCCATTGCATTAACAGAAGCTAA 67
                |||
sbjct 1268028  CTTGGAAAACCAATTTTACCTTTAGCACAATCCGCCGCCATTGCATTAACAGAAGCTAA 1267969

Query 68      TGCAAATAAAACC GCCATAAACATCTTCTCATGCTTAACTCCTTTATT-ACCCGTCTGT 126
                |||
sbjct 1267968  TGCAAATAAAACC GCCATAAACATCTTCTCATGCTTAACTCCTTTATTACCCGT-TGT 1267910

Query 127     AC-TAAAAACAGTGACTTCATCGCCAGAAAACGCAGCAGCAGTAATACAAAACCCATAACG 185
                |||
sbjct 1267909  ATATAAAAACGTGACTTTCT-GTTCAGAAAACGCTGCAGCTGTATTACTTTCCATAATG 1267851

Query 186     TAAAGCATAAAAAAC-TAACGGGCAGTCGCCAGCTACCAGACAAATAGGCCGACACA-TC 243
                |||
sbjct 1267850  TATTGTTTATTTTATAACAGGCCTGTGCCAGTTATCTGACATTCGTGGTTGACTCTCTT 1267791

Query 244     AAAACACGGCGCGAACAGAACGC GCCCCCTGACGACGGCAACCAGTATAACGGCCACAG 303
                |||
sbjct 1267790  CATTACGGCGCGAACAGAACGC GCCCCCTGATGATGGCAATTCAGTATAACGGCCACAG 1267731

Query 304     TCCCCAGTATCGCTGAC-TATTATTAAAGGATACTCTCCCCACTCTGACACCATCTCTC 362
                |||
sbjct 1267730  TCCCCAGTATCGCTGATATATTATTAAAGGATATCTCCCCACTCTGACACCATCTCTC 1267671

Query 363     CCCGATACTCCGGAAGCACATTGCTGATTCG G C C C CAGTTTCAGAGTGAGGTCCACGTC 422
                |||
sbjct 1267670  CCCGATACTCCGGAAGCACATTGCTGATTCG C C C C CAGTTTCAGAGTGAGGTCCACGTC 1267611

Query 423     CCGCGTCATCGTATACACAGGAGCAGTTTCAGACAGTGCCTGACGAAATTCCTCTGT 482
                |||
sbjct 1267610  CCGCGTCATCGTATACACAGGAGCAGTTTCAGACAGTGCCTGACGAAATTCCTCTGT 1267551

Query 483     TCTGCCTGAAGCGTAAGGCTTCTGCTGTGACAGTGACAAAACGCAGAACTGCTCTGGATG 542
                |||
sbjct 1267550  TCTGCCTGAAGCGTAAGGCTTCTGCTGTGACAGTGACAAAACGCAGAACTGCTCTGGATG 1267491

Query 543     CATCTCTGGTCATTGTATTACCACTGAACTCCATTAACGCCAGATATGATGAAACCAGTG 602
                |||
sbjct 1267490  CATCTCTGGTCATTGTATTACCACTGAACTCCATTAACGCCAGATATGATGAAACCAGTG 1267431

Query 603     AGTGACGACTGATTTGCATTCCGGAACGTTCCAGCGCTGCACACGTTGCAGAGTGGTAT 662
                |||
sbjct 1267430  AGTGACGACTGATTTGCATTCCGGAACGTTCCAGCGCTGCACACGTTGCAGAGTGGTAT 1267371

Query 663     AACTGCTGTCCGTTGTGTCATGGGAAACC GTTGTGACACC GGGGCACTGATATATGTGAAA 722
                |||
sbjct 1267370  AACTGCTGTCCGTTGTGTCATGGGAAACC GTTGTGACACC GGGGCACTGATATATGTGAAA 1267313

Query 723     ATCTGAAAAAACGGTAGAAAGTATTTGTTTGCCGTATTAACGAAACCCCGCCCATAA 782
                |||
sbjct 1267312  AT-CTG-AAAAACGGTAGAAAGTATTTG-TTGCCGTATTAACGAA--CCCGCCACAT-A 1267259

Query 783     TAAATTATTTTGTCTCAATAATCAGACGAAGATGGTCAAAACGCGCCTGATAGACATCAA 842
                |||
sbjct 1267258  TAAATTA-TTTTGTCTCAATAATCAGACGAAGATGGTCAAAACGCGCCTGATAGACATCAA 1267200

Query 843     GCCCTCGTATATCCACAGCAAATAACTGCCCGGTGGGGTGTGGTTAATAACAGACATC 902
                |||
sbjct 1267199  G-CCCTCGTATATCCACAGCAAATAACTGCCCGGTGGGGTGTGGTTAATAACAGACACC 1267141

Query 903     GATGTGGTCCCTGAGATA 921
                |||
sbjct 1267140  GATGTGGTCCCTGAGATA 1267122

```

**Figure 4.12: *E. coli* clone L94 sequence alignment.** Alignment of *E. coli* clone L94 to Accession NC\_002695.1 (*E. coli* O157:H7 strain Sakai, complete genome). Identity match was 92% and the mutation was observed (C→G) at nucleotide 395 of the query strand (see boxed area).

```

ALIGNMENTS
>ref|NC_002695.1| Escherichia coli O157:H7 str. Sakai, complete genome
Length=5498450

Score = 134 bits (148), Expect = 1e-31
Identities = 204/259 (78%), Gaps = 46/259 (17%)
Strand=Plus/Minus

Query 608      TCATTAGTATTTACCACTGAACTCCATTAAACGCCAGATATGGATGAAACCAGTGAAGTG 667
||||| ||||| ||||| ||||| ||||| ||||| ||||| ||||| ||||| ||||| |||||
sbjct 1267481   TCATT-GTATT-ACCACTGAACTCCATT-AACGCCAGATAT-GATGAAACCAGTG-AGTG 1267427

Query 668      ACGACTGATTTTGGCATTCCGGTAACGGTCCAGCGGCTGCACACGGTTTGCAGAGTT 727
||||| ||||| ||||| ||||| ||||| ||||| ||||| ||||| ||||| ||||| |||||
sbjct 1267426   ACGACTGATTT--GCATTCCGG-AACG--TTCCAGC-GCTGCACACG--TTGCAGAGT- 1267376

Query 728      GGCTATTAAGTGCCTGGTCCCGGTTTGTTCATGGAAAACCCGTTTGTTCACACTCGGGT 787
||| ||||| ||||| ||||| ||||| ||||| ||||| ||||| ||||| ||||| |||||
sbjct 1267375   -GGTA-TAACTGC--TGTC--GTT--GTCATGGAAA--CCGTT--GTCACAC-CGGG-- 1267331

Query 788      CATCTTGATTATATTTTGGTAAAAATCTTGAAAAAACCGGTAGAAAGGTATTTTGGTTG 847
||| ||||| ||||| ||||| ||||| ||||| ||||| ||||| ||||| ||||| |||||
sbjct 1267330   CA--CTGA-TATATGTGT----AAAATC-TGAAAAA--CGGTAGAAA-GTATTT--GTTG 1267284

Query 848      GCTCGCTATTAACGGAACC 866
| ||||| |||||
sbjct 1267283   ---CCGTATTAAC-GAACC 1267269

```

**Figure 4.13: *E. coli* clone L4 sequence alignment.** Alignment of *E. coli* clone L4 to Accession NC\_002695.1 (*E. coli* O157:H7 strain Sakai, complete genome). Identity match was 78% and the mutation was not observed (sequence quality was poor).

## 6.0 Discussion

Whether or not Stx-2 binds to Bcl-2 family proteins seems to be a controversial topic. Previous research has indicated that Stx-2 binds Bcl-2 (190) however this could not be repeated in the studies performed in Chapter 2. The effects that Stx-2 has on the apoptosis of neutrophils has also been debated in the past (51, 118) and studies performed in Chapter 3 showed that a Stx-2-induced delay in neutrophil apoptosis was observed for up to 12 h, and could be due to the binding of Stx-2 with Bak in the endoplasmic reticulum. An additional method to determine if binding between Stx-2 and apoptosis related proteins occurs is through the use of a Stx-2 mutant. Annis *et al.* (4) has used mutants to determine the contribution of Bcl-2 family proteins in the endoplasmic reticulum or mitochondria numerous times. One study performed by Yin *et al.* (225) indicated that a mutation to a portion of the NWGRI sequence of Bcl-2 resulted in failure of heterodimerization with Bax. It was believed that if Stx-2 bound with Bcl-2 family proteins through this same binding site, mutation of Stx-2 at the NWGRI sequence should also result in the failure of dimerization between Stx-2 and other proteins. The goal of these experiments was to perform a point mutation in the *stx2* gene, specifically to the region encoding the glycine residue within the pentameric sequence NWGRI at amino acid position 225, and change it to alanine in a manner similar to that performed by Yin *et al.* (225) with Bcl-2. This gene would then be ligated into pBR322, and finally transformed into *E. coli* O157:H7 strain 43888 (a Stx-2 negative strain) for purification. It was hypothesized that this mutation would result in a mutant protein that was less pathogenic than the wild-type due to its inability to trigger the apoptotic pathways. Data

obtained indicated successful mutation of glycine to alanine at position 225 within *stx2*. This mutant gene was also successfully inserted into pBR322 and transformed into *E. coli* O157:H7 strain 43888 which does not produce either Stx-1 or Stx-2.

In these experiments, a mutant Stx-2 protein was created containing an alanine at amino acid position 225 such that the pentameric sequence reads NWARI. Having a mutant toxin will help elucidate the mechanisms of Stx-2 action within host cells, especially when determining the role of Stx-2 in the apoptotic pathway. Further experiments with this mutant toxin will be done to determine the effects it has on Vero cell cytotoxicity, neutrophil apoptosis and necrosis rates, as well as activation of caspase-8 and caspase-9 within neutrophils.

## CHAPTER 5

### THE EFFECTS OF MUTANT STX-2 AND NATIVE STX-2 WITH AN INTERLEUKIN-8 INHIBITOR ON NEUTROPHIL APOPTOSIS, NECROSIS, AND CASPASE-8 AND CASPASE-9 ACTIVATION

#### 1.0 **Abstract**

Apoptosis is mediated by the Bcl-2 protein family (4, 151, 177, 181) and these may bind with Stx-2 through a conserved NWGRI amino acid motif. A mutation was introduced into Stx-2 to change the NWGRI sequence to NWARI, influencing apoptotic outcomes. Other factors that may influence human neutrophil apoptosis include the presence of Interleukin-8 (IL-8), which results in a delay of spontaneous and TNF- $\alpha$ -mediated apoptosis in both a dose- and time-dependent manner (96). This process is not reliant on inducing expression of Bcl-2 especially within the first 30 h (96). In this study, apoptosis and necrosis rates of isolated human neutrophils were examined at intervals of 0, 6, 12, 18, 24 and 48 h following exposure to Stx-2 from *E. coli* O157:H7 or to mutant Stx-2 (G225A cloned from *E. coli* O157:H7 strain 90-2380). An IL-8 inhibitor together with Stx-2 was studied to determine if IL-8 contributed to the delay in apoptosis. Caspase-8 and 9 levels were examined to determine which apoptotic pathway was involved. Data indicated that although there was no clear correlation between delayed apoptosis due to Stx-2, it was clear that cells exposed to mutant Stx-2 had apoptosis rates similar to those of the untreated cells.

## 2.0 Introduction

Human neutrophils routinely are subjected to relatively rapid apoptosis (programmed cell death) and typically have a short circulating lifespan of approximately 6-18 h (113). Approximately  $10^{10}$  neutrophils are produced daily, and these account for 45-75% of the total white blood cell count (113). Neutrophils are the first responders during infection, and these cells are capable of phagocytosing foreign material and in an attempt to clear the infection, they release reactive oxidative intermediates (113).

Apoptosis is a normal function of cells mediated by the Bcl-2 protein family (46). These proteins consist of anti-apoptotic (pro-survival) and apoptotic (pro-death) proteins that possess conserved homology domains. It is through these conserved homology domains that these proteins interact with each other, and the relative ratio of unbound protein type (i.e. pro-survival or pro-death) available in the cell determines the ultimate fate of the cell (46).

Exposure of neutrophils to Interleukin-8 (IL-8) results in a delay of spontaneous apoptosis as well as of TNF- $\alpha$ -mediated apoptosis in both a dose- and time-dependent fashion (96). During the early phases of apoptosis (within the first 30 h) this process is not determined by the expression of Bcl-2 (96). Phenomena that can be induced in human neutrophils following exposure to IL-8 included: changing shape (221); actin polymerization (216); degranulation (123); and up-regulation of adhesion molecules (43).

Stimulated neutrophils can release a variety of cytokines including IL-8 and TNF- $\alpha$  (6, 27). TNF- $\alpha$  can rapidly increase neutrophil apoptosis 2 h after exposure (97, 143, 192).

Data from previous studies have shown conflicting results as to whether neutrophil apoptosis is delayed following exposure to Stx-2. Liu *et al.* (118) concluded that Stx-2 derived from *E. coli* O157:H7 exhibited both a dose- and time- dependent inhibition of spontaneous neutrophil apoptosis, possibly involving the protein kinase C pathway. Flagler *et al.* (51) were unable to demonstrate a Stx-2 and neutrophil interaction nor did they observe an altered apoptosis rate when cells were exposed to 1 $\mu$ g/mL of Stx-1 or Stx-2. In agreement with Liu *et al.* (118), Suzuki *et al.* (190) reported that Bcl-2 did bind Stx-2. Further analysis of the Bcl-2 protein family (Chapter 2, pg. 56-57) indicated that Stx-2 has the potential to bind with all Bcl-2 family members through a conserved NWGRI amino acid motif, but binding was not detected to Bcl-2, Bcl-X<sub>L</sub> or Bax isolated from Caco-2 cells.

The timing (increase or delay in the rate) of human neutrophil apoptosis was examined over the course of 48 h following exposure of cells to 5 ng semi-purified Stx-2 from *E. coli* O157:H7 strain 90-2380 and also to 5 ng mutant Stx-2 (G225A cloned from *E. coli* O157:H7 strain 90-2380). The impact of IL-8 inhibitor at concentrations of 0.01mM was also examined at the same time as treatment with Stx-2 to determine if the presence of IL-8 contributed to a delay in apoptosis previously seen in past experimentation (Chapter 3, pg. 109-112). Caspase-8 and caspase-9, cellular components



critical to apoptosis induction, were evaluated to better understand which apoptotic pathways were involved.

### **3.0 Hypothesis**

Neutrophils treated with mutant Stx-2 will show apoptosis rates that align with the baseline (untreated) apoptosis rate, resulting from an inability to trigger the apoptosis pathway. Alternatively, neutrophils treated with Stx-2 in combination with an IL-8 inhibitor will also show apoptosis rates that align with the baseline (untreated) apoptosis rate. The presence of IL-8 will contribute to a delay in apoptosis as opposed to Stx-2 alone.

### **4.0 Materials and Methods**

#### **4.1 Purification of Stx-2**

*E. coli* O157:H7 strain 90-2380 was inoculated into LB broth and allowed to grow overnight at 37°C with shaking. The following day, the culture was aliquoted into sterile 100x15mm Petri dishes (10mL per dish). The lids were removed, and the culture was exposed to ultraviolet (UV) light in a biosafety cabinet for 30 minutes. Subsequent to UV exposure, the dishes were transferred to a 37°C incubator and allowed to incubate for an additional 48 h.

Following incubation, the culture samples were pooled and centrifuged at 16,000 x g for 15 min at 4°C. The supernatant fluid was collected and sterile filtered using Millex 0.45µm low protein-binding membranes (Millipore Corp, Bedford, MA). The toxin was precipitated using ammonium sulfate precipitation. First, ammonium sulfate was slowly added to the supernate until the concentration was 40%. The mixture was centrifuged and the supernatant fluid was transferred to a new beaker. The ammonium sulfate concentration was increased to 70%, and the mixture was again centrifuged. The pellet was resuspended in 25mL PBS and placed into a Slide-a-lyzer® 20 kDa molecular weight cut off dialysis cassette (Thermo Scientific, Rockford, IL). The cassette was inserted into a tank containing 4L PBS and incubated overnight at 4°C. On the following day, the buffer was exchanged and the cassette was incubated at room temperature for an additional 5 h with two buffer exchanges during the incubation period. The cassette was unloaded and the semi-purified Stx-2 was loaded into a 100 kDa Centricon device and spun at 3220 x g for 15 min. The filtrate was collected and processed through an Amicon 50 kDa device for 15 minutes. The retentate was collected and measured for total protein concentration using the  $A_{280}$  method on the Nanodrop spectrophotometer. An  $A_{280} / A_{260}$  reading was also performed to determine protein purity. Approximate protein concentrations were calculated from this data using the Warburg-Christian Method (211).

#### **4.2 Purification of Mutant Stx-2**

*Escherichia coli* O157:H7, strain 43888 (the otherwise toxin negative strain), L42 mutant with the Stx-2 insert was inoculated into LB broth containing 50µg/mL ampicillin

and allowed to grow for 72 h at 37°C with shaking. Following incubation, the culture was placed in a -20°C freezer for 48 h to aid in cellular disruption. The culture was then thawed and processed using a B-PER<sup>®</sup> Bacterial Protein Extraction Reagent (Thermo Scientific). The bacterial cells were centrifuged at 5,000 x g for 10 min and 4mL of B-PER<sup>®</sup> reagent was added per gram of cell pellet. The suspension was mixed by pipette to homogeneity and allowed to incubate for 15 min at room temperature. The lysate was centrifuged at 15,000 x g for 5 min to separate the soluble and insoluble proteins. The fluid phase was collected and processed through Pierce Detergent Removal Spin Columns (Thermo Scientific) according to the manufacturer's instructions. The sample was then loaded into a Slide-a-lyzer<sup>®</sup> 20 kDa molecular weight cut off dialysis cassette (Thermo Scientific), placed into a tank containing approximately 4L PBS and incubated for 48 h at 4°C. The buffer was exchanged and the cassette was incubated for 24 h at 4°C and the resultant semi-purified mutant Stx-2 was loaded into a 100 kDa Centricon device and centrifuged at 3220 x g for 15 min. The filtrate was collected and 20mL of PBS was added. The sample was then processed through an Amicon 50 kDa device for 15 min. The retentate was collected and measured for total protein concentration using the A<sub>280</sub> method on the Nanodrop spectrophotometer. An A<sub>280</sub> / A<sub>260</sub> reading was also performed to determine protein purity. Approximate protein concentrations were calculated from this data using the Warburg-Christian Method (211).

### **4.3 Conjugation of STX2-11E10 Antibody**

Horseradish peroxidase (HRP) was conjugated to the mouse STX2-11E10 antibody (Toxin Technology) using the EZ-Link™ Plus Activated Peroxidase Kit (Thermo Scientific). One mg of lyophilized EZ-Link™ Plus activated peroxidase was resuspended with 100µL of MilliQ water and added to 1mL PBS containing 1mg/mL of STX2-11E10. Ten µL of cyanoborohydride was added to this reaction mixture in the fume hood and allowed to incubate for 1 h at room temperature. Twenty µL of quenching buffer (3M ethanolamine, pH 9) was added and allowed to react at room temperature for 15 min.

The conjugated antibody was then purified using the Pierce Conjugate Purification Kit (Thermo Scientific). An immobilized Iminodiacetic acid column was activated by adding 10-20mL of TBS and allowing the fluid to drain through the column. When the flow of TBS had stopped, 2mL of Pierce column activator buffer was added and once the flow had stopped a second time, it was incubated for an additional 5 min. A column wash was then performed with 10-20mL of TBS to remove non-bound nickel. The conjugated antibody was added to the activated column followed by 5-10mL of TBS. This was then allowed to drain through. Elution buffer (1.7mL) was applied to the column forming a blue band indicating the elution front and an additional 0.8mL of elution buffer was added and the blue liquid was collected.

Buffer exchange was subsequently performed on the conjugate by loading it on a polyacrylamide desalting column that was previously equilibrated with 50mL of PBS. Half mL aliquots of PBS were added to the column for each fraction collected and 16 fractions were collected in total. Fractions were tested for enzyme activity by adding 2 $\mu$ L of each fraction to separate tubes containing 1mL TBS with 0.05% Tween-20. Five  $\mu$ L from each prepared tube was then added to a 96-well microtiter plate and 100 $\mu$ L of 1-step ABTS (Thermo Scientific) was added to each well. The first three fractions with the highest enzyme activity were pooled and stored at 2-8°C.

#### **4.4 Verification of Stx-2 and Mutant Stx-2 Presence and Activity**

SDS-PAGE and Western blot were performed to verify the presence of Stx-2 and mutant Stx-2 in the semi-purified preparations. SDS-PAGE was performed under both reducing and non-reducing conditions. Samples were diluted 1:2 in sample preparation buffer (Appendix A, 4.13), and treated in each of three ways; 1) samples were heated at 95°C for 5 min with  $\beta$ -mercaptoethanol added (reducing), 2) samples were heated at 95°C for 5 min 3) samples were not heated and  $\beta$ -mercaptoethanol was not added (non-reducing). Protein from the semi-pure Stx-2 samples was added at 2.4 $\mu$ g/well and from the mutant Stx-2 samples at 1.4 $\mu$ g/well. All samples were loaded onto a 4-20% Tris-HCl gel cassette (Bio-Rad, Hercules, CA), and run at 300V for 20 min. The gel was then stained with GelCode Blue Safe Protein Stain (Thermo Scientific) for 2 h, and destained with water overnight until the background was no longer blue, and visible protein bands were observed.

A Western blot was performed under reducing conditions with the Stx-2 and mutant Stx-2 samples which were diluted 1:2 in sample preparation buffer. These were heated at 95°C for 5 min with  $\beta$ -mercaptoethanol added. Samples were loaded onto a 4-20% Tris-HCl gel cassette (Bio-Rad) in duplicate and run at 300V for 20 min. The gel was aligned onto a polyvinylidene fluoride (PVDF) membrane (Millipore Corp), and placed into a transfer sandwich consisting of fiber pads and filter paper (Figure 2.1, pg. 49). The transfer sandwich was placed in a buffer tank containing Tris-glycine buffer (TGB) (Appendix A, 4.19) and proteins were transferred at 60V for 4-5 h. After transfer, the membrane was processed for Western blotting using the Snap ID Protein Detection System (Millipore Corp). The blot holder was opened and thoroughly soaked with MilliQ water. The pre-wet blot was placed into the blot holder protein side down and gently rolled to remove all air bubbles. A spacer was placed on top of the blot membrane and rolled again to ensure contact of the spacer with the blot membrane. The blot holder lid was closed and placed into the chamber of the Snap ID system ensuring that the blot holder tabs were aligned with the notches of the chamber. To block the membrane, 30mL of TBS containing 0.1% Tween 20 and 0.5% dry non-fat milk was added and the vacuum was turned on until all the fluid passed through the blot. Next, 3mL of HRP-conjugated mouse anti-Stx-2 antibody, STX2-11E10, (10 $\mu$ g/mL) (Toxin Technology, Sarasota, FL) containing 1 $\mu$ L of StrepTactin-HRP conjugate (to detect the bands of the Precision Plus Protein™ WesternC™ standards) (Bio-Rad) was added to the blot and incubated for 10 min at room temperature. Once the incubation was complete, the vacuum was turned on and the blot was washed three times with 30mL of TBS with 0.1% Tween 20. The blot

was removed from the Snap ID system and incubated with the Immun-Star WesternC™ kit (Bio-Rad) for CCD imaging.

In order to determine if the Stx-2 preparation was biologically active after the purification procedure and what type of biological activity the mutant Stx-2 preparation had, African green monkey kidney cells (Vero cells) were exposed to the semi-pure preparations for 96 h. Vero cells were grown in three 25cm<sup>2</sup> tissue culture flasks. Once confluent, the first flask remained untreated, to the second flask 50µL of mutant Stx-2 was added, and to the third 50µL of Stx-2 was added. The control and test flasks were incubated at 37°C in 5% CO<sub>2</sub> for 96 h. Each flask was observed at 200x total magnification using an inverted phase-contrast microscope for the presence of cytotoxic effects.

#### **4.5 Quantitation of Stx-2 and Mutant Stx-2 Using Enzyme-Linked Immunosorbent Assay (ELISA)**

The concentration of Stx-2 and mutant Stx-2 was determined using a sandwich “capture” ELISA (Figure 5.1). Two hundred µL of the primary antibody STX2-BB12 specific to the B-subunit of Stx-2 (20µg/mL) was added to the wells of a 96-well plate and allowed to incubate at room temperature for 2 h while shaking. Unbound antibody was removed from the wells and 300µL of PBS was added to each well and the plate was rinsed with shaking for 5 min to remove excess antibody. This wash was repeated three times and then 300µL of blocking buffer was added to the wells and incubated at room

temperature for an additional 2 h while shaking. Once again, the liquid was removed from the wells and they were washed three times using the same procedure described above. Once the plate had been copiously rinsed, 200 $\mu$ L of 1:2 dilutions containing 2  $\mu$ g/mL to 31.25 ng/mL of a commercial Stx-2 preparation (Toxin Technology) were added to the plate in triplicate to generate a standard curve (Figure 5.2). Next the Stx-2 and mutant Stx-2 were added to the wells of the plate in triplicate and the plate was incubated at room temperature for 2 h with shaking. After the wells of the plate were emptied and rinsed three times, 200 $\mu$ L of the secondary antibody STX2-11E10 HRP-conjugate (5 $\mu$ g/mL) was added to each well and incubated again for 2 h at room temperature with shaking. A final series of rinses was performed five times with 300 $\mu$ L of PBS incubated at room temperature for 5 min with shaking and 150 $\mu$ L of 1-Step ABTS (Thermo Scientific) was added to each well and developed for 10 min at room temperature. The reaction was stopped by the addition of 100 $\mu$ L of 1% SDS and measured for absorbance at 405nm.



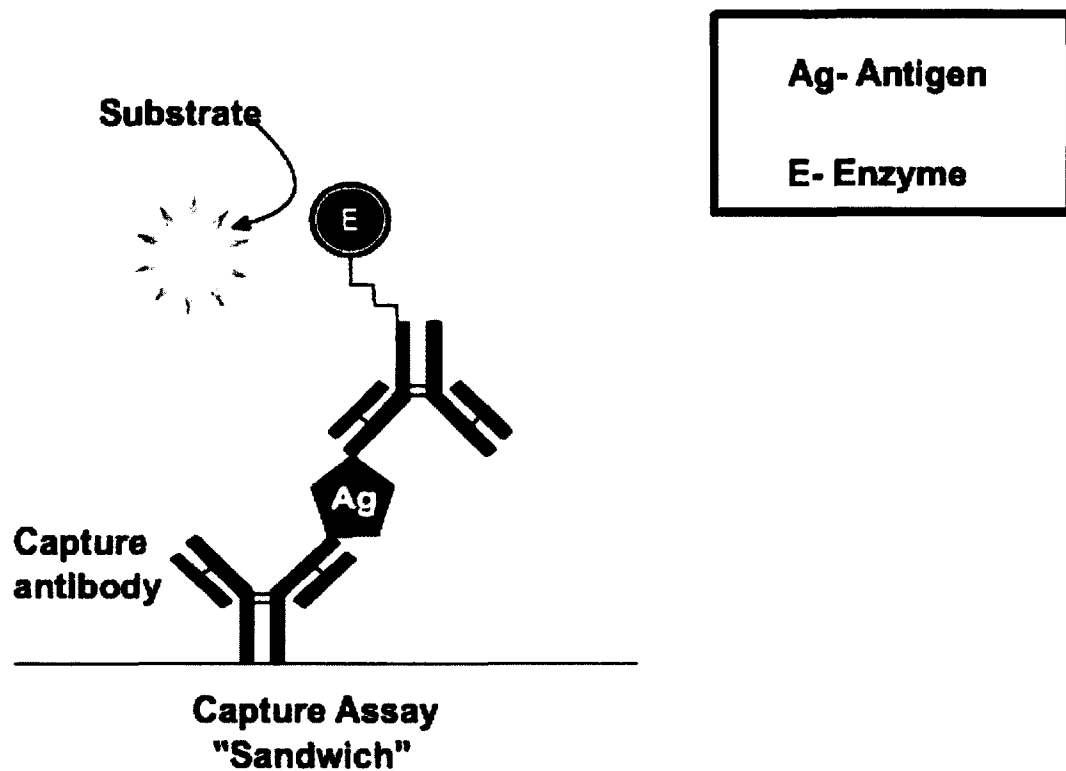


**Figure 5.1: Setup of a sandwich ELISA.** A primary or capture antibody is affixed to a microtiter plate and the antigen of interest is bound. A secondary antibody conjugated with an enzyme is bound to the antigen and developed with a substrate to produce a color change. Diagram courtesy of Amrita Vishwa Vidyapeetham University, Coimbatore, Tamil Nadu, India.

Row	1	2	3	4	5	6	7	8	9	10	11	12
A	400ng	200ng	100ng	50ng	25ng	12.5ng	6.25ng					
B	400ng	200ng	100ng	50ng	25ng	12.5ng	6.25ng					
C	400ng	200ng	100ng	50ng	25ng	12.5ng	6.25ng	N/A	N/A	N/A	N/A	N/A
D												
E												
F	N/A	N/A	N/A	N/A	N/A	N/A	N/A	N/A	N/A	N/A	N/A	N/A
G	N/A	N/A	N/A	N/A	N/A	N/A	N/A	N/A	N/A	N/A	N/A	N/A
H	N/A	N/A	N/A	N/A	N/A	N/A	N/A	N/A	N/A	N/A	N/A	N/A
<b>A1-C7</b>	= standard curve							= PBS Blank with entire process				
	= mutant Stx-2 sample							= ABTS Solution only!! (no antibody)				
	= Stx-2 sample						N/A	= empty well				

**Figure 5.2: Setup of the ELISA plate.** The standard curve was diluted 1:2 and tested in triplicate. Values listed represent the total number of nanograms of commercially prepared Stx-2 per well. Stx-2 and mutant Stx-2 samples were also diluted 1:2 and tested in triplicate along with PBS blank and ABTS controls (n=5).

#### **4.6 Isolation of Human Neutrophils**

Neutrophils were collected from human blood using the Sigma Aldrich leukocyte separation method shown in Figure 3.1 on pg. 96. Three mL of Histopaque™ 1119 was added to a 15mL conical tube and 3mL of Histopaque™ 1077 was carefully layered on top followed by 6mL of human blood. The tubes were centrifuged at 700 x g for 30 min at room temperature. After centrifugation, layer B containing the granulocytes was aseptically transferred using a pipette to a 50mL conical tube and an equal volume of modified Hank's balanced salt solution (HBSS) was added. The cells were washed by centrifugation at 250 x g for 10 min at room temperature and the supernatant fluid was removed. The cell pellet was resuspended in 12mL of 0.2% NaCl for 30 sec to lyse any remaining red blood cells. The suspension was then returned to an isotonic state with the addition of 12mL of 1.6% NaCl and centrifuged at 250 x g for 10 min. This was repeated three times until all red blood cells were lysed. The neutrophils were resuspended in 2mL RPMI-1640 (Appendix A, 5.4), assessed for viability with trypan blue, and counted using a hemocytometer.

#### **4.7 Analysis of Neutrophil Apoptosis and Necrosis Rates Following Exposure to Native and Mutant Stx-2**

Neutrophil apoptosis and necrosis rates were measured over time at 0, 6, 12, 18, 24 and 48 h using the Cell Death Detection ELISA kit (Roche Diagnostics). This ELISA detects fragmented DNA and histone complexes. Neutrophils were isolated as described

previously, a suspension was made in RPMI-1640 containing 50,000 cells/mL and 200 $\mu$ L was dispensed into each well of a 96-well plate (see Table 5.1 for time points). A separate plate was used for each time point. Three blood samples from different donors were tested in triplicate (n=9 total). The negative control consisted of neutrophils only (C), the IL-8 inhibitor control consisted of neutrophil suspension plus 0.01mM IL-8 inhibitor (I), while the test samples consisted of the neutrophil suspension plus the semi-pure protein preparations containing either 5 ng mutant Stx-2 (M) or 5 ng of Stx-2 (T), or the neutrophil suspension plus 5 ng Stx-2 and 0.01mM IL-8 inhibitor (TI).

For each time point, the 96-well plate was centrifuged at 200 x g for 10 min and the supernatants were collected and held at 2-8 $^{\circ}$ C to assay for necrosis. The cell pellet was lysed for 30 min at room temperature with the lysis buffer provided in the kit, the plate was centrifuged again at 200 x g for 10 min, and the supernatant fluid was analyzed for apoptosis. Twenty  $\mu$ L of each supernatant sample (pre-lysis and post-lysis), positive control (DNA-histone-complex), and background control (incubation buffer) were transferred to a streptavidin coated plate and 80 $\mu$ L of immunoreagent containing incubation buffer, anti-histone biotin, and anti-DNA-POD were added. The samples were shaken at 300 rpm for 2 h at room temperature, rinsed three times with 300 $\mu$ L incubation buffer each wash, and developed with 100 $\mu$ L ABTS. Absorbance was measured at 405nm using a SpectraMax M5 plate reader with SoftMax Pro v5.4.2 (Molecular Devices, Sunnyvale, CA).

**Table 5.1: Neutrophil Cell Death Detection Time Point Setup<sup>1</sup>**

96-well plate Row/Column	1	2	3	4	5	6	7	8	9	10	11	12
A	C	C	C	-				-				-
B	I	I	I	-				-				-
C	M	M	M	-				-				-
D	T	T	T	-				-				-
E	TI	TI	TI	-				-				-
F	-	-	-	-	-	-	-	-	-	-	-	-
G	-	-	-	-	-	-	-	-	-	-	-	-
H	-	-	-	-	-	-	-	-	-	-	-	-

<sup>1</sup> 10,000 cells were added to each well suspended in 200 $\mu$ L RPMI-1640. A separate plate was used for each time point.

**Sample Key:**

- 'C' = Negative control (neutrophils only)
- 'I' = IL-8 inhibitor added at final concentration 0.01mM (IL-8 inhibitor control)
- 'M' = 5 ng mutant Stx-2 added
- 'T' = 5 ng Stx-2 added
- 'TI' = 5 ng Stx-2 and IL-8 inhibitor added at final concentration 0.01mM
- = Blood Donor A
- = Blood Donor B
- = Blood Donor C
- '-' = Blank well

#### **4.8 Analysis of Neutrophil Caspase-8 and Caspase-9 Activation Following Exposure to Native and Mutant Stx-2**

Caspase-8 and Caspase-9 activation were monitored at times 0, 6, 12, 18, 24, and 48 h after exposure to Stx-2 and mutant Stx-2. In addition, the effect of an IL-8 inhibitor was analyzed to better understand the type of apoptotic trigger(s) involved. Enzyme activation was detected using the Caspase-Glo® 8 and Caspase-Glo® 9 Assays (Promega). All reagents were prepared according to the manufacturer's instructions with the addition of the MG-132 inhibitor. Neutrophils were isolated from whole blood and diluted in RPMI-1640 to give a concentration of 50,000 cells/mL. One mL was placed in glass test tubes and treated as follows: sample 1, negative control, untreated (C); sample 2, IL-8 inhibitor added at 0.1mM (I); sample 3 mutant Stx-2 added at 0.25 ng/μL (M); sample 4, Stx-2 added at 0.25 ng/μL (T); and sample 5, Stx-2 added together with IL-8 inhibitor at 0.25 ng/μL and 0.1mM, respectively (TI). All tubes were allowed to incubate at 37°C in 5% CO<sub>2</sub> until the elapsed time point. At each time point, the tubes were gently mixed and 20μL of neutrophil cell suspension was added in triplicate to wells of a 384-well plate for each caspase test. Twenty μL of caspase-8 or caspase-9 reagent was added to each well, gently mixed for 30 sec and allowed to incubate at room temperature for 45 min. After incubation was complete, the plate was assayed for luminescence using a SpectraMax M5 plate reader with SoftMax Pro v5.4.2 (Molecular Devices).

## **5.0 Results**

### **5.1 Verification of Stx-2 and Mutant Stx-2 Presence and Activity**

The purification of Stx-2 from *E. coli* O157:H7 strain 90-2380 (native Stx-2) and mutant Stx-2 from the L42 mutant of *E. coli* O157:H7 strain 43888 (mutant Stx-2) was achieved as demonstrated by total protein concentration and purity, SDS-PAGE, and Western blot.

To determine total protein concentration and purity of the native and mutant Stx-2 preparations, optical densities were taken at  $A_{280\text{nm}}$  and  $A_{260\text{nm}}$ . The total protein concentrations were determined to be 0.300 mg/mL for native Stx-2 and 0.110 mg/mL for mutant Stx-2 while the purity (as determined by the  $A_{280} / A_{260}$  ratio) was 1.05 for native Stx-2 and 0.810 for mutant Stx-2. These values indicate the presence of nucleic acid which can influence the total protein concentration accuracy. Correction factors of 0.81 and 0.63 were applied to the native and mutant Stx-2 values respectively in accordance with the Warburg-Christian Method (211). The final protein concentrations were determined to be 0.243 mg/mL protein with 3.5% nucleic acid (native Stx-2) and 0.069 mg/mL protein with 6.0% nucleic acid (mutant Stx-2).

SDS-PAGE of semi-purified native Stx-2 (panel A) and mutant Stx-2 (panel B) are shown in Figure 5.3. Target protein load was 2.4  $\mu\text{g}$  for native Stx-2 and 1.4  $\mu\text{g}$  for mutant Stx-2. As can be seen by comparing lanes 2, 3, and 4 with each other in panel A,

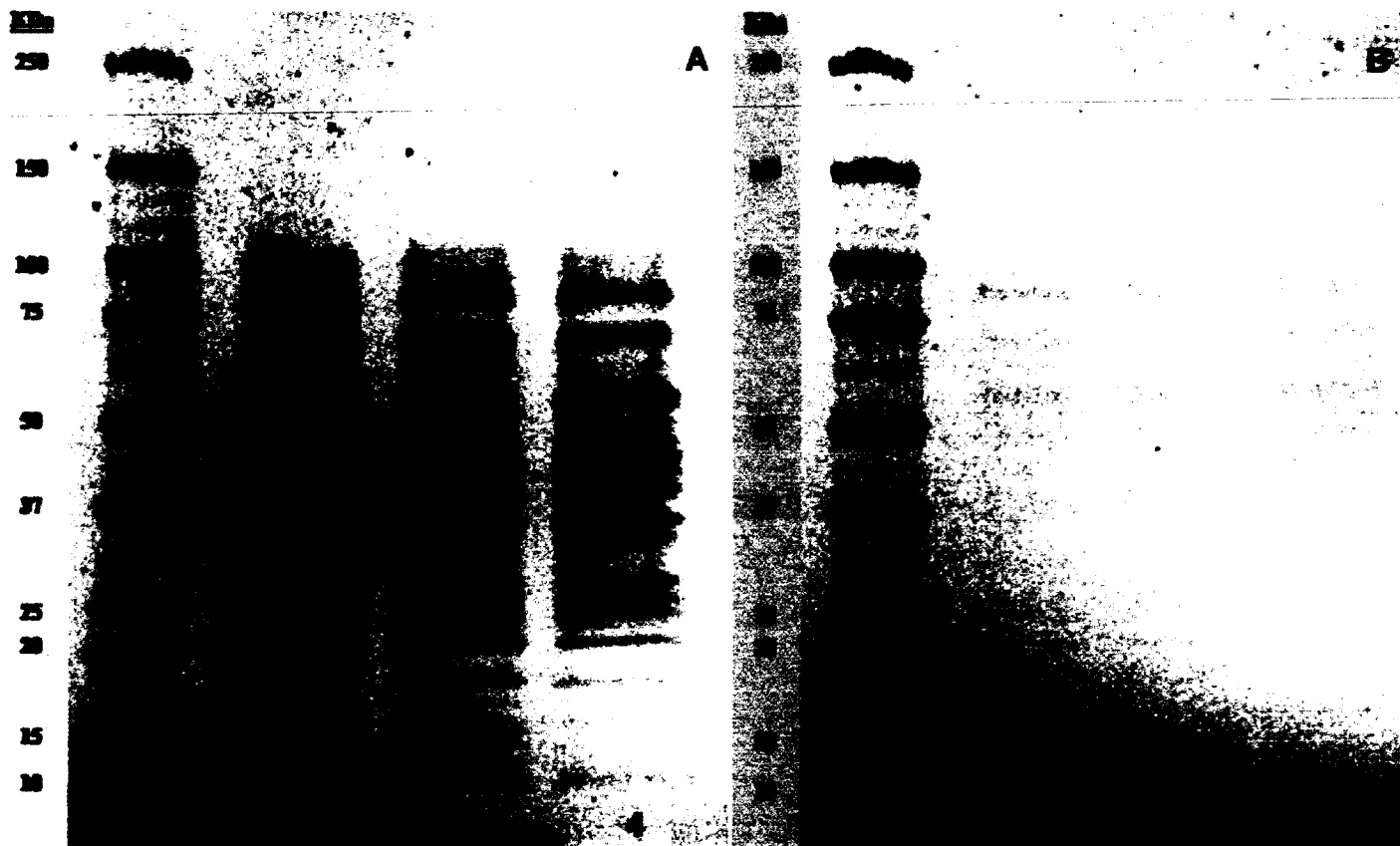


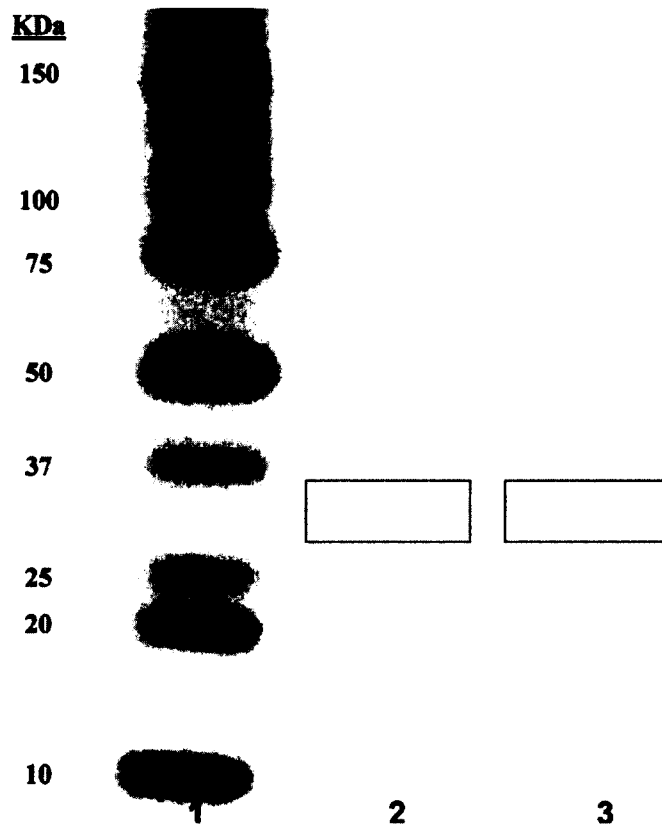
**Figure 5.3: SDS-PAGE analysis of semi-purified native and mutant Stx-2.** A) Broad-range Precision Plus Protein WesternC standards (Bio-Rad) are in Lane 1, semi-pure Stx-2 under non-reducing conditions is in Lane 2, semi-pure Stx-2 under heat only conditions is in Lane 3, and semi-pure Stx-2 under reducing conditions is in Lane 4. B) Broad-range Precision Plus Protein WesternC standards (Bio-Rad) are in Lane 1, semi-pure mutant Stx-2 under non-reducing conditions is in Lane 2, semi-pure Stx-2 under heat only conditions is in Lane 3, and semi-pure Stx-2 under reducing conditions is in Lane 4. No differences in band pattern were observed.



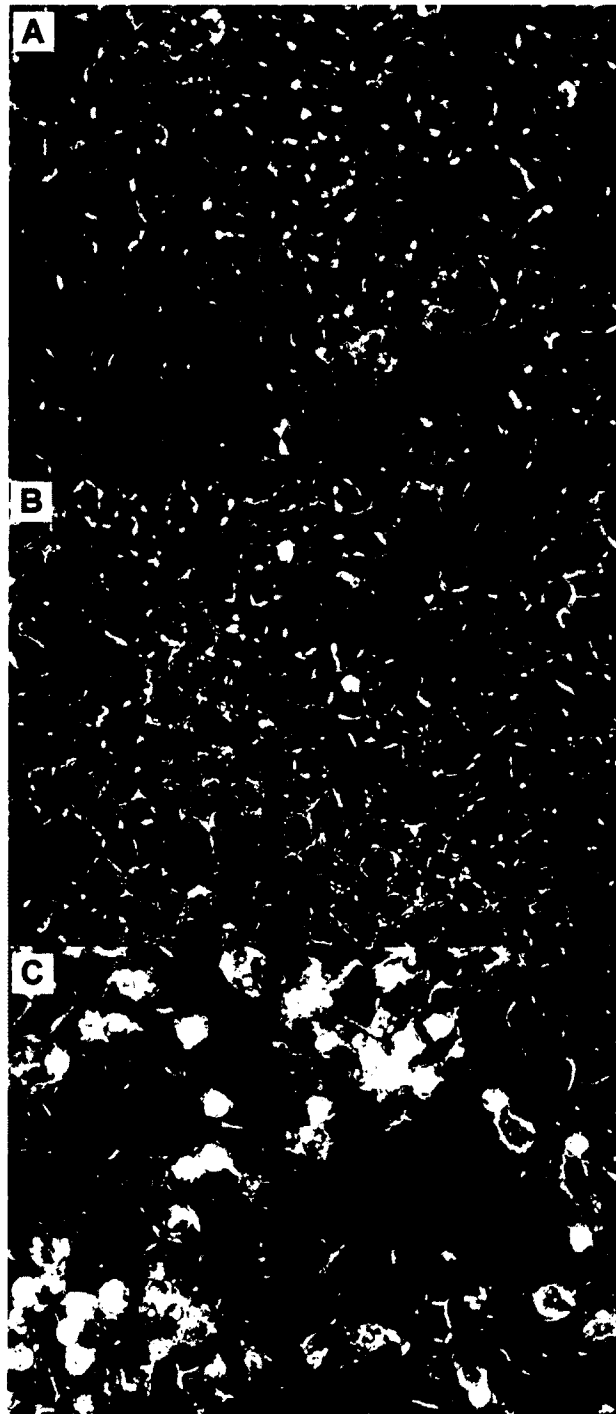
it was evident that there was no difference in the protein profile for the semi-purified toxin whether untreated, heated, or subjected to reducing conditions. Similarly, no differences were noted in the protein profiles of the mutant Stx-2 under reducing, non-reducing, or heated conditions despite the faintness of the band patterns. In addition there appears to be fewer bands in the mutant Stx-2 preparation than in the native Stx-2 preparation. It seems likely that this is due to the differences in loading concentration and in the purification procedure.

Figure 5.4 illustrates the Western blot of semi-purified native and mutant Stx-2 treated with the HRP-conjugated STX2-11E10 antibody. There was a band visible in each sample at approximately 32 kDa as highlighted by the boxed areas. These bands show the A-subunit of native and mutant Stx-2 and confirm the presence of the toxin in both samples.

The biological activity of Stx-2 and mutant Stx-2 on Vero cells was observed at 200x magnification and is illustrated in Figure 5.5. Panel A shows untreated Vero cells while panel B corresponds to Vero cells treated with 50 $\mu$ L of semi-purified mutant Stx-2 and panel C shows Vero cells treated with 50 $\mu$ L of semi-purified native Stx-2. Cytotoxic effects typical of Stx-2 were observed in the cell monolayers (rounded, refractile and dead cells with monolayer thinning) as evident in panel C of Figure 5.5. Minimal cytotoxic changes were observed in the cells from the mutant Stx-2 indicating that the point mutation within the NWGRI motif had a profound impact on the ability of Stx-2 to cause cellular damage in these otherwise highly sensitive cells.



**Figure 5.4: Western blot analysis of toxin preparations.** Broad-range Precision Plus Protein WesternC standards are in Lane 1, semi-pure native Stx-2 preparation probed with HRP-conjugated STX2-11E10 is in Lane 2, and semi-pure mutant Stx-2 preparation probed with HRP-conjugated STX2-11E10 is in Lane 3. The A-subunit of Stx-2 and mutant Stx-2 was detected in the boxed areas of Lane 2 and 3, respectively.



**Figure 5.5: Biological Activity of semi-purified Stx-2 and mutant Stx-2 viewed at 200x magnification.** A) Image of untreated Vero cells after 96 h. B) Image of Vero cells after 96 h incubation with 50 $\mu$ L semi-purified mutant Stx-2. C) Image of Vero cells after 96 h incubation with 50 $\mu$ L semi-purified native Stx-2. Cytotoxic effects are evident by the large number of rounded and refractile cells in panel C. Note that the cells treated with mutant Stx-2 were similar to controls and showed minimal cytopathic changes.

## **5.2 Quantitation of Stx-2 and Mutant Stx-2 Using ELISA**

Standard curves were assayed in triplicate and the results are shown in Figure 5.6. The average background absorbance was calculated between the quintuplet blanks, and this value was subtracted from the total absorbance reading in each well. Three points were used to generate a standard curve between 25 and 100ng of Stx-2. The triplicate standard curve values were averaged and plotted to produce an average standard curve with a correlation coefficient ( $r^2$ ) of 0.9673.

The total Stx-2 protein concentration for the semi-pure preparation was calculated by averaging the absorbance of the undiluted triplicate samples assayed as these values were within the center of the standard curve. This average value was then entered into the standard curve regression equation, and a final protein concentration of 6.42 $\mu$ g/mL was obtained.

The total mutant Stx-2 protein concentration for the semi-pure preparation was calculated by averaging the absorbance of the 1:2 diluted triplicate samples assayed as these values were within the center of the standard curve. The average value was entered into the standard curve regression equation, and a final protein concentration of 9.46 $\mu$ g/mL was obtained after adjusting for a 1:2 sample dilution.

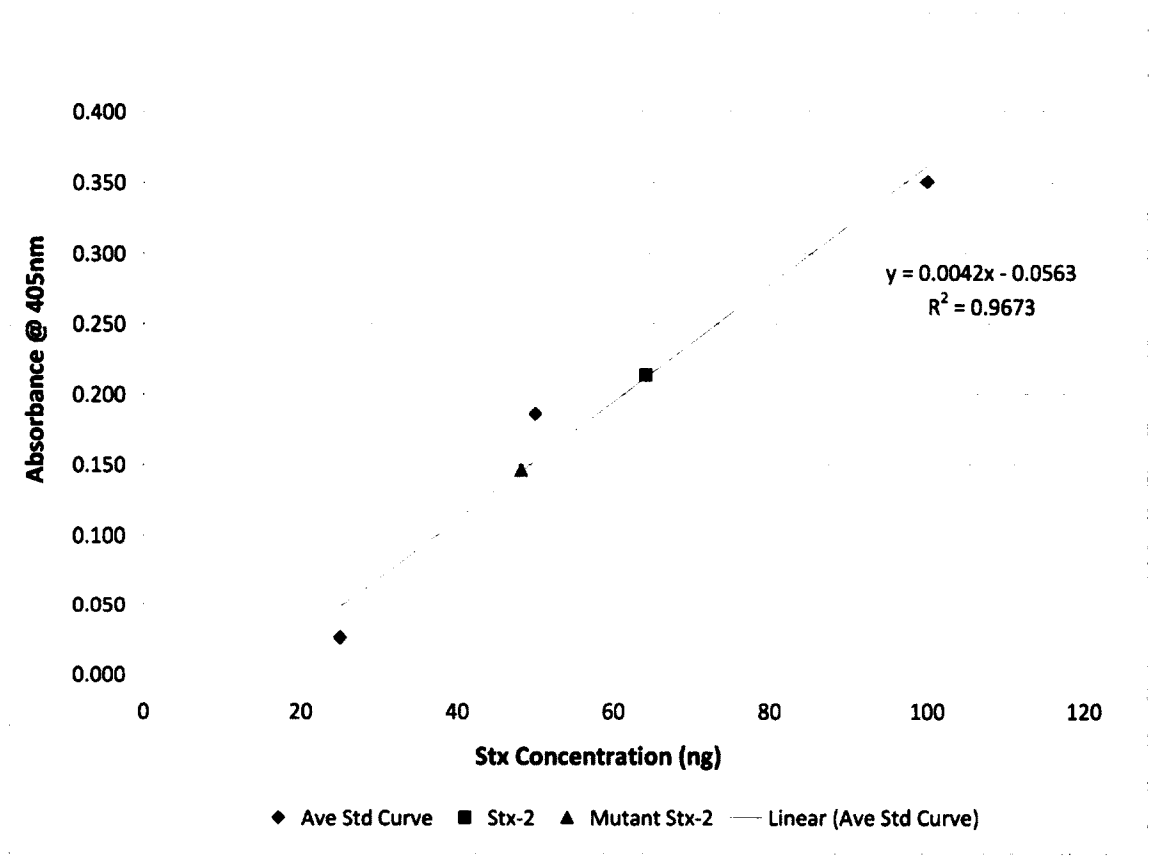


**Figure 5.6: Total protein concentration of toxin preparations.** Total protein concentration of Stx-2 and mutant Stx-2 in the semi-purified preparations. The average standard curve shown by the ◆ symbol with correlation coefficient of  $r^2 = 0.9673$  and regression equation of  $y = 0.0042x - 0.0563$ . The total calculated Stx-2 concentration was  $6.42\mu\text{g/mL}$  shown by the ■ symbol and the total calculated mutant Stx-2 concentration after 1:2 dilution adjustment was  $9.46\mu\text{g/mL}$  shown by the ▲ symbol.

### **5.3 Isolation of Human Neutrophils**

Neutrophils from three blood donors were isolated and counted using a hemocytometer and the total cell concentration and viability of each sample were obtained (Table 5.2). The viability of neutrophils from Donor B was much higher (97.3%) when compared to Donor A (85%) and Donor C (86.2%). This was most likely due to the effect of multiple red blood cell lysis steps on the suspension. In order to lyse contaminating red blood cells, neutrophil suspensions were osmotically shocked. This method lysed the red blood cells and undoubtedly some neutrophils accounting for the differences in viability noted. The overall health of isolated neutrophils also influences how susceptible they are to osmotic damage. Indeed, the maximum number of times the suspension can be shocked should be limited to three times. During this experiment, a high number of red blood cells were present after granulocyte collection and the full three rounds of osmotic shocking were needed to lyse and remove them. This accounted for the lower viability seen in the neutrophil suspensions from Donors A and C and this may have either increased the initial necrosis and/or apoptosis results or may have made the cells more susceptible to the effects of the toxin. Regardless, the results obtained for all three donor cell preparations have been presented. Based on the higher viability and the overall higher neutrophil cell count from Blood Donor B as compared with those from either Blood Donors A or C, all subsequent investigations on the action of native Stx-2, mutant Stx-2 or IL-8 inhibitor on necrosis or apoptosis was conducted on neutrophils collected from Blood Donor B. Similarly, the caspase-8 and caspase-9 levels were assayed in Blood Donor B neutrophils.

**Table 5.2: Viability of Neutrophils Collected from 3 Donors**

Sample Name	No. Live Cells Counted	No. Dead Cells Counted	% Viability	Total No. Neutrophils (cells/mL)
Blood Donor A	608	107	85.0	$6.08 \times 10^6$
Blood Donor B	1128	31	97.3	$1.1 \times 10^7$
Blood Donor C	638	102	86.2	$6.38 \times 10^6$

#### **5.4 Analysis of Neutrophil Necrosis and Apoptosis Rates After Exposure to Native Stx-2, Mutant Stx-2, and IL-8 Inhibitor**

Necrosis and apoptosis rates were examined for the neutrophil preparation isolated from Donor B after 0, 6, 12, 18, 24, and 48 h of treatment with native Stx-2, mutant Stx-2 or IL-8 inhibitor. Assays were performed in triplicate and the results were standardized by expressing the final result as a percent of the positive control provided in the kit for each assay. The mean and standard deviation of each test article was calculated, and a t-test was performed on seven sample comparisons (neg. control vs. native Stx-2, neg. control vs. mutant Stx-2, mutant Stx-2 vs. native Stx-2, neg. control vs. IL-8 inhibitor, neg. control vs. IL-8 inhibitor & native Stx-2, and IL-8 inhibitor vs. IL-8 inhibitor & native Stx-2) to assess the effects of native Stx-2, mutant Stx-2, and IL-8 inhibitor on neutrophil apoptosis and necrosis.

##### **5.4.1 Necrosis Rates**

Significant differences were observed between sample comparisons with a 95% confidence interval ( $p < 0.05$ ). Necrosis rates are shown in Figure 5.7 and a summary of the statistical comparison is shown in Table 5.3. In comparison with untreated neutrophils, the cells showed significantly more necrosis at 6 and 12 h when exposed to native Stx-2 and at 12, 24, and 48 h when exposed to mutant Stx-2. There were no significant differences in necrosis noted between cells exposed to native Stx-2 and mutant Stx-2 except at 48 h, where mutant Stx-2 exhibited significantly more necrosis. These



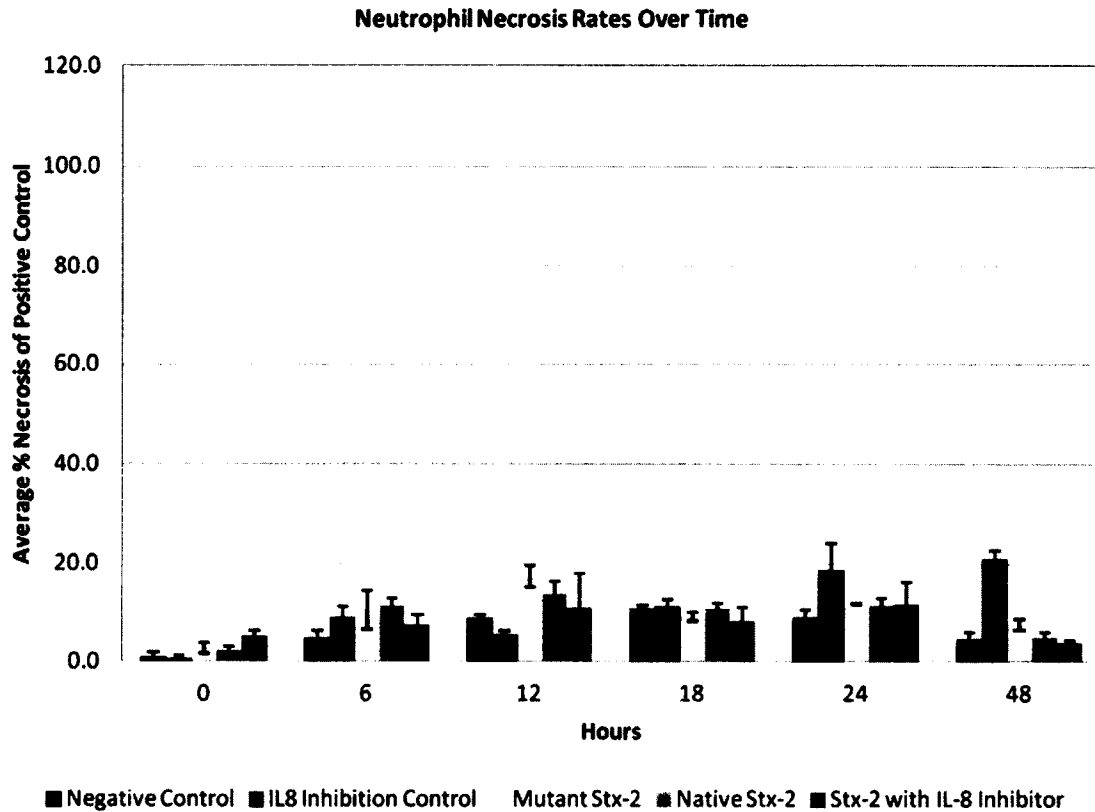


**Figure 5.7: Necrosis rates for blood donor B.** Data is presented as the average percent necrosis when compared to the positive assay control. Error bars represent the standard deviation calculated between triplicates. Significant differences were observed between treatments with peak necrosis rates for the IL-8 inhibition control at 48 h, mutant Stx-2 at 48 h, native Stx-2 between 6-12 h, and Stx-2 with IL-8 inhibitor peaking at 12 h.

**Table 5.3: Summary of Statistical Analysis for Blood Donor B: Necrosis**\* indicates a significant difference ( $p < 0.05$ )

<i>Sample</i>	<i>Time Point (h)</i>	<i>Unpaired t-test P-value</i>
Negative Control vs. Stx-2	0	0.0932
	6	0.0036*
	12	0.0354*
	18	0.8046
	24	0.1091
	48	0.5960
Negative Control vs. Mutant Stx-2	0	0.0864
	6	0.0836
	12	0.0026*
	18	0.0795
	24	0.0329*
	48	0.0418*
Mutant Stx-2 vs. Stx-2	0	0.6545
	6	0.7201
	12	0.1396
	18	0.0950
	24	0.6650
	48	0.0379*
Negative Control vs. IL-8 Inhibitor	0	0.6767
	6	0.0564
	12	0.0071*
	18	0.5407
	24	0.0328*
	48	0.0002*
Negative Control vs. IL-8 Inhibitor + Stx-2	0	0.0057*
	6	0.1243
	12	0.6162
	18	0.1980
	24	0.4065
	48	0.4844
IL-8 Inhibitor vs. IL-8 Inhibitor + Stx-2	0	0.0022*
	6	0.4521
	12	0.2681
	18	0.1508
	24	0.1422
	48	0.0001*
Stx-2 vs. IL-8 Inhibitor + Stx-2	0	0.0177*
	6	0.0410*
	12	0.5593
	18	0.1847
	24	0.9628
	48	0.1207

data show that necrosis is initiated in neutrophils exposed to both native and mutant Stx-2, with comparable necrotic effects until 48 h when the mutant Stx-2-treated cells showed elevated necrosis, possibly due to cell density differences between wells.

Neutrophils exposed to IL-8 inhibitor showed significantly less necrosis at 12 h, but significantly more necrosis at 24 and 48 h in comparison with the untreated control. In addition, neutrophils exposed to a combination of native Stx-2 and IL-8 inhibitor demonstrated significantly more necrosis at 0 h when compared to untreated and IL-8 inhibitor-treated samples, but also exhibited significantly less necrosis at 48 h when compared to IL-8 inhibitor-treated neutrophils. Finally, neutrophils exposed to native Stx-2 and IL-8 inhibitor were significantly more necrotic at 0 h and significantly less necrotic at 6 h than cells exposed to native Stx-2 alone. These data indicate that IL-8 inhibitor-induced necrosis occurs after 24 h, and that this inhibitor also lowers native Stx-2-induced necrosis overall, but only significantly at 6 h. It is believed that the significant increases in neutrophil necrosis at 0 h in samples treated with native Stx-2 and IL-8 inhibitor are not directly correlated with treatment, rather they are a result of cell damage from the neutrophil isolation procedure, especially since the necrosis rates were low overall (< 5.3%).

The effects of these treatments on neutrophil necrosis indicated that necrosis rates were changed significantly; Native Stx-2-induced necrosis was highest between 6-12 h of exposure, mutant Stx-2-induced necrosis peaked at 48 h, and IL-8-inhibitor-

induced necrosis peaked at 24-48 h, and IL-8 inhibitor with native Stx-2 necrosis rates peaked at 12 h.

#### **5.4.2 Apoptosis Rates**

Significant differences in apoptosis rates ( $p < 0.05$ , 95% confidence interval) were observed between samples. Apoptosis rates are shown in Figure 5.8 and a summary of the statistical comparison is shown in Table 5.4. There was significantly more apoptosis in cells exposed to native Stx-2 at 18 h than untreated cells. In addition, neutrophils exposed to mutant Stx-2 showed a significant increase in apoptosis when compared to untreated cells, however this was not observed until 48 h. It is believed that this significance may not be practical since the level of apoptosis detected was extremely low (0.02% vs. 0.28%). Comparing native Stx-2 to mutant Stx-2, only a significant increase in native Stx-2-induced apoptosis was observed at 18 h. No other statistical differences between the two treatments were noted. Overall, these data show that apoptosis was observed for a longer period of time in cells exposed to native Stx-2, but this does not equate to a delay in apoptosis as the results were the same as the control prior to 18 h. Cells exposed to mutant Stx-2 showed equivalent apoptosis rates to the control.

Neutrophils exposed to IL-8 inhibitor showed an overall trend of higher apoptosis than the untreated control at all time points, however significance was only achieved at 0 and 48 h. Cells exposed to IL-8 inhibitor and native Stx-2 showed equivalent results to untreated controls at 0, 6, 12, 24, and 48 h, but had significantly more apoptosis at 18 h.

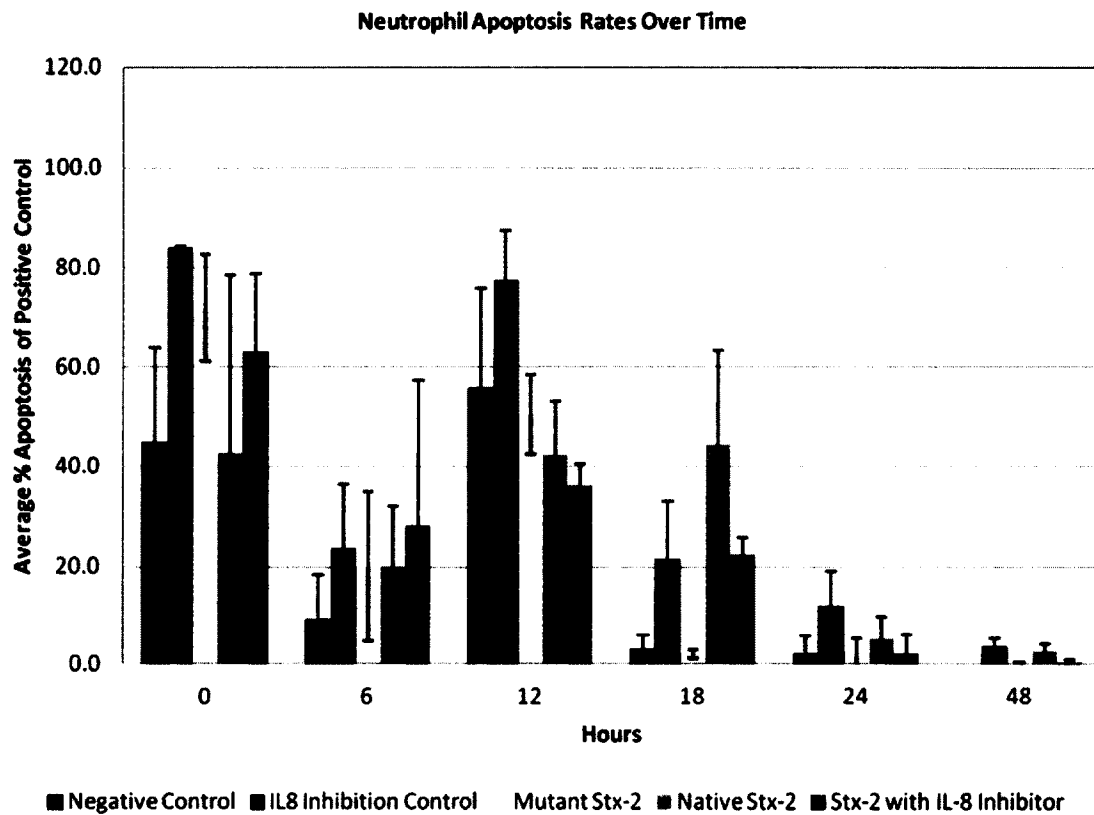


**Figure 5.8: Apoptosis rates for Blood Donor B.** Data are presented as the average percent apoptosis when compared to the positive assay control. Error bars represent the standard deviation calculated between triplicates. Significant differences were observed between treatments. The IL-8 inhibition control, mutant Stx-2, and Stx-2 with IL-8 inhibitor-treated samples showed peak apoptosis rates at 0 and 12 h, whereas native Stx-2-treated neutrophils showed peak apoptosis rates between 12-18 h. The data support that this 0 h apoptosis peak represents cell damage from the neutrophil isolation procedure, and the 12 h apoptosis peak observed was representative of spontaneous neutrophil apoptosis, unrelated to the treatment method. The peak observed at 18 h with Stx-2 treated neutrophils illustrated the apoptotic effect of the toxin.

**Table 5.4: Summary of Statistical Analysis for Blood Donor B: Apoptosis**  
 \* indicates a significant difference ( $p < 0.05$ )

<i>Sample</i>	<i>Time Point (h)</i>	<i>Unpaired t-test P-value</i>
Negative Control vs. Stx-2	0	0.9319
	6	0.3041
	12	0.3697
	18	0.0207*
	24	0.4065
	48	0.0545
Negative Control vs. Mutant Stx-2	0	0.0973
	6	0.3554
	12	0.6882
	18	0.5280
	24	0.8750
	48	0.0088*
Mutant Stx-2 vs. Stx-2	0	0.2487
	6	0.9865
	12	0.3662
	18	0.0183*
	24	0.4307
	48	0.0732
Negative Control vs. IL-8 Inhibitor	0	0.0223*
	6	0.1859
	12	0.1691
	18	0.0556
	24	0.0937
	48	0.0249*
Negative Control vs. IL-8 Inhibitor + Stx-2	0	0.2679
	6	0.3417
	12	0.1731
	18	0.0017*
	24	0.9492
	48	0.2939
IL-8 Inhibitor vs. IL-8 Inhibitor + Stx-2	0	0.0809
	6	0.8134
	12	0.0029*
	18	0.8963
	24	0.0972
	48	0.0395*
Stx-2 vs. IL-8 Inhibitor + Stx-2	0	0.4187
	6	0.6642
	12	0.3907
	18	0.1213
	24	0.4305
	48	0.0933

In addition these cells also showed significantly less apoptosis at 12 and 48 h than cells exposed to IL-8 inhibitor alone, and the presence of an IL-8 inhibitor had no effect on Stx-2-induced apoptosis. This data show that the apoptotic effect of Stx-2 is exhibited between 12 and 18 hours after exposure, despite the presence of IL-8.

The effects of these treatments illustrated that neutrophil apoptosis rates were significantly changed; native Stx-2-induced apoptosis peaked between 12-18 h, mutant Stx-2-induced apoptosis peaked at 0 h and again at 12 h, IL-8 inhibition control peaked at 0 and 12 h, and Stx-2 with IL-8 inhibitor peaked at 0 and 12 h. Apoptosis rates were highest overall at 0 h for all samples, however this peak represents that cell damage from the neutrophil isolation procedure did occur. The apoptosis peak observed at 12 h was related to spontaneous neutrophil apoptosis. The peak observed at 18 h with Stx-2 treated neutrophils illustrated the apoptotic effect of the toxin.

#### **5.5 Analysis of Neutrophil Caspase-8 and Caspase-9 Activation After Exposure to Native Stx-2, Mutant Stx-2, and IL-8 Inhibitor**

Caspase-8 and Caspase-9 levels were measured using luminescence after neutrophils isolated from Donor B were exposed in triplicate to native Stx-2, mutant Stx-2, and IL-8 inhibitor for 0, 6, 12, 18, and 24 h. No blanking was performed on these assays as there was a high background in the blanking wells resulting from luminescence signal carryover in adjacent positive control wells. The mean and standard deviation of measurements were calculated and t-tests performed on seven sample comparisons to

assess the effects of native Stx-2, mutant Stx-2, and IL-8 inhibitor on caspase-8 and caspase-9 activation.

### **5.5.1 Caspase-8**

Caspase-8 activation was significantly different ( $p < 0.05$ , 95% confidence interval) between five out of the seven comparisons. Caspase-8 activation is summarized in Figure 5.9 and sample comparisons are summarized Table 5.5. No significant differences were observed between native Stx-2-treated and untreated cells. A significant increase in caspase-8 activation was observed in mutant Stx-2-treated cells at 0 and 24 h compared to the control. In addition, there was a significant increase in caspase-8 activation at 0 h in cells exposed to mutant Stx-2 when compared to native Stx-2.

The IL-8 inhibitor treated cells showed lower caspase-8 activation overall when compared to the control; significance was achieved at 12 h and beyond. Neutrophils exposed to IL-8 inhibitor and Stx-2 showed significant decreases in caspase-8 activation at 12 and 18 h when compared to untreated cells, but did not show any significant differences when compared to IL-8 inhibitor-treated cells. Finally, neutrophils exposed to IL-8 inhibitor and native Stx-2 showed a sustained significant decrease in caspase-8 activation after 12 h when compared to native Stx-2 alone.

Caspase-8 activation was significantly different between these treatments; however they all followed the same overall pattern with activation rates peaking at 6 h. This is



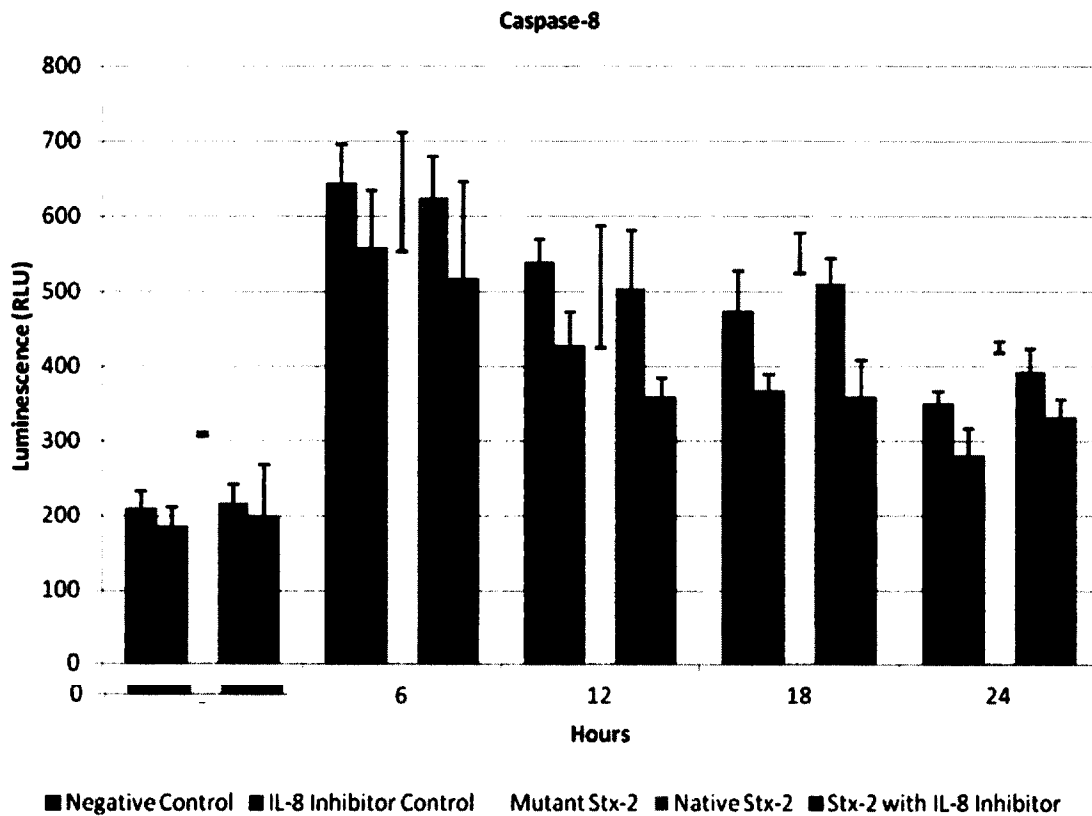


**Figure 5.9: Relative caspase-8 levels for blood donor B.** Relative caspase-8 levels in cells isolated from Blood Donor B. Error bars represent the standard deviation calculated between triplicates. Caspase-8 activation peaked in all samples at 6 h. It is believed that this peak is related to spontaneous neutrophil apoptosis observed at 12 h, independent of treatment method. Caspase-8 activation was significantly different between treatments; however they all followed the same overall pattern with activation rates peaking at 6 h. This is likely related to the spontaneous neutrophil apoptosis peak detected at 12 h, as caspase-8 activation occurs prior to DNA fragmentation, which is the antigen primarily detected in the ELISA. Note that no significant increase in caspase-8 activation was detected in the neutrophils treated with Stx-2.

**Table 5.5: Summary of Statistical Analysis for Blood Donor B: Relative Caspase-8 Levels**

<i>Sample</i>	<i>Time Point (h)</i>	<i>Unpaired t-test P-value</i>
Negative Control vs. Stx-2	0	0.7106
	6	0.6866
	12	0.5118
	18	0.3559
	24	0.0824
Negative Control vs. Mutant Stx-2	0	0.0018*
	6	0.8485
	12	0.5553
	18	0.0872
	24	0.0014*
Mutant Stx-2 vs. Stx-2	0	0.0032*
	6	0.8961
	12	0.9802
	18	0.1809
	24	0.1526
Negative Control vs. IL-8 Inhibitor	0	0.2962
	6	0.1826
	12	0.0245*
	18	0.0299*
	24	0.0317*
Negative Control vs. IL-8 Inhibitor + Stx-2	0	0.8268
	6	0.1857
	12	0.0014*
	18	0.0474*
	24	0.2861
IL-8 Inhibitor vs. IL-8 Inhibitor + Stx-2	0	0.7402
	6	0.6563
	12	0.0848
	18	0.7921
	24	0.0993
Stx-2 vs. IL-8 Inhibitor + Stx-2	0	0.6952
	6	0.2484
	12	0.0353*
	18	0.0104*
	24	0.0420*

\* indicates a significant difference ( $p < 0.05$ )

likely related to the spontaneous neutrophil apoptosis peaks detected at 12 h, as caspase-8 activation occurs prior to DNA fragmentation, which is detected in the ELISA. In addition, no significant increase in caspase-8 activation was detected in the neutrophils treated with Stx-2 which indicates that Stx-2 induced apoptosis does not occur through the extrinsic apoptosis pathway.

### **5.5.2 Caspase-9**

Caspase-9 activation was determined to be significantly different ( $p < 0.05$ , 95% confidence interval) for five out of seven comparisons. Caspase-9 activation is summarized in Figure 5.10 and sample comparisons are shown in Table 5.6. No difference in caspase-9 activation was detected for neutrophils exposed to native Stx-2 when compared to the untreated and mutant Stx-2-treated neutrophils. At 6 and 12 h there was significantly less caspase-9 activation and at 18 h significantly more caspase-9 activation in neutrophils exposed to mutant Stx-2 when compared to the control.

Neutrophils treated with IL-8 inhibitor demonstrated significantly less caspase-9 activation at 6, 12, and 18h when compared to untreated cells as well as IL-8 inhibitor and Stx-2-treated cells. In addition, significantly less caspase-9 activation was seen at 12 h in cells treated with IL-8 inhibitor and Stx-2 versus IL-8 inhibitor only. Finally, there was a significant sustained reduction of caspase-9 activation from 0 to 18 h in cells exposed to IL-8 inhibitor and Stx-2 as compared to Stx-2 only.

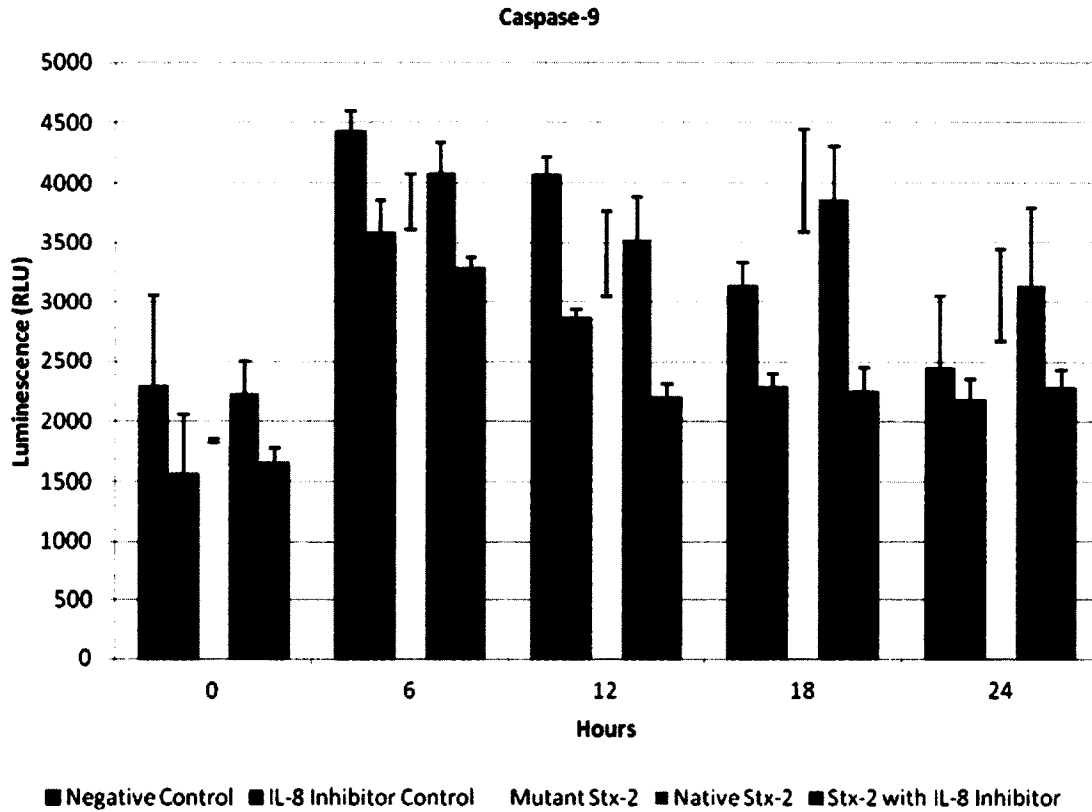


**Figure 5.10: Relative caspase-9 levels for blood donor B.** Relative caspase-9 levels in cells isolated from Blood Donor B. Error bars represent the standard deviation calculated between triplicates. Caspase-9 activation was significantly different between these treatments; samples treated with native and mutant Stx-2 showed overall higher caspase-9 activation at 18 h, related to mitochondrial membrane permeabilization (MMP). Caspase-9 activation was reduced in all samples treated with IL-8 inhibitor with significance achieved at 6, 12, and 18 h. This indicates that the intrinsic pathway is not utilized in association with spontaneous neutrophil apoptosis.

**Table 5.6: Summary of Statistical Analysis for Blood Donor B: Relative Caspase-9 Levels**

<i>Sample</i>	<i>Time Point (h)</i>	<i>Unpaired t-test P-value</i>
Negative Control vs. Stx-2	0	0.9039
	6	0.1096
	12	0.0712
	18	0.0544
	24	0.2457
Negative Control vs. Mutant Stx-2	0	0.3497
	6	0.0219*
	12	0.0387*
	18	0.0315*
	24	0.2173
Mutant Stx-2 vs. Stx-2	0	0.0562
	6	0.2818
	12	0.6754
	18	0.7072
	24	0.8474
Negative Control vs. IL-8 Inhibitor	0	0.2314
	6	0.0087*
	12	0.0002*
	18	0.0029*
	24	0.5053
Negative Control vs. IL-8 Inhibitor + Stx-2	0	0.2241
	6	0.0004*
	12	<0.0001*
	18	0.0054*
	24	0.6707
IL-8 Inhibitor vs. IL-8 Inhibitor + Stx-2	0	0.7526
	6	0.1296
	12	0.0006*
	18	0.8720
	24	0.4575
Stx-2 vs. IL-8 Inhibitor + Stx-2	0	0.0248*
	6	0.0059*
	12	0.0034*
	18	0.0042*
	24	0.0890

\* indicates a significant difference ( $p < 0.05$ )

Caspase-9 activation was significantly different between these treatments; samples treated with native and mutant Stx-2 showed overall higher caspase-9 activation at 18 h. Significance was only achieved for mutant Stx-2, however the p-value for Stx-2 was 0.0544 which is very close to the significance threshold. It is believed that the increase in caspase-9 activation is directly related to the effect of both mutant and native Stx-2 on the neutrophils, resulting from mitochondrial membrane permeabilization (MMP) which can occur simultaneously with DNA fragmentation (78, 160). Caspase-9 activation was reduced in all samples treated with IL-8 inhibitor with significance achieved at 6, 12, and 18 h. This indicates that the intrinsic pathway is not utilized in association with spontaneous neutrophil apoptosis.

## **6.0 Discussion**

During infection with *E. coli* O157:H7, it has been observed that disease pathogenesis is enhanced when neutrophils remain within the circulation and tissues to provide maximum distribution of toxin (37, 208). It is thought that neutrophils may provide a way for Stx-2 to be distributed throughout the body during infection (195). Therefore, it is critical that neutrophil necrosis and apoptosis is delayed to increase the number of neutrophils present. Previous studies on the impact of Stx-2-induced neutrophil apoptosis have shown conflicting results. Liu *et al.* (118) observed a time- and dose-dependent delay in spontaneous neutrophil apoptosis when exposed to Stx-2 whereas Flagler *et al.* (51) did not. Preliminary studies performed with supernatant from *E. coli* O157:H7 strain 90-2380 (Chapter 3) showed that a delay in apoptosis was

observed in samples up to 12 h. In order to assess why these differences were observed, a better understanding of the mechanisms of Stx-2 induced neutrophil apoptosis is needed. Yin *et al.* (225) used mutants to understand Bcl-2 family dimerization between Bcl-2 and Bax. It was thought the same technique could be utilized to understand Stx-2 and Bcl-2 family protein interactions, and confirm if they occur. The goal of these experiments was to assess the effects that semi-purified native Stx-2 and Stx-2 containing a G225A mutation had on the necrosis and apoptosis rates of neutrophils over a period of 48 h, and to determine the role that IL-8 plays in spontaneous and toxin-induced neutrophil apoptosis. Caspase-8 and caspase-9 levels were monitored over a period of 24 h to determine which apoptotic pathways were being utilized, either extrinsic (caspase-8-dependent) or intrinsic (caspase-9-dependent). It was hypothesized that neutrophils treated with mutant Stx-2 will show apoptosis rates that align with the baseline (untreated) apoptosis rate, resulting from an inability to bind to the BH1 domain of the Bcl-2 family pro-survival proteins, and that neutrophils treated with Stx-2 in combination with an IL-8 inhibitor will also show apoptosis rates that align with the baseline (untreated) apoptosis rate indicating that IL-8 was responsible for the delay in apoptosis as opposed to Stx-2.

The data obtained in this study on semi-purified Stx-2-induced neutrophil apoptosis were not consistent with the data obtained for neutrophils exposed to Stx-2-containing supernate from *E. coli* O157:H7 strain 90-2380 (Chapter 3). The supernate study showed a delay in apoptosis up to and including 12 h. The present data showed no significant differences in apoptosis at 0, 6, 12, 24, and 48h, but showed a significantly

higher rate of apoptosis after 18 h that was triggered through a caspase-9 dependent mechanism. The two major differences between the present and previous studies were sample concentration and purity. In the experiments performed in Chapter 3, the exact amount of Stx-2 tested was unknown; however in this study, 5 ng/mL of Stx-2 was added to each sample. It is possible that this concentration was insufficient to elicit the same response to that observed previously. However, the most likely scenario is that the supernate used in the previous study had residual LPS which is known to stimulate cytokine production in neutrophils including IL-8 and TNF- $\alpha$  (97). Production of these cytokines could impact the timing of apoptosis as IL-8 is known to delay neutrophil apoptosis (96). Neutrophils exposed to LPS release IL-8 in two phases; 20-30% of the total IL-8 production occurs in the first phase which begins approximately ½ hour after exposure and continues uninhibited over several hours, and the remaining IL-8 production occurs during the second phase (97) but it is more susceptible to the inhibitory effects of other cytokines such as IL-10 (26). In other words, the protective effect of IL-8 does not continue throughout the entire period that neutrophils are exposed to LPS resulting in a point at which apoptosis occurs. During the supernate study (Chapter 3), the delay in apoptosis observed with the Stx-2 exposed neutrophils ceased after 12 h thereby supporting this theory. In the present experiment, the chances that LPS were present in the semi-purified sample were low, therefore it is believed that these results give a better indication of the true effect of Stx-2 on neutrophil apoptosis.

The effect of native Stx-2 exposure on neutrophil necrosis, apoptosis, and caspase-8/-9 activation indicated that necrosis was significantly increased 6-12 h after



exposure and that native Stx-2-induced apoptosis was observed after 18 h and was associated with an increase in caspase-9 activation. It is possible that Stx-2-induced necrosis can be triggered by mechanisms other than N-glycosidase activity. Mitochondrial membrane permeabilization (MMP) results in programmed cell death (PCD) as shown in Figure 5.12, and can trigger three outcomes; the activation of caspase-9 which results in downstream apoptosis, the activation of apoptosis inducing factor (AIF) and EndoG which result in direct DNA fragmentation and apoptosis-like cell death, and the release of calcium and reactive oxygen species (ROS) which result in necrosis like cell death (78). Calcium is known to be released as part of a stress response originating from the ER (Figure 5.12), where Stx-2 is known to be located, or from MMP as explained above (78, 160) which may occur if Stx-2 interacts with Bak on the mitochondrial membrane. Previous research has stated that apoptosis is induced by Stx-1 through the ER stress response in human monocytic cells (110), and that DNA condensation can occur in cells that overexpress Bax, despite the presence of a caspase inhibitor (124, 222), which supports the use of alternative pathways that result in apoptosis-like cell death such as those with AIF and EndoG. The data obtained in these experiments support the theory that Stx-2 induced cytotoxicity is triggered by either by ER stress and calcium release, a direct interaction between Stx-2 and Bcl-2 family members at the mitochondrial membrane, or both, thereby resulting in apoptotic and necrotic cellular responses through MMP and autophagy, a process that is associated with autophagosomes and autolysosomes (199), respectively.

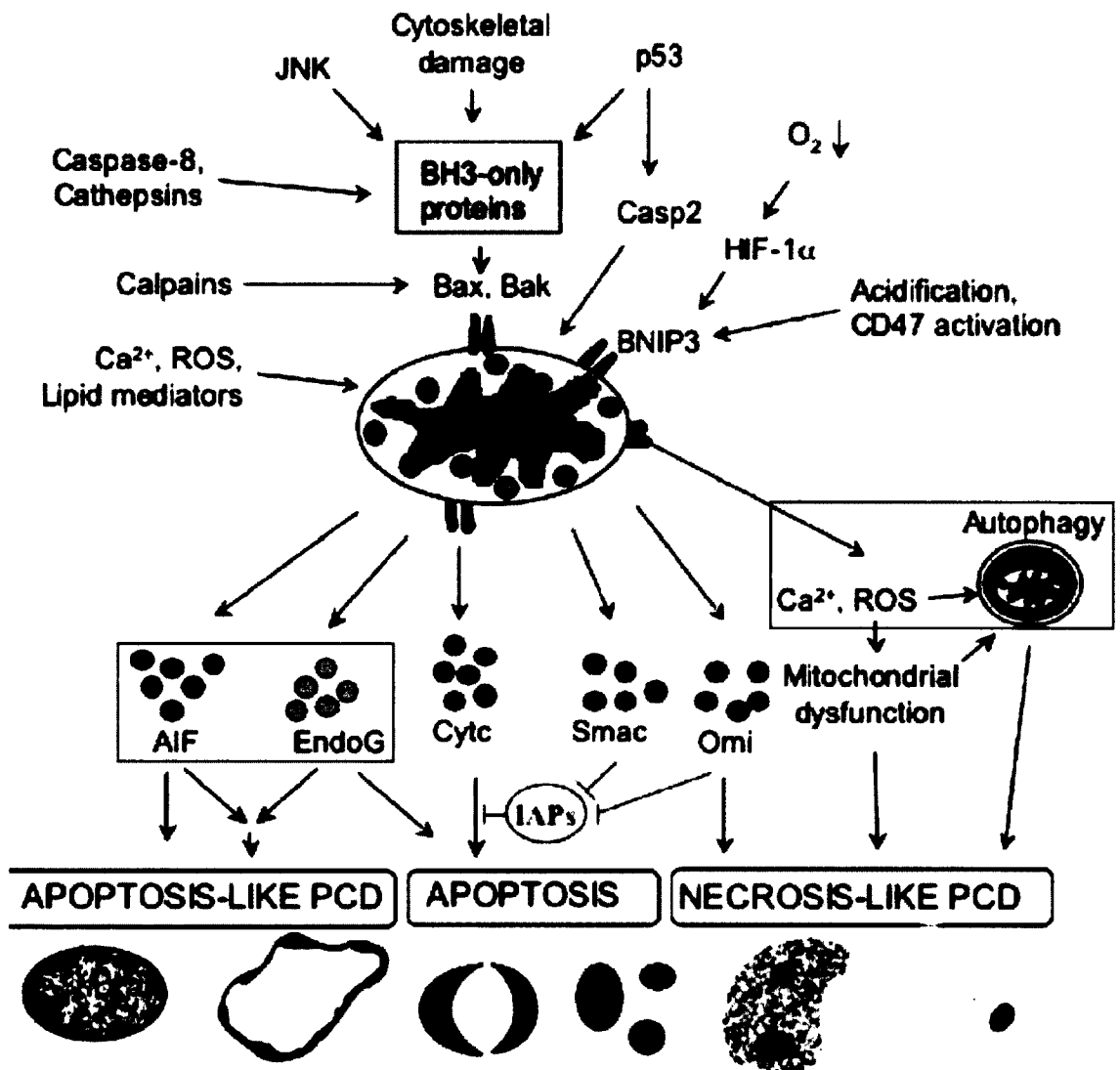


**Figure 5.11: The effects of mitochondrial membrane permeabilization (MMP) on programmed cell death (PCD).** Figure is adapted from M. Jaattela (78). MMP has many downstream cellular effects that can lead to apoptosis-like PCD, true apoptosis, and necrosis-like PCD. In these experiments, it is believed that apoptosis-inducing factor (AIF) or EndoG may be triggered by Bak activation as a result of cytokine withdrawal or binding to Stx-2 at the mitochondrial or ER surface (left box). In addition, the release of calcium from the ER may also trigger necrosis-like PCD through autophagy (right box).

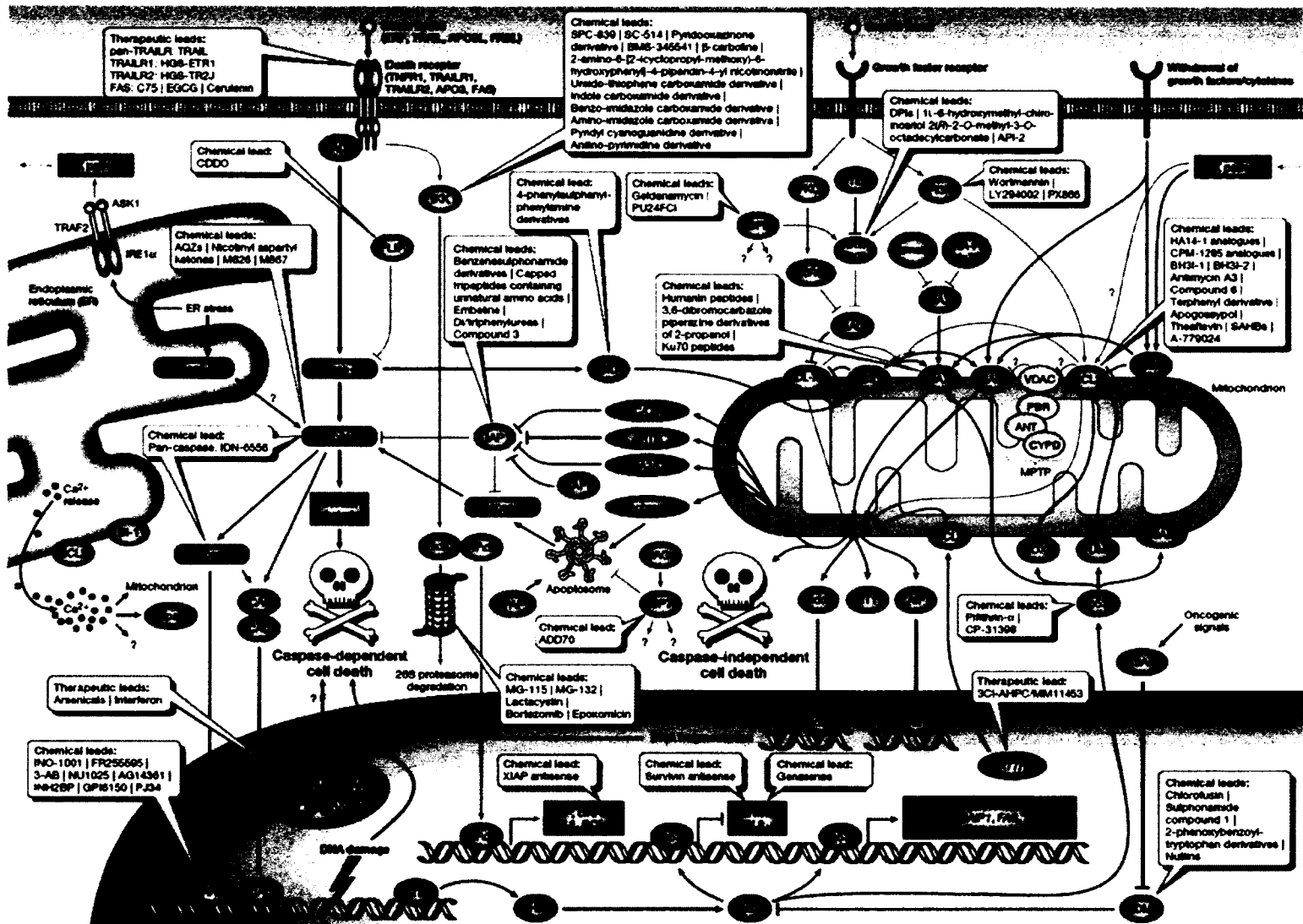


**Figure 5.12: Apoptotic pathways leading to caspase-dependent and -independent cell death.** This diagram is courtesy of Reed *et al.* (160). The pathways thought to be related to Stx-2-induced apoptosis are triggered by ER stress and calcium release, resulting in downstream caspase-independent cell death from mitochondrial membrane permeabilization and EndoG / AIF release.

The effect of mutant Stx-2 on neutrophil necrosis, apoptosis, and caspase-8/-9 activation indicated that necrosis was not remarkably different from native Stx-2, with only a slight increase after 48 h; however there was a lack of mutant Stx-2-induced apoptosis. In addition, no difference in caspase-8 and caspase-9 activation was detected between native and mutant Stx-2. This shows that the mutation did alter the cytotoxicity of the toxin, and did not cause apoptosis of cells at 18 h as seen with native Stx-2. This further supports that Stx-2 triggers ER stress followed by calcium release and/or directly interacts with Bcl-2 family members such as Bak at the mitochondrial membrane leading to downstream effects of MMP on cell death as explained by Jaattela (78) and Reed *et al.* (160).

The effect of IL-8 inhibitor on neutrophil necrosis, apoptosis, and caspase-8/-9 activation was remarkably different from native and mutant Stx-2. A steady increase in necrosis was observed after 12 h and apoptosis rates were highest at 12 h, but caspase-8 and caspase-9 levels were the lowest, even in the presence of Stx-2. This shows that the IL-8 inhibitor triggered programmed cell death through a caspase-independent apoptotic pathway. It is suspected that this pathway involved Bak and destabilization of the mitochondrial membrane which then caused the mitochondria to release apoptosis-inducing factor (AIF) and EndoG. These molecules lead to DNA fragmentation, chromatin condensation, and apoptosis-like programmed cell death, in a fashion similar to the pathway shown on the right side of Figure 5.12 entitled “withdrawal of growth factors/cytokines”. It is known that exposure to IL-8 results in a delay of spontaneous apoptosis, and without it TNF- $\alpha$  can rapidly increase neutrophil apoptosis 2 h after

exposure (97, 143, 192). Even though apoptosis rates of neutrophils treated with IL-8 inhibitor were consistently higher than the negative control at 6 h and beyond, the data from these experiments do not support that the induction of apoptosis was due to TNF- $\alpha$  because the low levels of caspase-8 activation indicated that the extrinsic pathway typically triggered by TNF- $\alpha$  was not used. These data do suggest that spontaneous neutrophil apoptosis occurred at approximately 12 h in all samples despite the level of IL-8 or Stx-2 present, however the negative control showed lower apoptosis rates indicating that IL-8 did have some protective effect against spontaneous neutrophil apoptosis, although it was not significant at all time points.

The experiments performed in this study did not show a clear correlation between a delay in apoptosis as a result of exposure to Stx-2; however they did demonstrate that Stx-2 induced apoptosis was observed at 18 h and that cells exposed to mutant Stx-2 had apoptosis rates similar to that of the untreated cells. Data from these experiments supported that the mechanism of action of Stx-2 was either through the ER stress response and/or interaction with Bcl-2 family members such as Bak at the mitochondrial membrane therefore inducing MMP and its downstream effects. Additionally, mutant Stx-2 was unable to interact with Bcl-2 family members such as Bak at the mitochondrial membrane, preventing the downstream effects of MMP and cell death. However mutant Stx-2 was still able to elicit the ER stress response, resulting in calcium release, autophagy, and necrosis-like cell death. IL-8 did not appear to play a major role in the delay of spontaneous apoptosis or to Stx-2 induced apoptosis in these experiments, and only showed a slight protective effect.

## CHAPTER 6

### CONCLUSIONS AND FUTURE STUDIES

#### 1.0 **Conclusion and Future Studies**

*Escherichia coli* O157:H7 is the prototype organism of the STEC group, and has caused numerous outbreaks in the United States associated with a wide variety of food types since it first emerged in the early 1980's (159). It is a dominant Shiga-toxin (Stx) producing *Escherichia coli* (STEC) and although many toxic virulence factors are produced by *E. coli* O157:H7, the Stx toxins have been implicated as the most likely inducers of Hemolytic uremic syndrome (HUS) and its symptoms (131). It is important to understand the mechanisms by which these toxins elicit cytotoxic responses and how they differ between host cell types. By doing so, novel therapies and/or vaccines can be created to supplement current treatments, which are currently focused on maintaining homeostasis (148). The experiments performed in these studies helped to elucidate the mechanisms of Stx-2-induced programmed cell death.

Different cell types within the human body are known to contain different levels of Bcl-2 family proteins, and are affected by cytokines and growth hormones in different ways. Therefore, apoptotic responses may differ between these cell types. Numerous

studies have been performed investigating the effects of Stx-1 and Stx-2-induced apoptosis on many different cell types. A study by Fujii *et al.* (54) determined that Stx-2 induced apoptosis is mediated by C/EBP homologous protein (CHOP) in human brain microvascular endothelial cells. Another study performed by Park *et al.* concluded that CHOP enhances NF $\kappa$ -B signals by repression of peroxisome proliferator-activated receptor  $\gamma$  in intestinal epithelial cells (147). NF $\kappa$ -B controls the up-regulation of IL-8 and inhibitor of apoptosis proteins (IAPs) and can inhibit apoptosis by preventing caspase-9/-3 activation (184). A third study concluded that shiga-like toxins induced apoptosis of Hep-2 cells by cleavage of Poly (ADP-Ribose) (PARP) and activation of caspases (35). All of these studies support that shiga-like toxins use different apoptotic pathways in the tested cells. This shows it is necessary to investigate the effects of Stx-2-induced programmed cell death on each cell type typically associated with disease in order to ensure the correct mechanisms are identified.

Human intestinal epithelial cells and neutrophils are two cell types that have been associated with the pathogenesis of HUS, and were used in the experiments performed in this research. Human intestinal epithelial cells allow toxins produced in the colon to translocate into the blood stream using either a microtubule-dependent or -independent method (75, 113). Neutrophils are the first line of defense in the human host immune system and constitutively undergo apoptosis in the circulation, and have an estimated half-life of 6 to 18 h (3, 67, 173, 213). Increased counts of both neutrophils and macrophages in circulation have been associated with an increased severity of renal failure during HUS (156), suggesting that the normal rate of apoptosis may be altered

during infection with Stx-2. Previous studies performed by Suzuki *et al.* (190) have indicated that Stx-2 but not Stx-1 interacts with a pentameric sequence, NWGRI within the BH1 domain (a highly conserved region) on the pro-survival protein, Bcl-2 (residues 143 to 147), and this induces target cell death from caspase-3 activation. This same sequence is found in other members of the Bcl-2 protein family as well as in Stx-2 (residues 222-228) (190). Therefore, it is possible that Stx-2 is acting in a similar manner to the Bcl-2 protein family by forming heterodimers with these proteins and influencing the outcome of the cell's fate.

The goal of this research was to elucidate how Stx-2 interacts with the Bcl-2 protein family and to determine what role it plays in host cell apoptosis, especially in human neutrophils. In these studies, protein interactions between Stx-2 and select Bcl-2 family proteins (Bcl-2, Bcl-X<sub>L</sub>, Mcl-1, Bcl-w, and Bax) were examined using Far Western Blot and Co-Immunoprecipitation in a human intestinal epithelial cell model (Caco-2). Necrosis and apoptosis rates of human neutrophils as well as the corresponding pathways used (e.g. caspase-8 and/or caspase-9) were also determined following exposure to Stx-2 and mutant Stx-2 (G225A) to determine the extent that the pentameric sequences plays in regulating apoptosis. The protein interaction studies concluded that protein binding between Stx-2 and Bcl-2, Bcl-X<sub>L</sub>, or Bax was not demonstrated in Caco-2 cells. One potential interaction was observed, but the identity of this protein was unknown. Identifying this interaction could be a challenge; however if the interaction was demonstrated in repeat experiments, the binding protein could be identified. First, this protein should be isolated from a PVDF membrane or gel, and the amino acid sequence



determined using Edman degradation or mass spectrometry. Once the protein sequence has been determined, it can be compared to a database of known protein sequences using the basic local alignment search tool (BLAST) to determine its identity. The protein interactions between Stx-2 and this protein can then be determined using the same methods used in these experiments, and the presence of this protein can also be identified in other cell types, such as neutrophils. In order to confirm protein interactions, alternative techniques should be used such as yeast or mammalian two-hybrid systems or ultracentrifugation of protein complexes labeled with fluorescent probes. Gaining this knowledge will further elucidate the pathway by which Stx-2 programmed cell death occurs.

The neutrophil apoptosis studies concluded that Stx-2-induced apoptosis is delayed for 12 h after exposure, but only in the presence of crude supernatant fluid. It is believed that this observation is due to LPS-induced IL-8 upregulation, which is known to delay neutrophil apoptosis (96). This delay was not observed in neutrophils treated with semi-purified Stx-2 as there was no reduction in spontaneous neutrophil apoptosis observed within the first 12 h. Instead, a distinct peak of Stx-2 induced apoptosis was observed at 18 h in addition to spontaneous neutrophil apoptosis peak observed at 12 h. Data supported that the mechanism of action of Stx-2 was either through the ER stress response and/or interaction with Bcl-2 family members such as Bak at the mitochondrial membrane therefore inducing MMP and its downstream effects. IL-8 did not appear to play a major role in the delay of spontaneous apoptosis or to Stx-2 induced apoptosis in these experiments, and only showed a slight protective effect. The neutrophil necrosis

studies concluded that Stx-2-induced necrosis was significantly increased 6-12 h after exposure, and that this was triggered by a mechanism other than N-glycosidase activity. It is believed that Stx-2 is able to elicit a stress response within the ER that results in calcium release, autophagy, and necrosis-like cell death. Further experiments should be performed to confirm that the proposed mechanisms are involved in Stx-2-induced programmed cell death. To determine if Stx-2 does indeed induce an ER stress response, intracellular calcium, calpain, and ROS levels in neutrophils exposed to Stx-2 in a dose-dependent manner should be examined. The transcription and protein levels of AIF and EndoG should also be examined to determine if these proteins are the cause of caspase-independent apoptosis. Cells exposed to Stx-2 in a dose-dependent manner should be observed using electron microscopy for the formation of autophagosomes and autolysosomes. The presence of all of the above plus confirmation of the identity of the unknown protein interaction described previously would confirm that Stx-2-induced apoptosis and necrosis is occurring as a result of an ER stress response.

The number of variables involved in toxin-mediated cellular programmed cell death provides a challenge when trying to elucidate the molecular mechanisms involved. The research performed in these experiments was conducted over a time frame of nine years, and hypotheses were initially developed in 2005. Three toxin batches were produced during this time and toxin potency was confirmed through Vero cell cytotoxicity testing to ensure no batch variation was present. Much progress has been made over the last decade to understand the complexities of both cellular apoptosis and Stx-2 mechanisms of action including the identification of a number of new proteins and

signaling pathways that are involved in determining the fate of a cell (78, 160). The research performed in these experiments was limited to a small number of proteins that were predominantly known to be involved in the process of apoptosis at the time the study was designed. However, from this research two molecular mechanisms for Stx-2 induced apoptosis and necrosis have been proposed. Providing increased knowledge of the mechanisms of Stx-2-induced programmed cell death will help future discoveries and open up new avenues for treatments and/or vaccines for *E. coli* O157:H7 infection.

## APPENDIX A:

### MICROORGANISMS, MEDIA, AND REAGENTS

#### 1.0 Microorganisms

The strains of *E. coli* O157:H7 used in these studies, the toxins they produced, and the origins of each are shown below.

##### *E. coli* O157:H7 strains used

Strain	Toxin Produced	Origin
90-2380	Stx-2	National Laboratory for Enteric Pathogens Canada
95-2157	Stx-1	National Laboratory for Enteric Pathogens Canada
43895	Stx-1, Stx-2	American Type Culture Collection
43888	None	American Type Culture Collection

#### 2.0 Microbiological Media

##### 2.1 Luria Bertani (LB) Agar

10 g Bacto-Tryptone (Difco 0123-01-1)  
5 g Bacto-yeast extract (Difco 0127-05-3)  
10 g NaCl  
15 g Bacto-agar (Difco 0140-01)  
Distilled H<sub>2</sub>O to 1 L

Add ingredients to an Erlenmeyer flask. Bring the volume up to 1L with distilled H<sub>2</sub>O and stir until all ingredients are dissolved. Autoclave on the liquid cycle for 20

minutes at 121°C, 15psi, and cool to 55 °C , and pour into sterile Petri dishes (20 mL/plate).

## **2.2 Luria Bertani (LB) Broth**

10g Bacto Tryptone  
5g Yeast Extract  
10g NaCl  
1L distilled H<sub>2</sub>O

Add ingredients to an Erlenmeyer flask. Bring the volume up to 1L with distilled H<sub>2</sub>O and stir until all ingredients are dissolved. Autoclave on the liquid cycle for 20 minutes at 121°C, 15psi, and store at room temperature.

## **2.3 LB Agar with 50µg/mL Ampicillin**

2.5 g Bacto-Tryptone (Difco 0123-01-1)  
1.25 g Bacto-yeast extract (Difco 0127-05-3)  
2.5 g NaCl  
3.75 g Bacto-agar (Difco 0140-01)  
Distilled H<sub>2</sub>O to 250mL

Add ingredients to an Erlenmeyer flask. Bring the volume up to 250mL with distilled H<sub>2</sub>O and stir until all ingredients are dissolved. Autoclave on the liquid cycle for 20 minutes at 121°C, 15psi and cool to 55 °C , add Ampicillin (2.5mL of a 5mg/mL stock solution per 250mL media) and pour into sterile Petri dishes (approx. 20 ml/plate).

## **2.4 LB Agar with 1% Glucose, 25µg/mL Chloramphenicol, 50µg/mL Ampicillin**

5 g Bacto-Tryptone (Difco 0123-01-1)  
2.5 g Bacto-yeast extract (Difco 0127-05-3)  
5 g NaCl  
5 g Glucose  
7.5 g Bacto-agar (Difco 0140-01)

Distilled H<sub>2</sub>O to 500mL

Add ingredients to an Erlenmeyer flask. Bring the volume up to 500mL with distilled H<sub>2</sub>O and stir until all ingredients are dissolved. Autoclave on the liquid cycle for 20 minutes at 121°C, 15psi, and cool to 55 °C , add antibiotics (2.5mL of 5mg/mL Chloramphenicol and 5mL of 5mg/mL Ampicillin per 500mL media) and pour into sterile Petri dishes (20 mL/plate).

## **2.5 LB Agar with 25ug/mL Kanamycin**

2.5 g Bacto-Tryptone (Difco 0123-01-1)  
1.25 g Bacto-yeast extract (Difco 0127-05-3)  
2.5 g NaCl  
3.75 g Bacto-agar (Difco 0140-01)  
Distilled H<sub>2</sub>O to 250mL

Add ingredients to an Erlenmeyer flask. Bring the volume up to 250mL with distilled H<sub>2</sub>O and stir until all ingredients are dissolved. Autoclave on the liquid cycle for 20 minutes at 121°C, 15psi, and cool to 55 °C , add Kanamycin (1.25mL of 5mg/mL stock solution per 250mL media) and pour into sterile Petri dishes (20 mL/plate).

## **2.6 Trypticase Soy Broth with 15% Glycerol**

30g Trypticase Soy Broth Powder  
7.5mL Glycerol  
500mL distilled H<sub>2</sub>O

Dissolve TSB powder in the distilled water and remove 7.5mL of broth. Add 7.5mL glycerol and mix well. Autoclave on the liquid cycle for 20 minutes at 121°C, 15psi, and store at room temperature.

## **2.7 SOC Medium**

20g Bacto Tryptone  
5g Bacto Yeast Extract  
2ml of 5M NaCl.  
2.5ml of 1M KCl.  
10ml of 1M MgCl<sub>2</sub>  
10ml of 1M MgSO<sub>4</sub>  
20ml of 1M glucose  
ddH<sub>2</sub>O to 1L

Add ingredients to 900mL of distilled H<sub>2</sub>O. Bring the volume up to 1L with distilled H<sub>2</sub>O and stir until all ingredients are dissolved. Autoclave on the liquid cycle for 20 minutes at 121°C, 15psi.

## **3.0 Antibiotic Stock Solutions**

Stock solutions of ampicillin, chloramphenicol, kanamycin, and tetracycline were prepared as needed per the recipes below. In all cases, antibiotics were mixed until dissolved, sterile filtered with 0.2µm filters (Pall), and added to media in the desired concentration.

### **3.1 Ampicillin (Amp): Stock of 5 mg/mL in sterile ddwater (sddH2O).**

0.5 g Ampicillin (Sigma A-9518)  
Sterile ddH<sub>2</sub>O to 100 ml

### **3.2 Chloramphenicol (Chl): Stock of 5 mg/mL in 95% ethanol (EtOH).**

0.05 g Chloramphenicol  
95% EtOH to 10 ml

**3.3 Kanamycin (Kan): Stock of 5 mg/ml in sterile ddwater (sddH2O).**

0.05 g Kanamycin  
Sterile ddH<sub>2</sub>O to 10 mL

**3.4 Tetracycline (Tet): Stock of 5 mg/ml in 95% ethanol (EtOH).**

0.05 g Tetracycline-HCl  
95% EtOH to 10 ml

**4.0 Biochemical Reagents**

**4.1 Phosphate Buffered Saline (PBS), pH 7.4**

1.44g Sodium phosphate, dibasic (Na<sub>2</sub>HPO<sub>4</sub>)  
8g Sodium chloride (NaCl)  
0.2g Potassium Chloride (KCl)  
0.24g Potassium Phosphate, monobasic (KH<sub>2</sub>PO<sub>4</sub>)  
1L distilled H<sub>2</sub>O

Add ingredients to flask, bring up the volume to 1L with distilled water, and stir until dissolved. Adjust pH to 7.4 using HCl. Autoclave on the liquid cycle for 20 minutes at 121°C, 15psi, and store at room temperature.

**4.2 0.5M Ethylene Diamine Tetraacetic Acid (EDTA), pH 8.0**

46.5 g NaEDTA (Sigma)  
200 mL distilled H<sub>2</sub>O

Adjust to pH 8.0 with approximately 5 g of NaOH pellets (Sigma). Autoclave on the liquid cycle for 20 minutes at 121°C, 15psi, and store at room temperature.



#### **4.3 50x Tris-Acetate-EDTA Buffer (TAE), pH 8.5**

242g Tris Base  
100mL 0.5M EDTA, pH 8.0  
57.1mL Glacial Acetic Acid  
distilled H<sub>2</sub>O

Add ingredients to flask, bring up the volume to 1L with distilled water, and stir until dissolved. Adjust pH to 8.5 with Glacial Acetic Acid. Store at room temperature.

#### **4.4 DNA Extraction Lysis Buffer**

250μL 10% SDS  
50μL 10N NaOH  
9.7mL dH<sub>2</sub>O

Add ingredients to a conical tube and mix well. If the SDS does not dissolve, place tube into a warm water bath for 5 minutes. Vortex to mix. Store at room temperature for no longer than 2 months.

#### **4.5 Loading Dye**

7mL 0.25% Bromophenol Blue  
7mL 0.25% Cylene Cyanol  
6mL Glycerol

Add ingredients to a conical tube and mix well. Store at room temperature.

#### **4.6 50x Native Gel Running Buffer (1M Tris, 1M Glycine, 0.1M EDTA), pH 8.8**

121.14g Tris  
75.07g Glycine  
32.73g EDTA  
Distilled H<sub>2</sub>O

Add ingredients to flask, bring up the volume to 1L with distilled water and stir until dissolved. Adjust pH to 8.8 with HCl. Store at room temperature or 2-8°C. To use, dilute stock 50-fold with deionized water to obtain a 1x solution for each native electrophoresis run. Mix thoroughly before use.

#### **4.7 5X Sample Loading Buffer**

2.423g Tris  
1.501g Glycine  
0.372g EDTA  
25mL Glycerol  
1mL Bromophenol blue  
Distilled H<sub>2</sub>O

Add ingredients to a flask containing 50mL distilled H<sub>2</sub>O, bring up the volume to 100mL with distilled water and stir until dissolved. Use 2.5mL per 10mL sample processed.

#### **4.8 1M PMSF**

0.1742g PMSF  
1mL methanol

Dissolve PMSF in methanol. Vortex to mix. Store at -20°C.

#### **4.9 Acrylamide/Bisacrylamide (30%T, 2.67%C)**

87.6g acrylamide  
2.4g N'N'-bis-methylene-acrylamide

Bring up volume to 300mL with deionized water. Filter using Whatman #1 paper and store at 4°C in the dark.

**4.10 10% (w/v) Sodium Dodecyl Sulfate (SDS)**

10g SDS  
Distilled H<sub>2</sub>O

Dissolve 10g SDS in 90mL water with gentle stirring and bring volume up to 100mL with deionized water.

**4.11 Resolving Gel Buffer (1.5M Tris-HCl), pH 8.8**

27.23g Tris base  
80mL deionized water

Adjust to pH 8.8 with 5N HCl. Bring total volume to 150mL with deionized water and store at 4°C.

**4.12 Stacking Gel Buffer (0.5M Tris-HCl), p 6.8**

6g Tris base  
60mL deionized water

Adjust to pH 6.8 with 5N HCl. Bring total volume to 100mL with deionized water and store at 4°C.

**4.13 Sample Buffer (SDS Reducing Buffer)**

3.55mL deionized water  
1.25mL 0.5M Tris-HCl, pH 6.8  
2.5mL glycerol  
2.0mL 10% (w/v) SDS  
0.2mL 0.5% (w/v) bromophenol blue

Add ingredients to a conical tube and mix well. Store at room temperature. Prior to use, add 50 $\mu$ L  $\beta$ -mercaptoethanol to 950 $\mu$ L sample buffer. Dilute the sample at least 1:2 with sample buffer and heat at 95°C for 4 minutes.

#### **4.14 10x Electrode SDS-PAGE (Running) Buffer, Tris-Glycine pH 8.3**

30.3g Tris base  
144.0g Glycine  
10.0g SDS  
Distilled H<sub>2</sub>O

Dissolve ingredients in 700mL deionized water and bring the total volume up to 1L. Do not adjust pH with acid or base. Store at 4°C. If precipitation occurs, warm to room temperature before use. Prior to use, dilute 50mL 10x stock with 450mL deionized water for each electrophoresis run. Mix thoroughly.

#### **4.15 10% Ammonium Persulfate (APS) (made fresh daily)**

100mg ammonium persulfate  
1mL deionized water

Dissolve 100mg ammonium persulfate in 1mL of deionized water and vortex to mix well.

#### **4.16 6% Stacking / 12% Resolving Acrylamide Gel**

Resolving Gel (10mL):

4 mL Acrylamide/Bisacrylamide (30%T, 2.67%C)  
2.5mL Resolving gel buffer  
3.5mL distilled H<sub>2</sub>O  
5 $\mu$ L TEMED  
50 $\mu$ L APS

Stacking Gel (5mL):

1mL Acrylamide/Bisacrylamide (30%T, 2.67%C)  
1.25 Stacking gel buffer  
2.75mL distilled H<sub>2</sub>O  
5μL TEMED  
25μL APS

Add resolving ingredients to a conical tube in the order listed. Mix gently and allow to de-gas for at least five minutes. Carefully pipette resolving gel solution into gel casting stand until ¾ full. Gently add a layer of water and allow to solidify. Pour off water and prepare stacking gel in the same manner. Insert comb into the top of the gel casting stand and allow to solidify.

#### **4.17 Coomassie Blue Staining Buffer**

1g Coomassie Blue R250  
100mL Glacial Acetic Acid  
400mL Methanol  
500mL Distilled H<sub>2</sub>O

Add acetic acid to distilled water followed by methanol and Coomassie blue. Mix well and filter with Whatman #1 filter paper to remove large particles. Store at room temperature.

#### **4.18 Coomassie Blue Destain Buffer**

200mL Methanol  
100mL Glacial Acetic Acid  
700mL Distilled H<sub>2</sub>O

Add 100mL glacial acetic acid to 700mL of dH<sub>2</sub>O followed by 200mL methanol and mix well. Store at room temperature.

**4.19 10x Western Blot Transfer Buffer (Tris Glycine), pH 8.3**

30.3g Tris base  
144.0g Glycine  
Distilled H<sub>2</sub>O

Dissolve ingredients in 700mL deionized water and bring the total volume up to 1L. Do not adjust pH with acid or base. Store at 4°C. If precipitation occurs, warm to room temperature before use. Prior to use, dilute 1:10 with deionized water for each electroblot transfer. Mix thoroughly.

**4.20 Blocking Buffer (5% Dehydrated Skim Milk)**

5g dehydrated skim milk powder  
100mL 1x Phosphate Buffered Saline (PBS)

Add 5g of dehydrated skim milk powder into 100mL PBS. Vortex until dissolved.

For extended storage, store at -20°C.

**4.21 10x Tris Buffered Saline (TBS)**

24.20g Tris Base  
292.4g NaCl  
Distilled H<sub>2</sub>O

Add ingredients to 500mL distilled water, adjust the pH to 7.5 with HCl and bring the volume up to 1L. Dilute 1:10 with distilled water prior to use. Store at 2-8°C.

**4.22 0.05% Tween Tris Buffered Saline (TTBS), pH 7.5**

1L 1x TBS  
0.5mL Tween 20

Add Tween 20 to 1L 1x TBS and mix well. Store at room temperature.

## **5.0 Cell Culture Media and Reagents**

### **5.1 Trypsin-EDTA Solution**

0.5g Trypsin  
0.2g EDTA  
1L HBSS modified

Add ingredients and mix until dissolved. Sterile filter with 0.2µm filters (Pall) and transfer aliquots into 15mL conical tubes. Store at -20°C.

### **5.2 Trypan Blue**

0.04g Trypan Blue  
100mL 1x Phosphate Buffered Saline (PBS)

Add ingredients and mix until dissolved. Sterile filter with 0.2µm filters (Pall) and store at room temperature.

### **5.3 HBSS Modified (no Ca<sup>++</sup> or Mg<sup>++</sup>)**

2 bottles pre-measured, powdered HBSS modified (no Ca<sup>++</sup> or Mg<sup>++</sup>) (Atlanta Biologicals, Atlanta GA)  
0.70g sodium bicarbonate  
2L distilled H<sub>2</sub>O

Add ingredients and mix well. Adjust pH to 7.2 with HCl. Sterile filter into autoclaved bottles using 0.2µm filter units (Nalgene Nunc, Rochester, NY). Incubate media overnight at 37°C for sterility check. Store at 2-8°C.

#### **5.4 RPMI-1640 with 10% FBS**

10.44g RPMI-1640 powder  
Distilled H<sub>2</sub>O up to 1L  
2.0g sodium bicarbonate  
10mL non-essential amino acids, 100x  
50mL Fetal Bovine Serum (FBS)

Add ingredients and mix well. Adjust pH to 7.2 with HCl if required. Sterile filter into autoclaved bottles using 0.2µm filter units (Nalgene). Incubate media overnight at 37°C for sterility check. Add 200mL FBS and return to incubator for an additional overnight sterility check. Store at 2-8°C.

#### **5.5 DMEM Modified (5% FBS, Hepes, Bicarbonate, High Glucose, and non-essential amino acids)**

2 bottles pre-measured, powdered DMEM modified (DMEM-4.5, high glucose with L-glutamine, 25mM HEPES buffer, without sodium pyruvate) (Atlanta Biologicals)  
7.40g sodium bicarbonate  
20mL non-essential amino acids, 100x  
1.8L distilled H<sub>2</sub>O  
100mL fetal bovine serum (FBS)

Add ingredients (except FBS) and mix well. Adjust pH to 7.2 with HCl. Sterile filter into autoclaved bottles using 0.2µm filter units (Nalgene). Incubate media overnight at 37°C for sterility check. Add 200mL FBS and return to incubator for an additional overnight sterility check. Store at 2-8°C.

#### **5.6 Caco-2 Media**

18.8g Eagles Minimal Essential Medium (Atlanta Biologicals)  
29.6g Leibovitz-15 Medium (Atlanta Biologicals)  
16.88g HEPES



1.168g L-glutamine  
3g Sodium bicarbonate  
40mL non-essential amino acids, 100x  
3.6L distilled H<sub>2</sub>O  
400mL Fetal Bovine Serum (FBS)

Add ingredients (except FBS) and mix well. Sterile filter into autoclaved bottles using 0.2µm filter units (Nalgene). Incubate media overnight at 37°C for sterility check. Add 400mL FBS and return to incubator for an additional overnight sterility check. Store at 2-8°C.

## APPENDIX B

### MAINTENANCE OF EUKARYOTIC CELL CULTURES

#### **1.0 Vero Cell Growth and Cryopreservation**

African green monkey kidney (vero) cells (designated CCL-81) were obtained from the American Type Culture Collection (ATCC) and cellular morphology was confirmed by microscopic analysis. Aliquots of vero cells (1mL containing  $1 \times 10^6$  cells/vial) were cryopreserved in DMEM modified with 5% FBS (Appendix A, 5.5) and 5% dimethylsulfoxide (DMSO), and stored in liquid nitrogen. Working cell lines were maintained in DMEM modified medium for five passages per stock vial, and grown at 37°C in an open system containing 5% CO<sub>2</sub>.

#### **2.0 Caco-2 Cell Growth and Cryopreservation**

Caco-2 cells (designated HTB-37) were obtained from the ATCC and cellular morphology was confirmed by microscopic analysis. Aliquots of cells were cryopreserved in Caco-2 media (Appendix A, 5.6) and 5% dimethylsulfoxide (DMSO), and stored in liquid nitrogen. Working cell lines were maintained in Caco-2 media for five passages (passage #42-46) per stock vial and grown at 37°C in a closed system.

**APPENDIX C**

**INSTITUTIONAL REVIEW BOARD PROJECT APPROVAL**

**(see next page)**

## University of New Hampshire

Research Integrity Services, Service Building  
51 College Road, Durham, NH 03824-3585  
Fax: 603-862-3564

21-Mar-2012

Rodgers, Frank G  
Molecular, Cellular & Biomedical Sciences, Rudman Hall  
Durham, NH 03824

**IRB #: 3679**

**Study:** Regulation of Escherichia coli Shiga-like Toxins and their Impact of Host Cell Apoptosis

**Review Level:** Expedited

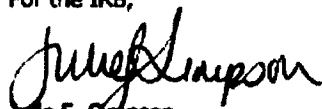
**Approval Expiration Date:** 28-Mar-2013

The Institutional Review Board for the Protection of Human Subjects in Research (IRB) has reviewed and approved your request for time extension for this study. Approval for this study expires on the date indicated above. At the end of the approval period you will be asked to submit a report with regard to the involvement of human subjects. If your study is still active, you may apply for extension of IRB approval through this office.

Researchers who conduct studies involving human subjects have responsibilities as outlined in the document, *Responsibilities of Directors of Research Studies Involving Human Subjects*. This document is available at <http://unh.edu/research/irb-application-resources> or from me.

If you have questions or concerns about your study or this approval, please feel free to contact me at 603-862-2003 or [Julie.simpson@unh.edu](mailto:Julie.simpson@unh.edu). Please refer to the IRB # above in all correspondence related to this study. The IRB wishes you success with your research.

For the IRB,



Julie F. Simpson  
Director

cc: File  
Jeffrey, Lia

**APPENDIX D**

**UNH INSTITUTIONAL BIOSAFETY COMMITTEE PROJECT APPROVAL**

**(see next page)**



# UNIVERSITY of NEW HAMPSHIRE

**Date:** February 19, 2007  
**To:** Frank Rodgers, Professor  
Microbiology  
**Cc:** Aaron Margolin, Chair  
UNH Institutional Biosafety Committee  
**From:** David R. Gillum, Assistant Director  
Environmental Health and Safety  
**Re:** Letter of Approval – Recombinant DNA Registration

The UNH Institutional Biosafety Committee (IBC) approved your recombinant DNA research project entitled, "Interactions in Neutrophils between Bcl-2 Family Proteins and Stx-2 Produced in *E. coli* 0157:H7," on February 15, 2007. The IBC approval number for this research project is **R:2-2007**. This project falls under category III-D of the *NIH Guidelines for Research Involving Recombinant DNA Molecules*, requiring IBC approval before initiation. Please review the following information with all personnel that will be working with recombinant DNA in your laboratories:

1. All research with recombinant DNA and infectious agents must be conducted in laboratories with a Biological Safety Level Two (BSL-2) rating. Information about BSL-2 ratings can be found in the CDC/NIH document, "Biosafety in Microbiological and Biomedical Laboratories," 5<sup>th</sup> edition (available online at <http://www.cdc.gov/od/ohs/biosfty/bmbl5/bmbl5toc.htm>).
2. Laboratory staff, students and visitors must be trained in safe handling, use and disposal of recombinant DNA technology and infectious agents. This training must be conducted prior to allowing them to work with this material. All training must include the date, instructor and participant names.
3. Any activity capable of producing aerosols or droplets of recombinant DNA or infectious agents must be done in an approved containment device (i.e. biological safety cabinet, fume hood).
4. All waste containing recombinant DNA or infectious agents must be autoclaved or chemically-disinfected prior to disposal.
5. A safety inspection of your laboratory must be conducted at least annually by OEHHS.
6. Approval of this project is valid for three years or until there are changes in your research protocol (whichever occurs first). Note: Any changes in your research protocol must be approved by the IBC.

I am attaching a document outlining your responsibilities as a researcher in a laboratory where recombinant DNA is present and used. Please contact me if you have any questions or concerns regarding this approval letter.

Thank you!

## LIST OF REFERENCES

1. Ackers ML, Mahon BE, Leahy E, Goode B, Damrow T, Hayes PS, *et al.* 1998. An outbreak of *Escherichia coli* O157:H7 infections associated with leaf lettuce consumption. *J Infect Dis.* 177: 1588–93.
2. Adams JM, Cory S. 1998. The Bcl-2 Protein Family: Arbiters of Cell Survival. *Science.* 281: 1322-1326.
3. Akgul C, Moulding DA, Edwards SW. 2001. Molecular control of neutrophil apoptosis. *FEBS Lett.* 487: 318-322.
4. Annis, MG, Yethon JA, Leber B, Andrews DW. 2004. There is more to life and death than mitochondria: Bcl-2 proteins at the endoplasmic reticulum. *Biochem Biophys Acta.* 1644: 115-123.
5. Armstrong GL, Hollingsworth J, and Morris JG Jr. 1996. Emerging foodborne pathogens: *Escherichia coli* O157:H7 as a model of entry of a new pathogen into the food supply of the developed world. *Epidemiol Rev.* 18: 29-51.
6. Baggiolini M, Dewals D, Moser B. 1994. Interleukin-8 and related chemotactic cytokines-CXC and CC chemokines. *Adv Immunol.* 55: 97-179.
7. Banatvala N, Griffin PM, Greene KD, Barrett TJ, Bibb WF, Green JH, *et al.* 2001. The United States national prospective hemolytic uremic syndrome study: microbiologic, serologic, clinical, and epidemiological findings. *J Infect Dis.* 183: 1063-1070.
8. Barrett TJ, Potter ME, Strockbine NA. 1990. Evidence for participation of the macrophage in Shiga-like toxin II induced lethality in mice. *Microbiol Pathog.* 9: 95–103.
9. Barry M, Bleackley RC. 2002. Cytotoxic T lymphocytes: all roads lead to death. *Nat Rev Immunol.* 2: 401–9.
10. Beg AA, Baltimore D. 1996. An essential role for NF-kappaB in preventing TNF-alpha-induced cell death. *Science.* 274: 782–784.
11. Bell BP, Goldoft M, Griffin PM, Davis MA, Gordon DC, Tarr PI, Bartleson CA, Lewis JH, Barrett TJ, Wells JG *et al.* 1994. A multistate outbreak of *Escherichia coli* O157:H7-associated bloody diarrhea and hemolytic uremic syndrome from hamburgers. The Washington experience. *JAMA.* 272: 1349–53.

12. Bell P, Griffin PM, Lozano P, Christie DL, Kobayashi JM, Tarr PI. 1997. Predictors of hemolytic uremic syndrome in children during a large outbreak of *Escherichia coli* O157:H7 infections. *Pediatrics* 100: 127 [Online] <http://www.pediatrics.org/e12>.
13. Besser RE, Lett SM, Weber JT, Doyle MP, Barrett TJ, Wells JG, Griffin PM. 1993. An outbreak of diarrhea and hemolytic uremic syndrome from *Escherichia coli* O157:H7 in fresh-pressed apple cider. *JAMA*.269: 2217–20.
14. Beuchat LR, Nail BV, Adler BB, Clavero MR. 1998. Efficacy of spray application of chlorinated water in killing pathogenic bacteria on raw apples, tomatoes, and lettuce. *J Food Prot.* 61: 1305–11.
15. Beuchat LR, Ryu JH. 1997. Produce handling and processing practices. *Emerg Infect Dis.* 3: 459–65.
16. Beutin LM, Montenegro A, Orskov I, Orskov F, Prada J, Zimmermann S, Stephan R. 1989. Close association of verotoxin (Shiga-like toxin) production with enterohemolysin production in strains of *Escherichia coli*. *J Clin Microbiol.* 27: 2559-2564.
17. Bitzan M, Moebius E, Ludwig K, Mueller-Wiefel DE, Heesemann J, Karch H. 1991. High incidence of serum antibodies to *Escherichia coli* O157:H7 lipopolysaccharide in children with hemolytic uremic syndrome. *J Pediatr.* 119: 380-385.
18. Boerlin P, McEwen SA, Boerlin-Petzold F, Wilson JB, Johnson V, Gyles CL. 1999. Associations between virulence factors of Shiga toxin-producing *Escherichia coli* and disease in humans. *J Clin Microbiol.* 37: 497–503.
19. Boyd B, Lingwood CA. 1989. Verotoxin receptor glycolipid in human renal tissue. *Nephron.* 51: 207–210.
20. Brach MA, deVos S, Gruss H-J, Hermann F. 1992. Prolongation of survival of human polymorphonuclear neutrophils by granulocyte-macrophage colony stimulating factor is caused by inhibition of programmed cell death. *Blood.* 80: 2920-2924.
21. Brenner DJ, Krieg NR, Staley JR, and Garrity G. 2005. *Bergey's Manual of Systematic Bacteriology. Volume II, Part B: The Gammaproteobacteria.* Springer Science & Business Media Inc. New York, NY.
22. Brunder W, Schmidt H, Karch H. 1997. EspP, a novel extracellular serine protease of enterohaemorrhagic *Escherichia coli* O157:H7 cleaves human coagulation factor V. *Mol Microbiol.* 24: 767–778.



23. Buteau C, Proulx F, Chaibou M, Raymond D, Clermont MJ, Mariscalco MM, Lebel MH, Seidman E. 2000. Leukocytosis in children with *Escherichia coli* O157:H7 enteritis developing the hemolytic uremic syndrome. *Pediatr Infect Dis J.* 19: 642-647.
24. Cai J, Yang J, Jones DP. 1998. Mitochondrial control of apoptosis: the role of cytochrome c. *Biochimica et Biophysica Acta.* 1366: 139-149.
25. Calderwood SB, Auclair F, Donohue-Rolfe A, Keusch GT, Mekalanos JJ. 1987. Nucleotide sequence of the Shiga-like toxin genes of *Escherichia coli*. *Proc Natl Acad Sci. USA* 84: 4364-4368.
26. Cassatella MA, Meda L, Bonora S, Ceska M, Constantin G. 1993. Interleukin 10 (IL-10) inhibits the release of proinflammatory cytokines from human polymorphonuclear leukocytes. Evidence for an autocrine role of tumor necrosis factor and IL-1 beta in mediating the production of IL-8 triggered by lipopolysaccharide. *J Exp Med.* 178: 2207-2211.
27. Cassatella MA. 1995. The production of cytokines by polymorphonuclear neutrophils. *Immunol Today.* 16: 21-26.
28. Cassatella, MA. 2003. *The Neutrophil. An emerging regulator of inflammatory and immune response.* Karger. Basel, Switzerland.
29. Centers for Disease Control (2011). *E. coli.* Online: <http://www.cdc.gov/ecoli>.
30. Centers for Disease Control and Prevention. 1995. *Escherichia coli* O157:H7 outbreak linked to commercially distributed dry-cured salami - Washington and California, 1994. *MMWR Morb Mortal Wkly Rep.* 44: 157-60.
31. Centers for Disease Control and Prevention. 2001. Reducing the risk for transmission of enteric pathogens at petting zoos, open farms, animal exhibits, and other venues where the public has contact with farm animals. *MMWR Morb Mortal Wkly Rep.* 50: 297.
32. Chao DT, Korsmeyer SJ. 1998. BCL-2 family: regulators of cell death. *Annu Rev Immunol.* 16: 395-419.
33. Cheng EH-Y, Levine B, Boise LH, Thompson CG, Hardwick JM. 1996. Bax-independent inhibition of apoptosis by BCL-XL. *Nature.* 379: 554-556.
34. Cherla, RP, Lee, S, Tesh VL. 2003. Shiga toxins and apoptosis. *FEMS Microbiology Letters.* 228: 159-166.

35. Ching JC, Jones NL, Ceponis PJ, Karmali MA, Sherman PM. 2002. Escherichia coli Shiga-like toxins induce apoptosis and cleavage of poly (ADP-ribose) polymerase via in vitro activation of caspases. *Infect Immun.* 70: 4669–4677.
36. Chittenden T, Flemington C, Houghton AB, Ebb RG, Gallo GJ, Elangovan B, Chinnadurai G, Lutz RJ. 1995. A conserved domain in Bak, distinct from BH1 and BH2, mediates cell death and protein binding functions. *EMBO J.* 14: 5589-5596.
37. Coad NA, Marshall T, Rowe B, Taylor CM. 1991. Changes in the postenteropathic form of the hemolytic uremic syndrome in children. *Clin Nephrol.* 35: 10–16.
38. Colotta F, Re F, Polentarutti N, Sozanni S, Mantovani A. 1992. Modulation of granulocyte survival and programmed cell death by cytokines and bacterial products. *Blood.* 80: 2012-2020.
39. Cory S, Strasser A, Jacks T, Corcoran LM, Metz T, Harris AW, Adams JM. 1994. Enhanced cell survival and tumorigenesis. *Cold Spring Harbor Symp Quant Biol.* 59: 365-375.
40. Cory S. 1995. Regulation of lymphocyte survival by the bcl-2 gene family. *Annu Rev Immunol.* 13: 513-543.
41. DeGrandis S, Ginsberg J, Toone M, Climie S, Friesen J, Brunton J. 1987. Nucleotide sequence and promoter mapping of the Escherichia coli Shiga-like toxin operon of bacteriophage H-19B. *J Bacteriol.* 169: 4313–4319.
42. Deng X, Ito T, Carr B, Mumby M, May WS Jr. 1998. Reversible phosphorylation of Bcl2 following interleukin 3 or bryostatin 1 is mediated by direct interaction with protein phosphatase 2A. *J Biol Chem.* 273: 34157-34163.
43. Detmers PA, Lo SK, Olsen-Egbert E, Walz A, Baggiolini M, Cohn ZA. 1990. Neutrophil-activating protein 1/ interleukin-8 stimulates the binding activity of the leukocyte adhesion receptor CD11b/CD18 on human neutrophils. *J Exp Med.* 171: 1155-1162.
44. Du C, Fang M, Li Y, Li L, Wang X. 2000. Smac, a mitochondrial protein that promotes cytochrome c-dependent caspase activation by eliminating IAP inhibition. *Cell.* 102: 33–42.
45. Dunican AL, Leuenroth SJ, Grutkoski P, Ayala A, Simms HH. 2000. TNF- $\alpha$ -induced suppression of PMN apoptosis is mediated through interleukin-8 production. *Shock.* 14: 284-289.

46. Elmore, S. 2007. Apoptosis: A Review of Programmed Cell Death. *Toxicol Pathol.* 35: 495-516.
47. Endo Y, Tsurugi K, Yutsudo T, Takeda Y, Ogasawara T, Igarashi K. 1988. Site of action of a Vero toxin (VT2) from *Escherichia coli* O157:H7 and of Shiga toxin on eukaryotic ribosomes. RNA N-glycosidase activity of the toxins. *Eur J Biochem.* 171: 335-337.
48. Escherich T. 1885. Die Darmbakterien des Neugeborenen und Säuglinge. *Fortschr. Med.* 3: 515-522.
49. Fitzpatrick MM, Shah V, Filler G, Dillon MJ, Barratt TM. 1992. Neutrophil activation in the haemolytic uraemic syndrome: free and complexed elastase in plasma. *Pediatr Nephrol.* 6: 50-53.
50. Fitzpatrick MM, Shah V, Trompeter RS, Dillon MJ, Barratt TM. 1992. Interleukin-8 and polymorphonuclear leucocyte activation in hemolytic uremic syndrome of childhood. *Kidney Int.* 42: 951-956.
51. Flagler MJ, Strasser JE, Chalk CL, Weiss AA. 2007. Comparative analysis of the abilities of Shiga toxins 1 and 2 to bind to and influence neutrophil apoptosis. *Infect Immun.* 75: 760-765.
52. Forsyth KD, Simpson AC, Fitzpatrick MM, Barratt TM, Levinsky RJ. 1989. Neutrophil-mediated endothelial injury in haemolytic uraemic syndrome. *Lancet.* 2: 411-414.
53. Friedman MS, Roels T, Koehler JE, Feldman L, Bibb WF, Blake P. 1999. *Escherichia coli* O157:H7 outbreak associated with an improperly chlorinated swimming pool. *Clin Infect Dis.* 29: 298-303.
54. Fujii J, Wood K, Matsuda F, Carneiro-Filho BA, Schlegel KH, Yutsudo T, Binnington-Boyd B, Lingwood CA, Obata F, Kim KS, Yoshida S, Obrig T. 2008. Shiga toxin 2 causes apoptosis in human brain microvascular endothelial cells via CEBP/homologous protein. *Infect Immun.* 76: 3679-3689.
55. Garred O, Dubinina E, Polesskaya A, Olsnes S, Kozlov J, Sandvig K. 1997. Role of the disulfide bond in shiga toxin A-chain for toxin entry into cells. *J Biol Chem.* 272: 11414-11419.
56. Garred O, van Deurs B, Sandvig K. 1995. Furin-induced cleavage and activation of Shiga toxin. *J Biol Chem.* 270: 10817-10821.
57. Garrido C, Galluzzi L, Brunet M, Puig PE, Didelot C, Kroemer G. 2006. Mechanisms of cytochrome c release from mitochondria. *Cell Death Differ.* 13: 1423-33.

58. Gauthier R, Harnois C, Drolet JF, Reed JC, Vezina A, Vachon PH. 2001. Human intestinal epithelial cell survival: differentiation state-specific control mechanisms. *Am J Physiol Cell Physiol.* 280: C1540-1544.
59. Ghosh RN, Mallet WG, Soe TT, McGraw TE, Maxfield FR. 1998. An endocytosed TGN38 chimeric protein is delivered to the TGN after trafficking through the endocytic recycling compartment in CHO cells. *J Cell Biol.* 142: 923-936.
60. Girard D, Paquet ME, Paquin R, Beaulieu AD. 1996. Differential effects of interleukin-15 (IL-15) and IL-2 on human neutrophils: modulation of phagocytosis, cytoskeleton rearrangement, gene expression and apoptosis by IL-5. *Blood.* 88: 3176-3184.
61. Girard D, Paquin R, Beaulieu AD. 1997. Responsiveness of human neutrophils to IL-4: induction of cytoskeletal rearrangements, de novo protein synthesis and delay of apoptosis. *Biochem J.* 325: 147-153.
62. Gorden J, Small PLC. 1993. Acid resistance in enteric bacteria. *Infect. Immun.* 61: 364-367.
63. Habib NF, Jackson MP. 1993. Roles of a ribosome-binding site and mRNA secondary structure in differential expression of Shiga toxin genes. *J Bacteriol.* 175: 597-603.
64. Hancock DD, Besser TE, Rice DH, Herriott DE, and Tarr PI. 1997. Epidemiology of *Escherichia coli* O157 in fourteen cattle herds. *Epidemiol Infect.* 118: 193-195.
65. Hancock DD, Rice DH, Herriott DE, Besser TE, Ebel ED, Carpenter LV. 1997. Effects of farm manure handling practices on *Escherichia coli* O157 prevalence in cattle. *J Food Prot.* 60: 462-465.
66. Haslett C, Savill JS, Whyte MKB, Stern M, Dransfield I, Meagher LC. 1994. Granulocyte apoptosis and the control of inflammation. *Philos Trans R Soc Lond Biol Sci.* 345: 327-333.
67. Haslett C. 1992. Resolution of acute inflammation and the role of apoptosis in the tissue fate of granulocytes. *Clin Sci.* 83: 639-648.
68. Hengartner M. 2000. The Biochemistry of Apoptosis. *Nature.* 407: 770-776.
69. Hidalgo IJ *et al.* 1989. Characterization of the human colon carcinoma cell line (Caco-2) as a model system for intestinal epithelial permeability. *Gastroenterology* 96: 736-49.

70. Higuchi R, Krummel B, Saiki RK. 1988. A general method of in vitro preparation and specific mutagenesis of DNA fragments: study of protein and DNA interactions. *Nucleic Acids Res.* 16: 7351–7367.
71. Horton RM, Cai ZL, Ho SN, *et al.* 1990. Gene splicing by overlap extension: tailor-made genes using the polymerase chain reaction. *Biotechniques.* 8: 528-35.
72. Hsu H, Xiong J, Goeddel DV. 1995. The TNF receptor 1-associated protein TRADD signals cell death and NF-kappa B activation. *Cell.* 81: 495–504.
73. Hsu YT, Youle RJ. 1997. Nonionic detergents induce dimerization among members of the Bcl-2 family. *J Biol Chem.* 272: 13829–13834.
74. Hughes DA, Smith GC, Davidson JE, Murphy AV, Beattie TJ. 1996. The neutrophils oxidative burst in diarrhea-associated haemolytic uraemic syndrome. *Pediatr Nephrol.* 10: 445–447.
75. Hurley BP, Jacewicz M, Thorpe CM, Lincicome LL, King AJ, Keusch GT, Acheson WK. 1999. Shiga toxins 1 and 2 translocate differently across polarized intestinal epithelial cells. *Infection and Immunity* 67: 6670-6677.
76. Igney FH, Krammer PH. 2002. Death and anti-death: tumour resistance to apoptosis. *Nat Rev Cancer.* 2: 277–88.
77. Inward CD, Howie AJ, Fitzpatrick MM, Rafaat F, Milford DV, Taylor CM. 1997. Renal histopathology in fatal cases of diarrhea-associated haemolytic uraemic syndrome. *Pediatr Nephrol.* 11: 556–559.
78. Jaattela M. 2004. Multiple cell death pathways as regulators of tumour initiation and progression. *Oncogene.* 23: 2746-2756.
79. Jacewicz MS, Acheson DWK, Binion DG, West GA, Lincicome LL, Fiocchi C, Keusch GT. 1999. Responses of human intestinal microvascular endothelial cells to Shiga toxins 1 and 2 and pathogenesis of hemorrhagic colitis. *Infect Immun.* 67: 1439-1444.
80. Jackson ME, Simpson JC, Girod A, Pepperkok R, Roberts LM, Lord JM. 1999. The KDEL retrieval system is exploited by *Pseudomonas* exotoxin A, but not by Shiga-like toxin 1, during retrograde transport from the Golgi complex to the endoplasmic reticulum. *J. Cell Sci.* 112: 467-475.
81. Jackson MP, Neill RJ, O'Brien AD, Holmes RK, Newland JW. 1987. Nucleotide sequence analysis and comparison of the structural genes for Shiga-like toxin I and Shiga-like toxin II encoded by bacteriophages from *Escherichia coli* 933. *FEMS Microbiol Lett.* 44: 109-114.

82. Jackson MP, Newland JW, Holmes RK, and O'Brien AD. 1987. Nucleotide sequence analysis of the structural genes for Shiga-like toxin I encoded by bacteriophage 933J from *Escherichia coli*. *Microb Pathog.* 2: 147–153.
83. Jin Z, Gao F, Flagg T, Deng X. 2004. Tobacco-specific nitrosamine 4-(methylnitrosamino)-1-(3-pyridyl)-1-butanone promotes functional cooperation of Bcl2 and c-Myc through phosphorylation in regulating cell survival and proliferation. *J Biol Chem.* 279: 40209-40219.
84. Jones E, Islur A, Haq R, Mascarenhas M, Karmali MA, Perdue MH, Zanke BW, Sherman PM. 2000. *Escherichia coli* Shiga toxins induce apoptosis in epithelial cells that is regulated by the Bcl-2 family. *Am J Physiol Gastrointest Liver Physiol.* 278: G811-G819.
85. Joza N, Susin SA, Daugas E, Stanford WL, Cho SK, Li CY, Sasaki T, Elia AJ, Cheng HY, Ravagnan L, Ferri KF, Zamzami N, Wakeham A, Hakem R, Yoshida H, Kong YY, Mak TW, Zuniga-Pflucker JC, Kroemer G, Penninger JM. 2001. Essential role of the mitochondrial apoptosis-inducing factor in programmed cell death. *Nature.* 410: 549–54.
86. Kaper JB, O'Brien AD. 1998. *Escherichia coli* O157:H7 and other shiga toxin-producing *E. coli* strains. ASM Press, Washington DC.
87. Karmali M. 1989. Infection by Verocytotoxin-Producing *Escherichia coli*. *Clin Microbiol Rev* 2:15-38.
88. Karmali MA, Petric M, Lim C, Cheung R, Arbus G. 1985. The association between idiopathic hemolytic uremic syndrome and infection by Verotoxin-producing *Escherichia coli*. *J Infect Dis* 151: 775-782.
89. Karmali, MA, Steele BT, Petric M, Lim C. 1983. Sporadic cases of hemolytic uremic syndrome associated with fecal cytotoxin and cytotoxin-producing *Escherichia coli*. *Lancet* i: 619–620.
90. Karpman D, Connell H, Svensson M, Scheutz F, Alm P, Svanborg C. 1997. The role of lipopolysaccharide and Shiga-like toxin in a mouse model of *Escherichia coli* O157:H7 infection. *J Inf Dis.* 175: 611–620.
91. Karpman D, Hakansson A, Perez M-TR, Isaksson C, Carlemalm E, Capriolo A, Svanborg C. 1998. Apoptosis of renal cortical cells in the hemolytic-uremic syndrome: in vivo and in vitro studies. *Infect Immun.* 66: 636-644.
92. Kataoka T, Schroter M, Hahne M, Schneider P, Irmeler M, Thome M, Froelich CJ, Tschopp J. 1998. FLIP prevents apoptosis induced by death receptors but not by perforin/granzyme B, chemotherapeutic drugs, and gamma irradiation. *J Immunol.* 161: 3936–42.

93. Keane, W. F., R. Welch, G. Gekker, and P. K. Peterson. 1987. Mechanism of *Escherichia coli* alpha-hemolysin-induced injury to isolated renal tubular cells. *Am. J. Pathol.* 126:350–357.
94. Kelekar A, Chang BS, Harlan JE, Fesik SW, Thompson CB. 1997. Bad is a BH3 domain-containing protein that forms an inactivating dimer with Bcl-XL. *Mol Cell Biol.* 17: 7040-7046.
95. Kelekar A, Thompson CB. 1998. Bcl-2 family proteins: the role of the BH3 domain in apoptosis. *Trends Cell Biol.* 8: 324-330.
96. Kettritz R, Gaido ML, Haller H, Luft FC, Jennette CJ, Falk RJ. 1998. Interleukin-8 delays spontaneous and tumor necrosis factor- $\alpha$ -mediated apoptosis of human neutrophils. *Kidney International.* 53: 84-91.
97. Kettritz R, Gaido ML, Jennette JC, Falk RJ. 1997. Neutrophil super-oxide release is required for spontaneous and FMLP-mediated but not for TNF- $\alpha$ -mediated apoptosis. *J Am Soc Nephrol.* 8: 1091-1100.
98. Kim JS, Kim JM, Jung HC, Song IS. 2001. Caspase-3 activity and expression of Bcl-2 family in human neutrophils by *Helicobacter pylori* water-soluble proteins. *Helicobacter.* 6: 207-15.
99. Kimmit PT, Harwood CR, Barer MR. 2000. Toxin gene expression by Shiga toxin-producing *Escherichia coli*: The role of antibiotics and the bacterial SOS response. *Emerg Infect Dis.* 6: 458-465.
100. King AJ, Sundaram S, Cendoroglo M, Acheson DW, Keusch GT. 1999. Shiga toxin induces superoxide production in polymorphonuclear cells with subsequent impairment of phagocytosis and responsiveness to phorbol esters. *J Infect Dis.* 179: 503-507.
101. Kischkel FC, Hellbardt S, Behrmann I, Germer M, Pawlita M, Krammer PH, Peter ME. 1995. Cytotoxicity-dependent APO-1 (Fas/CD95)- associated proteins form a death-inducing signaling complex (DISC) with the receptor. *Embo J.* 14: 5579-88.
102. Klebanoff SF, Olszowski S, Voorhis WCV, Ledbetter JA, Waltersdorph AM, Schlechte KG. 1992. Effects of  $\gamma$ -interferon on human neutrophils: Protection from deterioration on storage. *Blood.* 80: 225-234.
103. Knutton S, Lloyd DR, McNeish AS. 1987. Adhesion of enteropathogenic *Escherichia coli* to human intestinal enterocytes and cultured human intestinal mucosa. *Infect Immun.* 55: 69-77.

104. Konowalchuk, J, Speirs JI, Stavric S. 1977. Vero response to a cytotoxin of *Escherichia coli*. *Infect. Immun.* 18: 775-779.
105. Kothakota S, Azuma T, Reinhard C, Klippel A, Tang J, Chu K, McGarry TJ, Kirschner MW, Koths K, Kwiatkowski DJ, Williams LT. 1997. Caspase-3-generated fragment of gelsolin: effector of morphological change in apoptosis. *Science.* 278: 294-8.
106. Kozlov YV, Kabishev AA, Lukyanov EV, Bayev AA. 1988. The primary structure of the operons coding for *Shigella dysenteriae* toxin and temperate phage H30 Shiga-like toxin. *Gene.* 67:213–221.
107. Krajewski S, Tanaka S, Takayama S, Schibler MJ, Fenton W, Reed JC. 1993. Investigation of the subcellular distribution of the Bcl-2 oncoprotein: residence in the nuclear envelope, endoplasmic reticulum, and outer mitochondrial membranes. *Cancer Res.* 53: 4701–4714.
108. Kroemer G *et al.* 2009. Classification of cell death: recommendations of the Nomenclature Committee on Cell Death. *Cell Death Diff.* 401: 3-11.
109. Law D, Kelly J. 1995. Use of heme and hemoglobin by *Escherichia coli* O157 and other Shiga-like-toxin-producing *E. coli* serogroups. *Infect Immun.* 63:700–702.
110. Lee SY, Lee MS, Cherla RP, Tesh VL. 2008. Shiga toxin 1 induces apoptosis through the endoplasmic reticulum stress response in human monocytic cells. *Cellular Microbiology.* 10: 770–780.
111. Leuenroth SJ, Grutkoski PS, Ayala A, Simms Hank H. 2000. The loss of Mcl-1 expression in human polymorphonuclear leukocytes promotes apoptosis. *J Leukocyte Biology.* 68: 158-166.
112. Li LY, Luo X, Wang X. 2001. Endonuclease G is an apoptotic DNase when released from mitochondria. *Nature.* 412: 95–9.
113. Li Y, Frey E, Mackenzie AMR, Finlay BB. 2000. Human response to *Escherichia coli* O157:H7 infection: antibodies to secreted virulence factors. *Infection and Immunity.* 68: 5090-5095.
114. Lieberman J, Fan Z. 2003. Nuclear war: the granzyme A-bomb. *Curr Opin Immunol.* 15: 553–9.
115. Lingwood, CA, Law H, Richardson S, Petric M, Brunton JL, DeGrandis S, Karmali, M. 1987. Glycolipid binding of natural and cloned *Escherichia coli* produced verotoxin in vitro. *J Biol Chem.* 262: 8834–8839.



116. Lingwood, CA. 1996. Role of verotoxin receptors in pathogenesis. *Trends Microbiol.* 4: 147–153.
117. Litalien C, Proulx F, Mariscalco MM, Robitaille P, Turgeon JP, Orrbine E, Rowe PC, McLaine PN, Seidman E. 2000. Circulating inflammatory cytokine levels predict severity of renal failure in hemolytic uremic syndrome. *Pediatr Nephrol.* 35: 28-34.
118. Liu J, Akahoshi T, Sasahana , Kitasato H, Namai R, Sasaki T, Inoue M, Kondo H. 1999. Inhibition of neutrophil apoptosis by Verotoxin 2 derived from *Escherichia coli* O157:H7. *Infect Immun* 67: 6203-6205.
119. Locksley RM, Killeen N, Lenardo MJ. 2001. The TNF and TNF receptor superfamilies: integrating mammalian biology. *Cell.* 104: 487–501.
120. Louise CB, Obrig TG. 1992. Shiga toxin-associated hemolytic uremic syndrome: combined cytotoxic effects of Shiga toxin and lipopolysaccharide (endotoxin) on human vascular endothelial cells in vitro. *Infect Immun.* 60:1536–1543.
121. Lund AH, Duch M, Pendersen FS. 1996. Increased cloning efficiency by temperature-cycle ligation. *Nucleic Acid Res.* 24: 800-801.
122. Martin DL, MacDonald KL, White KE, Soler JT, Osterholm MT. 1990. The epidemiology and clinical aspects of the hemolytic uremic syndrome in Minnesota. *N Engl J Med.* 323: 1161–1167.
123. Masure S, Proost P, Van Damme J, Opdenakker G. 1991. Purification and identification of 91-kDa neutrophils gelatinase-Release by the activating peptide interleukin-8. *Eur J Biochem.* 198: 391-398.
124. McCarthy NJ, Whyte MK, Gilbert CS, Evan GI. 1997. Inhibition of Ced-3/ICE-related proteases does not prevent cell death induced by oncogenes, DNA damage, or the Bcl-2 homologue Bak. *J Cell Biol.* 136: 215-27.
125. Mead PS, Slutsker L, Dietz V, McCaig LF, Bresee JS, Shapiro C, *et al.* 1999. Food-related illnesses and death in the United States. *Emerg Infect Dis.* 5: 607-625.
126. Meng J, Doyle MP, Zhao S, Zhao T. 1994. The detection and control of *Escherichia coli* O157:H7 in foods. *Trends Food Sci Technol.* 5: 179-185.
127. Milford D, Taylor CM, Rafaat F, Halloran H, Dawes J. 1989. Neutrophil elastases and haemolytic uraemic syndrome. *Lancet.* 2: 1153.

128. Moulding DA, Quayle JA, Hart CA, Edwards SW. 1998. Mcl-1 expression in human neutrophils: Regulation by cytokines and correlation with cell survival. *Blood*. 92: 2495-2502.
129. Muchmore SW, Sattler M, Liang H, Meadows RP, Harlan JE, Yoon HS, Nettesheim D, Chang BS, Thompson CB, Wong SL, Ng SL, Fesik SW. 1996. X-ray and NMR structure of human Bcl-xL, an inhibitor of programmed cell death. *Nature*. 381: 335-41.
130. Myrianthefs P, Venetsanou K, Grouzi E, Boutzouka E, Evagelopoulou P, Fildissis G, Spiliotopoulou I, Baltopoulos G. 2002. Monocyte normal immune response to LPS stimulation. *Critical Care*. 6: 101 [Online]  
<http://ccforum.com/content/6/S1/P101>
131. Nataro JP, Kaper JB. 1998. Diarrheagenic *Escherichia coli*. *Clin Microbiol Rev*. 11: 142-201.
132. Nelson, DL Cox MM. 2000. *Lehninger Principles of Biochemistry*. Worth Publishers. New York, NY.
133. Nikado, H. 1996. Outer membrane. In Neidhardt, Curtiss, Ingraham Lin, Low, Magasanik, Reznikoff, Riley, Schaechter and Umberger (Editors), *Escherichia coli* and *Salmonella*: Cellular and Molecular Biology, 2nd Ed., ASM Press, Washington DC. pg. 27-29.
134. Niwa M, Hara A, Kanamori Y, Hatakeyama D, Saio M, Takami T, Matsuno H, Kozawa O, Uematsu T. 2000. Nuclear factor- $\kappa$ B activates dual inhibition sites in the regulation of tumor necrosis factor- $\alpha$ -induced neutrophil apoptosis. *Eur J Pharmacol*. 407: 211-219.
135. Nolan B, Kim R, Duffy A, Sheth K, De M, Miller C, Chari R, Bankey P. 2000. Inhibited neutrophil apoptosis: Proteasome dependent NF- $\kappa$ B translocation is required for TRAF-1 synthesis. *Shock*. 14: 290-294.
136. Norbury CJ, Hickson ID. 2001. Cellular responses to DNA damage. *Annu Rev Pharmacol Toxicol*. 41: 367-401.
137. Nutt LK, Pataer A, Pahler J, Fang B, Roth J., McConkey DJ, Swisher DG. 2002. Bax and Bak promote apoptosis by modulating endoplasmic reticular and mitochondrial Ca<sup>2+</sup> stores. *J Biol Chem*. 277: 9219- 9225.
138. O'Brien AD, Holmes RK. 1987. Shiga and Shiga-like toxins. *Microbiol Rev*. 51: 206-220.

139. O'Brien, AD, La Veck GD. 1983. Purification and characterization of a *Shigella dysenteriae* 1-like toxin produced by *Escherichia coli*. *Infect. Immun.* 40: 675–683.
140. O'Brien, AD, LaVeck GD, Thompson MR, Formal SB. 1982. Production of *Shigella dysenteriae* type 1-like cytotoxin by *Escherichia coli*. *J Infect Dis.* 146: 763–769.
141. Obrig TG, Moran TP, Brown JE. 1987 The mode of action of Shiga toxin on peptide elongation of eukaryotic protein synthesis. *Biochem J.* 244: 287–294.
142. Obrig TG. 1998. Interaction of Shiga toxins with endothelial cells, p. 303–311. In Kaper JB and O'Brien AD (ed.), *Escherichia coli* O157:H7 and other Shiga toxin-producing *E. coli* strains. American Society for Microbiology, Washington, D.C.
143. Ohta H, Yatomi Y, Sweeney EA, Hakomori S, Igarashi Y. 1994. A possible role of sphingosine in induction of apoptosis by tumor necrosis factor- $\alpha$  in human neutrophils. *FEBS Lett.* 355: 267-270.
144. Oltvai ZN, Milliman CL, Korsmeyer SJ. 1993. Bcl-2 functions in an antioxidant pathway to prevent apoptosis. *Cell.* 75: 241-251.
145. Ostroff SM, Tarr PI, Neill MA, Lewis JH, Hargrett-Bean N, Kobayashi JM. 1998. Toxin genotypes and plasmid profiles as determinants of systemic sequelae in *Escherichia coli* O157:H7 infections. *J Infect Dis.* 160: 994–998.
146. Pardo J, Bosque A, Brehm R, Wallich R, Naval J, Mullbacher A, Anel A, and Simon MM. 2004. Apoptotic pathways are selectively activated by granzyme A and/or granzyme B in CTL-mediated target cell lysis. *J Cell Biol.* 167: 457.
147. Park SH, Choi HJ, Yang H, Do KH, Kim J, Lee DW, Moon Y. 2010. Endoplasmic reticulum stress-activated C/EBP homologous protein enhances nuclear factor-kappaB signals via repression of peroxisome proliferator-activated receptor gamma. *J Biol Chem.* 285: 35330–35339.
148. Paton JC, Paton AW. 1998. Pathogenesis and diagnosis of Shiga-toxin producing *Escherichia coli* infections. *Clin Microbiol Rev* 11: 450-479.
149. Pericle F, Liu JH, Diaz JI, Blanchard DK, Wei S, Forni G, Djeu JY. 1994. Interleukin-2 prevention of apoptosis in human neutrophils. *Eur J Immunol.* 24: 440-444.
150. Petros AM, Medek A, Nettesheim DG, Kim DH, Yoon HS, Swift K, Matayoshi ED, Oltersdorf T, Fesik SW. 2001. Solution structure of the antiapoptotic protein Bcl-2. *Proc Natl Acad Sci USA.* 98: 3012–3017.

151. Petros AM, Olejniczak ET, Fesik SW. 2004. Structural biology of the Bcl-2 family of proteins. *Biochem Biophys Acta*. 1644: 83-94.
152. Phillips AD, Navabpour S, Hicks S, Dougan G, Wallis T, Frankel G. 2000. Enterohemorrhagic *Escherichia coli* O157:H7 target Peyer patches in humans and cause attaching/effacing lesions in both human and bovine intestine. *Gut*. 47: 377-381.
153. Pinto M *et al.* 1983. Enterocyte-like differentiation and polarization of the human colon carcinoma cell line Caco-2 in culture. *Biol Cell* 47: 323–30.
154. Proulx F, Seidman E, Mariscalco MM, Lee K, Carroll SF 1999. Increased circulating levels of lipopolysaccharide binding protein in children with *Escherichia coli* O157:H7 hemorrhagic colitis and hemolytic uremic syndrome. *Clin Diagn Lab Immunol*. 6:773.
155. Proulx F, Litalien C, Turgeon JP, Mariscalco MM, Seidman E. 1998. Inflammatory mediators in hemorrhagic colitis and hemolytic uremic syndrome. *Pediatr Inf Dis*. 17: 899–904.
156. Proulx F, Seidman EG, Karpman D. 2001. Pathogenesis of Shiga toxin-associated hemolytic uremic syndrome. *Ped Res*. 50: 163- 171.
157. Public Health Agency of Canada. 2001. Material Safety Data Sheet- *Escherichia coli*, enterohemorrhagic. Online: <http://www.phac-aspc.gc.ca/msds-ftss/msds63e-eng.php>
158. Quintiliani, RJ, Courvalin R. 1995. Mechanisms of resistance to antimicrobial agents. In Murray, Baron, Tenover and Tenover (Editors), *Manual of Clinical Microbiology*, 6th Ed., ASM Press, Washington D.C. pg. 1308-1326.
159. Rangel JM, Sparling PH, Crowe C, Griffin PM, Swerdlow DL. 2005. Epidemiology of *Escherichia coli* O157:H7 outbreaks, United States, 1982-2002. *Emerg Infect Dis* 11: 603-609.
160. Reed JC, Huang Z. 2004. Apoptosis pathways and drug targets poster. *Nature Reviews*. [Online] <http://www.nature.com/reviews/poster/apoptosis/index.html#top>.
161. Richardson SE, Karmali MA, Becker LE, Smith CR. 1988. The histopathology of the hemolytic uremic syndrome associated with verocytotoxin-producing *Escherichia coli* infections. *Hum Pathol*. 19: 1102–1108.

162. Riley, LW, Remis RS, Helgerson SD, McGee HB, Wells JG, Davis BR, Hebert RJ, Olcott ES, Johnson LM, Hargrett NT, Blake PA, Cohen ML. 1983. Hemorrhagic colitis associated with a rare *Escherichia coli* serotype. *N Engl J Med.* 308: 681-685.
163. Ruemmele FM, Dionne S, Qureshi I, Sarma DS, Levy E, Seidman EG. 1999. Butyrate mediates Caco-2 cell apoptosis via up-regulation of pro-apoptotic BAK and inducing caspase-3 mediated cleavage of poly-(ADP-ribose) polymerase (PARP). *Cell Death Differ.* 6: 729-35.
164. Russell JH, Ley TJ. 2002. Lymphocyte-mediated cytotoxicity. *Annu Rev Immunol.* 20: 323-70.
165. Saelens X, Festjens N, Vande Walle L, van Gurp M, van Loo G, Vandenabeele P. 2004. Toxic proteins released from mitochondria in cell death. *Oncogene.* 23: 2861-74.
166. Sakahira H, Enari M, Nagata S. 1998. Cleavage of CAD inhibitor in CAD activation and DNA degradation during apoptosis. *Nature.* 391: 96-9.
167. Saleh, MT, Ferguson J, Boggs JM, Garipey J. 1996. Insertion and orientation of a synthetic peptide representing the C-terminus of the A1 domain of Shiga toxin into phospholipid membranes. *Biochemistry.* 35: 9325-9334.
168. Salzman MB, Ettenger RB, Cherry JD. 1991. Leukocytosis in hemolytic uremic syndrome. *Pediatr Infect Dis J.* 10: 470-471.
169. Sandvig K, van Deurs B. 1996. Endocytosis, intracellular transport, and cytotoxic action of Shiga toxin and ricin. *Physiol. Rev.* 76: 949-966.
170. Sandvig, K. 2001. Shiga toxins. *Toxicon* 39: 1629-1635.
171. Sattler M, Liang H, Nettlesheim D, Meadows RP, Harlan JE, Eberstadt M, Yoon HS, Shuker SB, Chang BS, Minn AJ, Thompson CB, Fesik SW. 1997. Structure of Bcl-XL-Bak peptide complex: recognition between regulators of apoptosis. *Science.* 275: 983.
172. Savarino SJ, McVeigh A, Watson J, Cravioto A, Molina J, Echeverria P, Bhan MK, Levine MM, Fasano A. 1996. Enteroaggregative *Escherichia coli* heat-stable enterotoxin is not restricted to enteroaggregative *E. coli*. *J Infect Dis.* 173: 1019-1022.
173. Savill JS, Wyllie AH, Henson JE, Walport MJ, Henson PM, Haslett C. 1989. Macrophage phagocytosis of aging neutrophils in inflammation. *J Clin Invest.* 83: 865-875.

174. Scaffidi C, Schmitz I, Krammer PH, Peter ME. 1999. The role of c-FLIP in modulation of CD95-induced apoptosis. *J Biol Chem.* 274: 1541–8.
175. Schimmer AD. 2004. Inhibitor of apoptosis proteins: translating basic knowledge into clinical practice. *Cancer Res.* 64: 7183–90.
176. Schmidt H, Karch H, Beutin L. 1994. The large-sized plasmids of enterohemorrhagic *Escherichia coli* O157 strains encode hemolysins which are presumably members of the *E. coli* alpha-hemolysin family. *FEMS Microbiol Lett.* 117: 189–196.
177. Scorrano L, Korsmeyer S J. 2003. Mechanisms of cytochrome c release by proapoptotic BCL-2 family members. *Biochem Biophys Res Commun.* 304: 437-444.
178. Scorrano L, Oakes SA, Opferman JT, Cheng EH, Sorcinelli MD, Pozzan T, Korsmeyer SJ. 2003. BAX and BAK regulation of endoplasmic reticulum Ca<sup>2+</sup>: a control point for apoptosis. *Science.* 300: 135– 139.
179. Scotland SM, Willshaw GA, Smith HR, Rowe B. 1987. Properties of strains of *Escherichia coli* belonging to serogroup O157 with special reference to production of vero cytotoxins VT1 and VT2. *Epidemiol Infect.* 99: 613–62437.
180. Seto M, Jaeger U, Hockett RD, Graninger W, Bennett S, Goldman P, Korsmeyer SJ. 1988. Alternative promoters and exons, somatic mutation and deregulation of the Bcl-2-Ig fusion gene in lymphoma. *EMBO J.* 7: 123-131.
181. Sharpe JC, Arnoult D, Youle RJ. 2004. Control of mitochondrial permeability by Bcl-2 family members. *Biochem Biophys Acta.* 1644: 107-113.
182. Slee EA, Adrain C, Martin SJ. 2001. Executioner caspase-3, -6, and -7 perform distinct, non-redundant roles during the demolition phase of apoptosis. *J Biol Chem.* 276: 7320–6.
183. Sperandio V, Mellies JL, Nguyen W, Shin S, Kaper JB. 1999. Quorum sensing controls expression of the type III secretion gene transcription and protein secretion in enterohemorrhagic and enteropathogenic *Escherichia coli*. *Proc Natl Acad Sci USA.* 96: 15196–15201.
184. Stehlik C, de Martin R, Binder BR, Lipp J. 1998. Cytokine induced expression of porcine inhibitor of apoptosis protein (iap) family member is regulated by NF- $\kappa$ B. *Biochem Biophys Res Commun.* 243: 827–832.

185. Strasser S, Huang DCS, Vaux DL. 1997. The role of the bcl-2/ced-9 gene family in cancer and general implications of defects in cell death control for tumourigenesis and resistance to chemotherapy. *Biochim Biophys Acta.* 1333: F151-78.
186. Stringer RE, Hart CA, Edwards SW. 1996. Sodium butyrate delays neutrophil apoptosis. Role of protein biosynthesis in neutrophil survival. *Br J Haematol.* 92: 169-175.
187. Strockbine, NA, Jackson MP, Sung LM, Holmes RK, O'Brien AD. 1988. Cloning and sequencing of the genes for Shiga toxin from *Shigella dysenteriae* type 1. *J Bacteriol.* 170: 1116-1122.
188. Susin SA, Daugas E, Ravagnan L, Samejima K, Zamzami N, Loeffler M, Costantini P, Ferri KF, Irinopoulou T, Prevost MC, Brothers G, Mak TW, Penninger J, Earnshaw WC, Kroemer G. 2000. Two distinct pathways leading to nuclear apoptosis. *J Exp Med.* 192: 571-80.
189. Suttrop N, Floer B, Schnittler H, Seeger W, Bhakdi S. 1990. Effects of *Escherichia coli* hemolysin on endothelial cell function. *Infect Immun.* 58: 3796-3801.
190. Suzuki A, Hirofumi B, Fumiko M, Aikawa S, Takiguchi K, Kawano H, Hayashida M, Ohno S. 2000. Bcl-2 antiapoptotic protein mediates verotoxin II-induced cell death: possible association between Bcl-2 and tissue failure by *E. coli* O157:H7 *Gene Develop.* 14: 1734-1740.
191. Suzuki T, Yan Q, Lennardz WJ. 1998. Complex, two-way traffic of molecules across the membrane of the endoplasmic reticulum. *J Biol Chem.* 273: 10083-10086.
192. Takeda Y, Watanabe H, Yonehara S, Yamashita T, Saito S, Sendo F. 1993. Rapid acceleration of neutrophils apoptosis by tumor necrosis factor- $\alpha$ . *Int Immunol.* 5: 691-694.
193. Taylor CM, Milford DV, Rose PE, Roy TCF, Rowe B. 1990. The expression of blood group P1 in post-enteropathic haemolytic uraemic syndrome. *Pediatr Nephrol.* 4: 59-61.
194. Te Loo, Monnens LA, van Der Velden TJ, Vermeer MA, Preyers F, Demacker PN, van Den Heuvel LP, van Hinsbergh VW. 2000. Binding and transfer of verocytotoxin by polymorphonuclear leukocytes in hemolytic uremic syndrome. *Blood.* 95: 3396-3402.

195. Te Loo, Monnens LA, van Der Velden TJ, Vermeer MA, Preyers F, Demacker PN, van Den Heuvel LP, van Hinsbergh VW. 2000. Binding and transfer of verocytotoxin by polymorphonuclear leukocytes in hemolytic uremic syndrome. *Blood*. 95: 3396-3402.
196. Thomas A, Chart H, Cheasty T, Smith HR, Frost JA, Rowe B 1993 Vero cytotoxin-producing *Escherichia coli*, particularly serogroup O157, associated with human infections in the United Kingdom: 1989–1991. *Epidemiol Infect*. 110: 591–600.
197. Thorpe CM, Hurley BP, Lincicome LL, Jacewicz MS, Keusch GT, Acheson DW. 1999. Shiga toxins stimulate secretion of interleukin-8 from intestinal epithelial cells. *Infect Immun* 67: 5985–5993.
198. Trapani JA, Smyth MJ. 2002. Functional significance of the perforin/granzyme cell death pathway. *Nat Rev Immunol*. 2: 735–47.
199. Tsujimoto Y, Shimizu S. 2005. Another way to die: autophagic programmed cell death. *Cell Death and Differ*. 12: 1528–1534.
200. U.S. Food and Drug Administration. 1993. Food Code: 1993 recommendations of the United States Public Health Service, Food and Drug Administration. Pub. no. PB94-11394. Washington: National Technical Information Service.
201. Van Antwerp DJ, Martin SJ, Kafri T, Green DR, Verma IM. 1996. Suppression of TNF-alpha-induced apoptosis by NF-kappaB. *Science*. 274: 787–789.
202. van Loo G, van Gurp M, Depuydt B, Srinivasula SM, Rodriguez I, Alnemri ES, Gevaert K, Vandekerckhove J, Declercq W, Vandenaabeele P. 2002. The serine protease Omi/HtrA2 is released from mitochondria during apoptosis. Omi interacts with caspase-inhibitor XIAP and induces enhanced caspase activity. *Cell Death Differ*. 9: 20–26.
203. Van Setten PA, Hinsbergh MV, Van Den Heuvel LPWJ, Preyers F, Dijkman HPBM, Assmann KJM, Ven Der Velden TJAM, Monnens LAH. 1998. Monocyte chemoattractant protein-1 and interleukin-8 in urine and serum of patients with hemolytic uremic syndrome. *Pediatr Res*. 43: 759–767.
204. Van Setten PA, Monnens LA, Verstraten RG, van den Heuvel LP, van Hinsbergh VW. 1996. Effects of verocytotoxin-1 on nonadherent human monocytes: binding characteristics, protein synthesis and induction of cytokine release. *Blood*. 88: 174-183.



205. Vierzig A, Roth B, Querfeld U, Michalk D. 1998. A 12-year-old boy with fatal hemolytic uremic syndrome, excessive neutrophilia and elevated endogenous granulocyte-colony-stimulating-factor serum concentrations. *Clin Nephrol.* 50: 56-69.
206. Waddell T, Head S, Petric M, Cohen A, Lingwood CA. 1988. Globotriosyl ceramide is specifically recognized by the *Escherichia coli* Verotoxin 2. *Biochem Biophys Res Commun.* 152: 674–679.
207. Wajant H. 2002. The Fas signaling pathway: more than a paradigm. *Science.* 296: 1635–6.
208. Walters MD, Matthei IE, Kay R, Dillon MJ, Barratt TM. 1989. The polymorphonuclear leukocyte count in childhood haemolytic uraemic syndrome. *Pediatr Nephrol.* 3: 130–134.
209. Wang CY, Mayo MW, Baldwin AS Jr. 1996. TNF- and cancer therapy-induced apoptosis: potentiation by inhibition of NF-kappaB. *Science.* 274: 784–787.
210. Wang G, Clark CG, Rodgers FG. 2002. Detection in *Escherichia coli* of the genes encoding the major virulence factors, the genes defining the O157:H7 serotype, and components of the type 2 Shiga toxin family by multiplex PCR. *J Clin Microbiol.* 40: 3613-3619.
211. Warburg, O, Christian W. 1941. Isolation and crystallization of the enzyme enolase. *Biochem Z.* 310: 384-421.
212. Ward C, Chilvers ER, Lawson MF, Pryde JG, Fujihara S, Farrow SN, Haslett C, Rossi AG. 1999. NF-κB activation is a critical regulator of human granulocyte apoptosis in vitro. *J Biol Chem.* 274: 4309-4318.
213. Ward C, Dransfield I, Chilvers ER, Haslett I, Rossi AG. 1999. Pharmacological manipulation of granulocyte apoptosis: Potential therapeutic targets. *Trends Pharmacol Sci.* 20: 503-509.
214. Ward C, Dransfield I, Murray J, Farrow SN, Haslett C, Rossi AG. 2002. Prostaglandin D2 and its metabolites induce caspase-dependent granulocyte apoptosis that is mediated via inhibition of IκB-α degradation using a peroxisome proliferator-activated receptor-γ-independent mechanism. *J Immunol.* 168: 6232-6243.
215. Watanabe-Takahashi M, Sato T, Dohi T, Noguchi N, Kano F, Murata M, Hamabata T, Natori Y, Nishikawa K. 2010. An orally applicable Shiga toxin neutralizer functions in the intestine to inhibit the intracellular transport of the toxin. *Infect Immun.* 78: 177–183.

216. Westlin WF, Kiely JM, Gimbrone MAJ. 1992. Interleukin-8 induces changes in human neutrophils actin conformation and distribution: relationship to inhibition of adhesion to cytokine-activated endothelium. *J Leukocyte Biol.* 52: 43-51.
217. Wilson JW, Nostro MC, Balzi M, Faraoni P, Becciolini A, Potten CS. 2000. Bcl-w expression in colorectal adenocarcinoma. *British Journal of Cancer.* 82: 178-185.
218. Wong CS, Jelacic S, Habeeb RL, Watkins S, Tarr PI. 2000. The risk of the hemolytic uremic syndrome after antibiotic treatment of *Escherichia coli* O157:H7 infections. *N Engl J Med.* 26: 1930-1936.
219. Wong CS, Jelacic S, Habeeb RI, Watkins SL, Tarr PI. 2000. The risk of hemolytic-uremic syndrome after antibiotic treatment of *Escherichia coli* O157:H7 infections. *N Engl J Med.* 26: 1930-1936.
220. Woodward DL, Clark CG, Caldeira RA, Ahmed R, Rodgers FG. 2002. Verotoxigenic *Escherichia coli* (VTEC): A major public health threat in Canada. *Canad J Infect Dis.* 13: 321-330.
221. Wymann MP, Kernen P, Deranleau DA, Dewald B, Von Tscherner V, Baggiolini M. 1987. Oscillatory motion in human neutrophils responding to chemotactic stimuli. *Biophys Res Commun.* 147: 361-368.
222. Xiang J, Chao DT, Korsmeyer SJ. 1996. Bax-induced cell death may not require interleukin 1 beta-converting enzyme-like proteases. *Proc Natl Acad Sci USA.* 93: 14559-63.
223. Yamasaki C, Natori Y, Zeng XT, Ohmura M, Yamasaki S, Takeda Y, Natori Y. 1999. Induction of cytokines in a human colon epithelial cell line by Shiga toxin 1 and 2 but not by non-toxic mutant Stx 1 which lacks N-glycosidase activity. *FEBS Lett.* 442: 231-234.
224. Yang E, Korsmeyer SJ. 1996. Molecular thanatopsis: a discourse on the BCL2 family and cell death. *Blood.* 88: 386-401.
225. Yin XM, Oltavi ZN, Korsmeyer SJ. 1994. BH1 and BH2 domains of Bcl-2 are required for inhibition of apoptosis and heterodimerization with Bax. *Nature.* 369: 321-323.
226. Zamzami N, Kroemer G. 1999. Apoptosis: Condensed matter in cell death. *Nature.* 401: 168-73.

227. Zhang Z, Lapolla SM, Annis MG, Truscott M, Roberts J, Miao Y, Shao Y, Tan C, Peng J, Johnson AE, Zhang XC, Andrews DW, Lin J. 2004. Bcl-2 homodimerization involves two distinct binding surfaces, a topographic arrangement that provides an effective mechanism for Bcl-2 to capture activated Bax. *J Biol Chem.* 279: 43920-43938.